ISBN 978-82-326-0950-5 (printed version)
ISBN 978-82-326-0951-2 (electronic version)
ISSN 1503-8181

Doctoral theses at NTNU, 2015:147

Anders Willersrud

Model-Based Diagnosis of Drilling Incidents

NTNU
Norwegian University of
Science and Technology
Faculty of Information Technology,
Mathematics and Electrical Engineering
Department of Engineering Cybernetics

NTNU – Trondheim
Norwegian University of
Science and Technology

Doctoral theses at NTNU, 2015:147

NTNU

NTNU – Trondheim
Norwegian University of
Science and Technology

Anders Willersrud

Model-Based Diagnosis of Drilling Incidents

Thesis for the degree of Philosophiae Doctor

Trondheim, May 2015

Norwegian University of Science and Technology

NTNU – Trondheim
Norwegian University of
Science and Technology

NTNU
Norwegian University of Science and Technology

Thesis for the degree of Philosophiae Doctor

ISBN 978-82-326-0950-5 (printed version)
ISBN 978-82-326-0951-2 (electronic version)
ISSN 1503-8181
ITK Report 2015-2-W

Doctoral theses at NTNU, 2015:147

Printed by Skipnes Kommunikasjon as

To Cecilie

Summary

Oil and gas drilling is an advanced process with very little instrumentation, where drilling fluid is transported through rotating drillstrings of up to several kilometers, possibly at extreme depths with high pressure and temperature. A drilling bit is used at the bottom of the drillstring to crush the formation, and the drilling fluid is used to carry the cuttings to the surface, as well as maintain the pressure in the well. Drilling is a costly operation, especially offshore. Incidents can occur that may slow down the progress. Detecting such incidents manually, especially those occurring down in the well, may be difficult. Early symptoms may give small variations in pressure, temperature, and flow rates, possibly covered in measurement noise.

The push for drilling more complex wells in more remote locations demands more from the drilling control and monitoring system. With advances in drilling control technology such as managed pressure drilling, and sensor technology such as wired drill pipe, the complexity of the control system greatly increases. With a high data rate of sensor readings, as well as lower operation margins, an efficient automatic diagnosis system is instrumental in reducing operational delays. This thesis presents different model-based methods for achieving early diagnosis of different drilling incidents, possibly distinguished from sensor bias, and with estimation of the incident magnitude. The model-based diagnosis system consists of two parts; first some residuals are generated using either adaptive observers or analytical redundancy relations, then changes to these residuals are detected using a statistical change detection algorithm, required due to measurement noise. Univariate and multivariate generalized likelihood ratio tests are applied, using the probability density function that best matches the noise of the residuals. The thresholds are found using the probability distribution of the test statistic, determined by a specified probability of false alarms. The probability of fault detection is also found as a function of the threshold, where data during the incidents are available.

Data from a medium-scale flow loop is used to test the diagnosis method, where the noise of the residuals fits the t-distribution well. A multivariate change detection method considering multiple residuals jointly is found to be superior over a univariate method considering each residual separately, and is used to detect and isolate the different incidents occurring in the test data. Furthermore, the t-distribution is shown to give an increased probability of detection compared with assuming the more common Gaussian distribution. Simulation of a drilling incident in the high-fidelity multi-phase simulator OLGA with Gaussian noise in the measurements is also considered.

The diagnosis framework proposed in this thesis is module-based, where the methods in each module are simple enough to be implemented in drilling monitoring

software at the rig, and can be run in real-time. However, a limitation with the proposed method is that good data during the normal operating mode is required for reliable detection and isolation. Future work and implementations should take this into account, and facilitate automatic acquisition of new data when changes to the process are made.

Preface

This thesis is submitted in partial fulfillment of the requirements for the degree of Philosophiae Doctor (PhD) at the Norwegian University of Science and Technology (NTNU). The research has been conducted at the Department of Engineering Cybernetics (ITK) from January 2011 to March 2015. Funding for the research has been provided by the Norwegian Research Council and Statoil ASA, for which I am very grateful.

I would first and foremost like to thank my supervisor Professor Lars Imsland. He encouraged me to pursue a PhD degree, and has since the beginning been an excellent supervisor. I am very grateful for his support, motivation and guidance. Professor Imsland has always encouraged me to improve my work, and has throughout this period provided valuable feedback and suggestions for further research directions.

I would especially like to thank Professor Mogens Blanke at the Technical University of Denmark and Center for Autonomous Marine Operations and Systems (AMOS) at NTNU for the close collaboration. I have had the privilege to work with Professor Blanke from September 2013 until today, which I am very thankful for. Professor Blanke is a well renowned expert within the fields of fault diagnosis and fault-tolerant control, and has contributed to most of the major results in this thesis.

I would also like to thank my co-supervisor Dr. Alexey Pavlov from Statoil for his ideas, comments and suggestions to the work. Dr. Pavlov has valuable industry experience, but also a substantial theoretical background which is greatly valuable to the work. From Statoil I would also like to thank Adjunct associate professor Glenn-Ole Kaasa (now Managing director at Kelda Drilling Controls), Dr. Henrik Manum and Dr. Qin Li for sharing their industry expertise, and giving valuable feedback to my work.

I would like to thank my research group for discussions and feedback, including Ulf Jakob Aarsnes, Amirhossein Nikoofard, Torbjørn Pedersen, Dr. Agus Hasan and Assistant professor Florent Di Meglio, as well as the supervisors and collaborators in the project Professor Ole Morten Aamo, Professor Tor Arne Johansen, Adjunct professor John-Morten Godhavn, Dr. Jan Einar Gravdal and Adjunct professor Gerhard Nygaard.

During my time at the department I have enjoyed the close friendship and good colleagueship with Joakim Haugen, Anne Mai Ersdal, Brage Knudsen, Tor Aksel Heirung, Bjarne Grimstad and the rest of the PhD students. I have greatly enjoyed the time with them, with many social and technical discussions.

I would like to thank my mother and father, Aase and Terje, and my sister Line, for always supporting and encouraging me. Finally I would like to express my deepest gratitude to Cecilie, for her love, support and encouragement, agreeing to move with me to Trondheim for the sole purpose of me pursuing this thesis.

Anders Willersrud
Trondheim, February 2015

Contents

Abbreviations

Oil and gas drilling

BHP	Bottomhole pressure
BOP	Blowout preventer
ECD	Equivalent circulating density
NCS	Norwegian continental shelf
NPT	Non-productive time
MPD	Managed pressure drilling
TVD	True vertical depth

Statistics and fault diagnosis

ARR	Analytical redundancy relations
CDF	Cumulative distribution function
CUSUM	Cumulative sum
FDI	Fault detection and isolation
GLRT	Generalized likelihood ratio test
IID	Independent and identically distributed
PDF	Probability density function

Chapter 1

Introduction

Oil and gas reservoirs are hydrocarbons contained in subsurface sedimentary porous rock formations. The hydrocarbons are reached by drilling a well into the formation. Geologists determine probable locations for oil and gas, which then may result in drilling of *exploration wells*. Once a sufficient amount of hydrocarbons are determined, it can be decided to develop the field. *Production wells* are then drilled at positions determined by the reservoir engineering group, maximizing expected production (Bourgoyne Jr. et al., 1986).

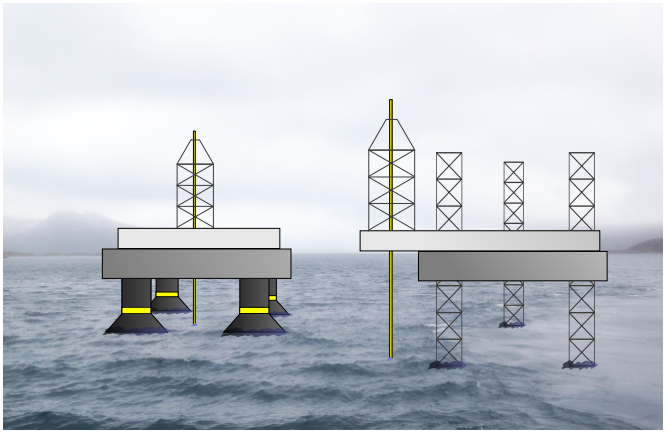

Figure 1.1: Offshore rigs: semisubmersible to the left, jackup rig to the right.

Hydrocarbon formations can exits both in *onshore* and *offshore* locations. Whereas onshore wells can be drilled with relatively small equipment, offshore drilling is a high cost operation requiring expensive drilling rigs and personnel. Offshore wells can be drilled in the range of shallow waters close to land, to deep-water drilling, and ranging from equatorial locations to a harsh arctic environment. Typical drill rigs include self-contained platform rigs and jackup rigs for shallow water, and semisubmersible rigs and offshore drillships for deep water and locations with high mobility requirements. An illustration of a semisubmersible rig and a jackup rig is shown in Fig. 1.1.

Cost of drilling is a major part of the total field development cost. In a recent report by the Norwegian Petroleum Directorate (2014) on costs at the Norwegian

Continental Shelf (NCS), it is stated that *"drilling new development wells has accounted for about 50 per cent of the investment"* for oil and gas fields, where offshore wells are drilled exclusively. Furthermore is it stated that *"most developement wells on the NCS are drilled from mobile units. Rig hire and various forms of well services account for the bulk of the cost of drilling such wells. Rig hire alone comprises 45 per cent of the cost of a well."*. The report also states that the drilling efficiency has great significance for the cost of the well, where efficiency can be measured as drilled meters per day. The cost development in the latest 15 years is shown in Fig. 1.2, showing the increasing marked rig rate for semisubmersible rigs, as well as the in increased cost per well on the Norwegian Continental Shelf. These figures are also representative for offshore drilling costs in other parts of the world.

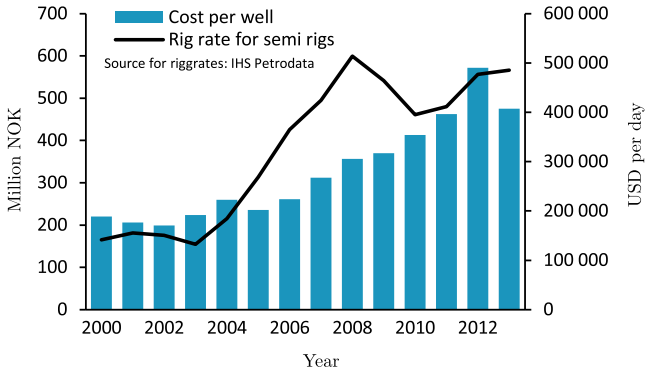

Figure 1.2: Global rig rates in USD/day (black line) and cost per well on the Norwegian Continental Shelf (blue bars). From the Norwegian Petroleum Directorate (2014).

1.1 Drilling oil and gas wells

This section will give an introduction to rotary drilling for oil and gas, describing different subsystems and equipment on the rig, and new emerging technologies. During drilling different incidents can occur which may delay progress, or lead to abandonment of the well. Diagnosis of these incidents is the topic of this thesis. The different incidents which can occur are presented, and challenges in detecting them are discussed.

1.1.1 Rotary drilling

The drilling rig consists of multiple subsystems, each with a specific task. The most important parts are briefly described in this section which are necessary for understanding the problems encountering in the following chapters, however for a more thorough introduction the reader is referred to drilling literature, such as Bourgoyne Jr. et al. (1986); Mitchell and Miska (2011). An overview of equipment

and systems on a drilling rig is shown in Fig. 1.3, showing miscellaneous equipment, the *hoisting system*, the *drilling fluid circulation system*, the *blowout preventer* (BOP), and the drillstring with the *bottomhole assembly* and *drill bit*.

Drilling fluid circulation

When drilling into a formation, a drilling fluid is circulated through the drillstring, through the rotating drilling bit crushing the formation, and back to the surface through the annular section surrounding the drillstring, see Fig. 1.3 for details. The main purpose of the drilling fluid is to transport out the crushed formation particles, while maintaining pressure in the well. Other purposes include cooling and lubrication of the rotating bit and drillstring, fluid loss avoidance, chemical functions, and transmitting hydraulic power to the rotating bit. Drilling fluids are typically either water-based or oil-based, and contain several additives giving certain density, viscosity and lubricity properties (Mitchell and Miska, 2011).

Hoisting system

The hoisting system is used to move the drillstring in and out of the well, called *tripping* (Mitchell and Miska, 2011), and is mounted in the derrick as shown in Fig. 1.3. As drilling is progressing, a new drillpipe is connected to the drillstring in an operation called a *connection*. The opposite operation is when the drillstring is removed from the well for various reasons, where the drillpipes are disconnected and stored at the rig. Reasons may be due to replacement of a worn drill bit, maintenance of downhole logging equipment or the drillstring, or completion of the well.

Rotary system

The rotary system using a *rotary table* consists of a *swivel* connecting the rotary system and the circulation system, and a *kelly*, used to transmit torque to the drillstring using *kelly bushings*. On modern rigs a *topdrive* replaces the kelly, kelly bushings, and the rotary table (Mitchell and Miska, 2011), and is illustrated in Fig. 1.3.

Casings and well pressure margin

To stabilize the formation and seal it from the well, a series of steel casing pipes are cemented at different depths. The lowest casing position is called the *casing shoe*, and marks the beginning of the contact between the well and the formation. At this position and downwards, the pressure in the well is required to stay within the formation pore pressure and the formation fracture pressure, illustrated in Fig. 1.4. This is often denoted as the *pressure window* or *drilling margin*. If the formation is permeable, and the pressure in the well is lower than in the formation, fluids will start to flow into the well. This *influx* of formation fluids, often called a *kick*, may

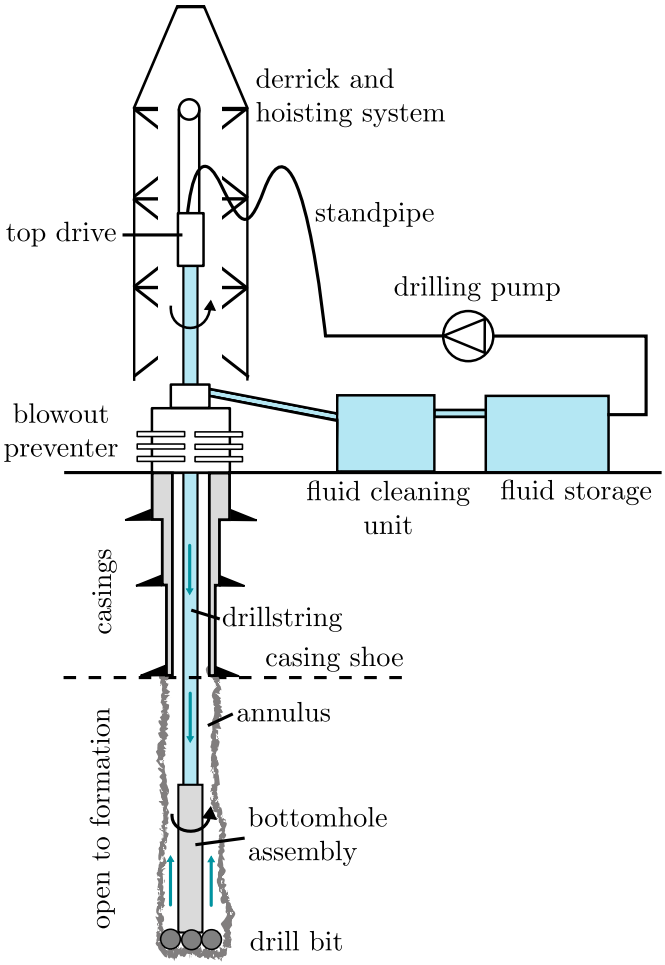

Figure 1.3: Components of rotary drilling including derrick with hoisting system, the circulation system, and the drillstring, bit and casings. In offshore drilling a marine riser is used from the seabed up to the rig (not shown).

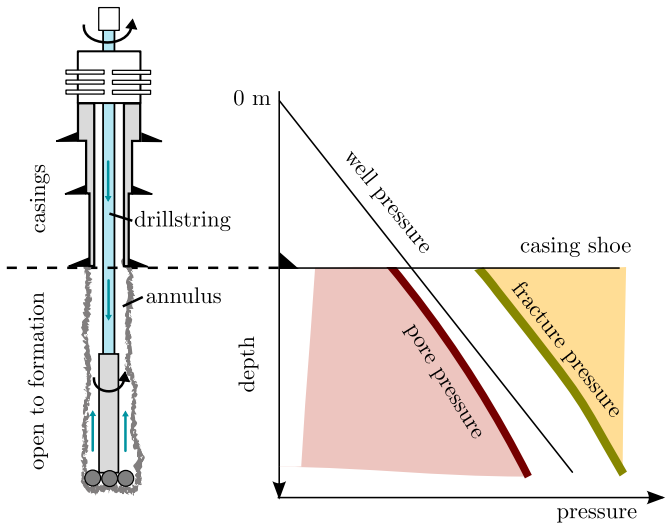

Figure 1.4: Overview of drilling with pressure margins. The well is open to the formation below the casing shoe, and in conventional drilling this part must have a well pressure above the pore pressure and below the fracture pressure.

in the worst case lead to a *blowout* if left unhandled (Bourgoyne Jr. et al., 1986). In the other end of the pressure window is the fracture pressure. This is the pressure where the formation starts to fracture, which can give permanent damage and loss of drilling fluid to the formation, reducing production capabilities and inducing significant costs.

If the well is drilled with a well pressure above the pore pressure, it is drilled *overbalanced*, which is the conventional way of drilling. If the well pressure is intentionally kept lower than formation pore pressure, the well is drilled *underbalanced*. Only the overbalanced case is discussed in this thesis.

Casings are cemented in sections and planned based on gathered information on the pore and fracture pressure in the well. The operation of cementing in casings is very expensive, and a major cost of drilling (Mitchell and Miska, 2011). It will also halt the drilling progress. Casing programs should therefore be planned to minimize cost. How often new casings are needed are dependent on the pressure window. With a narrow pressure window, new casings are required at a short interval. Since new smaller casings often are cemented inside above wider ones, there is a limit on how many segments of casings that can be placed. A possible solution to this limitation is to use *managed pressure drilling* (MPD), which is discussed in Sec. 1.1.2.

Another defining factor of how often new casings are needed is the *kick tolerance*, which is the maximum influx volume of formation fluids before a possible fracture of the weakest point in the well, which typically is at the casing shore (Redman Jr., 1991).

Safety systems

Well control is the task of maintaining a pressure in the well inside the pressure window. This is achieved by using '*at least two independent barriers between hydrocarbons in the reservoir and the environment at all times*' (Bellarby, 2009). During normal drilling conditions this is achieved using an overbalanced hydraulic column of the drilling fluid and a *filter cake* as a primary barrier, and casings and a blowout preventer (BOP) as the secondary barrier.

If the pressure in some parts of the open well decreases below the pore pressure, an unwanted influx in the well can occur. This inflow of formation fluids into the annulus can be stopped using the BOP. In other words did the primary barrier fail, necessitating the secondary barrier. A stack of different BOPs is installed making it possible to run the drillstring in and out of a closed well, as well as being able to close a well without a drillstring inside the BOP.

Rotary control devices are used to achieve a closed circulation of drilling fluid, and is used in managed pressure drilling and underbalanced drilling. In a recent study by Jablonowski and Podio (2011) it was found that using a rotary control device decreases the occurrence of blowouts, thus increasing safety.

1.1.2 Drilling technologies

The oil and gas industry is quite conservative, where new technology takes years of maturing before it is applied in the field. However, there has in later years been introduced several new technologies which increases control and monitorability of the drilling process, where available real-time data yield great value to the drilling crew (Macpherson et al., 2013). As easy accessible reservoirs become more scarce, field development is moving towards remote areas and deep high-pressure and high-temperature wells. For some of these cases, conventional drilling with little well control possibilities and little instrumentation can be a challenge, if possible to drill at all. Two of the new technologies maturing on the marked today is managed pressure drilling (MPD) for increased well control (Elliott et al., 2011) and *wired drill pipe* for increased instrumentation along the well.

Wired drill pipe has been used in over 100 wells worldwide as of the writing of Pixton et al. (2014), and is often used together with MPD with a high requirement of well control precision. However, the volume of raw data is already too high to process manually by the drilling operator, and is expected to grow even more in the future with expected growth in drilling-system complexity (Macpherson et al., 2013). This motivates the need for automated drilling monitoring and analyzing tools, detecting and isolating possible drilling incidents. This thesis explores different methods for designing such tools.

Managed pressure drilling

In conventional drilling the pressure in the well can be controlled by changing the fluid density and the pump flow rate. Since the top of the annulus is open to atmosphere, the pressure in the well is a function of hydrostatic pressure of the fluid column, and the friction due to fluid circulation. The combination of hydrostatic pressure and friction is often called *equivalent circulating density* (ECD) in the drilling community. Since a certain flow rate is required for sufficient hole cleaning, the well pressure is typically only changed by changing the density of the fluid pumped into the well. This is a slow process, since the fluid already present must be replaced by a new fluid with another density. In wells with small pressure margin between the pore pressure and fracture pressure, referring to Fig. 1.4, it may be difficult to maintain within the pressure window in the whole open borehole. The result is an increased need for new casings sealing off the well from the formation. This is a time-consuming process, slowing down drilling progress. In addition, since each new casing section often is cemented inside the previous ones, there is a limit on how many times new casings can be cemented in, and thus a limit on the total length of the well.

One technology handling these difficulties is managed pressure drilling. By sealing off the top of the annulus with a what is called a *rotating control device*, and using a choke manifold, the induced *back-pressure* (pressure upstream the chokes) can be controlled directly and with a high accuracy. With a pressure in the top of the annulus higher than atmospheric pressure, a better pressure gradient in the well can be applied using an appropriate drilling fluid density, which is illustrated in Fig. 1.5, thus opening possibilities to drill in wells with narrow pressure windows and reducing the need for new casings.

Incident diagnosis with managed pressure drilling is studied in this thesis as a case study. This is a case where there are even higher demands for narrow pressure margins compared to conventional drilling, making early diagnosis instrumental. Another important reason for choosing MPD as a case study is the fact that the experimental flow-loop used in major parts of the thesis was rigged for MPD technology. However, the diagnosis methods can also be applied to conventional drilling, since it can be viewed as a special case of MPD, where the choke is permanently in a fully opened position.

Wired drill pipe measurement technology

The most common downhole measurement tool is the *mud pulse telemetry* technology where the signal is transported in the drilling fluid as pressure pulses (Jellison et al., 2003). These pulses travel with the speed of sound, compared to the speed of light using electrical signals. For wells of up to ten kilometers long, this is causing several seconds of signal delay. Furthermore does the sensor technology require a continuous circulation of drilling fluid, and has a limited bandwidth.

Wired drill pipe is a new sensor technology with a dedicated signal wire along the

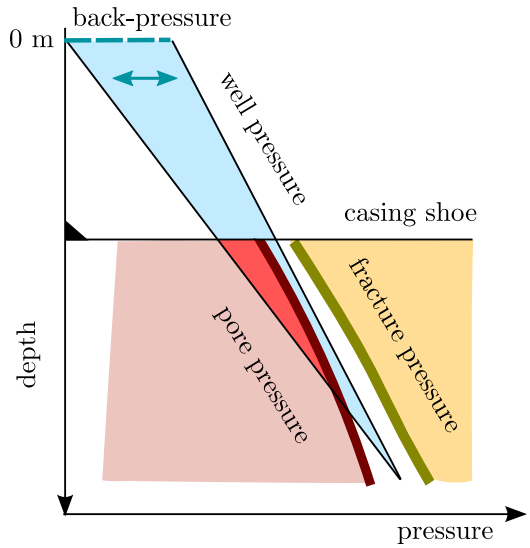

Figure 1.5: Managed pressure drilling with a narrow pressure window between pore pressure and fracture pressure. Note that with conventional drilling the well pressure would be lower than the pore pressure, making the well underbalanced in some parts of the open hole.

drillstring, see, e.g. Jellison et al. (2003); Pixton et al. (2014). This enables low-latency, high-bandwidth transmission of downhole data to the topside monitoring system. Dedicated pressure and temperature sensors can be installed at desired positions along the well, giving available measurements in real-time. Downhole pressure data is valuable information which makes it possible to take actions to prevent or fix borehole problems almost as soon as they develop, giving increased diagnostic possibilities (Dalton et al., 2003). In addition to increased monitorability of the well pressures and temperatures, the wired pipe technology can be used for optimizing casing point selection, eliminating wireline log runs, and monitoring of drillstring and bit wear and vibrations (Jellison et al., 2003).

The diagnosis methods developed in this thesis assumes wired drill pipe installed, but would still work without these measurements available. However, without the downhole measurements there will be fewer fault isolation possibilities, limiting the possibility to differentiate different incidents from each other, and determining the position of the incident. This is studied as a case in Chapter 6, where no downhole measurements are available.

1.1.3 Drilling incidents

Cost of drilling is a major part of the total field development cost, where rig hire and various forms of well services account for the bulk of the cost of drilling such wells. With high drilling costs, especially for offshore drilling, keeping the *non-productive*

time (NPT) to a minimum is of great interest for the oil and gas companies. In Godhavn (2010) the NPT for all wells drilled in Europe is reported to have been between 20-30 % in the period of 1997-2007, with an average today being between 20-25 %. A significant part of the downtime is related to well instabilites and lost circulation, another significant part is due to failure of equipment including pumps, valves, sensors, and communication. Maintaining effective drilling with a high reliability in equipment and reducing downhole incidents is therefore a high priority.

Equipment topside can be monitored with suited condition monitoring solutions. Health status of topside pumps, valves, pumps and sensors can be logged and analyzed using a monitoring software that gives feedback to relevant personnel responsible for drilling the well.

Monitoring of downhole incidents which can delay or even damage the well is a more challenging task. Traditionally, there has been very little instrumentation downhole, which makes it difficult to detect and diagnose incidents at an early stage. As a problem develops undetected, its severity may increase resulting in possible major drilling downtimes, or abandonment of the well or even more severe consequences. Methods for early detection and diagnosis are therefore instrumental in decreasing downtime, keeping costs at a minimum, which is the research focus of this thesis. Some of the incidents which can occur downhole are illustrated in Fig. 1.6 and presented in the following subsections, which are successfully detected and isolated in the work done in this thesis. To some extent, the position and magnitude of the incidents are also localized and estimated.

Influx of formation fluids

An influx of formation fluids can occur when the pressure in the well is lower than in the formation. An influx, often called a *kick*, is a severe incident in drilling. If left unhandled, the situation can develop into a full blowout, which is a danger for personnel, the rig, and also the environment.

Referring to Figs. 1.4 and 1.5, an influx can occur when the well pressure drops below the formation pore pressure in some parts of the well open to the reservoir (below the *casing shoe*). Fluids then start flowing from the pores in the rock into the well. If the fluid contains gas, the mixture in the well changes. Since gas has lower density, gas bubbles (not dissolved in the drilling fluid) will reduce the mixture density noticeably. As the gas travels upwards in the well, the pressure decreases and thus the gas volume increases, further decreasing the mixture density. With reduced density, the pressure in the well decreases due to decreased hydrostatic pressure. This will increase the difference in pressure between the reservoir and the well, called the *drawdown*, further increasing the gas influx into the well. If this continues without interference, a possible scenario is a well filled with gas with pressure close to the reservoir pressure in the whole well (up to several hundred bar pressure), also at the rig topside.

Due to its severity, kick detection is a widely studied drilling incident. Detection

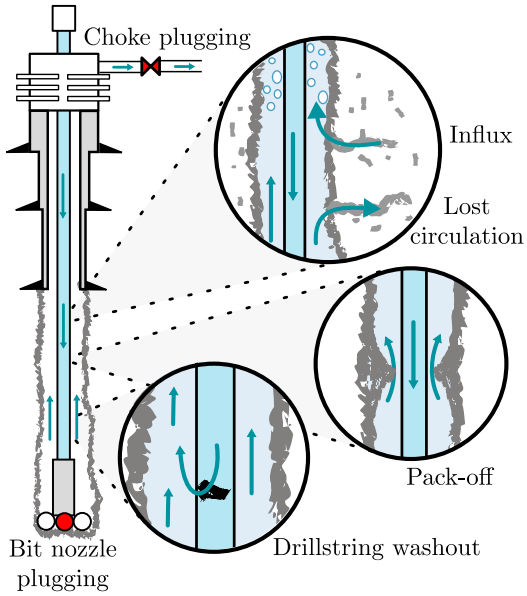

Figure 1.6: Downhole drilling incident studied in this thesis, including choke plugging, bit nozzle plugging, influx of formation fluid, loss of drilling fluid to the reservoir, pack-off and drillstring washout.

methods range from simple methods (Jardine et al., 1994; Swanson et al., 1997; Choe et al., 2007; Reitsma, 2010), to more complex ones (Hargreaves et al., 2001; Santos et al., 2007; Gravdal et al., 2010a; Cayeux et al., 2012b; Hauge et al., 2013).

Today, kicks are mainly detected by monitoring the difference between flow out and in of the well. If this difference in flow is greater than zero, it is a primary indicator of a kick (Mitchell and Miska, 2011). Detection can be done by using flow rate measurements of pump flow, and out flow, and comparing the difference. If these measurement are not available, the volume of the drilling fluid storage tank, called the *mud pit*, is monitored. An increase indicates a kick. A secondary indicator is *drilling breaks*, which is a sudden increase in bit penetration rate. Another indicator is a change in the pump pressure, but this can also be a result of a drillstring washout or twist-off (Mitchell and Miska, 2011).

If a kick is detected and the drilling crew decides to take action, the well is shut in, the pump is stopped and the blowout preventer (BOP) is closed around the drillstring. Then follows a lengthy operation of handling the kick, including circulating it out and replacing the drilling fluid to a heavier *kill mud*. This downtime contributes to slowing down the overall drilling progress.

Lost circulation

In conventional overbalanced drilling, one control objective is to keep the pressure in the well above the formation pore pressure. In normal conditions the drilling fluid remains in the well, due to additives in the fluid forming a thin, low-permeability layer called a *filter cake* (Mitchell and Miska, 2011). Loss of fluid to the formation, also called *circulation loss*, occurs due to high-permeability formations or if fractured formations are encountered or created due to too high well pressure (Bourgoyne Jr. et al., 1986). The upper limit in the drilling window, which is the fracture pressure, is therefore also important referring to Fig. 1.4. Lost circulation is one of the most common and troublesome downhole problem in drilling. If the drilling fluid enters an oil and gas reservoir, productivity can be reduced and thus possibly lowering the total production potential from the reservoir (Mitchell and Miska, 2011). Lost circulation is detectable by a lower flow rate out of the well than into it. Detection of fluid loss can partly be viewed as the opposite as an influx, and thus are many of the detection methods for influx also applicable for detecting fluid loss, see, e.g., Reitsma (2010); Cayeux et al. (2012b); Hauge et al. (2013).

Three different diagnosis steps for lost circulation are listed in Mitchell and Miska (2011), where the first step is to determine at what depth the loss is occurring, the second step is to describe the type of loss zone, and the third step is to evaluate the severity of the loss. Different lithologies will affect the loss differently. If the loss is slowly increasing, the loss zone is typically a high-permeability and porous layer, such as sandstone. If a large and sudden loss is encountered, a fracture is a probable cause.

Different methods for finding the lost circulation zone are described in Mitchell and Miska (2011). The effect of temperature change of the drilling fluid is logged by using a temperature recording device that is run on wire in the well. Another possibility is to use a radioactive-tracer survey, or a spinner survey where a spinner changes rotation where there is a loss. All these methods are time-consuming and require halting of normal operation. Motivated by this fact, methods in this thesis investigate what kind of diagnosis can be done real-time during drilling without interfering with normal operation.

Drillstring washout

Drillstrings can be up to several kilometers long and are rotating with high torque and speed, and will get fatigued over time. Forming cracks and holes are severe indicators of durability loss of the drillstring. If left unhandled, these weak spots may break with a result in a complete twist-off of the pipe. In such an event, the broken pipe needs to be removed in a lengthy *fishing operation* (Bert et al., 2009). An unsuccessful job means that a sidetrack needs to drilled. This operation can can take between two and twelve days to complete (Macdonald and Bjune, 2007). The cost of equipment is alone around one million USD, and the rig rate in the range of 0.2-6 million USD, referring to Fig. 1.2. If the fatigue is detected prior

to twist-off, called *leak-before-break state*, the cost is 1/10 (Macdonald and Bjune, 2007). Drillstring washouts, which are leakage from the drillstring to the annulus, are thus important to detect as soon as possible in order to reduce costly delays.

Pack-off

A pack-off is a collection of debris concentrated around the drillstring, failed to be transported out of the well. This will partially or fully restrict circulation flow, which typically result in a stuck pipe and significantly increase the possibility of a fractured formation (Dalton et al., 2003). A cause of pack-offs can be loose or unconsolidated formation sands which collapse into the wellbore, or schists and shales which restrict drillstring movement and circulation flow. Other effects which cause caving of the wellbore include drillstring vibration and overpressured shales which collapse around the pipe (Johnson et al., 2013).

To avoid cuttings (crushed formation particles) to pack off around the drillstring, a high rotation of the drillstring can be used, as well as a high circulation rate. However, these actions may increase the likelihood of a washout and a complete twist-off (Johnson et al., 2013).

Plugging of drill bit nozzles

When drilling, small particles from the cuttings may enter the drill bit nozzles, partially or fully plugging one or several of them (Cayeux et al., 2012a). A plugging will increase the pressure drop over the bit, and thus the pump pressure. However, since the pressure in the well is unchanged, this incident is not as severe as some of the other incidents described above. Diagnosis is nevertheless important as it is important to know if the increased pump pressure is due to a plugging of the bit nozzles, or, for example, a pack-off. If a plugging of some of the nozzles is diagnosed, the drilling crew will be notified about the incident, and correct assessment of the situation can be done.

Plugging and washout of MPD choke

If managed pressure drilling is applied, the drilling fluid with cuttings are transported through the MPD choke manifold. Similarly as with the drill bit, the chokes can thus be partially (or fully) plugged, increasing the pressure over the chokes. This will affect the pressure in the annulus, and actions must be taken immediately (Cayeux et al., 2012a). Pressure loss over the choke is not sufficient to diagnose a choke plugging; the combination of circulation flow, fluid properties, and pressure drop over the choke has to be taken into account to correctly diagnose a choke plugging. Similarly, the MPD chokes may also be washed out, reducing controllability of pressure in the well.

Sensor faults

A diagnosis system relies on sensors integrity for correct diagnosis. In the oil and gas industry, redundant safety critical sensors are often installed. A simple method is to use a voting function on the sensors, see, e.g., Willsky (1976); Venkatasubramanian et al. (2003c). If one of the sensors is behaving irregularly, an alarm is activated and the measurement is discarded. Downhole measurements in drilling is not usually available today. If available, redundant sensors can not be expected. A fault diagnosis system which handles sensor faults will thus be important in diagnosis of the drilling process. These concerns are discussed in Sec. 1.2.1 about system redundancy.

A dedicated detection algorithm may be applied to detect signals which completely drops out. Such an implementation would be possible to implement without process knowledge. Measurement bias is a more challenging task. If, e.g., a pressure sensor starts to drift, it may look like an actual increase in pressure. If not detected and handled by the diagnosis system, a false alarm may be set off. If a diagnosis system continues to provide false alarms, it will be regarded as unreliable, and may no longer be used. Handling sensors errors and faults is thus instrumental for the integrity of the diagnosis system.

1.1.4 Challenges in detecting and isolating different drilling incidents

One question one might ask is why more advanced diagnosis methods are needed. With an increased number of sensors available with a high update rate, keeping manual track of changes in the signals may be a tiresome and overwhelming task for the driller. Another problem is that effects of a beginning incident on measurements are usually marginal and therefore hard to notice. Moreover, they can be covered in measurement noise, making early detection manually quite a challenging task. With an integrated diagnosis system running in the background which detects small changes to process variables as well as handling measurement noise, the driller can be notified at an early time of an incident, increasing the probability of handling the situation correctly before it escalates. Furthermore, the different incidents described above will affect pressure and flow differently. It is a challenging task to systematically detect these incidents and isolate them from one another.

Detection and isolation of different drilling incidents have been studied extensively, where a major part of the methods addresses influx diagnosis. Different methods range from only suggesting solutions (Aldred et al., 1998; Reitsma, 2010; Johnson et al., 2014), to using simple mathematical models of the process (Jardine et al., 1994; Swanson et al., 1997; Choe et al., 2007; Daison and Belavadi, 2008), to methods using advanced process models, advanced estimation, or both (Gravdal et al., 2010a; Cayeux et al., 2012a,b; Hauge et al., 2013). An alternative to using physical models is to use neural networks (Arehart, 1990) or so-called case-based reasoning (Skalle et al., 2013; Kucs et al., 2015). Other solutions suggest to add sensors such as an acoustic interferometer (Vestavik et al., 1990), or to use alter-

native drilling methods such as micro-flux control (Santos et al., 2007). Several of these publications and solutions describe methods for detecting one or several of the incidents, but only a few handle most or all. There also exist a numerous of commercial software and solutions with varying complexity, such as DrillEdge by Verdande Technology using case-based reasoning (Raja et al., 2011; Gundersen et al., 2013), eDrilling by eDrilling Solutions (Rommetveit et al., 2007, 2008), and the FLAG influx and loss detection service technology by Schlumberger (Schlumberger, 2014). Using statistical methods has been suggested in Hargreaves et al. (2001); Gulsrud et al. (2009), although detection and isolation of small incidents covered in measurement noise is not commonly handled.

In this thesis different diagnosis methods using a simple hydraulics model together with statistical change detection are used to detect that some drilling incident is evolving, to find out which incident it is, and to isolate the part of the well where it is occurring. Diagnosis of pack-offs is studied in Chapters 2 and 5, and different diagnosis methods for drillstring washouts are derived and tested in Chapter 3. Diagnosis of multiple incidents is conducted in Chapter 4, as well as in Chapter 6 where also sensor bias drift is correctly detected and isolated.

1.2 Introduction to fault diagnosis

This section will give an introduction to the concept of fault diagnosis. Some terminology will be presented, and an overview of possible system representations and classifications are given. Methods applied in the following chapters are presented and put into context of different fault diagnosis methods. The motivation is to detect and isolate the incidents described in Sec. 1.1.3 as early as possible, with as few false alarms as possible, using methods which are easy to tune and implement in a drilling system.

1.2.1 System redundancy

A wide range of applications are dependent on control and monitoring systems to function. They range from large and complex processes such as oil refineries or a nuclear power plants, and in this case a drilling rig, to smaller fast moving jet fighters, or small equipment such as a hard disk drive. Common for all is that they have a normal operating mode which serves to maintain safety and operational objectives. For the nuclear power plant, cooling of control rods in the reactor is the necessary safety and operating objective for the overall goal of power production. A hard disk drive can be used in a server handling sensitive information, while the fighter jet has to maintain the safety of the pilot of all costs.

In order to make these systems *fault tolerant*, redundant systems are often implemented. It is possible to differentiate between hardware and analytical redundancy (Blanke et al., 2006). *Hardware redundancy*, or *physical redundancy*, is achieved by installing separate physical systems (Frank, 1990). In process facilities there are

independent safety systems, as well as parallel critical equipment such as pumps and valves, and planned emergency shutdowns. An aircraft has several independent control systems, hardwired for increased safety. The server handling sensitive information will have redundant hard disk drives, should one fail. *Analytical redundancy* is achieved by having software systems which are tolerant to faults. As an example can an observer estimate process values should a sensor fail. Moreover, a fault tolerant control system can reconfigure the control structure if a fault occurs. The reconfiguration may decrease performance, but the alternative could be a system failure. Fault diagnosis plays an instrumental part in these systems. In this thesis, methods using analytical redundancy will be studied for diagnosing drilling incidents.

1.2.2 Terminology

Some terminology is presented in this section, including different types of faults in the sense of position and time scale, the difference between additive and multiplicative faults are defined, as well as defining differences between faults, disturbances and modeling error.

System faults

It is typical to divide the location of the fault to three different locations (Blanke et al., 2006).

- *Sensor fault*: loss of signal from the sensor, or bias in the measurements.
- *Actuator fault*: loss or partial loss of control of an actuator.
- *Process fault*: An unwanted change in the system, changing the dynamical input/output behavior.

Different faults happen on different time scales. In Isermann (1997) the time dependency of faults are categorized into the three following:

- *Abrupt faults*,
- *Incipient faults*,
- *Intermittent faults*.

Abrupt faults are sudden faults such as a component breakdown. Incipient faults are slowly varying faults such as changes to the process or wear of actuators and bias drift of sensors. Intermittent faults are irregular faults coming and going, such as faults in a computer system or instability in connection with a field measurement. Different diagnosis methods are beneficial for the different time dependency of the faults, which will be described in Sec. 1.4, as well as in later chapters.

Additive and multiplicative faults

Faults can be classified as either *additive faults* or *multiplicative* (Isermann, 1997, 2005). Additive faults occur in the model as unknown functions of time multiplied with known system matrices, whereas multiplicative faults are known functions of time multiplied with unknown matrices (Venkatasubramanian et al., 2003c). Typical additive faults can be sensor bias, whereas multiplicative faults are typically changes in process parameters. Consider the nonlinear system

$$\dot{x} = g(x, u, \theta_0) \tag{1.1}$$
$$y = h(x, u, \theta_0) \tag{1.2}$$

with inputs u, states x, nominal parameters θ_0 and outputs y, which is subject to some faults. If the fault affects the system parameters, changing them from θ_0 to θ_f, the system representation with multiplicative faults can be written as

$$\dot{x} = g(x, u, \theta_f) \tag{1.3}$$
$$y = h(x, u, \theta_f). \tag{1.4}$$

If the fault is additive, the system can be written as

$$\dot{x} = g(x, u, \theta_0) + f_x + f_u \tag{1.5}$$
$$y = h_f(x, u, \theta_0) + f_y \tag{1.6}$$

where f_x are system faults, f_u actuator faults and f_y sensor faults.

Faults, disturbances and modeling errors

If the process is not correctly modeled, modeling errors may look like faults in the fault diagnosis algorithm. The sensitivity to modeling error is thus a key problem in methods based on analytical redundancy (Frank, 1990). In order to minimize false alarms the model should try to capture:

- Faults in actuators, sensors and components in the process.
- Disturbances.
- System noise and measurement noise.

It is important to note that faults are not considered as disturbances or noise, since a fault is some change in the process which should be detected and handled. Not all disturbances and noise can be perfectly modeled. It is therefore common to use a threshold on the decision function, where a trade-off between false alarms and detection rate has to be considered, see, e.g., Venkatasubramanian et al. (2003c); Blanke et al. (2006); Ding (2008). In this thesis, measurement noise is handled by using statistical change detection, together with thresholds determined by the noise distribution of the test statistic in the fault-free case.

1.2.3 Fault diagnosis definition

Faults in sensors, actuators, or in the plant itself are in many cases crucial to detect and handle. There are several levels of how accurate the location and position of a fault can be pinpointed. Fault diagnosis is usually a term (Isermann, 1997) which can be divided into

- *Fault detection*: detect that an abnormal situation has occurred.
- *Fault isolation*: determine the type and location of the fault.
- *Fault estimation*: estimate fault magnitude.

1.3 Fault diagnosis methods

Methods for fault diagnosis are quite wide-ranging, covering a large range of research fields. In the three series paper collection Venkatasubramanian et al. (2003a,b,c) the authors try to classify the different methods, where the main families of methods are *model-based methods* and *data-based methods*, also called *process history-based methods*. Model-based methods can be divided into *quantitative model-based methods* which rely on some first-principles model of the system, whereas in *qualitative model-based methods* the physics of the process is expressed in qualitative functions around different units in the process (Venkatasubramanian et al., 2003a). Data-driven methods do not use known process knowledge, but analyse large amount of historical process data to enable later diagnosis, see, e.g., (Venkatasubramanian et al., 2003b; Yin et al., 2012). The different methods are illustrated in Fig. 1.7.

Model-based fault diagnosis has typically been used in aerospace, electrical and mechanical systems. For complex nonlinear systems, such as chemical plants, data-based system for fault diagnosis has been most common (Zhang and Jiang, 2008). Data driven methods may be beneficial for large systems where modeling may be difficult or too cumbersome, while model-based methods utilize some known model structure in diagnosing faults. Quantitative model-based methods are often called *observer-based fault diagnosis methods* (Frank, 1990; Frank and Ding, 1997; Ding, 2008). The idea in these methods is to apply well-known observer design from control theory in order to estimate occurring faults. Dependent on the system and the residual generation, different observer designs can be applied. Another type of the quantitative methods is to use *analytical redundancy relations* (ARR) to generate residuals which are only functions of known inputs and outputs, and possibly their derivatives. For linear system this includes the *parity relations* approach.

1.3.1 Diagnosis research in drilling

Due to their severity, a major part of research in drilling incident diagnosis concerns detection of influx and lost circulation. For influx detection it is common to only

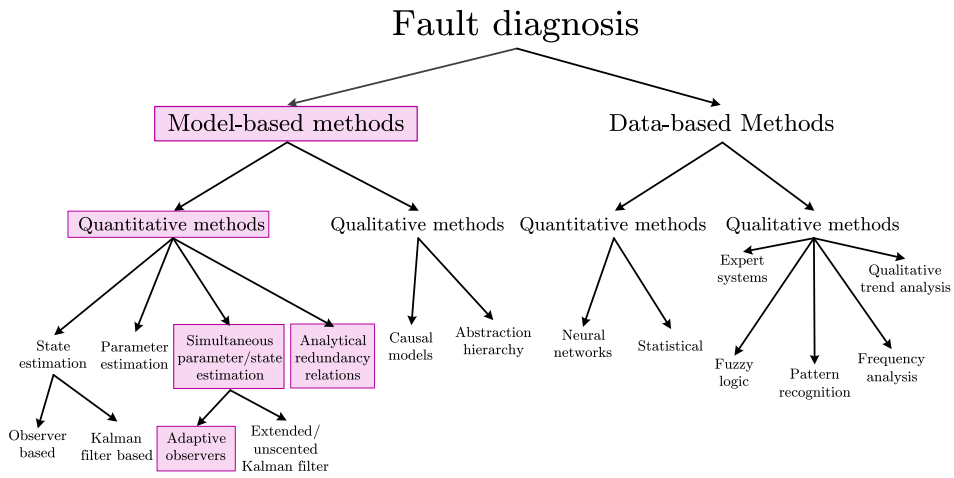

Figure 1.7: Classification of fault diagnosis methods. The methods used in this thesis are highlighted, namely model-based quantitative methods using adaptive observers and analytical redundancy relations. Adapted from Venkatasubramanian et al. (2003c); Zhang and Jiang (2008).

use the difference in flow rate in and out of the well (Mitchell and Miska, 2011). Either by measuring directly, or indirectly measuring the drilling fluid storage, as described in Sec. 1.1.3. However, as argued in Sec. 1.1.4, for early detection and correct incident type isolation, more advanced methods are required.

Methods for systematic diagnosis of drilling incidents can be divided into the three approaches defined in Sec. 1.3. The first approach is the *quantitative model-based method*, where some physical model of the well is used. Research concerning detection of influxes was studied in Hargreaves et al. (2001); Santos et al. (2007); Gravdal et al. (2010a); Hauge et al. (2013), poor hole cleaning was diagnosed in Gulsrud et al. (2009), and several incidents were diagnosed in Cayeux et al. (2012a,b); Ghilardi et al. (2013); Martins et al. (2013). Wired drill pipe measurements were used together with a very simple model for estimating the equivalent circulating density for pack-off detection and isolation in Coley and Edwards (2013). Torque and drag diagnosis was studied in Niedermayr, Michael Pearse et al. (2010).

In Abdollahi et al. (2008); Skalle et al. (2013), a *qualitative model-based method* was used to diagnose different incidents by using a symptom-recognition system with qualitative measures such as “sudden loss” and “increased rate of penetration”.

A *data-driven approach* was used in Raja et al. (2011); Gundersen et al. (2012), where case-based reasoning using real-time data was matched to previous known experiences of drilling incidents. In Nybø (2010), possibilities for using data-centric methods using soft computing and machine learning were discussed. A Bayesian network was used in Ashok et al. (2013); Ambrus et al. (2013) to detect drilling incidents and sensor faults.

1.3.2 Selecting methods for drilling incident diagnosis

As pointed out in Venkatasubramanian et al. (2003c), the different diagnosis methods can be quite far apart, and it can be difficult to select the best suited method for the problem at hand. In choosing diagnosis methods in this thesis we have chosen to follow the philosophy of using simple methods, which can be implemented and installed as a part of a drilling process monitoring system. Since simple models of the drilling hydraulics are available, this thesis will focus on the *quantitative methods* of the *model-based methods family*, highlighted in Fig. 1.7. The simple model (Kaasa et al., 2012) (with some extensions) has been thoroughly studied and tested within our research group, see, e.g., Stamnes et al. (2011b,a); Zhou et al. (2011); Hauge et al. (2013); Landet et al. (2013); Mahdianfar et al. (2013). This insight gives a benefit for designing good model-based diagnosis methods. Data-driven diagnosis methods could also be used, as discussed in Sec. 1.3.1. However, these methods require training based on historical data, exposing them to data with known faults. This can be a challenge if data during faults are scarce or not available, and diagnosing new types of incidents may be difficult without prior recorded data.

1.4 Model-based fault diagnosis methods

In order to quantify the fault, a residual sensitive to faults is designed in such a way that it has zero value in the fault-free case and a nonzero value during faults. If possible, the residual function should also be designed such that different faults will affect the residual in different ways, making it possible to identify and isolate the different faults from each other. Designing such residuals are often called *residual generation*. Then doing a *residual evaluation*, a fault may be detected and isolated, possibly with an estimation of its magnitude. The different stages in a model-based fault diagnosis system is shown in Fig. 1.8. The residuals generated are evaluated in order to detect, and possibly isolate and estimate the faults. The result can be given as an alarm, and possibly be applied in a fault-tolerant control system.

There exists many books and survey papers on the topic of change detection and fault diagnosis. Noticeable books include Basseville and Nikiforov (1993); Gertler (1998); Chen and Patton (1999); Patton et al. (2000); Blanke et al. (2006); Isermann (2006); Ding (2008); Isermann (2011), and book chapters Frank et al. (1999). Some of the survey papers are Willsky (1976); Isermann (1984); Chow and Willsky (1984); Frank (1990); Gertler (1997); Isermann (1997); Alcorta García and Frank (1997); Frank and Ding (1997); Venkatasubramanian et al. (2003c,a,b); Isermann (2005); Zhang and Jiang (2008); Hwang et al. (2010). The methods used in this thesis are presented in the following sections, as well as putting them in context related to other model-based diagnosis methods.

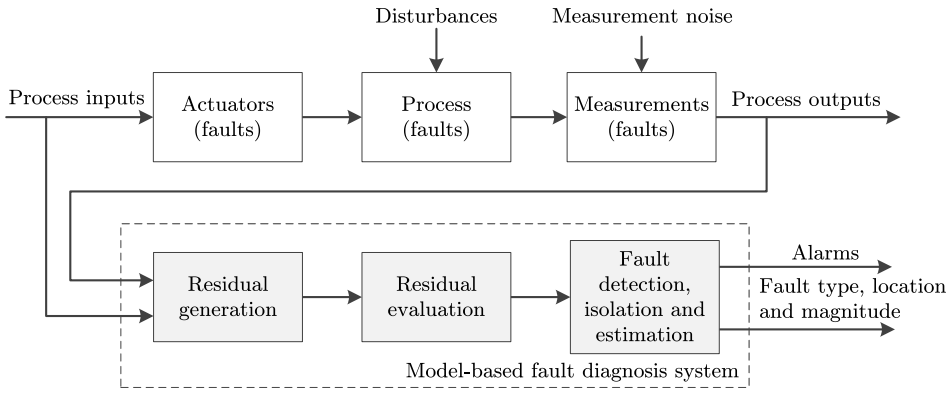

Figure 1.8: Model-based fault diagnosis. Adapted from Ding (2008).

1.4.1 Residual generation

The first part of a model-based fault diagnosis method is the residual generation. A model of the process and the faults is used together with the inputs and outputs of the process to determine the consistency between the system and the model (Blanke et al., 2006).

Faults can occur in the actuators, the process, and in the measurements, illustrated in Fig. 1.8. In addition, there can be process disturbances and measurement noise. The measured outputs of the process is compared to the process model output in some way to generate the residual r. The residual should be designed sensitive to process faults such that

$$r = 0, \quad \mathcal{H}_0 : \text{null hypothesis} \tag{1.7a}$$
$$r \neq 0, \quad \mathcal{H}_1 : \text{alternative hypothesis} \tag{1.7b}$$

where $\mathcal{H}_0$ is the hypothesis that no fault has occurred, and $\mathcal{H}_1$ is the hypothesis that the system is subject to some fault.

In order to be less sensitive to noise and modeling errors, a threshold h can be applied on the residual. The threshold can be fixed to a given constant value h,

$$g(k) \leq h, \quad \mathcal{H}_0 : \text{null hypothesis} \tag{1.8a}$$
$$g(k) > h, \quad \mathcal{H}_1 : \text{alternative hypothesis} \tag{1.8b}$$

where $g(k)$ is some decision function as a function of the residual r at sample time k.

Early methods for residual generation were mostly developed for linear systems, whereas generalization to non-linear systems has been derived in later years. Of the model-based quantitative methods (recall Fig. 1.7) it is common to use observer techniques from control theory, such as state observers, Kalman filters, parameter estimation and adaptive observers, as well as analytical redundancy relations

(Venkatasubramanian et al., 2003c; Ding, 2008). The different methods are briefly described in the following subsections, where adaptive observers and analytical redundancy relations will be used in later chapters.

State estimation

State estimation in the form of Luenberger-type observers or Kalman filters can be used to generate residuals used for fault diagnosis. There are different approaches described in the litterature, including the *dedicated observer approach* and the *fault detection filter* (Frank, 1990).

In the dedicated observer approach, full-order or reduced order observers can be applied, which are either linear or nonlinear. One observer can be used, or a bank of observers. There are two ways of using a bank of observers for fault diagnosis (Zhang et al., 2002). In the *dedicated observer scheme* (DOS) proposed by Clark (1978) each observer is sensitive to one fault, while in the *generalized observer scheme* (GOS) proposed by Frank (1990), each observer is sensitive to all faults but one. The fault detection filter is a full-order state estimator with a special choice of the observer gain matrix (Frank, 1990).

Parameter estimation

Detecting a non-measurable parameter drift requires online parameter estimation (Venkatasubramanian et al., 2003c). Multiplicative faults cause changes to the system parameters, see Sec. 1.2.2, and can be estimated using a parameter estimation method. If the different faults cause changes to different system parameters, fault isolation is also possible. However, for large systems, parameter estimation may be too complex for online fault diagnosis (Venkatasubramanian et al., 2003c).

Using parameter estimation for fault diagnosis may be particularly useful for incipient (slowly varying) faults (Frank, 1990; Isermann, 2006). These observers often require that the change in the parameter θ is piece-wise constant, i.e., $\dot{\theta} = 0$. This is an assumption best suited for slowly varying faults. Furthermore will this behavior of the parameter estimation give slower reaction to sudden changes than state-observer and analytical redundancy relations methods (Isermann, 2006).

Joint state and parameter estimation

If parameter and state estimation is combined, both multiplicative and additive faults are possible to detect (Isermann, 2006). Adaptive observers may be used to jointly estimate parameters and states. An overview of adaptive observers can be found in, e.g., Besançon (2000); Zhang (2002, 2005). Another possibility is to augment the parameters in the state vector in Kalman filters.

The benefit of jointly estimating states and parameters using such methods is that early abrupt changes can be detected, as well as slowly varying incipient faults caused by parameter drifts. Another benefit is improved robustness against model uncertainties (Frank and Ding, 1997). Adaptive observers for fault diagnosis has

been a subject for extensive research in later years, including Zhang (2000); Jiang et al. (2004); Xu and Zhang (2004); Caccavale et al. (2008); Zhang et al. (2010); Fan et al. (2013).

Analytical redundancy relations

Analytical redundancy relations (ARR) are functions of the inputs and outputs and their derivatives, and can be used to generate non-linear residuals (Staroswiecki and Comtet-Varga, 2001). These residuals can be used for fault detection and isolation by checking for inconsistencies between the actual plant and the model. The benefit of using ARR is that systematic methods for matching inputs and outputs can be used to generate the residuals, such as using graph matching (Blanke et al., 2006; Svärd et al., 2013), giving specified detection and isolation capabilities.

Parity relations are one specific type of analytical redundancy relations for linear systems (Blanke et al., 2006). The parity space method developed by Chow and Willsky (1984) is a systematic way of generating a residual for systems with a linear state model, using the parity relation.

The residuals generated by ARR typically have very fast reaction time after sudden faults (Isermann, 2006). For linear systems, is was shown in Gertler (1991) that once the design objectives are selected, parity equations and observers lead to identical or equivalent residual generators.

Comparing residual generation methods

Combining parameter and state estimation gives benefits from both state estimation methods and parameter estimation methods, as discussed above. This can be achieved using, e.g., an adaptive observer or a Kalman filter with parameters included in the state vector. Another method is to use the analytical redundancy relations to generate the residuals, giving some other properties. Similarities and differences between the two approaches are listed in Tab. 1.1, with the preferred method for each property highlighted. The table is based on Tab. 14.1 in Isermann (2006), and is an extension of Tab. 6.1 in Chapter 6.

With combined state and parameter estimation, it may be possible to estimate the fault magnitude, while maintaining relatively fast detection, whereas this may require additional estimation using analytical redundancy relations. The strength of using ARR is a possibility of fast detection of changes, combined with a systematic framework for fault detection and isolation, also isolating actuator and sensor faults. Fault diagnosis using adaptive observers is the topic in Chapters 2-5, whereas diagnosis using ARR is investigated in Chapter 6.

1.4.2 Residual evaluation

In model-based fault diagnosis the residual generated is ideally only sensitive to the faults, and insensitive to disturbances and noise. Due to model discrepancies,

Table 1.1: Comparison of state and parameter estimation with analytical redundancy relations for fault diagnosis. The text is highlighted for preferable methods. Adapted from Isermann (2006).

Characteristics	**State estimation**	**Parameter estimation**	**Combined state and parameter estimation**	**Analytical redundancy relations**
Fast detection	Relatively fast, dependent on tuning	Relatively fast, dependent on tuning	Relatively fast, dependent on tuning	*Fast*
Detecting and isolating sensor and actuator bias	Dependent on model and setup	Dependent on model and setup	Dependent on model and setup	*Inherent*
Estimation of fault magnitude	Possible, if fault is a state	Possible, if fault is a parameter	*Possible, but dependent on model and setup*	Requires additional estimation
Propagation of measurement noise	*Dependent on tuning*	*Dependent on tuning*	*Dependent on tuning*	Needs to be handled if measurement differentiation is required
Design of method	Dependent on model and observer stability	Dependent on model and observer stability	Dependent on model and observer stability	*Straightforward if tools are available*
Model parameters	Known, constant	*Unknown, time-varying*	*Unknown, time-varying*	Known, constant
Excitation requirements	*No*	Possibly	Possibly	*No*

these external effects will affect the residual. It is thus necessary with a *residual evaluation* to determine if the change in the residuals is due to a fault, minimizing the effect of disturbance and noise.

According to Ding (2008) there are two types of residual evaluation methods, which are

- *Norm based methods*,
- *Statistical methods*.

Both methods evaluate the generated residual, where a threshold is used to detect a fault. The threshold is selected with a trade-off between false alarms and fault detection rate. The norm-based method generates some norm of the residual which is compared to the threshold. However, often statistical methods are required in the decision making (Venkatasubramanian et al., 2003c). Of the statistical methods, the most common are the *cumulative sum* (CUSUM) and the *generalized likelihood test* (GLRT) (Blanke et al., 2006; Basseville and Nikiforov, 1993). Due to measurement noise and unknown residual values after a change, the GLRT statistical method is used for residual evaluation in Chapters 3-6.

Norm-based methods for change detection

The norm-based methods have less online calculation compared to statistical methods, and allows a systematic threshold computation using robust control theory (Ding, 2008). It is thus a method which is closer to control theory, where the idea is to generate some norm of the residual r and compare it to the threshold h,

$$\|r\| \leq h, \quad \mathcal{H}_0 : \text{null hyptohesis} \tag{1.9a}$$

$$\|r\| > h, \quad \mathcal{H}_1 : \text{alternative hypothesis} \tag{1.9b}$$

Some common intuitive evaluation functions using the output directly are listed in Ding (2008), such as the *the peak value*,

$$h_{\text{peak}} = \|r\|_{\text{peak}} = \sup_{t \geq 0} \left(\sum_{i=1}^{N_r} r_i(t)^2 \right)^{1/2}, \tag{1.10}$$

the *trend analysis*,

$$h_{\text{trend}} = \|\dot{r}(t)\|_{\text{trend}}, \tag{1.11}$$

the *root mean square* (RMS) value over the time interval of length T,

$$h_{\text{RMS}} = \|r(t)\|_{\text{RMS}} = \left(\frac{1}{T} \int_t^{t+T} \|r(\tau)\|^2 d\tau \right)^{1/2}, \tag{1.12}$$

and the *average value*,

$$h_{\text{avg}} = \|r(t)\|_{\text{avg}} = \sup_{t \geq 0} \|\bar{r}(t)\|_{\text{peak}}, \quad \bar{r} = \frac{1}{T} \int_t^{t+T} r(\tau) d\tau. \tag{1.13}$$

The norm-based methods are not used in this thesis and thus not studied in any further details.

Measurement noise

The Gaussian distribution is most commonly used to model the distribution of measurement noise. However, it is applied for convenience rather than necessarily motivated by the nature behind the generation of data (Agamennoni et al., 2012). Outliers are one cause of non-Gaussian noise in measurement data, which occur quite often (Pearson, 2002). Outliers are data points which do not match the majority of the available data, and can be seen as spikes in a trend plot. Other causes are due to process effects, such as in Wu (1993), where non-Gaussian measurement noise with heavier tails was reported in a radar system.

One such heavier-tailed distribution is the t-distribution, which is found to best match the noise in estimated parameters and ARR residuals in this thesis, using experimental field data. Reports of non-Gaussian t-distributed measurement noise in data from gravitational-wave detectors are given in Röver et al. (2011), where measurement noise originates partly from instrumental noise, partly from physical sources.

If X has the p-variate t-distribution with ν degrees of freedom, center μ and correlation matrix S, it is related to the normal distribution (Kotz and Nadarajah, 2004) as

$$X = R^{-1}Y + \mu, \tag{1.14}$$

if Y is a p-variate normal distribution with zero mean and covariance matrix R, and if $\nu R^2/\sigma$ is a χ^2 random variable with degrees of freedom ν, independent of Y.

As will be shown in the following chapters, noise in the studied test data is found to match the t-distribution quite well. However, for the sake of simplicity, the statistical methods described in this chapter concern Gaussian noise which is independent and identically distributed (IID).

Statistical methods for change detection

Typically, a fault will result in some changes in process variables and/or parameters. However, due to measurement noise, estimated states and parameters will be affected. This is the case found in the experimental data used in this thesis. One way of detecting such changes is to use a change detection algorithm on a given set of estimated parameters or residuals which are constant for the fault-free case $\mathcal{H}_0$, which is the method applied in later chapters. A good overview of algorithms is given in Basseville and Nikiforov (1993); Blanke et al. (2006).

Given a random variable $z(k)$ with probability function $f(z;\Pi)$, and with statistical parameters Π. If $z(k)$ has a Gaussian distribution with mean value μ and variance σ^2, the statistical parameters will be $\Pi = \{\mu, \sigma\}$, with probability density function (PDF)

$$f(z;\mu,\sigma) = \frac{1}{\sigma\sqrt{2\pi}} \exp\left(-\frac{(z-\mu)^2}{2\sigma^2}\right). \tag{1.15}$$

The change detection algorithm needs to determine when the statistical parameters Π change from Π_0 to Π_1. Several of these algorithms use the log-likelihood

ratio of an observation z,

$$s(z) = \ln \frac{f(z;\Pi_1)}{f(z;\Pi_0)}. \tag{1.16}$$

with the fundamental statistical property

$$\mathrm{E}(s;\Pi_0) < 0, \tag{1.17a}$$
$$\mathrm{E}(s;\Pi_1) > 0. \tag{1.17b}$$

One of the simplest algorithms for change detection is the *geometric moving average* (GMA) algorithm, where an exponential weighting of the observations is used. Given a forgetting factor α, the decision function can be written recursively as

$$g(k) = (1-\alpha)g(k-1) + \alpha s(k), \quad g_0 = 0, \tag{1.18}$$

where $s(k)$ is the log-likelihood in (1.16).

Of the more advanced change detection algorithms, the cumulative sum (CUSUM) algorithm by Page (1954) is commonly used, see, e.g., Basseville and Nikiforov (1993); Blanke et al. (2006). This algorithm uses a hypothesis test of whether the statistical parameters Π are more likely to be Π_0 or Π_1. It is thus a requirement that the statistical parameters are known before and after a change. If this is not the case, the generalized likelihood ratio test (GLRT) algorithm can be used (Willsky and Jones, 1976). Both algorithms are based on the log-likelihood ratio (1.16) of a series of observations $z(k),\ k = \{1,\dots,N\}$. Based on knowledge of the statistical parameters after change, these algorithms can be applied:

- The cumulative sum (CUSUM) algorithm if Π_1 is *known*,
- The generalized likelihood ratio test (GLRT) if Π_1 is *unknown*.

Cumulative sum (CUSUM) algorithm

Consider the cumulative sum of the log-likelihood function (1.16) of a random variable $z(k)$ with N observations,

$$S(k) = \sum_{i=1}^{k} s(z(i)) = \sum_{i=1}^{k} \ln \frac{f(z(i);\Pi_1)}{f(z(i);\Pi_0)}, \tag{1.19}$$

where k is the current sample time. From the statistical properties (1.17), $S(k)$ will tend to have a negative drift before the change, and a positive drift after. A possible decision function is then

$$g(k) = S(k) - \min_{1\le j\le k} S(j). \tag{1.20}$$

If there is only a change in the mean $\mu = \mathrm{E}(z)$ without change in the variance $\sigma^2 = \mathrm{VAR}(z)$ of a Gaussian distributed signal $z(k)$ with PDF given by (1.15), the decision function can be written recursively as

$$g(k) = \max\left(0, g(k-1) + \frac{\mu_1 - \mu_0}{\sigma^2}\left((z(k) - \frac{\mu_0+\mu_1}{2})\right)\right), \tag{1.21}$$

see, e.g., Blanke et al. (2006). A change between the two hypotheses

$$\begin{aligned} \text{null hypothesis } \mathcal{H}_0: &\quad \Pi = \Pi_0, \\ \text{alternative hypothesis } \mathcal{H}_1: &\quad \Pi = \Pi_1, \end{aligned}$$

is detected if $g(k)$ increases above a threshold h, namely

$$\begin{aligned} &\text{if} \quad g(k) \leq h \quad \text{accept} \quad \mathcal{H}_0, \\ &\text{if} \quad g(k) > h \quad \text{accept} \quad \mathcal{H}_1. \end{aligned}$$

Generalized likelihood ratio test (GLRT)

In the CUSUM algorithm it is assumed that the parameters Π_1 are known. In the generalized likelihood ratio test (GLRT) algorithm this requirement is relaxed so that also the case with unknown Π_1 can be handled. As with the CUSUM algorithm, the cumulative sum of the log-likelihood between the two probability density functions can be defined as

$$S_j^k(\Pi_1) = \sum_{i=j}^{k} \ln \frac{f(z(i); \Pi_1)}{f(z(i); \Pi_0)}. \tag{1.22}$$

In (1.22) the statistical parameters Π_1 at $\mathcal{H}_1$ are unknown. To estimate these, the maximum likelihood of the parameters can be used (Basseville and Nikiforov, 1993; Blanke et al., 2006), obtained by solving

$$\hat{\Pi}_1 = \arg \max_{1 \leq j \leq k} \max_{\Pi_1} S_j^k(\Pi_1). \tag{1.23}$$

To limit the data window, only the last M samples are used, giving a GLRT decision function

$$g(k) = \max_{k-M+1 \leq j \leq k} \max_{\Pi_1} S_j^k(\Pi_1), \tag{1.24}$$

where a change is detected if $g(k) > h$, where h is a threshold.

If the probability density function for the scalar signal $z(k)$ is Gaussian, and if only the mean is changing, the GLRT statistic is given by (see, e.g., Basseville and Nikiforov (1993); Blanke et al. (2006)),

$$g(k) = \frac{1}{2\sigma^2} \max_{k-M+1 \leq j \leq k} \frac{1}{k-j+1} \left[\sum_{i=j}^{k} (z(i) - \mu_0) \right]^2. \tag{1.25}$$

Determining thresholds and probability of detection

In control theory, robustness and sensitivity of the control system are important aspects. In the same way, the performance of a fault diagnosis system is measured based on a low *probability of false alarms*, P_{FA}, and high *probability of detection*,

P_D, (Kay, 1998; Ding, 2008). A trade-off between false alarms and detection rate has to be made when selecting thresholds, since these are conflicting properties.

The threshold value h can be determined based on the distribution of the test statistic $g(k)$, with a specified probability of false alarm, P_{FA}. If the signal $z(k)$ has a Gaussian distribution, where each sample is independent and identically distributed (IID), the GLRT statistic (1.25) follows asymptotically the χ^2_r distribution under $\mathcal{H}_0$, with r degrees of freedom (Kay, 1998).

However, if the data is non-Gaussian and/or not IID, other distributions such as the Weibull and the lognormal distributions better describe the test statistic, see, e.g., Galeazzi et al. (2013); Blanke et al. (2012); Fang et al. (2015).

Given a distribution $f_g(x;\Pi)$ with statistical parameters Π, which accurately describes the GLRT statistic $g(k)$. Let $F(x;\Pi)$ be the cumulative distribution, and $Q(P;\Pi)$ be the inverse cumulative distribution with probability P. Let Π_0 be the statistical parameters of the test statistic data under $\mathcal{H}_0$ fitted to the distribution $f_g(x;\Pi)$. Then the threshold value h can be determined based on a specified probability of false alarms, P_{FA} (Kay, 1998),

$$h = Q(1 - P_{FA};\Pi_0). \tag{1.26}$$

If sufficient data is available to determine the statistical parameters Π_1 under $\mathcal{H}_1$, the probability of detection P_D with given a threshold h is

$$P_D = 1 - F(h;\Pi_1). \tag{1.27}$$

This method for determining thresholds, and in some cases the probability of detection, will be studied in Chapters 3-6.

1.4.3 Fault isolation

In most systems it is desired to know where the fault has happened. If a processing plant has a leakage or a broken valve, it is much faster to replace the part if the operators and technicians know where the faulty equipment is located. If the fault diagnosis system is used as a part of a fault-tolerant control system, fault isolation can be a requirement. If an aircraft has a stuck rudder, the control system has to know what kind of fault that is occurring and where it is, in order to counter-act for it.

The generated residuals $r \in \mathbb{R}^{N_r}$ may be viewed as a vector, where changes to the elements can be detected using an appropriate change detection algorithm. There are different procedures for fault isolation based on the residuals. A simple approach is to evaluate each element r_i in r against a corresponding threshold h_i. The different faults can then be isolated if each fault has a unique effect on the residuals. If a priori knowledge of the cause and effects between residuals and faults are known, the faults and residuals can be organized in a fault look-up table, see, e.g., Gertler and Singer (1990); Blanke et al. (2006).

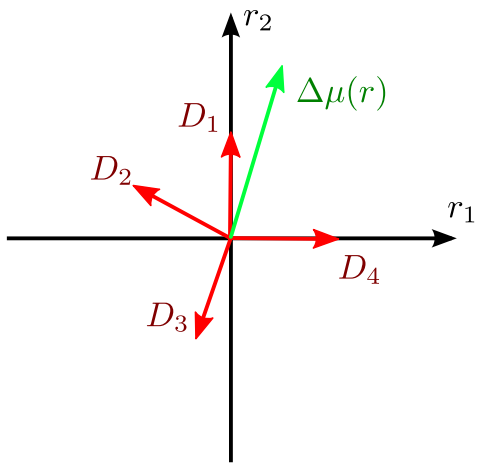

Figure 1.9: Change direction of mean $\Delta\mu$ of residual $r \in \mathbb{R}^2$. The fault with change direction D_1 has the lowest Euclidean distance, and is thus isolated.

A challenge with a *univariate* method as explained above is that it can be difficult to determine a threshold for each residual r_i. If the residual value is close to the threshold, correct isolation may be difficult. This can partly be solved by using more complex logic, but this logic may be cumbersome to service over time, and difficult to expand. An alternative is to use a *multivariate* method, using the change direction of r or a subset of it for fault isolation, see, e.g., Gertler and Monajemy (1995); Yin (1998); Venkatasubramanian et al. (2003c). A fault can be isolated if the change direction of the residual is in a neighborhood of a fault vector. This is illustrated as an example in Fig. 1.9, where a fault is represented by the change in mean of r, and is closest to the unit fault direction D_1. A challenge with this method is that the computational complexity can be quite high for even a moderate number of residuals.

A graphical comparison between a univariate and a multivariate approach is shown in Fig. 1.10 for a case with two residuals normally distributed with standard deviation σ, and with mean $\mu = 0$ for the fault-free case and $\mu = 1$ for the fault case. By using thresholds $h_1 = 3\sigma$ for residual r_1 and $h_2 = 3\sigma$ for residual r_2 independently, a large portion of the $\mathcal{H}_1$ data (red crosses) will be below either one of the thresholds (below h_2 and to the left of h_1). This results in a lot of missed detections, giving a low detection rate P_D. If a higher detection rate is desired, the cost is an increased false alarm rate. Using a multivariate approach with the same threshold of 3σ, the detection rate is greatly increased, with an unchanged false alarm rate. In the figure, false alarms are blue data circles outside the solid black threshold circle, while missed detection is red data points inside the threshold circle.

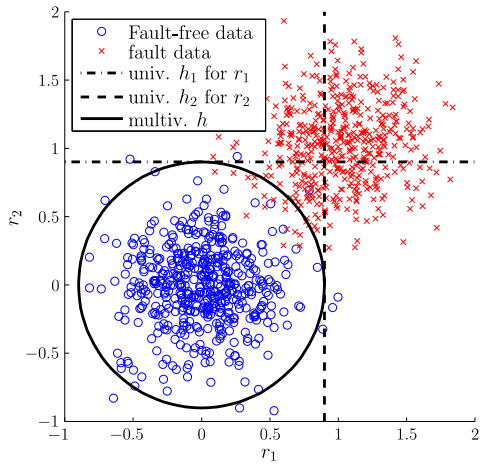

Figure 1.10: Example where data at $\mathcal{H}_0$, shown in blue circles, is normally distributed with $\mu = 0$ and $\sigma = 0.3$ for two residuals r_1 and r_2. Fault data is shown with red crosses, with $\mu = 1$ and unchanged variance. Different thresholds of 3σ are plotted, using two independent univariate tests (dashed and dashed dotted lines), and a multivariate test (solid circle). Notice that the multivariate method covers approximately the same amount of $\mathcal{H}_0$ data, but much less of the $\mathcal{H}_1$ data. The result is that detection rate is noticeably increased with the same false alarm rate.

1.5 Research objective

The main objective of this thesis is to develop methods which detects and isolates the downhole drilling incidents described in Sec. 1.1.3 as early as possible, with a low number of false alarms. Early detection of an event, as well as determining type and location, greatly reduces the outcome of the incident. This will save time, additional cost, and maintain safe operations in oil and gas drilling. The main research objective of the thesis can be summarized as follows:

Research objective

Develop efficient fault diagnosis methods for oil and gas drilling which are easy to use with little tuning needed, while at the same time have early detection and isolation properties and with a low false alarm rate.

1.6 Outline and contributions of the thesis

Of the model-based methods, the main parts of this thesis will use adaptive observers for parameter and state estimation, in particular friction parameters and flow rates. These are then used for fault diagnosis of the different incidents. Due to noticeable noise in the estimates using test data, statistical change detection

methods are proven to be necessary. Detuning the observers can be used to reduce the effect of the noise, but this will increase detection time, which is not a desired behavior. As pointed out in Sec. 1.4.1, analytical redundancy relations have some other properties for diagnosis. This is studied in Chapter. 6, where also diagnosis of sensor bias is possible, but with limitations in fault magnitude estimation. The main contributions in each of the following chapters are summarized as:

- **Chapter 2** contains preliminary results using model-based fault diagnosis of pack-offs in drilling, where the main contribution is the development of the adaptive observer used in later chapters. A bank of observers is used to estimate friction parameters, used to detect and isolate the position of the pack-off, where the model is correct for the correct position of the incident. The method is tested on a simulation case where the process model has the same structure as the observer model, but with a slightly more advanced friction model.

  This part consists of Willersrud and Imsland (2013).

- **Chapter 3** continues the work of Chapter 2, applying the adaptive observer on data from an experimental flow-loop test case, containing tests of a drillstring washout. For small washouts, changes to the estimated parameters are small, and covered in noise. The distribution of the noise of the estimated parameters is determined to fit the t-distribution well after white filtering, which has heavier tails compared to the Gaussian distribution. Due to noise, changes to the mean of the estimated parameters are detected using a statistical change detection algorithm. Three different change detection methods are tested, one univariate and two multivariate, where the multivariate approach showed superior detection properties. The main contributions of the chapter is the development of the univariate and multivaritate GLRT for the t-distribution, combining this with an adaptive observer and specified threshold levels based on probability of false alarm, and applying this as a drilling incident diagnosis method.

  This part consists of Willersrud et al. (2015c), based on preliminary results in Willersrud et al. (2013b).

- **Chapter 4** applies the methods developed in Chapter 3 on a series of downhole drilling incidents tested in the flow-loop, including gas influx, lost circulation, bit nozzle plugging, and drillstring washout. A multivariate generalized likelihood ratio test is used to detect the incidents, and isolate the type. Detection properties assuming a t-distribution of the noise in the estimated parameters is compared to assuming Gaussian distribution, showing a clear benefit with the t-distribution. The main contribution of this paper is to apply previous results on a series of different drilling incidents, developing and testing an isolation method based on change direction of carefully selected parameters and states.

This part consists of Willersrud et al. (2015d), based on preliminary results in Willersrud et al. (2013b).

- **Chapter 5** investigates how the method in Chapter 3 and 4 can be applied for diagnosing pack-offs, which was not tested in the flow-loop. The diagnosis framework is tested on simulated data from the high-fidelity multi-phase simulator OLGA, also showing diagnosis where the noise is Gaussian distributed. The main contribution in this chapter is to demonstrate the diagnosis method developed in Chapters 3 and 4 on a full-scale pack-off simulation case, where the noise is Gaussian.

  This part consists of Willersrud et al. (2015a).

- **Chapter 6** investigates the use of analytical redundancy relations (ARR) for fault detection and isolation, as opposite to using adaptive observers as in the previous chapters. Benefits and drawbacks of the two methods are compared, where ARR gives isolation of sensor bias drift and and actuator faults, in addition to downhole incident isolation. However, estimation of fault magnitude requires additional estimation methods. The main contribution of this chapter is to derive residuals using analytical redundancy relations for the specific drilling model, and demonstrate diagnostic properties on the flow-loop data using the framework developed in Chapter 3 and 4. Detection and isolation capabilities without downhole sensors is also investigated. The paper has a discussion of benefits and challenges using ARR, compared to using adaptive observers which was done in the previous chapters.

  This part consists of Willersrud et al. (2015b).

- **Chapter 7** concludes the thesis, discussing the different diagnosis methods applied on both experimental flow-loop data as well as simulated data. Possible future research directions are indicated.

Comment on the contents of the thesis chapters

Each chapter contains one peer-reviewed conference or journal paper, and is therefore *self-contained*. As such, parts of the introduction and background material will have some slight repetition, including model description and presentation of the experimental flow-loop.

1.6.1 Publications

The following list of publications forms the basis of the thesis:

Journal publications

- Willersrud, A., Blanke, M., and Imsland, L. (2015b). Incident detection and isolation in drilling using analytical redundancy relations. *Control Engineer-*

ing Practice, 41:1–12.

- Willersrud, A., Blanke, M., Imsland, L., and Pavlov, A. (2015d). Fault diagnosis of downhole drilling incidents using adaptive observers and statistical change detection. *Journal of Process Control*, 30:90–103.

- Willersrud, A., Blanke, M., Imsland, L., and Pavlov, A. (2015c). Drillstring Washout Diagnosis using Friction Estimation and Statistical Change Detection. *IEEE Transactions on Control Systems Technology*, PP(99).

Conference papers

- Willersrud, A., Blanke, M., and Imsland, L. (2015a). Early pack-off diagnosis in drilling using an adaptive observer and statistical change detection. In *Proc. IFAC Workshop on Automatic Control in Offshore Oil and Gas Production*, Florianopolis, Brazil.

- Willersrud, A. and Imsland, L. (2013). Fault Diagnosis in Managed Pressure Drilling Using Nonlinear Adaptive Observers. In *Proc. European Control Conference*, pages 1946–1951, Zürich, Switzerland.

Additional publications

The following additional conference papers are not included directly in the thesis, but acts as preliminary and background work. The first paper is an overview paper, which Sec. 1.1 in the introduction is based upon. The next paper is preliminary work which included in in Chapters 3 and 4.

- Willersrud, A., Imsland, L., Blanke, M., and Pavlov, A. (2015e). Early Detection and Localization of Downhole Incidents in Managed Pressure Drilling. In *Managed Pressure Drilling and Underbalanced Drilling Operations Conf. and Expo., SPE/IADC 173816*, pages 1–9, Dubai, UAE.

- Willersrud, A., Imsland, L., Pavlov, A., and Kaasa, G.-O. (2013b). A Framework for Fault Diagnosis in Managed Pressure Drilling Applied to Flow-Loop Data. In *Proc. Dynamics and Control of Process Systems*, pages 625–630, Mumbai, India.

The following publication was written in the period of the PhD study, but is not included in the thesis:

- Willersrud, A., Imsland, L., Hauger, S. O., and Kittilsen, P. (2013a). Short-term production optimization of offshore oil and gas production using nonlinear model predictive control. *Journal of Process Control*, 23(2):215–223.

Chapter 2

Fault diagnosis in managed pressure drilling using nonlinear adaptive observers

The work in this chapter was published in Willersrud and Imsland (2013).

Summary

A bank of nonlinear adaptive observers is used for fault diagnosis in oil and gas drilling where managed pressure drilling (MPD) is applied. The particular fault considered is formation of a pack-off, causing increased friction in one part of the annulus. The process model is a simplified hydraulics model with a Newtonian fluid. All states in the model are assumed measurable, an assumption based on planned implementation of the wired drill pipe measurement technology. A fault detection observer is used to detect that a pack-off is being formed somewhere in the annulus. Then a set of fault isolation and approximation observers, one for each possible fault, is used to isolate the location of the pack-off and estimating its magnitude. Isolation is done by using residuals of annular friction estimation. The method for fault diagnosis is illustrated in a simulation study.

2.1 Introduction

Drilling of onshore and offshore oil and gas wells has traditionally been done manually by a driller. As technology has advanced, more sophisticated online measurements have been available, e.g., depth, penetration rate, topside pump rates and pressures, and drilling fluid ("mud") flow return rate from the borehole. These measurements have mainly been used as information to the driller, and have to a little extent been used for automated closed-loop control or automated diagnosis of the operation. One of the exceptions where automated control has been applied is managed pressure drilling (MPD), where closed loop control of topside chokes keeps annular wellbore pressure within margins of pore pressure and fracture pressure.

A new measurement technology called wired drill pipe has recently been introduced (e.g., Nygaard et al. (2008)), which increases the bandwidth and sampling rate drastically compared to traditional mud pulse telemetry. It will then be possible to have a more continuous measurement of downhole conditions during drilling

such as downhole pressure and rate of penetration, as well as added measurements such as flow through the bit and distributed pressure and temperature sensors along the drillstring (Long and Veeningen, 2011). This technology may become instrumental in future drilling operations, as an increasing number of wells are less accessible, at high depths with small pressure margins. Operating within smaller margins, increased supervision of the drilling operation will be even more important. Incidents such as kicks (uncontrolled influx into the wellbore), pack-off (wellbore plugged around the drill string), loss of drilling fluid to the formation, and blocking of the drill bit need to be detected and handled.

In this paper the work done in, e.g., Stamnes et al. (2011a); Grip et al. (2010) will be used as background for including early fault warning of when and where a pack-off is being formed in the annulus, using a bank of adaptive nonlinear observers. By utilizing the wired drill pipe technology, the pack-off can be located with much higher accuracy. A similar study has also recently been done on a well in the Gulf of Mexico, but with manual detection of the pack-off formation (Long and Veeningen, 2011). Detection was done by observing an increase in equivalent circulating pressure for all pressure sensors below the pack-off. Another example of using the technology for diagnosis has recently been studied in Gravdal et al. (2010b), where an uncented Kalman filter (UKF) has been used to detect and isolate a kick.

This rest of the paper is organized in seven short sections. In the following section the concept of fault diagnosis is explained with emphasis on application in an MPD system. In Sec. 2.3 the model of the drilling process is presented, with some unknown parameters representing process friction and faults. In Sec. 2.4 a nonlinear adaptive observer for the process is presented, and in Sec. 2.5 the concept of using a bank of these observers for fault diagnosis is described. How this can be implemented for the drilling process is explained in Sec. 2.6. We then carry out a simulation case in Sec. 2.7 and give some concluding remarks in Sec. 2.8.

2.2 Fault diagnosis

System faults, disturbances and modeling error will all alter a system's behavior. The difference is that disturbances and modeling error are factors which typically are suppressed by filtering and robust control, whereas faults in a system must be detected and handled. There have been published several books on the subject lately (Blanke et al., 2006; Isermann, 2006; Ding, 2008). The problem of *fault diagnosis* consist of first detecting the error through *fault detection*, finding the source of the problem through *fault isolation* and then identify its magnitude through *fault identification*. Fault diagnosis is not only important in itself, but also key if a good fault-tolerant control system is to be implemented Zhang and Jiang (2008). Adaptive observers for fault diagnosis has been studied in, e.g., Xu and Zhang (2004); Besancon and Zhang (2002). The ideas have then been extended to have a bank of adaptive observers (Zhang, 2000; Zhang and Jiang, 2006; Zhang et al., 2010). Extended Kalman filters can also be used to design adaptive observers, but will

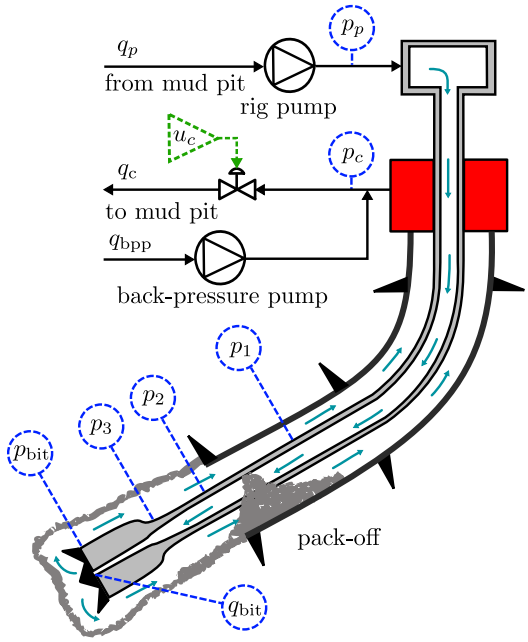

Figure 2.1: Detection of pack-off in MPD (Adapted from Kaasa et al. (2012)). The measurements are labelled with blue circles.

usually only guarantee local convergence (Xu and Zhang, 2004; Zhang, 2000).

The method in this paper is to use a bank of Lyapunov based adaptive observers in order to detect and isolate a fault using measurements from the wired drill pipe. The formation of a pack-off is typically an incipient (slowly varying) fault represented by increased friction, favoring the use of adaptive observers with parameter estimation (Frank, 1990). In addition there is an overall annular wall friction which can vary for other reasons. The idea behind the fault diagnosis setup is that a fault between two pressure sensors will give an increased pressure differential between these sensors. The bank of observers consists of one observer detecting that a fault has occurred, and one observer for each possible fault each assuming that only the corresponding fault has occurred. Then only the observer estimating the actual fault will get a correct estimate, isolating the fault.

2.3 Hydraulic drilling model

The model used is based on the simple hydraulics model in Kaasa et al. (2012), where a schematic overview is shown in Fig. 2.1. The model has simple one-phase

incompressible flow relationships for a Newtonian fluid, and can be represented as

$$\frac{dp_p}{dt} = \frac{\beta_d}{V_d}(q_p - q_{\text{bit}}) \tag{2.1a}$$

$$\frac{dp_c}{dt} = \frac{\beta_a}{V_a}(q_{\text{bit}} + q_{\text{bpp}} - q_c) \tag{2.1b}$$

$$\frac{dq_{\text{bit}}}{dt} = \frac{1}{M}(p_p - p_c - F(q_{\text{bit}}, \theta) - (\rho_a - \rho_d)gh_{\text{TVD}}) \tag{2.1c}$$

where p_p [bar] is the drilling pump pressure, p_c [bar] is the choke pressure, q_{bit} [L/s] is the flow through the drill bit, and q_{bpp} [L/s] is the back-pressure pump. In the drill string and annulus, respectively, the bulk modulus is $\beta_{\{d,a\}}$ [bar] and the volume is $V_{\{d,a\}}$ [L]. The vector θ is the unknown parameters. The choke flow can be represented by the choke equation (Manring, 2005)

$$q_c = C_v u_c \sqrt{p_c - p_0}$$

where C_v is the choke constant, u_c is the choke opening, and p_0 is atmospheric pressure. The densities $\rho_{\{d,a\}}$ [kg/m^3] and cross sections $A_{\{d,a\}}$ [m^2] of the drill pipe and annulus are assumed known. Thus

$$M_i = \int_{L_{i-1}}^{L_i} \frac{\rho_i(x)}{A_i(x)} dx, \quad i \in \{d, a\}$$

is assumed know, where M_i [bar $\cdot$ s^2/L] is the integrated density per cross section over the segment $\Delta L_i = L_i$ [m] $- L_{i-1}$ [m]. We will use $M = M_d + M_a$ as the total integrated value of the hydraulic system from the the pump to the choke. Furthermore, the true vertical depth h_{TVD} [m] is assumed known.

2.3.1 Friction model

The total friction $F(q, \theta)$ in the system (2.1) can be divided into friction through the drillstring $F_d(q)$, including pipe friction and bit friction, and annular friction $F_a(q, \theta)$. As argued in Kaasa et al. (2012) the flow dynamics will be faster than the pressure dynamics, and we can thus assume that the flow through the system can be approximated by the measured flow q_{bit} through the bit. Furthermore, since we measure the pressure drop $p_{\text{bit}} - p_p$ over the drill string and assume known density ρ_d and viscosity μ_d, the friction $F_d(q)$ in the drill string can be assumed known and given as

$$F_d(q) = F_{\text{pipe}}(\rho_d, \mu_d, L_d, q) + k_{\text{bit}}(\rho_d)q^2$$

where pipe friction is modeled based on Newtonian fluid assumption including laminar flow, turbulent flow, and a transition zone.

The flow in the annulus is modeled in a similar way, but for the observer design we will assume that this flow is laminar, without loss of generality. For laminar flow of a Newtonian fluid, the pressure drop $F_{a,i}(q, \theta) = \psi c_i q$ in an annular segment

i will be dependent on the length and diameter of the segment by a factor c_i, as well as some unknown parameter $\theta = \psi$. The constant c_i can be calculated as

$$c_i = \int_{L_i}^{L_{i+1}} \frac{1}{\left(d_h(l) - d_o(l)\right)^2 \left(d_h^2(l) - d_o^2(l)\right)} dl$$

where $d_h(l)$ [m] is the annular diameter and $d_o(l)$ [m] is the outer drill string diameter. $\Delta L_i = L_{i+1} - L_i$ [m] is the length of the segment.

2.3.2 Pack-off in the annulus

The fault studied in this paper is the formation of a pack-off, which is a (partially) plugged annulus around the drill string caused by accumulation of cuttings. One of the reasons for this to happen can be a too low circulation flow (Aadnoy et al., 2009). Pack-off is modeled using the orifice equation for incompressible fluids (Manring, 2005). The friction $F_a(q, \theta)$ in the annulus can thus be represented as

$$F_a(q, \theta) = \sum_{i=1}^{N} F_{a,i}(q, \theta) = \sum_{i=1}^{N} \left(\psi c_i q + \phi_i q^2\right) \tag{2.2}$$

where $\theta = \begin{bmatrix} \psi, & \phi^\top \end{bmatrix}^\top$ are the unknown parameters we wish to estimate, and N is the number of annular segments between pressure measurements, and thus also number of faults. We will distinguish between the unknown annular friction parameter ψ and the parameters representing the set of possible faults

$$\mathcal{F} := \{\phi_1, \ldots, \phi_N\} \tag{2.3}$$

where each element is the friction parameter ϕ_i in (2.2) corresponding to increased pressure due to, e.g., pack-off.

2.3.3 Measurements with wired drill pipe

In addition to the topside pressures p_p and p_c, wired drill pipe is used to measure downhole pressure p_{bit} and flow q_{bit}, as well as three pressure measurements p_1, p_2, p_3 along the annulus, see Fig. 2.1. By defining $F_{a,i}(q, \theta)$ in (2.2) as the friction between the pressure sensors in the annulus, the following equations represent the relation between pressure and friction

$$\begin{aligned} p_1 &= p_c + F_{a,1}(q, \theta) + G_1(\rho_a) \\ p_2 &= p_1 + F_{a,2}(q, \theta) + G_2(\rho_a) \\ p_3 &= p_2 + F_{a,3}(q, \theta) + G_3(\rho_a) \\ p_{\text{bit}} &= p_3 + F_{a,4}(q, \theta) + G_4(\rho_a) \end{aligned}$$

where $G_i(\rho_a)$ is the hydrostatic pressure difference between the two measurement points.

2.4 Nonlinear adaptive observer framework

In this section we will present the nonlinear adaptive observer used as a basis for parameter and fault estimation. It is assumed that all states are measured, giving the system on the form

$$\dot{x} = \alpha(x, z, u) + \beta(x, z, u)\theta \tag{2.4a}$$
$$z = \eta(x, z, u) + \lambda(x, z, u)\theta \tag{2.4b}$$

where $x(t) \in \mathbb{R}^n$ are the states, $z(t) \in \mathbb{R}^m$ are additional measurements, $u(t) \in \mathbb{R}^p$ are the inputs, $\theta \in \mathbb{R}^q$ are unknown parameters, and $\alpha(\cdot)$, $\beta(\cdot)$, $\eta(\cdot)$ and $\lambda(\cdot)$ are locally Lipschitz. The observer with theorem and proof is based on an observer in Besançon (2000), adapted to the system representation (2.4).

Theorem 2.1. *Given an observer on the form*

$$\dot{\hat{x}} = \alpha(x, z, u) + \beta(x, z, u)\hat{\theta} - K_x(\hat{x} - x) \tag{2.5a}$$
$$\dot{\hat{\theta}} = -\Gamma\beta^\top(x, z, u)(\hat{x} - x) - \Lambda\lambda^\top(x, z, u)(\hat{z} - z) \tag{2.5b}$$
$$\hat{z} = \eta(x, z, u) + \lambda(x, z, u)\hat{\theta} \tag{2.5c}$$

where $K_x, \Lambda, \Gamma > 0$ are tuning matrices, and with $\dot{\theta} = 0$. Let $e_x = \hat{x} - x$ and $e_\theta = \hat{\theta} - \theta$ be variables for the error dynamics, where $e = \begin{bmatrix} e_x^\top, & e_\theta^\top \end{bmatrix}^\top = 0$ is an equilibrium point. Then $e = 0$ is globally exponentially stable if

$$\Gamma^{-1}\Lambda\lambda^\top(\cdot)\lambda(\cdot) - \beta^\top(\cdot)K^\top K\beta(\cdot) > kI_q \tag{2.6}$$

for some constant $k > 0$, where $I_q \in \mathbb{R}^{q\times q}$ is the identity matrix.

Proof. Let a continuously differentiable positive definite Lyapunov function be given by $V = \frac{1}{2}e_x^\top K_x^{-1}e_x + \frac{1}{2}e_\theta^\top\Gamma^{-1}e_\theta$. Then the time-derivative of V is given by

$$\begin{aligned}
\dot{V} &= e_x^\top K_x^{-1}\dot{e}_x + e_\theta^\top\Gamma^{-1}\dot{e}_\theta \\
&= e_x^\top K_x^{-1}\beta(\cdot)e_\theta - e_x^\top e_x - e_\theta^\top\beta^\top(\cdot)e_x - e_\theta^\top\Gamma^{-1}\Lambda\lambda^\top(\cdot)e_z \\
&= e_x^\top K_x^{-1}\beta(\cdot)e_\theta - e_x^\top e_x - e_\theta^\top\beta^\top(\cdot)e_x - e_\theta^\top\Gamma^{-1}\Lambda\lambda^\top(\cdot)\lambda(\cdot)e_\theta
\end{aligned}$$

where it has been used that $\dot{e}_x = \beta(\cdot)e_\theta - K_x e_x$, $\dot{e}_\theta = \dot{\hat{\theta}} - \dot{\theta} = \dot{\hat{\theta}} = \Gamma\beta^\top(\cdot)e_x - \Lambda\lambda^\top(\cdot)e_z$, $e_z = \lambda(\cdot)e_\theta$. Using that $e_x^\top K_x^{-1}\beta(\cdot)e_\theta - e_\theta^\top\beta^\top(\cdot)e_x = -\frac{1}{2}e_x^\top\left(I_n - K_x^{-1}\right)\beta(\cdot)e_\theta - \frac{1}{2}e_\theta^\top\beta^\top(\cdot)\left(I_n - K_x^{-1}\right)^\top e_x$, we can write

$$\begin{aligned}
\dot{V} &= -\begin{bmatrix} e_x^\top, & e_\theta^\top \end{bmatrix}\begin{bmatrix} I_n & K\beta(\cdot) \\ \beta^\top(\cdot)K^\top & \Gamma^{-1}\Lambda\lambda^\top(\cdot)\lambda(\cdot) \end{bmatrix}\begin{bmatrix} e_x \\ e_\theta \end{bmatrix} \\
&= -e^\top\Phi(\cdot)e
\end{aligned}$$

where $K = \frac{1}{2}(I_n - K_x^{-1})$. From Proposition 16.2 in Gallier (2011) on the Schur complement, we have that $\Phi(\cdot) > kI_{n+q}$, if and only if $\Gamma^{-1}\Lambda\lambda^\top(\cdot)\lambda(\cdot) - \beta^\top(\cdot)K^\top K\beta(\cdot) >$

kI_q, using that I_q is invertible and positive definite. Provided that (2.6) holds, $\dot{V} < -k\|e\|^2$ and thus according to Theorem 4.10 in Khalil (2002) the equilibrium point $e = 0$ is globally exponentially stable. □

Note that if $\beta(\cdot)$ is bounded and $\lambda^\top(\cdot)\lambda(\cdot) > 0$ there exist some tuning parameters K_x, Γ and Λ such that (2.6) is fulfilled. The matrix function $\beta(\cdot)$ is bounded as the physical flow $x_3 = q_{\text{bit}}$ through the system always will be bounded, while $\lambda^\top(\cdot)\lambda(\cdot) > 0$ can be interpreted as a requirement for persistence of excitation.

2.5 A bank of observers for fault diagnosis

The procedure of making a bank of $N+1$ observers, where N is the number of faults in some fault class $\mathcal{F}$, is based on the methods presented in Zhang (2000); Zhang et al. (2002). The idea is to have one *fault detection observer* (FDO) to detect faults. After a fault is detected, the N remaining *fault isolation and approximation observers* (FIAOs) are used to isolate the fault and estimate its magnitude. There are two ways of using a bank of observers for fault diagnosis Zhang et al. (2002). In the *dedicated observer scheme* (DOS) proposed by Clark Clark (1978) each observer is sensitive to one fault, while in the *generalized observer scheme* (GOS) proposed by Frank (1990) each observer is sensitive to all faults but one.

In this paper we will use the DOS scheme. The FDO only estimates the unknown process parameters ψ, while the jth FIAO in addition estimates one possible fault parameter ϕ_j in $\mathcal{F}$, while assuming the rest of ϕ zero.

2.5.1 Fault detection observer (FDO)

The FDO will be used to detect that a fault has occurred by detecting changes in the estimate of the plant parameters ψ without estimating the fault parameters ϕ. The observer (2.5) with $\phi_j = 0$ will be

$$\dot{\hat{x}}_0 = \alpha(x,u) + \beta_0(x)\hat{\psi}_0 - K_x(\hat{x}_0 - x) \tag{2.7a}$$

$$\dot{\hat{\psi}}_0 = -\Gamma_0\beta_0^\top(x,z)(\hat{x}_0 - x) - \Lambda_0\lambda_0^\top(x)(\hat{z}_0 - z) \tag{2.7b}$$

$$\hat{z}_0 = \eta(x,z) + \lambda_0(x)\hat{\psi}_0 \tag{2.7c}$$

where $\beta_0(x)$ and $\lambda_0(x)$ are reduced matrices with columns corresponding to ψ in $\beta(x)$ and $\lambda(x)$, respectively. The gain matrices are K_x, Γ_0 and Λ_0.

2.5.2 Fault isolation and approximation observers (FIAOs)

The FIAOs are designed such that each observer only estimates one of the faults ϕ_j in $\mathcal{F}$, in addition to the plant parameter ψ. The fault isolation observer for fault

ϕ_j can then be written as

$$\dot{\hat{x}}_j = \alpha(x,u) + \beta_0(x)\hat{\psi}_j + \beta_j(x)\hat{\phi}_j - K_x(\hat{x} - x) \tag{2.8a}$$

$$\dot{\hat{\psi}}_j = -\Gamma_0\beta_0^\top(x,z)(\hat{x}_j - x) - \Lambda_0\lambda_0^\top(x)(\hat{z}_j - z) \tag{2.8b}$$

$$\dot{\hat{\phi}}_j = -\Gamma_j\beta_j^\top(x,z)(\hat{x}_j - x) - \Lambda_j\lambda_j^\top(x)(\hat{z}_j - z) \tag{2.8c}$$

$$\hat{z}_j = \eta(x,z) + \lambda_0(x)\hat{\psi}_j + \lambda_j(x)\hat{\phi}_j \tag{2.8d}$$

where $\beta_0(x)$ and $\lambda_0(x)$ are the same as in the FDO (2.7), and $\beta_j(x)$, $\lambda_j(x)$ are the corresponding regressors for $\hat{\phi}_j$. The tuning parameters will be the same as for the FDO in addition to Γ_j and Λ_j. Not that this observer is on the same form as (2.5), but with θ split into ψ and ϕ_j.

2.6 Fault diagnosis of the drilling process

In this section the methods for fault diagnosis presented in Sec. 2.5 will be applied to the drilling case. The simplified hydraulics drilling model (2.1) can be written on the form (2.4) where $z = \begin{bmatrix} p_1, & p_2, & p_3, & p_{\text{bit}} \end{bmatrix}^\top$, $x = \begin{bmatrix} p_p, & p_c, & q_{\text{bit}} \end{bmatrix}^\top$, $u = \begin{bmatrix} q_p, & q_{\text{bpp}}, & u_c \end{bmatrix}^\top$, and with system matrices

$$\alpha(x,u) = \begin{bmatrix} -\frac{\beta_d}{V_d}(x_3 - u_1) \\ \frac{\beta_a}{V_a}(x_3 + u_2 - C_v u_3\sqrt{x_2 - p_0}) \\ \frac{1}{M}(x_1 - x_2 - F_d(x_3) - \Delta\rho g h_{\text{TVD}}) \end{bmatrix} \tag{2.9a}$$

$$\eta(x,z) = \begin{bmatrix} x_2 - G_1 \\ z_1 - G_2 \\ z_2 - G_3 \\ z_3 - G_4 \end{bmatrix} \tag{2.9b}$$

where we have used $\Delta\rho = \rho_a - \rho_d$. Further will θ, $\beta(x)$ and $\lambda(x)$ be dependent on the specific FDO or FIAO.

2.6.1 Fault detection observer

In the fault detection observer a fault-free system is assumed, and thus only the annular friction $\theta = \psi$ of the parameters is estimated using the observer (2.7). In addition to (2.9) the corresponding system vectors will be

$$\beta_0(x) = \frac{1}{M}\begin{bmatrix} 0, & 0, & -x_3 \end{bmatrix}^\top \tag{2.10a}$$

$$\lambda_0(x) = \begin{bmatrix} c_1 x_3, & c_2 x_3, & c_3 x_3, & c_4 x_3 \end{bmatrix}^\top \tag{2.10b}$$

The requirement for convergence (2.6) will be $\frac{\Lambda_0}{\Gamma_0}(\sum_{i=1}^N c_i^2)x_3^2 + K_{3,3}^2 x_3^2 > k$, where $K_{3,3}^2$ is the third row and third column of $\frac{1}{2}(I_3 - K_x^{-1})$. This will be fulfilled for non-zero flow $x_3 = q_{\text{bit}}$, and appropriate Γ_0, Λ_0, K.

2.6.2 Fault isolation and approximation observers

For each of the jth fault isolation and approximation observers the unknown friction ψ and the possible fault ϕ_j will be estimated, giving an unknown parameter vector $\theta = \begin{bmatrix}\psi, & \phi_j\end{bmatrix}^\top$. The system vectors $\beta_0(x)$ and $\lambda_0(x)$ are the same as (2.10), while the FIAO specific vectors will be

$$\beta_j(x) = \frac{1}{M}\begin{bmatrix}0, & 0, & -x_3^2\end{bmatrix}^\top, \quad \lambda_j(x) = x_3 e_j \tag{2.11}$$

where e_j is the jth column of the identity matrix I_4. Here the requirement for convergence (2.6) will be

$$\begin{bmatrix}\frac{\Lambda_0}{\Gamma_0} & 0 \\ 0 & \frac{\Lambda_j}{\Gamma_j}\end{bmatrix}\begin{bmatrix}\left(\sum_{i=1}^N c_i^2\right)x_3^2 & c_j^2 x_3^3 \\ c_j^2 x_3^3 & x_3^4\end{bmatrix} + \frac{K_{3,3}^2}{M^2}\begin{bmatrix}x_3^2 & x_3^3 \\ x_3^3 & x_3^4\end{bmatrix} > kI_2$$

which also is fulfilled if x_3 is non-zero with some positive tuning parameters. Note that the last term is only positive semi-definite, meaning that convergence is enforced by the first term, representing the additional measurements z.

2.6.3 Residual generation and evaluation

Residuals are generated from the fault diagnosis method and define some measure on the fault in the system. In this paper the total annular friction $F_a(q,\theta)$ in (2.2) will be the basis for the residual generation and evaluation. Using the approach in Zhang (2000), we can define the residual as

$$\xi_j := \hat{F}_a(q,\hat{\psi}_0,0) - \hat{F}_a(q,\hat{\psi}_j,\hat{\phi}_j) \tag{2.12}$$

where $\hat{F}_a(q,\hat{\psi}_0,0)$ is the estimated annular friction in the FDO and $\hat{F}_a(q,\hat{\psi}_j,\hat{\phi}_j)$ is the estimated friction in the jth FIAO. The idea is that if there is a fault ϕ_j in the fault set $\mathcal{F}$ defined in (2.3), the jth FIAO will successfully estimate the friction, making ξ_j (close to) zero. Note that as in Zhang (2000), this method is limited to the case of a single fault happening.

The FDO for the drilling process is designed to detect increases in the total annular pressure which is similar to finding the equivalent circulating density. Of the available additional measurements z, only the pressure in the top and bottom of the annulus will be used for the FDO, making $z = p_{\text{bit}}$.

A threshold μ_{det} on $\hat{\psi}_0$ will be used for fault detection, giving a fault time t_{fault} if the threshold is exceeded, i.e., $\hat{\psi}_0 > \mu_{\text{det}}$. Then a threshold μ_{isol} on ξ_j is used for fault isolation, where a fault is isolated if $\xi_j < \mu_{\text{isol}}$. The magnitude of the fault will then be $\hat{F}_{\text{fault}} := \hat{\phi}_j q^2$. In order to make the detection and isolation more robust, a simple exponential moving average filter (Basseville and Nikiforov, 1993)

$$s_k = (1-\alpha)s_{k-1} + \alpha s_k \tag{2.13}$$

with forgetting factor α is used to filter $\hat{\psi}_0$ and ξ_j.

2.7 Simulation of the drilling model

The drilling model (2.1) is simulated using a fifth order fixed step solver with added Gaussian measurement noise with standard deviations $\sigma_x = \begin{bmatrix}0.5, & 0.1, & 0.1\end{bmatrix}^\top$ and $\sigma_z = \begin{bmatrix}0.5, & 0.5, & 0.5, & 0.5\end{bmatrix}^\top$. The parameter values are given in Tab. 2.1 based on an example in API (2006), and where the the back-pressure pump is not used ($q_{\text{bpp}} = 0\,\text{L/s}$). The model contains a marine riser, drill collars, drill pipe and drill bit, giving different diameters for different sections of the drill string and annulus. The model's initial values $x(0)$ are $p_p(0) = 230\,\text{bar}$, $p_c(0) = 2.2\,\text{bar}$ and $q_{\text{bit}}(0) = 22\,\text{L/s}$ The observers are initialized with $\hat{x}(0) = 0.7x(0)$, $\hat{\psi}_j(0) = 0.7$, and $\hat{\phi}_j(0) = 0$. The observer gains found through tuning are $K_x = \text{diag}\{0.5, 0.5, 3\}$, $\Gamma_0 = \Lambda_0 = 1 \times 10^{-3}$ and $\Gamma_j = \Lambda_j = 1 \times 10^{-6}$. The pump is initially running with flow $q_p = 22\,\text{L/s}$. At 10 minutes the pump is turned off resulting in zero flow through the bit until it is turned on again at 30 minutes. This mimics the common situation of a pipe connection. Note that the initial pump flow gives turbulent flow in the annulus, even though the observer was designed for laminar flow, see Sec. 2.3.1.

Table 2.1: Drilling model parameters.

β_a	5 000 bar	Effective bulk modulus annulus
β_d	14 000 bar	Effective bulk modulus drill string
M_a	$5.2\,\text{bar} \cdot \text{s}^2/\text{L}$	Integrated density per cross section
M_d	$10.8\,\text{bar} \cdot \text{s}^2/\text{L}$	Integrated density per cross section
V_a	$287 \times 10^3\,\text{L}$	Volume of fluid in annulus
V_d	$61 \times 10^3\,\text{L}$	Volume of fluid in drill string
ρ_a	1.30 kg/L	Density of fluid in annulus
ρ_d	1.10 kg/L	Density of fluid in drill string
μ_d, μ_a	$0.038\,\text{Pa} \cdot \text{s}$	Viscosity of drilling fluid
h_{TVD}	3760 m	True vertical depth of bit
L_d, L_a	6609 m	Length of drill string/annulus
u_c	30 %	Choke opening
μ_{det}	1.0 bar s/L	Fault detection threshold
μ_{isol}	0.20 bar	Fault isolation threshold

The simulated state estimation is shown in Fig. 2.2. The good state estimation is as expected, since all states are directly measured. When the flow is zero, the pump pressure p_p is reduced to the difference in hydrostatic pressure between the drill string and the annulus, caused by different densities. The choke pressure p_c is now atmospheric. The parameter estimation is shown in Fig. 2.3 where $\hat{\psi}_0$ is the annular friction coefficient estimated by the FDO and $\hat{\psi}_j$, $j \in \{1, \ldots, 4\}$ are the parameters estimated by the FIAOs. A fault is detected when a filtered $\hat{\psi}_0$ exceeds the threshold μ_{det}. This happens at $t_{\text{fault}} = 26.23\,\text{min}$. The actual pack-off ϕ_2 between pressure sensors p_1 and p_2 starts to form at $t = 16.7\,\text{min}$, shown in the lower plot in Fig. 2.3. The estimates $\hat{\phi}_j$ shown in the same plot are the

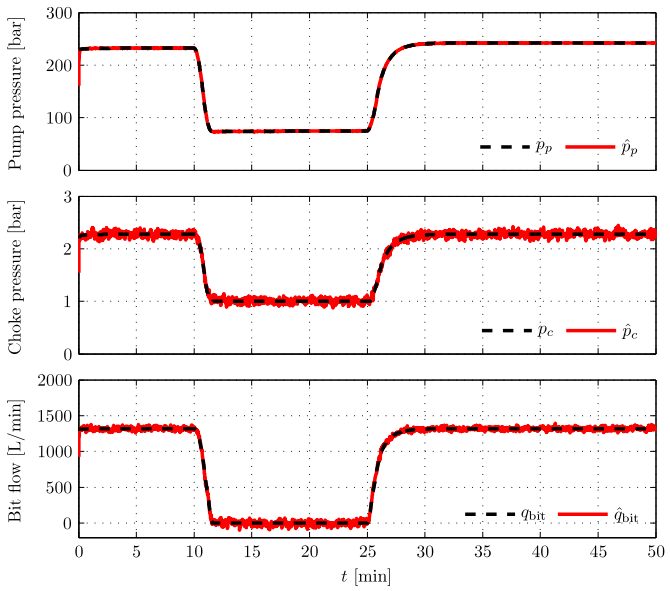

Figure 2.2: State estimation of pump pressure, choke pressure and bit flow.

estimates of fault ϕ_j by the jth FIAO. It can clearly be seen that the fault ϕ_2 is correctly estimated by the FIAO number 2, while the other FIAOs erroneously tries to estimate the fault to be in ϕ_1, ϕ_3 and ϕ_4, respectively. The reason that the fault is detected first after circulation resumes, is the requirement of a non-zero $q_{\text{bit}} = x_3$, as discussed in Sec. 2.6. Intuitively, this can be explained by the fact that the effect of increased friction is not seen when there is no flow, which also can be seen from the friction estimate in the upper plot in Fig. 2.4.

The residuals shown in the lower plot in Fig. 2.4 are the filtered signal of (2.12) using filter (2.13). A fault is isolated if after $t > t_{\text{fault}}$, the filtered ξ_j is below the threshold μ_{isol}. This happens for residual ξ_2, thus isolating the fault to a pack-off being formed between measurements p_1 and p_2, see Fig. 2.1. The magnitude of the fault in terms of pressure loss due to friction will then be given as $\hat{F}_{\text{fault}} = \hat{\phi}_2 x_3^2 = 9.7\,\text{bar}$ at full circulation.

2.8 Conclusion

In this paper a simplified nonlinear hydraulics model for drilling of oil and gas is combined with a bank of nonlinear adaptive observers in order to detect, isolate and identify that a pack-off is being formed. Utilizing the additional measurements available in the novel wired drill pipe technology, all states in the model are assumed directly measured in addition to a set of pressure transmitters distributed along the drill string. A fault detection observer is used in order to detect that a fault occurs.

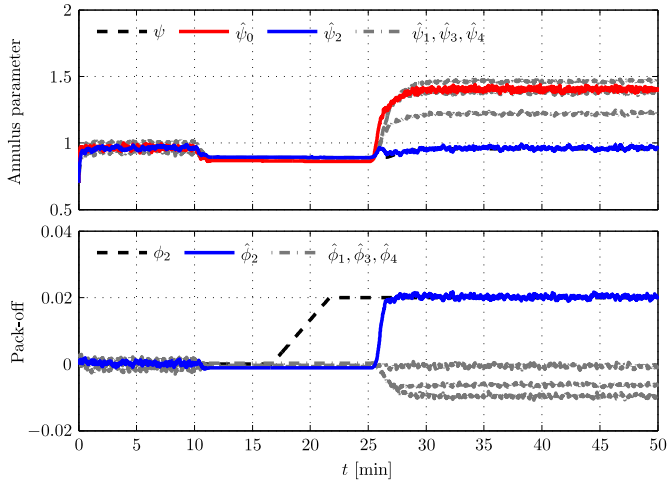

Figure 2.3: Estimation of friction parameter ψ_0 in the annulus by the FDO (red), and fault parameter ϕ_j by the jth FIAO. The fault is correctly estimated by $\hat{\phi}_2$ (blue), and incorrectly by the other $\hat{\phi}_j$ (grey).

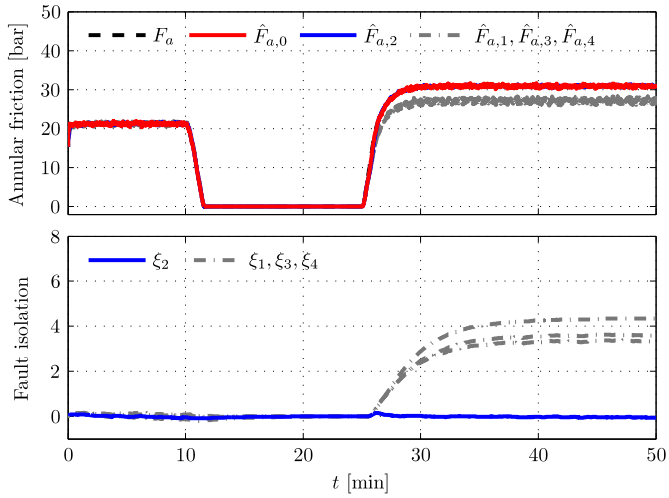

Figure 2.4: Friction estimates $\hat{F}_a$ and filtered fault isolation ξ_j. In the lower plot, the fault (blue) is isolated by FIAO-2 to be ϕ_2, while the other ξ_j are plotted in grey.

Then a set of fault isolation and approximation observers are used to isolate the position of the fault as well as its magnitude. Simulation of the simplified model shows that a fault is successfully detected and isolated between two pressure sensors as long as there is circulation of drilling fluid. As future work we hope to apply this method in a high-fidelity drilling simulation environment as well as on a real data set.

Chapter 3

Drillstring washout diagnosis using friction estimation and statistical change detection

The work in this chapter was published in Willersrud et al. (2015c), which is partly based on preliminary results in Willersrud et al. (2013b).

Summary

In oil and gas drilling, corrosion or tensile stress can give small holes in the drillstring, which can cause leakage and prevent sufficient flow of drilling fluid. If such washout *remains undetected and develops, the consequence can be a complete twist-off of the drillstring. Aiming at early washout diagnosis, this paper employs an adaptive observer to estimate friction parameters in the nonlinear process. Non-Gaussian noise is a nuisance in the parameter estimates, and dedicated generalized likelihood tests are developed to make efficient washout detection with the multivariate t-distribution encountered in data. Change detection methods are developed using logged sensor data from a horizontal 1400 m managed pressure drilling test rig. Detection scheme design is conducted using probabilities for false alarm and detection to determine thresholds in hypothesis tests. A multivariate approach is demonstrated to have superior diagnostic properties and is able to diagnose a washout at very low levels. The paper demonstrates the feasibility of fault diagnosis technology in oil and gas drilling.*

3.1 Introduction

Drilling is a major part of the total oil or gas field development cost. As the easy available reservoirs are being depleted, there is a trend that boundaries for drilling is pushed in the sense of more extreme environments, such as the arctic, or deep wells with high pressure and high temperature. With increasing depth and drilling at more remote locations, the cost of drilling is further increased and it is essential to minimize non-productive time, that amounts to 20-25 % of total time in operation (Godhavn, 2010).

Different incidents can happen downhole or topside that cause downtime, or even abandonment of a well. Emerging advanced drilling methods such as *managed*

pressure drilling (MPD) (Godhavn, 2010; Godhavn et al., 2011) brings along new instrumentation to the rig, which allows one to have methods for detecting abnormal situations. One such situation is *drillstring washout*, which will be studied in this paper. A drillstring washout is a hole or cracks in the drillstring caused by wear, such as corrosion or tensile stress (Bert et al., 2009). Such weakness can result in a complete twist-off of the pipe, which may cause an extra three to twelve days of drilling, in worst case abandonment of the well (Macdonald and Bjune, 2007). Early yet sure diagnosis of a drillstring washout is essential. The challenge is that a small washout gives tiny changes in pressure and flow rate of the circulated drilling fluid, and is difficult to detect in noisy measurements signals. In addition to detecting the occurrence of the washout it is of great value to isolate the position of the defect, making inspection and replacement more effective.

Detection of other critical incidents have been studied using different detection methods. Probably the most studied case is an influx of formation fluid, or *kick*, see Hargreaves et al. (2001); Gravdal et al. (2010a); Cayeux et al. (2012b); Hauge et al. (2013). Others are *lost circulation* of drilling fluid to the formation, *pack-off* of drilling cuttings around the drillstring, and *plugging* of the drill bit nozzles. All of these will affect drilling operation. Simulation and detection of different downhole drilling incidents, including drillstring washout, were discussed in Cayeux et al. (2012a) with some tests on real data in Cayeux et al. (2012b). There a high fidelity model was fitted to data and used to detect abnormalities. Knowledge-modeling was used for classification of different incidents by Skalle et al. (2013) and a Bayesian network was shown to detect sensor and process faults in Ambrus et al. (2013).

A challenge with monitoring and diagnosis of downhole conditions in drilling is the lack of measurements. Most commonly, low frequency measurements with mud pulse telemetry from the downhole assembly has been available (Godhavn, 2010). With high data rate, low latency transmission from downhole sensors, actions can be taken at an earlier stage in order to avoid borehole stability problems (Dalton et al., 2003). Recently, *wired drill pipe technology* has emerged as a technology with distributed sensors along the drillstring, providing measurements at high sample rate in real time (Godhavn, 2010; Veeningen et al., 2012).

Although increased instrumentation facilitates increased diagnosis, there are still problems with measurement noise. Different statistical methods can be applied in order to increase detection. In Hargreaves et al. (2001), a statistical cumulative sum (CUSUM) algorithm was applied in order to increase kick detection while maintaining a low false alarm rate. In Gulsrud et al. (2009), skewness of the statistical distribution was used to detect poor hole cleaning. An adaptive observer for friction estimation was presented in Willersrud and Imsland (2013) and applied on data in Willersrud et al. (2013b), but direct washout diagnosis was not feasible due to very poor signal to noise properties on the parameter estimates.

This paper proposes to use statistical change detection methods to diagnose downhole drilling incidents. The focus is on drillstring washout. The proposed method, depicted in Fig. 3.1, consists of using a reasonably simple mathematical model together with a nonlinear adaptive observer to estimate a set of friction

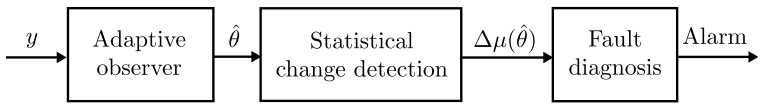

Figure 3.1: Overview of fault diagnosis method using an adaptive observer and statistical change detection for fault diagnosis, where y are measurements, $\hat{\theta}$ are estimated parameters, and $\Delta\mu(\hat{\theta})$ is the change in mean of the estimated parameters.

parameters and combine this with dedicated change detection. The estimated parameters will remain (close to) constant during normal operation, but change when there is a washout in the system. Data from a medium scale flow loop designed and tested by the oil and gas company Statoil ASA is used to test the diagnosis method. Due to noise in the measurements the friction estimates are shown to be noticeably affected. Detection and isolation possibilities are studied using the changes that develop in estimated parameters during a washout. Dedicated change detection algorithms are derived for the multivariate t-distribution that is observed from data, based on a generalized likelihood ratio test (GLRT) approach. A GLRT for each parameter is tested against a threshold using univariate probability distributions of the noise, and changes to all parameters jointly can be considered using multivariate distributions. Detectors are derived for both univariate and multivariate distributions and their performances are compared.

Referring to Fig. 3.1, the scope of the paper is as follows. Sec. 3.2 presents the test rig and test scenarios, Sec. 3.3 presents the nonlinear dynamic model of the process, and the nonlinear adaptive observer used for parameter estimation (first block in the figure). Sec. 3.4 motivates the need for statistical change detection, and Sec. 3.5 presents an analysis of the noise distribution of the estimated parameters. A dedicated diagnosis scheme is derived in Sec. 3.6 for the multivariate t-distribution at hand (second block), and isolation of the washout position is analyzed in Sec. 3.7 (third block). Findings are validated using experimental data in Sec. 3.8. A discussion and conclusion completes the paper.

3.2 Flow-loop test facility

To test the diagnosis methodology, we will use data from tests on managed pressure drilling technology conducted by Statoil in a 1400 m horizontal flow loop test setup at premises of the International Research Institute of Stavanger (IRIS), Norway. The flow loop was rigged with the possibility of emulating various faults including drillstring washout.

Fig. 3.2 shows a schematics with drillstring washout highlighted, and parts of the physical setup is shown in Fig. 3.3. Water is used as drilling fluid and pumped by a piston rig pump with flow rates in the range of 0–2000 L/min (0–0.033 m^3/s). The drill bit consists of three parallel valves, and the pipes are 700 meter circular steel pipes of 0.124 m and 0.155 m inner diameter, for drillstring and annulus respectively.

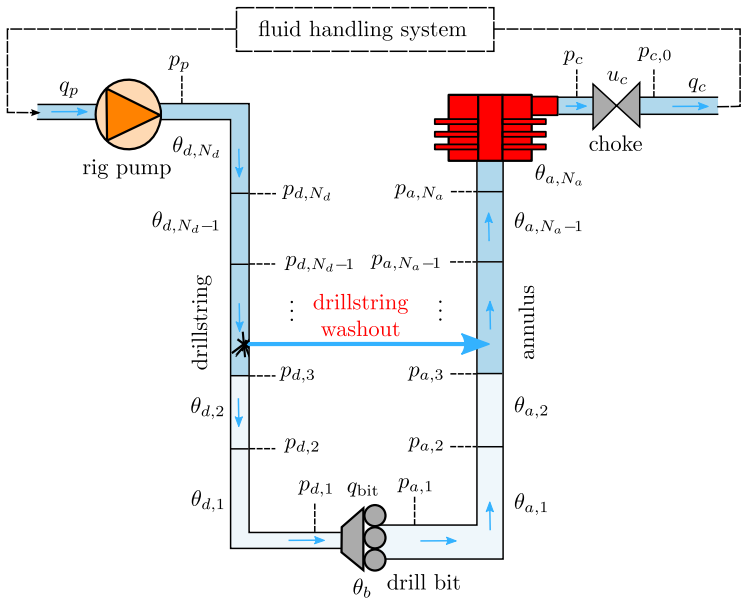

Figure 3.2: Drilling system with measurements p, q, choke opening u_c, and friction parameters θ. A drillstring washout is a leakage from the drillstring to the annulus, resulting in less flow in the lower part of the system and drill bit.

The flow loop is instrumented with topside measurements including standpipe and choke pressure, and pump and choke flow. Four pressure sensors in the annulus and one in the drillstring, upstream the bit, emulate a wired drill pipe. The technology quality for wired drill pipe pressure sensors is presently not as good as the pressure sensors used in the flow loop. Whether the accuracy is sufficient for the use we propose here, has not been investigated.

Although the flow loop is designed to capture key dynamics in a real drilling circulation system, there are some obvious differences. Since the loop is horizontal, the effects of gas expanding as the gas is percolating up the annulus will not be captured. Other differences is lack of annular effects and drillstring rotation. Cuttings (crushed formation rocks) transportation is also not included. However, the flow loop uses pumps and chokes that are used in real drilling, and measurements will be affected by bias and noise as at a real rig.

Data from a series of tests carried out by Statoil at the test rig is used to test the fault diagnosis method. Even though several incidents are tested, for clarity of presentation only the drillstring washout case will be used in this paper. Diagnosis of other incidents is the topic in Willersrud et al. (2015d). Drillstring washout is a challenging case with small changes to pressure due to friction, without any net change of flow in and out of the well. To emulate drillstring washout, a valve located half way along the flow loop was gradually open, releasing the flow from the drillstring section of the flow loop to the annulus section.

Figure 3.3: Flow-loop setup components for drillstring washout and gas injection (left) and for drill bit nozzles (right).

Table 3.1: Flow-loop physical parameters.

$\beta_{d,a}$	2.2×10^9 Pa	Effective bulk modulus
$\rho_{d,a}$	$1000\,\mathrm{kg/m^3}$	Drilling fluid density
M_a	3.74×10^7 Pa $\mathrm{s^2/m^3}$	Integrated density per cross section
M_d	5.81×10^7 Pa $\mathrm{s^2/m^3}$	Integrated density per cross section
V_a	$13.2\,\mathrm{m^3}$	Volume of fluid in annulus
V_d	$8.56\,\mathrm{m^3}$	Volume of fluid in drillstring
h_{TVD}	2.14 m	True vertical depth of bit
L_d, L_a	700 m	Length of drillstring/annulus

3.3 System model and adaptive observer

The model-based fault diagnosis method in this paper is based on parameter estimation using the simplified hydraulics model in Kaasa et al. (2012) as a process model together with an adaptive observer. As the authors argue, the simple model manages to capture the key components of the flow dynamics in drilling. Furthermore, a high-fidelity model with many parameters may not give a better result in practice, due to challenges in configuration and calibration. However, the simple model has some limitations. In realistic situations, the particular *bottom hole assembly* (tools at the end of the drillstring) used may give other setups near the bottom which may imply that detected changes in friction can be caused by other incidents than those considered herein. Moreover, we assume that the friction pressure loss is in steady state, which means that care must be taken in interpreting detections in periods just after known transients such as changing pump rates, drilling bit off bottom, and change of drillstring rotational velocity.

The simple model has been applied for estimation and control purposes in Hauge et al. (2013); Grip et al. (2010); Zhou et al. (2011); Stamnes et al. (2011a). This section presents the model as well as the adaptive observer utilizing wired drill

pipe measurements. The adaptive observer was derived in Willersrud and Imsland (2013), and used in a preliminary study on fault diagnosis of the flow loop data in Willersrud et al. (2013b), with simpler assumptions about the noise probability distribution, detecting changes to each friction parameter separately.

3.3.1 Simplified hydraulic model

Referring to Fig. 3.2, let p_p be the pressure at the pump, p_c be the pressure upstream the choke, and q_{bit} the flow through the bit. The pump flow is denoted by q_{p}, and q_c is flow through the choke. The model used is based on the model in Kaasa et al. (2012), given by

$$\frac{dp_p}{dt} = \frac{\beta_d}{V_d}(q_p - q_{\text{bit}}), \tag{3.1a}$$

$$\frac{dp_c}{dt} = \frac{\beta_a}{V_a}\left(q_{\text{bit}} - q_c(p_c, u)\right), \tag{3.1b}$$

$$\frac{dq_{\text{bit}}}{dt} = \frac{1}{M}\left(p_p - p_c - F(\theta, q_{\text{bit}}) - (\rho_a - \rho_d)gh_{\text{TVD}}\right), \tag{3.1c}$$

where ρ_j is the density, V_j the volume, and β_j the bulk modulus of the control volume indexed $j \in \{d, a\}$ for drillstring and annulus, respectively. The true vertical depth of the well is h_{TVD}, g is the acceleration of gravity, and the integrated fluid density per cross section is $M = \int_0^L \frac{\rho(x)}{A(x)}dx$ where L is the total length from pump to choke, and $A(x)$ is the cross section at position x. The unknown friction parameter vector θ is estimated by the adaptive observer. The total friction is modeled by

$$F(\theta, q) = \theta_b f_b(q) + \sum_{i=1}^{N_d} \theta_{d,i} f_d(q) + \sum_{i=1}^{N_a} \theta_{a,i} f_a(q), \tag{3.2}$$

where $f_d(q)$, $f_b(q)$, and $f_d(q)$ model the flow characteristics in the drillstring, bit, and annulus, respectively, and θ is a vector of assumed constant friction parameters to be estimated. The friction is more accurately modeled by complex models depending on well geometry and the non-Newtonian properties of drilling fluids, but in the spirit of simple models to be updated by measurements, we will here assume that $f(q)$ is given by $f(q) = q$ for laminar flow and $f(q) = q^2$ for turbulent flow. The flow through the choke is given by

$$q_c(p_c, u) = \text{sgn}(p_c - p_{c,0}) g_c(u_c) \sqrt{|p_c - p_{c,0}|}, \tag{3.3}$$

where $g_c(u_c)$ is the choke characteristics found empirically for choke opening $u_c \in [0, 100]$, $p_{c,0}$ is the pressure downstream the choke.

Wired drill pipe technology extends the number of pressure measurements downhole. Let $p_{d,i}, i \in \{1, \ldots, N_d\}$ be the measurements in the drillstring, and $p_{a,i}, i \in$

$\{1, \ldots, N_a\}$ in the annulus, see Fig. 3.2. The pressure difference is a function of friction and hydrostatic pressure,

$$p_{d,i} = p_{d,i+1} - \theta_{d,i} f_d(q) + G_{d,i}, \tag{3.4a}$$
$$p_{a,i} = p_{a,i+1} + \theta_{a,i} f_a(q) + G_{a,i}, \tag{3.4b}$$

where $G_{j,i} = \rho_j g(h_{j,i} - h_{j,i+1})$ is the hydrostatic pressure difference between sensor $p_{j,i}$ at depth $h_{j,i}$ and sensor $p_{j,i+1}$ at depth $h_{j,i+1}$. The corresponding friction between the sensors is given by $\theta_{j,i} f_j(q)$, where $\theta_{j,i}$ is the constant friction parameter and $f_j(q)$ is the flow characteristics in the drillstring and annulus, respectively. For typical flow rates in the test rig the Reynolds number is large enough to indicate turbulent flow in both drillstring and annulus, giving $f_d(q) = f_a(q) = q^2$, which also was found empirically in Willersrud et al. (2015d). The pressure drop over the drill bit is given by

$$p_{a,1} = p_{d,1} - \theta_b f_b(q), \tag{3.5}$$

where θ_b is the friction parameter in the drill bit. The flow characteristics $f_b(q)$ is typically given by $f_b(q) = q^2$, see, e.g., Bourgoyne Jr. et al. (1986).

3.3.2 Nonlinear adaptive observer

Estimation of parameters in the nonlinear system could be achieved by extensions to the extended Kalman filtering (EKF) techniques that estimate noise covariance online and hence would not need knowledge of noise and process disturbance covariances. This is described for linear systems in Ljung (1979), and Zhou and Blanke (1989) extended the EKF to continuous nonlinear systems with discrete time measurements. Also the later particle filter approaches could be applied. Here, a nonlinear observer approach is used that is based on deterministic stability analysis but still relies on persistent excitation to get parameter convergence.

An adaptive observer for system (3.1) was suggested in Willersrud and Imsland (2013) and is repeated here for completeness. The model is developed such that all states are measured, and such that the friction parameters, θ, are unknown but constant (on the time scale considered here) in the fault-free case. The system (3.1) can be written as

$$\dot{x} = \alpha(x, u) + \beta(x)\theta, \tag{3.6a}$$
$$z = \eta(x, z) + \lambda(x)\theta, \tag{3.6b}$$

where $x(t) \in \mathbb{R}^{N_x}$ are the states, $z(t) \in \mathbb{R}^{N_z}$ are the additional measurements, $u(t) \in \mathbb{R}^{N_u}$ are the inputs, $\theta \in \mathbb{R}^{N_\theta}$ are unknown parameters, and $\alpha(x, u) \in \mathbb{R}^{N_x}$, $\beta(x) \in \mathbb{R}^{N_x \times N_\theta}$, $\eta(x, z) \in \mathbb{R}^{N_z}$ and $\lambda(x) \in \mathbb{R}^{N_u \times N_\theta}$ are locally Lipschitz functions. The observer is based on a nonlinear observer in Besançon (2000), adapted to the system representation (3.6) with additional measurements z. It is assumed that z in (3.6b) is given explicitly.

Specifically, the system (3.1) with measurements (3.4) written on the form (3.6) will have system vectors and matrices

$$x = \begin{bmatrix} p_p,\ p_c,\ q_{\text{bit}} \end{bmatrix}^\top,\ u = \begin{bmatrix} q_p,\ u_c \end{bmatrix}^\top, \tag{3.7a}$$

$$z = \begin{bmatrix} p_{d,1},\ \ldots,\ p_{d,N_d},\ p_{a,1},\ p_{a,1},\ \ldots,\ p_{a,N_a} \end{bmatrix}^\top, \tag{3.7b}$$

$$\theta = \begin{bmatrix} \theta_{d,1},\ \ldots,\ \theta_{d,N_d},\ \theta_b,\ \theta_{a,1},\ \ldots,\ \theta_{a,N_a} \end{bmatrix}^\top, \tag{3.7c}$$

$$\alpha(x,u) = \begin{bmatrix} \frac{\beta_d}{V_d}(u_1 - x_3) \\ \frac{\beta_a}{V_a}(x_3 + u_2 - q_c(x_1,u_3)) \\ \frac{1}{M}(x_1 - x_2 - (\rho_a - \rho_d)g h_{\text{TVD}}) \end{bmatrix}, \tag{3.7d}$$

$$\beta(x) = \begin{bmatrix} 0 & & 0 \\ 0 & \cdots & 0 \\ -\frac{1}{M}x_3^2 & & -\frac{1}{M}x_3^2 \end{bmatrix}, \tag{3.7e}$$

$$\lambda(x) = \begin{bmatrix} -x_3^2 & & \\ & \ddots & \\ & & x_3^2 \end{bmatrix}, \tag{3.7f}$$

$$\eta(x,z) = \begin{bmatrix} z_2 + G_{d,1},\ \ldots,\ z_{N_d} + G_{d,N_d-1},\ x_1 + G_{d,N_d},\ z_1, \\ z_{N_d+3} + G_{a,1},\ \ldots,\ z_{N_d+N_a+1} + G_{a,N_a-1},\ x_2 + G_{a,N_a} \end{bmatrix}^\top. \tag{3.7g}$$

Theorem 3.1 (Willersrud and Imsland (2013))**.** *Given an observer on the form*

$$\dot{\hat{x}} = \alpha(x,u) + \beta(x)\hat{\theta} - K_x(\hat{x} - x), \tag{3.8a}$$

$$\dot{\hat{\theta}} = -\Gamma\beta^\top(x)(\hat{x} - x) - \Lambda\lambda^\top(x)(\hat{z} - z), \tag{3.8b}$$

$$\hat{z} = \eta(x,z) + \lambda(x)\hat{\theta}, \tag{3.8c}$$

where $K_x, \Lambda, \Gamma > 0$ are tuning matrices, and with $\dot{\theta} = 0$. Let $e_x = \hat{x} - x$ and $e_\theta = \hat{\theta} - \theta$ be variables for the error dynamics, where $e = \begin{bmatrix} e_x^\top,\ e_\theta^\top \end{bmatrix}^\top = 0$ is an equilibrium point. Then $e = 0$ is globally exponentially stable if

$$\Gamma^{-1}\Lambda\lambda^\top(\cdot)\lambda(\cdot) - \beta^\top(\cdot)K^\top K\beta(\cdot) > kI_{N_\theta}, \tag{3.9}$$

for some constant $k > 0$, where $K = \frac{1}{2}(I_{N_x} - K_x^{-1})$, and $I_N \in \mathbb{R}^{N\times N}$ is the identity matrix.

The proof of Thm. 3.1 is given in Willersrud and Imsland (2013) and is based on a Lyapunov function for the error dynamics (see also, e.g., Besançon (2000); Rajamani and Hedrick (1995)). Note that if $\beta(\cdot)$ is bounded and $\lambda^\top(\cdot)\lambda(\cdot) > 0$, there exist some tuning parameters K_x, Γ and Λ such that (3.9) is fulfilled. The matrix function $\beta(\cdot)$ is bounded as the physical flow $x_3 = q_{\text{bit}}$ through the system always will be bounded, while $\lambda^\top(\cdot)\lambda(\cdot) > 0$ can be interpreted as a requirement for persistence of excitation and will be fulfilled whenever there is flow through the well. If $\Gamma > 0$ and $\Lambda > 0$ are fixed, it can be seen from (3.9) that there is a maximum value of $K^\top K$, thus a minimum and maximum value of K_x, with $K^\top K$

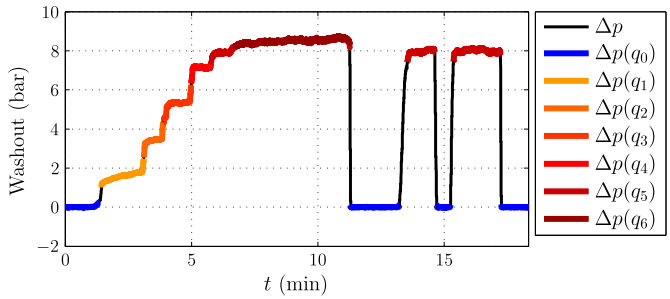

Figure 3.4: Actual washout in experiment measured over washout emulation valve, measured as pressure loss at different flow rates $\{q_0, \ldots, q_6\}$. The color coding shown to the right shows the pressure drop $\Delta p(q_i)$ for each flow rate q_i, where higher flow rates give higher pressure drop. This information is *not* known to the diagnosis methods, but shown for reference.

smallest for $K_x = I_{N_x}$. Furthermore, (3.9) shows that there is a lower bound on $\Gamma^{-1}\Lambda$ as a function of K_x, $\beta(\cdot)$ and $\lambda(\cdot)$, where increasing Λ and Γ gives higher noise magnification, while lowering them gives slower parameter updates. Since these estimates are used for detection, it is desirable with fast updates of estimated parameters after a change, giving requirements on the tuning matrices. Noise in the estimates is hence inevitable.

3.3.3 Estimating parameters from flow-loop measurements

The adaptive observer (3.8), with system vectors and matrices (3.7) is applied on data from the flow-loop experiments sampled at 10 Hz, during a time interval when a drillstring washout is occurring. The actual washout in the experiment is plotted in Fig. 3.4, measured as a pressure drop over an opened valve. This information is *not* known to the detection algorithm, but shown for reference. As described in Sec. 3.2, the test setup has $N_a = 4$ pressure measurements in the annulus and $N_d = 1$ pressure measurements in the drillstring. For appropriate scaling in the model, bar is used as unit for pressures, and L/s for flow rates. All parameters in Tab. 3.1 are scaled accordingly. The observer is initialized with $\hat{x}(0) = \begin{bmatrix}16, & 5, & 15\end{bmatrix}^\top$, $\hat{\theta}(0) = 10^{-4} \times \begin{bmatrix}9.7, & 23.5, & 1.7, & 0.24, & 0.34, & 4.9\end{bmatrix}^\top$, and configured with the parameters listed in Tab. 3.1. The observer gains are chosen such that (3.9) is fulfilled and with sufficiently fast response of the observer such that a stepwise change in a friction parameter could be tracked with a rise time of 1 s. The values used are $K_x = \mathrm{diag}(3, 3, 3)$, $\Gamma = \Lambda = 5 \times 10^{-5} \times \mathrm{diag}(1, 1, 10, 10, 10, 10)$, where 'diag' denotes a diagonal matrix.

The estimated topside pump pressures p_p and p_c are shown in the upper panel of Fig. 3.5, and the flow through the bit in the lower panel. Both pressures are directly measured, giving good estimates as expected. The flow through the bit q_{bit} is not measured. By ignoring flow dynamics in the drillstring, bit flow can be

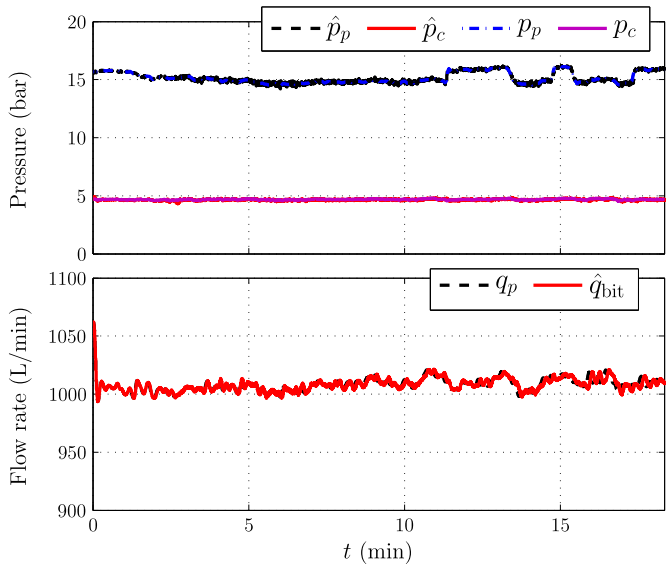

Figure 3.5: State estimation and measurements of pump pressure (p_p), choke pressure (p_c), and bit flow/pump flow (q_{bit}/q_p) during a washout. The flow rate and choke pressure is constant, while the pump pressure decreases during the washout due to reduced friction in the system.

assumed equal to the pump flow, $q_{\text{bit}} = q_p$. This assumption is no longer valid during a washout, resulting in a change in estimated parameters $\hat{\theta}$. The estimated parameters are shown in Fig. 3.6. These plots show that the effect of a washout is visible in the parameters $\hat{\theta}_d$ and $\hat{\theta}_b$, but much less in $\hat{\theta}_{a,1}, \ldots, \hat{\theta}_{a,4}$. The latter are essential to isolate the washout location.

3.4 Statistical change detection

Detecting change of parameters in a linear system is a classical problem in statistics. An overview of methods that are applicable for linear systems with Gaussian noise is provided in Basseville and Nikiforov (2002). When the quantities for which change detection are desired have non-Gaussian distributed noise, the change detection problem is harder but solvable. When the quantities under test are time-wise correlated and non-Gaussian, tests can be achieved but analytical methods may not be available to determine thresholds that give desired false alarm and detection probabilities.

A widely applied methodology is based on a likelihood ratio test, which maximizes the probability of detection P_D with a given false alarm probability P_{FA} (Kay, 1998). The test will differentiate between the *null hypothesis* $\mathcal{H}_0$ and the *alternative hypothesis* $\mathcal{H}_1$ using the probability density function (PDF) under each hypothesis.

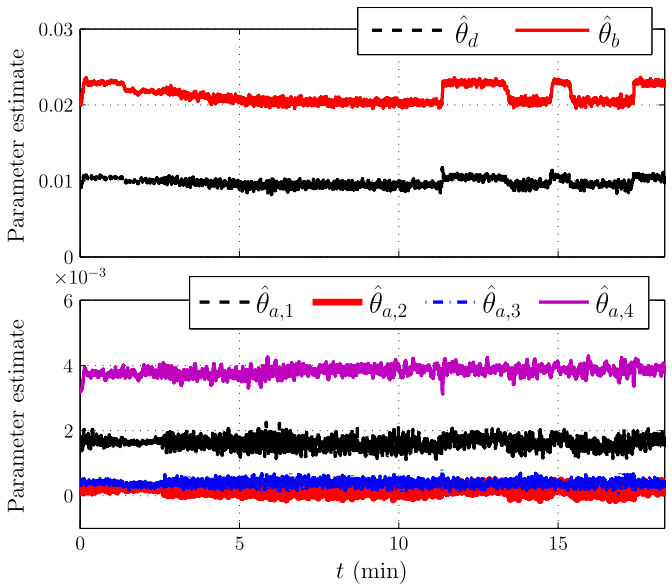

Figure 3.6: Estimated parameters $\hat{\theta}_d$, $\hat{\theta}_b$ and $\hat{\theta}_{a1}$ to $\hat{\theta}_{a4}$.

If the statistical parameters under $\mathcal{H}_1$ are unknown, the generalized likelihood ratio test (GLRT) can be applied.

The proposed method in this paper is to use parameter estimation to track physical changes in friction. With noise in the measurement, and with desired fast detection, parameter estimates are inevitably subjected to random variation. Thus is statistical change detection used to obtain desired false alarm rate and detection properties. Statistical change detection furthermore gives us isolation capability with known statistical properties. Methods for statistical change detection in fault diagnosis were applied in Galeazzi et al. (2013); Hansen and Blanke (2014) and applications are referred in Hwang et al. (2010) where GLRT was employed for detecting change in estimated parameters.

The need for statistical change detection is illustrated by inspecting $\hat{\theta}_d$ and $\hat{\theta}_b$ plotted in Fig. 3.6, which are affected the most by a drillstring washout. Fig. 3.7 shows the fault free case $\mathcal{H}_0$, and the fault-case $\mathcal{H}_1(q_i)$ for different washout flow rates q_i, see Fig. 3.4. The contour lines show two and three standard deviations calculated as if data were Gaussian. The upper plot illustrates that the small washout flow rate q_1 is difficult to detect from the parameters while keeping the false alarm rate low. For the friction parameters $\hat{\theta}_{a,1}$ and $\hat{\theta}_{a,2}$ in the annulus in the lower plot in Fig. 3.7, it is not possible to distinguish the different cases. Without a statistical change detection approach, it may be possible to detect a washout through change in $\hat{\theta}_d$ and $\hat{\theta}_b$, albeit with poor false alarm versus detection performance, but it would not be possible to determine the washout position.

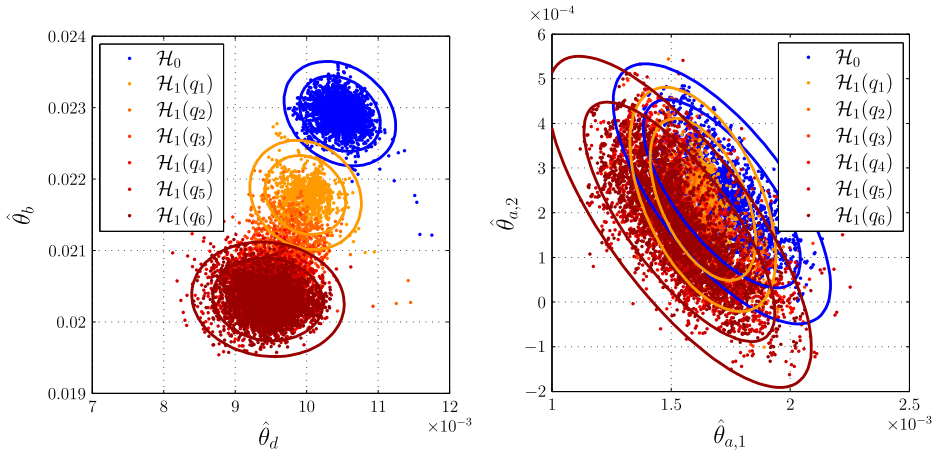

Figure 3.7: Scatter plot of estimated parameters without washout ($\mathcal{H}_0$), and with different flows of washout ($\mathcal{H}_1(q_i)$), where flow rates are corresponding to the washout pressure drop shown in Fig. 3.4. Ellipsoids show 2σ and 3σ for no washout (blue), minimum (yellow) and maximum washout (dark red).

3.5 Probability distribution

The statistical change detection algorithm presented in Sec. 3.6 utilizes the probability density function (PDF) of the noise in order to detect a change. With a vector of estimated parameters $\hat{\theta}$, it is possible to detect a change in each parameter isolated, using *univariate* distributions, or to jointly detect change in the *multivariate* distribution. The different distributions will be presented in this section.

3.5.1 Probability distribution of estimated parameters

Most commonly the noise of a signal is assumed to be independent, identically distributed (IID) Gaussian white noise. However, if the noise of the signal has heavier tails it will be more accurately represented with another distribution. The estimated parameters are nonlinear functions of the measurements, which are not independent due to the nature of the observer, where the innovations are integrated from one time step to the next. For most distributions, it is rather difficult to find analytical expressions for the *likelihood ratio* $L(x)$ over a window N,

$$L(x) = \frac{f(x_{k-N+1}, \dots x_k; \mathcal{H}_1)}{f(x_{k-N+1}, \dots x_k; \mathcal{H}_0)} = \frac{f(x_k; \mathcal{H}_1 | x_{k-1}, \dots x_{k-N+1}) \cdots f(x_{k-N+1}; \mathcal{H}_1)}{f(x_k; \mathcal{H}_0 | x_{k-1}, \dots x_{k-N+1}) \cdots f(x_{k-N+1}; \mathcal{H}_0)}, \quad (3.10)$$

if the signal is non-white, since conditional probabilities would have to be included. If the signal has non-white noise, a whitening filter can be applied in order to get close to white noise. IID Gaussian noise for $\hat{\theta}$ was assumed in Willersrud et al. (2013b), whereas a closer look on the distribution after white-filtering will be studied in this paper.

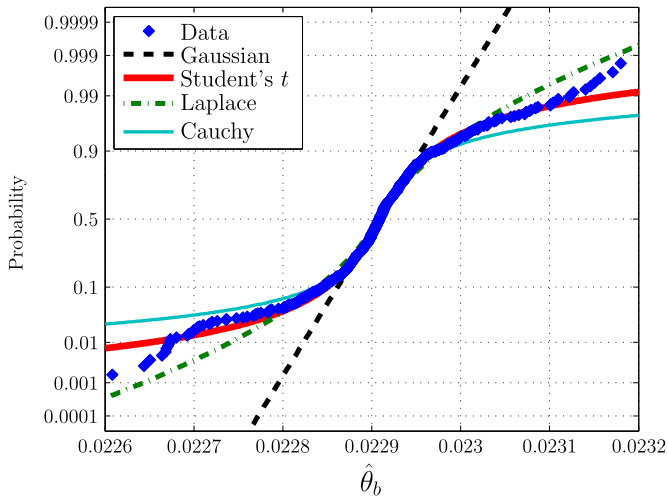

Figure 3.8: Normal probability plot of white-filtered estimated parameter $\hat{\theta}_b$ for different distributions. Data plotted in blue.

To find a candidate distribution, the cumulative distribution of the white-filtered estimated parameter $\hat{\theta}_b$ is plotted as illustration in the probability plot in Fig. 3.8 for different distributions. The dashed straight line represents the Gaussian cumulative distribution function (CDF), whereas the heavier-tails distributions, such as the Student t, Laplace and Cauchy will have a curved profile. Laplace and Cauchy distributions have been applied in other detection problems in Hansen and Blanke (2014, 2012). Comparing with the estimated parameter in blue, these heavier tail-distributions clearly better fit the data. The Kolmogorov-Smirnov test p-values of the white-filtered estimated parameters for the different distributions are given in Tab. 3.2. Here only Student t and Cauchy distributions have a p-value above 0.05 for all estimated parameters, which is a typical threshold used to reject the hypothesis that data have the corresponding distribution. Due to the high p-value for the Student t-distribution, this is chosen as best fit, although the Cauchy distribution could also be a candidate.

Table 3.2: p-value for different distributions.

Parameter	Gaussian	Student t	Laplace	Cauchy
$\hat{\theta}_d$	$\sim 10^{-10}$	0.57 ($\nu = 2.2$)	0.14	0.16
$\hat{\theta}_b$	$< 10^{-12}$	0.94 ($\nu = 2.1$)	0.069	0.14
$\hat{\theta}_{a1}$	$< 10^{-12}$	0.26 ($\nu = 1.8$)	0.0024	0.28
$\hat{\theta}_{a2}$	$< 10^{-12}$	0.58 ($\nu = 1.7$)	0.075	0.17
$\hat{\theta}_{a3}$	$\sim 10^{-8}$	0.58 ($\nu = 2.4$)	0.38	0.16
$\hat{\theta}_{a4}$	$< 10^{-12}$	0.44 ($\nu = 1.6$)	0.0031	0.49

3.5.2 p-variate t-distribution

Generally, the p-variate t-distribution with center μ, correlation matrix S, and degrees of freedom $\nu > 0$ has the joint probability density function

$$f(x;\mu,S,\nu) = \frac{\Gamma((p+\nu)/2)}{\Gamma(\nu/2)(\pi\nu)^{p/2}|S|^{1/2}} \left[1+\frac{1}{\nu}(x-\mu)^\top S^{-1}(x-\mu)\right]^{-\frac{p+\nu}{2}}, \tag{3.11}$$

where $\Gamma(z) = \int_0^\infty t^{z-1}e^{-1}dt$ is the Gamma function. For $\nu > 1$, $\mathrm{E}(x) = \mu$, for $\nu > 2, \mathrm{Var}(x) = S\nu/(\nu-2)$ (Kotz and Nadarajah, 2004).

If each parameter is considered individually, a univariate t-distribution with $p = 1$ can be used to represent the distribution of the estimated parameters. If changes to all parameters are considered simultaneously, the $p = N_\theta$ multivariate distribution will have to be used.

The degrees of freedom ν in the univariate Student t-distribution are also listed in Tab. 3.2 for each estimated parameter. Note that the if $\nu = 1$, (3.11) is the p-variate Cauchy distribution. If $\nu \to \infty$, (3.11) is the p-variate Gaussian distribution (Kotz and Nadarajah, 2004).

3.6 Generalized likelihood ratio test

The size of the washout affects the magnitude of change in the friction parameters, but the magnitude of change is unknown. A generalized likelihood ratio test (GLRT) can hence be applied for change detection. The GLRT utilizes the distribution of the noise in the estimated parameters to best fit a t-distribution. In this section, the GLRT for univariate distributions is described, together with multivariate distributions where the direction of change is assumed known or unknown, respectively.

Change detection for parameters with Gaussian noise were thoroughly treated in Basseville and Nikiforov (2002), a GLRT detector was derived for Cauchy distributed test quantities in Blanke and Hansen (2013), but a GLRT detector for the t-distribution has not been found in the literature.

3.6.1 GLRT with univariate Student t-distribution

To detect changes in the vector of estimated friction parameters, changes to each parameter can be considered independently, using a generalized likelihood ratio test with univariate Student t-distributions. The detection problem is to differentiate whether a signal x belongs to the null hypothesis $\mathcal{H}_0$ or the alternative hypothesis $\mathcal{H}_1$. If only the statistical parameter μ changes, whereas σ and ν are assumed constant, the detection problem with $\hat{\theta} \in \mathbb{R}$ is

$$\mathcal{H}_0: \quad \hat{\theta} \sim t(\mu_0, \sigma, \nu), \tag{3.12a}$$

$$\mathcal{H}_1: \quad \hat{\theta} \sim t(\mu_1, \sigma, \nu). \tag{3.12b}$$

To reduce computational cost, the window-limited GLRT is used where $0 \leq \tilde{N} < N$ (Willsky and Jones, 1976; Lai, 1995), which is given by

$$g(k) = \max_{k-N+1 \leq j \leq k-\tilde{N}} \ln \frac{\prod_{i=j}^{k} f(\hat{\theta}(i); \hat{\mu}_1, \sigma, \nu)}{\prod_{i=j}^{k} f(\hat{\theta}(i); \mu_0, \sigma, \nu)}, \tag{3.13}$$

where $\hat{\mu}_1$ is the maximum likelihood estimate of the mean μ_1 at $\mathcal{H}_1$, and $f(x; \mu, \sigma, \nu)$ is the univariate PDF (3.11) with $p = 1$.

A change between the hypotheses (3.12) is detected if the decision function $g(k)$ is above a threshold h,

$$\begin{aligned} &\text{if} \quad g(k) \leq h \quad \text{accept} \quad \mathcal{H}_0, \\ &\text{if} \quad g(k) > h \quad \text{accept} \quad \mathcal{H}_1. \end{aligned}$$

With univariate distributions, N_θ decision functions $g(k; \theta_i)$ will have to be checked against corresponding thresholds h_i.

3.6.2 GLRT with multivariate t-distribution and known direction of change

Detecting a change in a multivariate Gaussian distribution where the direction is known but magnitude unknown, is described in Basseville and Nikiforov (1993); Blanke et al. (2006). This is generalized to the multivariate t-distribution in this section, and the derivation is provided in Appendix 3.A.2.

Let the change detection problem with $\hat{\theta} \in \mathbb{R}^{N_\theta}$ be

$$\begin{aligned} \mathcal{H}_0 : &\quad \hat{\theta} \sim t(\mu_0, S, \nu), \\ \mathcal{H}_1 : &\quad \hat{\theta} \sim t(\mu_0 + w\Upsilon, S, \nu), \end{aligned}$$

where w is the change magnitude and Υ is the change direction with $\|\Upsilon\| = 1$, assuming that S and ν are unchanged. The generalized likelihood ratio decision function (Basseville and Nikiforov, 1993; Kay, 1998) is given by

$$g(k) = \max_{k-N+1 \leq j \leq k-\tilde{N}} \ln \frac{\sup_w \prod_{i=j}^{k} f(\hat{\theta}(i); \mu_0 + w\Upsilon, S, \nu)}{\prod_{i=j}^{k} f(\hat{\theta}(i); \mu_0, S, \nu)}. \tag{3.14}$$

With a derivation (see Appendix 3.A.2) similar to that of a multivariate normal distribution in Basseville and Nikiforov (1993); Blanke et al. (2006), the estimate of magnitude of change with distribution (3.11) is

$$\hat{w}(k, j) = \frac{\Upsilon^\top S^{-1} (\bar{\Theta}(k, j) - \mu_0)}{\Upsilon^\top S^{-1} \Upsilon}, \tag{3.15}$$

where

$$\bar{\Theta}(k, j) = \frac{1}{k-j+1} \sum_{i=j}^{k} \hat{\theta}(i). \tag{3.16}$$

The resulting decision function will then be

$$g(k) = \max_{k-N+1\leq j\leq k-\tilde{N}} \frac{p+\nu}{2} \sum_{i=j}^{k} \left[-\ln\left(1+\frac{1}{\nu}(\hat{\theta}(i)-\mu_0-\hat{w}\Upsilon)^\top S^{-1}(\hat{\theta}(i)-\mu_0-\hat{w}\Upsilon)\right) + \ln\left(1+\frac{1}{\nu}(\hat{\theta}(i)-\mu_0)^\top S^{-1}(\hat{\theta}(i)-\mu_0\right)\right]. \quad (3.17)$$

3.6.3 GLRT with multivariate t-distribution and unknown direction of change

If no assumption of direction of change is assumed, the MLE $\hat{\mu}_1$ of the mean at $\mathcal{H}_1$ has to be found. From Appendix 3.A.1, the MLE of the mean μ_1 is given by

$$\hat{\mu}_1 = \frac{1}{k-j+1} \sum_{i=j}^{k} \hat{\theta}(i), \quad (3.18)$$

and the GLR decision function is given by

$$g(k) = \max_{k-N+1\leq j\leq k-\tilde{N}} \frac{p+\nu}{2} \sum_{i=j}^{k} \left[-\ln\left(1+\frac{1}{\nu}(\hat{\theta}(i)-\hat{\mu}_1)^\top S^{-1}(\hat{\theta}(i)-\hat{\mu}_1)\right) + \ln\left(1+\frac{1}{\nu}(\hat{\theta}(i)-\mu_0)^\top S^{-1}(\hat{\theta}(i)-\mu_0)\right)\right]. \quad (3.19)$$

3.6.4 Thresholds based on GLRT test statistic approximated by a Weibull distribution

If the GLRT input was Gaussian and IID, the test statistic $g(k)$ would asymptotically follow a χ^2_r distribution and with r unknown parameters, r degrees of freedom under $\mathcal{H}_0$, and a non-central $\chi'^2_r(\lambda)$ distribution with non-centrality parameter λ under $\mathcal{H}_1$ (Kay, 1998). This would make it possible to set a threshold corresponding to a desired probability of false alarms and of detection. However, for real applications with correlated input, $g(k)$ is not χ^2_r distributed. Distributions seen in real applications depend on properties of the case. A Weibull distribution best fitted residuals from aircraft attitude data in Hansen and Blanke (2014); a lognormal distribution best fitted the GLRT test statistic from narrow band correlated ship motion data in Galeazzi et al. (2013). The distribution of the test statistic is therefore studied in this section, based on real data.

Having tested several possibilities, the Weibull distribution was found to give a good fit to the test statistic. The Weibull distribution has the probability distribution $F(x;\alpha,\beta)$ and the density function $f(x;\alpha,\beta)$, given by

$$F(x;\alpha,\beta) = 1 - e^{-(x/\alpha)^\beta}, \quad x \geq 0, \quad (3.20a)$$

$$f(x;\alpha,\beta) = \frac{\beta}{\alpha}\left(\frac{x}{\alpha}\right)^{\beta-1} e^{-(x/\alpha)^\beta}, \quad x \geq 0, \quad (3.20b)$$

where $\alpha > 0$ is the scale parameter and $\beta > 0$ the shape parameter.

Let P_{FA} be the probability of false alarm under $\mathcal{H}_0$. Then using the inverse CDF gives a threshold h with the given probability P_{FA},

$$h = Q(1 - P_{FA}; \mathcal{H}_0, \alpha_0, \beta_0) = \beta_0 \left(-\ln(P_{FA})\right)^{1/\alpha_0}. \tag{3.21}$$

The given threshold h will also determine the probability of detecting a fault under hypothesis $\mathcal{H}_1$ with probability P_D,

$$P_D = 1 - F(h; \mathcal{H}_1, \alpha_1, \beta_1) = e^{-(h/\alpha_1)^{\beta_1}}. \tag{3.22}$$

3.7 Fault diagnosis

Changes to the different parameters are used to detect a washout and isolate its position. As seen in Fig. 3.2, a washout will decrease the flow in the lower parts of the drillstring and the annulus, as well as in the drill bit. This will result in a decrease in the estimated parameters, since the estimator assumes equal flow throughout the system. Friction changes in the drillstring and bit are considerably higher than in the annulus, and they are thus used for detection. A washout is detected if both $\hat{\theta}_d$ and $\hat{\theta}_b$ have a negative change, as listed in Tab. 3.3. At the position of the washout, the related friction parameter will have a positive change. There will still be some friction loss in this section, however only the pressure sensor in the beginning of the section will be affected by reduced flow. The net effect is an increase in pressure drop in this section, which is used to isolate the washout. The other annular friction parameters must be unchanged or changing in negative direction.

Table 3.3: Fault isolation of drillstring washout with increasing (+), decreasing (−) and unchanged (0) variables. X denotes ignored change in parameter.

	Detection		Isolation			
	$\hat{\theta}_d$	$\hat{\theta}_b$	$\hat{\theta}_{a,1}$	$\hat{\theta}_{a,2}$	$\hat{\theta}_{a,3}$	$\hat{\theta}_{a,4}$
Washout 1 (f_1)	−	−	+	−/0	−/0	−/0
Washout 2 (f_2)	−	−	−/0	+	−/0	−/0
Washout 3 (f_3)	−	−	−/0	−/0	+	−/0
Washout 4 (f_4)	−	−	−/0	−/0	−/0	+
W.o., unknown pos. (f_0)	−	−	X	X	X	X

3.7.1 Isolation based on individual parameter changes with univariate distributions

If changes to each parameter are individually considered, a GLRT on each estimated parameter is used for fault diagnosis. There will be one threshold for each estimated

parameter, determined based on a specified probability P_{FA} of false alarm. Let the possible faults be

$$f_i \in \mathcal{F}, \tag{3.23}$$

where f_i represents a washout between sensor $p_{a,i}$ and $p_{a,i+1}$, corresponding to friction parameter $\theta_{a,i}$, and $\mathcal{F}$ are all possible locations of washout. Location of washout position from friction parameters are listed in Tab. 3.3, based on the changes to friction shown in Fig. 3.2. If the changes in estimated annulus parameters are inconsistent with regards to rows in Tab. 3.3, the position cannot be isolated, although a washout may still detected if $\hat{\theta}_d$ and $\hat{\theta}_b$ have a negative change (f_0).

3.7.2 Isolation in multivariate distribution with known direction of change

If the direction of change is limited to the possible known vectors of change directions $\Upsilon_i \in \mathcal{Y}$, isolation is done by finding the Υ_i with the largest change magnitude w. This will reduce the problem of inconsistent changes to parameters as found in the univariate case in Sec. 3.7.1, due to some parameters being below its threshold.

For each data sample, the largest $\hat{w}(\Upsilon_i)$ is found from (3.15) with fault isolation position

$$f_{\text{isol}} := \arg\max_i \hat{w}(\Upsilon_i) = \frac{\Upsilon_i^\top S^{-1}(\bar{\Theta}(k,j) - \mu_0)}{\Upsilon_i^\top S^{-1} \Upsilon_i}, \tag{3.24}$$

and used to find the value of $g(k)$ in (3.17) with $\hat{w}(\Upsilon_i | i = f_{\text{isol}})$. Hence is it only necessary to calculate $g(k)$ for one type of fault, although (3.15) will have to be calculated for each Υ_i.

3.7.3 Isolation in multivariate distribution with unknown direction of change

In this case, the fault $f_{\text{isol}} \in \mathcal{F}$ can be isolated by finding the largest projection of change in mean $(\hat{\mu}_1 - \mu_0)$ onto the vectors $\Upsilon_i \in \mathcal{Y}$,

$$f_{\text{isol}} = \arg\max_i \frac{\Upsilon_i^\top (\hat{\mu}_1 - \mu_0)}{\Upsilon_i^\top \Upsilon_i}. \tag{3.25}$$

The difference between this method and the known direction case in Sec. 3.7.2 is that $\hat{\mu}_1$ is used explicitly in the decision function $g(k)$, giving the possibility to detect other faults not specified in $\mathcal{Y}$. If the change direction is close to orthogonal to $\mathcal{Y}$, $g(k)$ in (3.19) would still be affected, whereas $\hat{w}$ in (3.15) would be close to zero, giving close to zero value for the decision function (3.17). However, isolation is still dependent on finding the minimum distance to some possible fault vectors, such as $\mathcal{Y}$. Comparing isolation (3.24) and (3.25), the difference is in fact that the changes are scaled with S^{-1} in $\hat{w}$ in (3.17), taking the correlation into account.

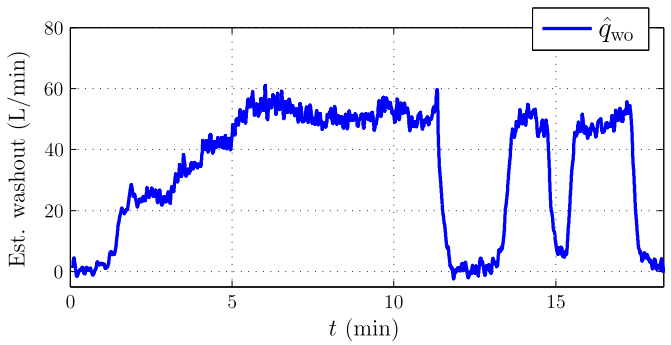

Figure 3.9: Estimated flow rate of drillstring washout. Can not be validated due to lack of measurements.

3.7.4 Estimating washout magnitude

In addition to isolating the position of the washout, described in Sec. 3.7, it is also of great value to get an estimate of the leakage magnitude. During normal operation, the flow through the bit will be equal to the pump flow at steady state, $q_{\text{bit}} = q_p$. During a washout, some of the flow is diverted through the leaking hole, giving $q_{\text{wo}} = q_p - q_{\text{bit}}$ at steady state, where q_{wo} denotes the washout flow rate. Since the observer (3.8) assumes all states measured, including q_{bit}, the estimated friction parameters will change during a washout. Friction loss over the bit will be $\Delta p_{\text{bit}}^{\mathcal{H}_0} = k_{\text{bit}} q_p^2$ with no washout, and $\Delta p_{\text{bit}}^{\mathcal{H}_1} = k_{\text{bit}}(q_p - q_{\text{wo}})^2$ during a washout, where the bit friction parameter k_{bit} is unknown. However, the pressure losses are estimated to be $\Delta \hat{p}_{\text{bit}}^{\mathcal{H}_0} = \hat{\theta}_b^{\mathcal{H}_0} q_p^2$, $\Delta \hat{p}_{\text{bit}}^{\mathcal{H}_1} = \hat{\theta}_b^{\mathcal{H}_1} q_p^2$. An estimate for steady state washout is therefore

$$\hat{q}_{\text{wo}} = q_p \left(1 - \sqrt{\frac{\hat{\theta}_b^{\mathcal{H}_1}}{\hat{\theta}_b^{\mathcal{H}_0}}} \right). \tag{3.26}$$

The estimated washout (3.26) is low-pass filtered and plotted in Fig. 3.9, showing flow rates in the range 0–60 L/min (0–0.001 m^3/s), which is up to 6 % of the total flow. Note that the actual washout plotted in Fig. 3.4 is measured in pressure loss, not in flow rate, and thus cannot be used to validate (3.26), although a significant co-variation can be observed. Furthermore is the estimated washout flow rate only valid if a fault is isolated as a washout. If not, the change in estimated parameter $\hat{\theta}_b$ could have other causes.

3.8 Fault diagnosis based on experimental data

The estimated parameters from the case of drillstring washout are analyzed using the three different methods described in Sec. 3.6 for change detection, namely univariate change detection, multivariate change detection with known direction,

and multivariate change detection with unknown change in mean and unknown direction.

3.8.1 Change in univariate distributions

The first approach is to consider each parameter individually, testing each estimated parameter against a corresponding threshold. As seen in Tab. 3.3, a washout is detected if $\hat{\theta}_d$ and $\hat{\theta}_b$ have a negative change, and the estimated annular parameters $\hat{\theta}_{a,i}$ are used to locate the washout.

The parameters during $\mathcal{H}_0$ are assumed known in the decision function (3.13). However, relevant data for the fault free case before the washout is sparse, hence are the statistical parameters μ_0, σ and ν found by using maximum likelihood estimation of the estimated parameters between 685 and 775 s (11:30 and 13:00 min), and between 1045 and 1100 s in a previous test. The GLRT decision function (3.13) for each estimated parameter is plotted in the two upper panels in Fig. 3.10, using window lengths $N = 150$ samples for detection and $N = 400$ for isolation, with $\tilde{N} = N/4$. To find thresholds, the probability of false alarm is specified to be $P_{FA} = 10^{-5}$ (0.0024 false alarms per hour) for detection and $P_{FA} = 10^{-3}$ (0.09 false alarms per hour) for isolation. Comparing these plots with the actual washout in Fig. 3.4, changes to $\hat{\theta}_d$ and $\hat{\theta}_b$ seem quite easy to detect, with large numerical values of $g(k)$ during a washout and small without it. However, $\hat{\theta}_{a,i}$ are less affected making isolation more challenging, although in a real drilling situation the isolation window could easily be chosen 10 to 20 times larger.

In Fig 3.11, the GLRT of $\hat{\theta}_{a,3}$ with data during $\mathcal{H}_0$ is plotted in a probability plot together with a fitted Weibull distribution. This friction parameter will determine isolation of the washout. Also plotted is data under hypothesis $\mathcal{H}_1$ with washout flow rate q_1 corresponding to a pressure loss between 1 and 2 bar, see Fig. 3.5, and flow rate q_6 with pressure loss of 8 bar. The statistical parameters of the fitted Weibull distributions (3.20a) during $\mathcal{H}_0$, $\mathcal{H}_1(q_1)$ and $\mathcal{H}_1(q_6)$ are listed in Tab. 3.4, also showing the corresponding threshold values and detection probabilities P_D. For convenience, the table shows the missed detection probability $P_M = 1 - P_D$.

Table 3.4: Threshold and probability of detection based on fitted Weibull distributions with parameters α and β, with changes to independent univariate distributions.

	P_{FA}	N	h	α_0	β_0	$\alpha_1(q_1)$	$\beta_1(q_1)$	$\alpha_1(q_6)$	$\beta_1(q_6)$	$P_M(q_1)$	$P_M(q_6)$
$\hat{\theta}_d$	10^{-5}	150	39.0	3.68	1.04	141	4.65	264	8.62	2.54×10^{-3}	$\sim 10^{-9}$
$\hat{\theta}_b$	10^{-5}	150	38.3	3.1	0.971	405	8.07	645	28	$\sim 10^{-10}$	$< 10^{-12}$
$\hat{\theta}_{a,1}$	10^{-3}	400	40.1	6.49	1.06	78.7	4.36	187	4.21	0.0515	1.54×10^{-3}
$\hat{\theta}_{a,2}$	10^{-3}	400	15.7	3.98	1.41	11.5	1.28	65.2	5.56	0.775	3.66×10^{-4}
$\hat{\theta}_{a,3}$	10^{-3}	400	21.8	5.56	1.41	24	1.2	58.3	2.26	0.59	0.102
$\hat{\theta}_{a,4}$	10^{-3}	400	11.0	4.19	2.0	31.9	3.52	4.99	1.61	0.0233	0.972

As illustrated in Fig. 3.11, $\hat{\theta}_{a,3}$ has a quite small value for probability of detection at q_1, meaning that isolation for small washout flow rates is quite uncertain. If P_D was to increase, the threshold should be lower with a penalty in increased P_{FA}.

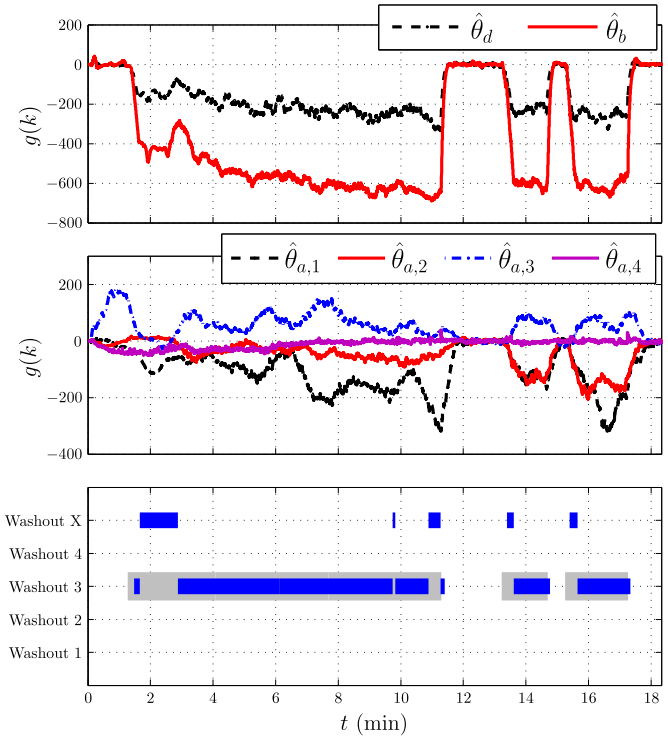

Figure 3.10: Decision function $g(k)$ for each estimated parameter and resulting fault isolation. Actual washout shown in grey.

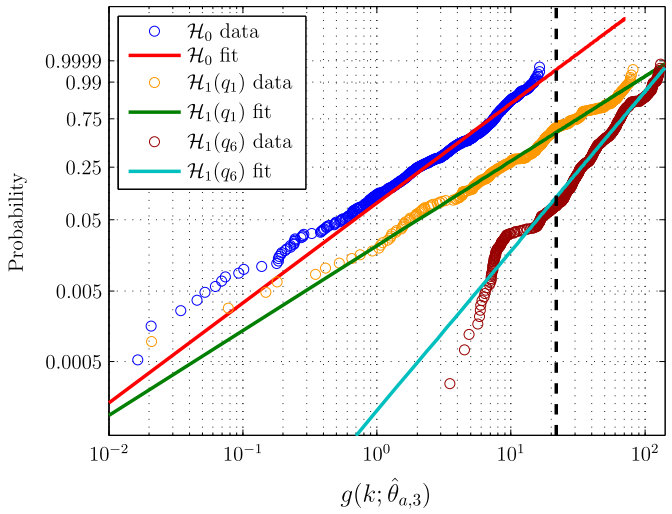

Figure 3.11: Weibull probability plot of GLRT under $\mathcal{H}_0$, $\mathcal{H}_1(q_1)$ and $\mathcal{H}_1(q_6)$ for estimated parameter $\hat{\theta}_{a,3}$ fitted to Weibull distributions. Threshold shown with dashed line.

Using the thresholds listed in Tab. 3.4, the resulting fault isolation is shown in the bottom of Fig. 3.10. Isolation of the position is quite uncertain in the first 3 min where the washout is ramping up (q_1 and q_2). When the washout rate reaches a high level, isolation is quite certain. The reason for no isolation for a short period at around 13 and 15 min is due to a longer window for isolation than for detection, combined with a sudden change in washout flow rate. The estimated $\hat{\theta}_{a,3}$ is above the threshold for the first 2 min, even though there are no faults. The reason is probably due to external factors (disturbances) in the process.

3.8.2 Multivariate distribution with known direction of change

The second case is to use the multivariate distribution, and limit the possible directions of change to a predefined set of vectors $\Upsilon_i \in \mathcal{Y}$, as described in Sec.3.6.2, with isolation as described in Sec. 3.7.2. The assumed possible change directions for detection and isolation are column vectors of

$$\bar{\Upsilon}_{\text{det}} = \begin{bmatrix} -1 \\ -3 \end{bmatrix}, \quad \bar{\Upsilon}_{\text{isol}} = \begin{bmatrix} 1 & -1 & -1 & -1 \\ 0 & 1 & -1 & -1 \\ 0 & 0 & 1 & -1 \\ 0 & 0 & 0 & 1 \end{bmatrix}, \tag{3.27}$$

where $\Upsilon_i = \bar{\Upsilon}_i / ||\bar{\Upsilon}_i||$. The magnitude of the friction parameter in the bit increases approximately three times the magnitude of the friction parameter in the drillstring. It is assumed that all parameters in the annulus are affected equally.

The white-filtered estimated parameters $\hat{\theta}_{\text{det}} \in \mathbb{R}^{N_d+1}$ and $\hat{\theta}_{\text{isol}} \in \mathbb{R}^{N_a}$ are fitted to multivariate t-distributions using the Expectation-Conditional Maximization Either (ECME) algorithm (Liu and Rubin, 1995). The decision functions for detection and isolation are plotted in Fig. 3.12, together with resulting isolation. In the middle panel, the isolation functions $g_{\text{isol}}(k)$ are plotted for each $\Upsilon_i \in \mathcal{Y}$, showing that a washout at position three gives the highest value. Note that isolation is based on maximum $\hat{w}(\Upsilon_i)$ given by (3.24), and thus only one decision function is required to be calculated. Parameter values, thresholds and detection probabilities are listed in Tab. 3.5. The threshold value h for $g_{\text{det}}(k)$ was selected to give a false alarm probability $P_{FA} = 10^{-5}$ from the data under $\mathcal{H}_0$, for isolation $P_{\text{FA}} = 10^{-3}$ is used.

Table 3.5: Threshold and probability of missed detection P_M based on Weibull fit with known change direction Υ of a multivariate distribution.

	P_{FA}	N	h	α_0	β_0	$\alpha_1(q_1)$	$\beta_1(q_1)$	$\alpha_1(q_6)$	$\beta_1(q_6)$	$P_M(q_1)$	$P_M(q_6)$
Detection	10^{-5}	150	65.6	3.81	0.858	527	7.70	782	17.6	$\sim 10^{-7}$	$< 10^{-12}$
Isolation	10^{-3}	400	76.5	14.1	1.14	55.8	1.14	592	14.2	0.761	$\sim 10^{-12}$

No washout is isolated in the first 3 min. The reason may be that changes in the parameters do not correspond directly to the directions (3.27). Furthermore, these directions may not be entirely accurate, where also correlation S affects the change direction (3.15). Compared to the univariate case in Fig. 3.10, accuracy in isolated

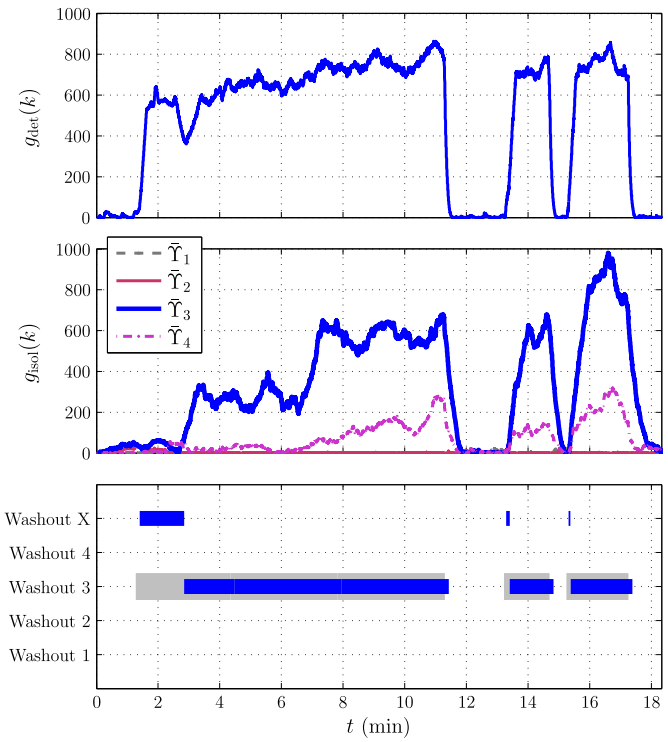

Figure 3.12: Decision function $g(k)$ with known direction of change Υ. Isolation based on largest $\hat{w}$ for each direction of change $\Upsilon_i \in \mathcal{Y}$, with $g(k)$ plotted for each direction. Actual washout shown in grey.

position is increased for higher washout flow rates (after 6 min). The detection probability P_D is higher for the multivariate method, and for higher washout rates the detection probability in isolation is significantly higher (lower P_M).

3.8.3 Multivariate distribution with unknown change in mean and unknown direction

In the third case, no assumption about change direction is made in the decision function, making it sensitive to all changes. Isolation given by (3.25) is done by finding the change in mean closest to possible change vectors, here given by (3.27).

The decision function $g_{\text{det}}(k)$ for the multivariate distribution of $\hat{\theta}_d$ and $\hat{\theta}_b$ is plotted in the top of Fig. 3.13, which is used for detection. The parameters $\hat{\theta}_{a,i}$ are used for isolation, with detection function $g_{\text{isol}}(k)$ plotted in the middle panel. Isolation is plotted in the lower panel. The thresholds are based on fitted data to Weibull probability functions, plotted for $g_{\text{isol}}(k)$ in Fig. 3.14. Comparing with the univariate method in Fig. 3.11, much less of the $\mathcal{H}_1$ data is left of the threshold,

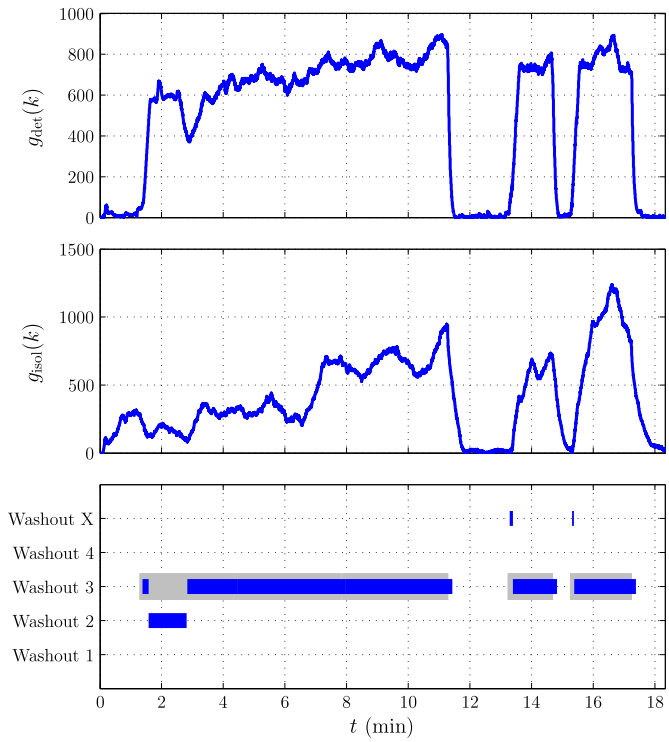

Figure 3.13: Decision function $g(k)$ with unknown change in mean and unknown direction of change. Isolation based on finding change in mean closest to possible change directions $\Upsilon_i \in \mathcal{Y}$. Actual washout shown in grey.

giving better isolation. Parameter values, thresholds and detection probabilities are listed in Tab. 3.6.

With this method a washout is detected almost immediately and is isolated around the 3 min time stamp. The difference between this very successful approach and the previous method is that assumption about direction is only made for isolation. Furthermore, isolation is only done based on changes in mean (3.25), not scaled with S as in (3.24).

Table 3.6: Threshold and probability of missed detection P_M based on Weibull fit with change in μ_1 of a multivariate distribution.

	P_{FA}	N	h	α_0	β_0	$\alpha_1(q_1)$	$\beta_1(q_1)$	$\alpha_1(q_6)$	$\beta_1(q_6)$	$P_M(q_1)$	$P_M(q_6)$
Detection	10^{-5}	150	61.6	6.64	1.10	550	7.11	810	16.5	$\sim 10^{-7}$	$< 10^{-12}$
Isolation	10^{-3}	400	88.5	24.2	1.49	154	5.82	711	7.34	0.0392	$\sim 10^{-7}$

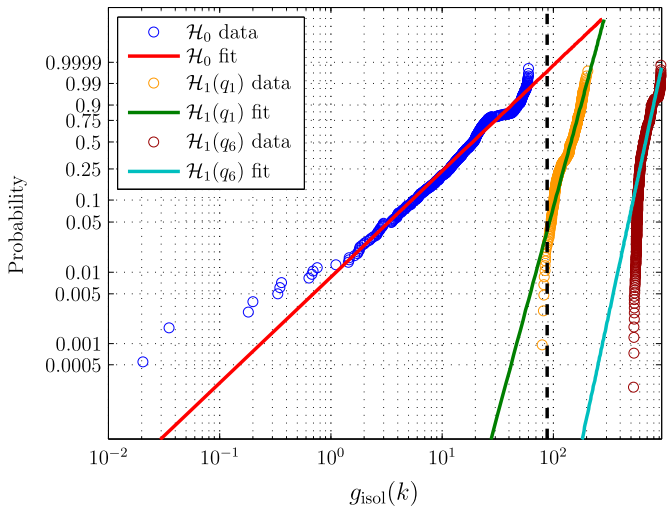

Figure 3.14: GLRT for isolation under $\mathcal{H}_0$, $\mathcal{H}_1(q_1)$ and $\mathcal{H}_1(q_6)$ for multivariate distribution with unknown direction of change, fitted to Weibull distributions in a Weibull probability plot. Threshold shown with dashed line.

3.9 Discussion

The friction model used in the adaptive observer is quite simple, but proved to work satisfactory for the washout case. If the method was to be applied during a large range of pump flow rates and with different drilling fluid densities, a more sophisticated friction model may be required. Nevertheless, for the current process, it has been sufficient in order to provide convincing detection of washout and isolation of the position of the leakage.

Two vector-based (multivariate) methods were compared. Method one, $GLRT_{w\Upsilon}$, assumed a known direction Υ, but unknown magnitude w. The direction vectors were determined from expected changes to the parameters with different washout locations. The second method, $GLRT_{\mu_1}$, assumed an unknown direction and magnitude of change in the vector μ_1.

The main difference between the two multivariate methods was that method one limits detection to already specified fault directions, other faults may not be detected. Method two calculates $g(k)$ based on the new estimated direction of change, and then isolates the position based on already assumed known directions. A disturbance not corresponding to the defined directions would impact the decision function in the second case, but much less in the first. A challenge can be to find the correct change directions. In this study, there was only data from one washout location available, the others are assumed with same structure and values.

Detection was based on both drillstring and bit parameters changing in the negative direction, and probability of detection was clearly best using the multivariate methods.

Isolation was also efficiently done with the multivariate methods, with the multivariate $GLRT_{\mu_1}$ approach being clearly superior in isolation performance. Isolation during the first 3 min was difficult, both due to transients in the system during the test and definitely due to the tiny changes in friction compared to a significant noise level in the parameter estimates. In a real drilling operation, the window size could be 10 min or more instead of the 40 s used here for reasons of the short duration of each washout level during the experiments. The longer isolation window would give significantly better isolation properties while fast detection could still be obtained since different window sizes are used for detection and isolation.

Based on the experiments reported here, it would be feasible to implement a diagnostic method using $\mathcal{H}_0$ data from normal operation to learn a feasible threshold h from test statistic data for given operational conditions. The detection scheme would be sufficiently sensitive to detect and locate a drillstring washout.

The methods presented in this paper have been successfully tested on the difficult drillstring washout case, but are applicable on all downhole incidents during drilling, that would cause detectable changes to friction and flow. This is studied in Willersrud et al. (2015d), detecting and isolating numerous incidents. It is noted that the validation of the proposed method is based on drilling conditions and problems represented by the test rig. In other drilling configurations, the models used for parameter estimation and incident isolation may need to be adjusted. Examples include drilling operation that uses a hole-opener or an under-reamer inside the bottom hole assembly. Such tools have side ports and this would need to be accounted for in the model. The state of cutter arms (extended or retracted) might also need be included in the model and, if a downhole motor is used, the associated bottom leakage at the motor shaft should be included.

3.10 Conclusion

This paper has developed change detection methods for washout detection and localization in oil and gas drilling, and tested the methods on data from a managed pressure drilling test facility. Using estimated friction coefficients in pipe segments as indicators for change, the combination of an adaptive observer to estimate friction parameters and stochastic change detection provides a setup that is able to detect and locate a washout with convincing performance. The parameters were determined to be t-distributed, and generalized likelihood ratio tests were derived for this particular distribution. Different diagnostic algorithms were tested, showing that a multivariate test with unknown change direction and unknown magnitude gave the most accurate detection and isolation as judged from experimental data. The methods presented in this paper are believed to be generic but application to other drilling conditions and problems would require that the model used for parameter estimation and the incident isolation approach are adopted to the specific conditions of the operation.

3.A Appendix

3.A.1 GLRT for unknown change in mean of a multivariate t-distribution

Given a sequence of N IID observations of a vector $z(j)$, $j = k-N+1, ..., k$. Determine whether z most likely belongs to $p(z; \mathcal{H}_0)$ or to $p(z; \mathcal{H}_1)$, where

$$\mathcal{H}_0 : \quad p(z(j)) \sim t(\mu_0, S, \nu), \quad j = k-N+1, ..., k, \tag{3.28}$$

$$\mathcal{H}_1 : \quad p(z(j)) \sim t(\mu_1, S, \nu), \quad j = k-N+1, ..., k, \tag{3.29}$$

where μ_0 is a known vector, μ_1 is unknown, S and ν are known parameters of the multivariate t-distribution (3.11). The generalized likelihood ratio decision function (Basseville and Nikiforov, 1993) is given by

$$\begin{aligned} g(k) &= \max_{k-N+1 \le j \le k} \ln \frac{\sup_{\mu_1} \prod_{i=j}^{k} f(z(i); \mu_1, S, \nu)}{\prod_{i=j}^{k} f(z(i); \mu_0, S, \nu)} \\ &= \max_{k-N+1 \le j \le k} \sup_{\mu_1} G_j^k(\mu_1), \end{aligned} \tag{3.30}$$

detecting a change in mean vector μ from μ_0 to μ_1, with S and ν constant. Using that

$$\frac{f(z(i); \mu_1, S, \nu)}{f(z(i); \mu_0, S, \nu)} = \frac{\left[1 + \frac{1}{\nu}(z(i)-\mu_1)^\top S^{-1}(z(i)-\mu_1)\right]^{-\frac{p+\nu}{2}}}{\left[1 + \frac{1}{\nu}(z(i)-\mu_0)^\top S^{-1}(z(i)-\mu_0)\right]^{-\frac{p+\nu}{2}}}$$

for the multivariate t-distribution with S and ν constant, $G_j^k(\mu_1)$ is given by

$$\begin{aligned} G_j^k(\mu_1) &= \sum_{i=j}^{k} \ln \frac{f(z(i); \mu_1, S, \nu)}{f(z(i); \mu_0, S, \nu)} \\ &= \frac{p+\nu}{2} \sum_{i=j}^{k} \left[-\ln\left(1 + \frac{1}{\nu}(z(i)-\mu_1)^\top S^{-1}(z(i)-\mu_1)\right) \right. \\ &\left. + \ln\left(1 + \frac{1}{\nu}(z(i)-\mu_0)^\top S^{-1}(z(i)-\mu_0)\right) \right]. \end{aligned}$$

The supremum is found by equating $\frac{\partial G_j^k(\mu_1)}{\partial \mu_1}$ to zero, yielding

$$\sum_{i=j}^{k} \frac{\partial}{\partial \mu_1} \ln\left(1 + \frac{1}{\nu}(z(i)-\mu_1)^\top S^{-1}(z(i)-\mu_1)\right) = 0$$

$$\implies \sum_{i=j}^{k} \frac{-2S^{-1}(z(i)-\mu_1)}{\nu + (z(i)-\mu_1)^\top S^{-1}(z(i)-\mu_1)} = 0.$$

Hence is the maximum likelihood estimate (MLE) of the mean μ_1 given by

$$\hat{\mu}_1 = \frac{1}{k-j+1} \sum_{i=j}^{k} z(i), \tag{3.31}$$

and the GLRT decision function

$$g(k) = \max_{k-N+1 \le j \le k} \frac{p+\nu}{2} \sum_{i=j}^{k} \left[-\ln \left(1 + \frac{1}{\nu} (z(i)-\hat{\mu}_1)^\top S^{-1} (z(i)-\hat{\mu}_1) \right) \right.$$
$$\left. + \ln \left(1 + \frac{1}{\nu} (z(i)-\mu_0)^\top S^{-1} (z(i)-\mu_0) \right) \right]. \tag{3.32}$$

3.A.2 Change in mean with known direction but unknown magnitude

If the direction of change is known, the mean after change is represented by $\mu_1 = \mu_0 + w\Upsilon$, where Υ is the unit direction vector and w is the unknown magnitude. Now the GLRT decision function will be slightly different, using that

$$\frac{\partial}{\partial w} (z(i) - \mu_0 - w\Upsilon)^\top S^{-1} (z(i) - \mu_0 - w\Upsilon)$$
$$= 2w\Upsilon^\top S^{-1} \Upsilon - 2\Upsilon^\top S^{-1} (z(i) - \mu_0) \tag{3.33}$$

$$\frac{\partial G_j^k(w)}{\partial w} = 0 \implies \sum_{i=j}^{k} \left[w\Upsilon^\top S^{-1} \Upsilon - \Upsilon^\top S^{-1} (z(i) - \mu_0) \right] = 0. \tag{3.34}$$

The MLE of change magnitude is given by

$$\hat{w}(k, j) = \frac{\Upsilon^\top S^{-1} (\bar{Z}_j^k - \mu_0)}{\Upsilon^\top S^{-1} \Upsilon}, \tag{3.35}$$

where

$$\bar{Z}_j^k = \frac{1}{k-j+1} \sum_{i=j}^{k} z(i). \tag{3.36}$$

Using (3.32) with $\hat{\mu}_1 = \mu_0 + \hat{w}\Upsilon$, and $\hat{w}$ from (3.35), the GLRT test statistic will hence be

$$g(k) = \max_{k-N+1 \le j \le k} \frac{p+\nu}{2} \sum_{i=j}^{k} \left[-\ln \left(1 + \frac{1}{\nu} (z(i)-\mu_0-\hat{w}\Upsilon)^\top S^{-1} (z(i)-\mu_0-\hat{w}\Upsilon) \right) \right.$$
$$\left. + \ln \left(1 + \frac{1}{\nu} (z(i)-\mu_0)^\top S^{-1} (z(i)-\mu_0) \right) \right]. \tag{3.37}$$

Chapter 4

Fault diagnosis of downhole drilling incidents using adaptive observers and statistical change detection

The work in this chapter was published in Willersrud et al. (2015d), which are using some of the methods published in Willersrud et al. (2015c), as well as being partly based on preliminary results in Willersrud et al. (2013b).

Summary

Downhole abnormal incidents during oil and gas drilling cause costly delays, and may also potentially lead to dangerous scenarios. Different incidents will cause changes to different parts of the physics of the process. Estimating the changes in physical parameters, and correlating these with changes expected from various defects, can be used to diagnose faults while in development. This paper shows how estimated friction parameters and flow rates can be used to detect and isolate the type of incident, as well as isolating the position of a defect. Estimates are shown to be subjected to non-Gaussian, t-distributed noise, and a dedicated multivariate statistical change detection approach is used that detects and isolates faults by detecting simultaneous changes in estimated parameters and flow rates. The properties of the multivariate diagnosis method are analyzed, and it is shown how detection and false alarm probabilities are assessed and optimized using data-based learning to obtain thresholds for hypothesis testing. Data from a 1400 m horizontal flow loop is used to test the method, and successful diagnosis of the incidents drillstring washout (pipe leakage), lost circulation, gas influx, and drill bit nozzle plugging are demonstrated.

4.1 Introduction

Drilling for oil and gas is a high-cost operation, especially for offshore wells. Here large drilling vessels are used, or the oil and gas platform is designed with drilling capabilities. An unwanted cost driver is non-productive time (NPT), which typically is between 20-25 % of the total drilling time (Godhavn, 2010). One of the major contributors to non-productive time is unforeseen incidents happening

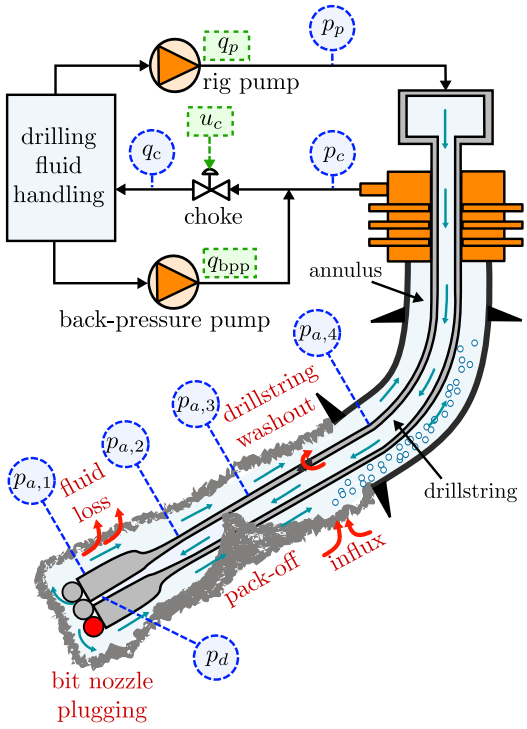

Figure 4.1: Drilling process with possible downhole incidents shown in red, including lost circulation, drillstring washout, formation fluid influx, bit nozzle plugging, and pack-off. Actuators shown in green, measurements in blue.

with the equipment on the rig, or downhole in the well. Early detection and isolation of an incident is of great importance (Godhavn, 2010), since early detection and mitigation can reduce the impact of an incident. Downhole incidents may in particular be challenging to detect, and to distinguish one type of incident from another may be even more difficult. Detecting and isolating the type and position of downhole incidents as soon as possible is the subject of this paper. A key issue is to avoid false alarms as these in themselves could cause unplanned stops in drilling operation while investigations are carried out to confirm an event.

A schematic of the possible downhole incidents in a drilling system is shown in Fig. 4.1. The main components of the system are the *drillstring* rotating the drill bit, with circulating drilling fluid pumped down inside the drillstring that transports crushed formation cuttings out of the *annulus*. The following incidents are of specific concern and are studied in this paper:

- An *influx* of formation fluid (gas, water, oil), also called a *kick*, is probably the most critical downhole incident. This is caused by a lower pressure in the well than in the formation. A gas kick will reduce the hydrostatic pressure,

thus further worsening the situation, and possibly leading to a dangerous full blowout. Detection of kicks is one of the most studied detection scenarios in drilling, see Hargreaves et al. (2001); Santos et al. (2007); Gravdal et al. (2010a); Hauge et al. (2013), and the importance of early detection is evident.

- Loss of drilling fluid to the formation is referred to as *lost circulation*. This is caused by either a very high permeability formation, or by a fractured formation (Bourgoyne Jr. et al., 1986). If large amounts of fluid is lost to the formation there may be problems maintaining a full fluid column in the annulus, which again may lead to an influx.

- A *pack-off* is a build-up of formation solids around the drillstring, partially or fully blocking the flow of drilling fluid. The result is typically stuck drillpipe and risk of formation fractures (Dalton et al., 2003).

- *Drillstring washout* is a hole in the drillstring caused by wear, which may cause leakage to the annulus. Such weakness can result in a complete twist-off of the pipe, resulting in extra three to twelve days of drilling (Macdonald and Bjune, 2007). A washout is difficult to detect at an early stage because changes in pressure and flow rate are tiny when the leakage is small.

- Small crushed formation particles may restrict one or several of the drill bit nozzles, which is called a *drill bit nozzle plugging*. Status monitoring of the drill bit is important to reduce downtime, where service and replacement of the bit is better planned with increased monitoring.

Different models and methods have been applied for detecting and isolating different kinds of incidents. Simple hydraulics models and observers were used by Gravdal et al. (2010a); Hauge et al. (2013), a high fidelity model was fitted to data in Cayeux et al. (2012a,b), and Skalle et al. (2013) applied a knowledge-modeling method. Due to measurement noise, a statistical cumulative sum (CUSUM) algorithm was tested on flow measurements in Hargreaves et al. (2001), and in Gulsrud et al. (2009), skewness of the statistical distribution was used to detect poor hole cleaning. Estimation and diagnosis has been demonstrated in process context in Nagy-Kiss and Schutz (2013) for a waste-water treatment plant where a bank of parallel linear observers were used for direct fault detection and isolation in a nonlinear plant, considering uncertainty but not stochastic elements. In our application, with a high sampling rate, the computational burden of this approach would be heavy when a high number of parallel observers were needed to adequately represent the nonlinearities of the system and different cases of parameter changes due to incidents listed above.

This paper employs a computationally simple mathematical model of the process in a nonlinear adaptive observer (Willersrud and Imsland, 2013) to estimate friction parameters and fluid flow rates. The estimates were found to follow a t-distribution and a dedicated generalized likelihood ratio test (GLRT) was developed

for this particular distribution in Willersrud et al. (2015c). This paper makes use of the adaptive observer in Willersrud and Imsland (2013) and the GLRT algorithm for the t-distribution from Willersrud et al. (2015c), to provide a multivariate test statistic in order to distinguish between the various types of downhole incidents that could happen. The purpose of this paper is to determine which of the possible incidents have happened, to where in the well the issue can be localized and which magnitude the incident has, hence which severity it has. The paper investigates the particular signatures of the different incidents in the test statistics and it develops rigorous methods to obtain both isolation and localization with desired probabilities of detection and false alarm. This result is achieved after a detailed analysis of properties of the vector comprising the test statistic and simultaneous analysis of estimated flow rates and friction parameters in the downhole process. The contribution of this paper is to find a vector-based evaluation method for the test statistic such that all of the types of incidents listed above can be diagnosed with convincing diagnostic properties. The paper demonstrates the efficacy of the method on data from a medium-scale horizontal flow loop designed and tested by Statoil, and compares the performance of the t-distribution and vector-based evaluation methodology with that of a standard Gaussian detection approach from Willersrud et al. (2013b) and shows the new method to be clearly superior.

The paper is organized as follows. Details about the test rig are first presented, and an overview of the fault diagnosis methodology is given. The hydraulic model is then detailed in Sec. 4.4, and changes to the different states and parameters in the model due to different incidents are discussed. Then, the adaptive observer is introduced, and a multivariate change detection algorithm is suggested. Tests with flow-loop induced faults data are finally presented, and the paper is completed with a discussion and conclusions.

4.2 Flow-loop test setup

The experimental rig is a water-based horizontal flow loop of 1400 meters, designed to emulate and test different contingencies, including *gas influx*, *lost circulation*, *bit nozzle plugging*, and *drillstring washout*. The test setup is designed by Statoil, and is located at the International Research Institute of Stavanger (IRIS), in Stavanger, Norway. The experimental test rig was designed to capture the main fluid dynamics in a real drilling rig using *managed pressure drilling* as closely as possible. In this configuration, the annulus is sealed off, and a choke is used to control the back-pressure. The schematics in Fig. 4.1 illustrates the process and incidents that can be imitated in the test rig.

A conventional piston pump is used to circulate the drilling fluid, and circular steel pipes of 124 mm and 155 mm inner diameter are used for the drillstring and annulus respectively, giving typical values of volume and bulk modulus. The back-pressure pump is omitted in the installation. Instrumentation is also typical for a real process. Pressure sensors downstream the pump (standpipe pressure),

Figure 4.2: Experimental flow loop with choke manifold to the left, gas influx and washout emulation in the middle, and bit and loss emulation to the right.

choke pressure, and pump flow are commonly available in a real rig. Downhole measurements along the drillstring and over the drill bit may be available with *wired drill pipe* technology (Godhavn, 2010; Veeningen et al., 2012).

However, some aspects of a real drilling process will not be captured in the test rig, where one of the more noticeable differences is caused by the loop being close to horizontal. In an inclined well with up to thousands of meters height difference between top and bottom, the volume of a gas influx will increase as it is approaching the surface, due to decreasing pressure. The result is a decreasing pressure in the bottom of the well. This effect will be much less noticeable when the hydrostatic pressure differences in the well are small, which is the case with the test rig. However, note that this effect is only occurring during multi-phase flow, which is the case during an influx. Other aspects are the lack of crushed formation particles in the annulus, annular effects and effects due to drillstring rotation. Nevertheless, flow rates and volumes, as well as a high-pressure environment, will give flow dynamics similar to real drilling.

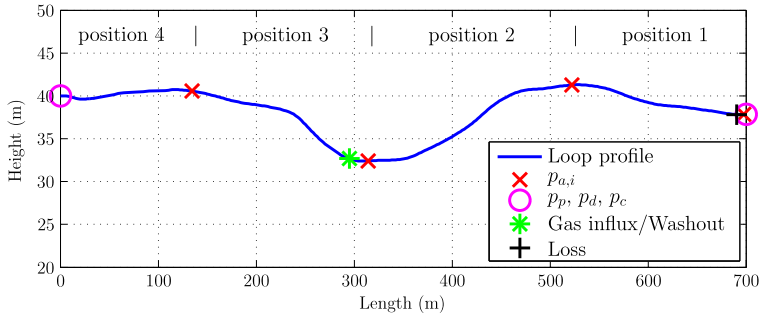

Figure 4.3: Flow-loop profile showing location of incident emulation at different positions in between pressure sensors.

Key parts of the process that are emulated are: drill bit; choke manifold; gas influx; drillstring washout; lost circulation. These are illustrated in Fig. 4.2. Gas influx is emulated by nitrogen injection in the middle of the annulus. At the same location, a valve can be opened, rerouting the flow from the drillstring to the annulus to emulate a drillstring washout. In the end of the drillstring, three adjustable valves emulate the bit nozzles with the possibility of partial plugging. The loop profile is shown in Fig. 4.3, illustrating that the loop does have height differences and therefore a hydrostatic pressure that varies along the line, albeit not as much as in real drilling. Location of the different incidents and pressure sensors are also shown in the figure.

4.3 Fault diagnosis methodology

This section presents the fault diagnosis method proposed for this problem. Fault diagnosis (Isermann and Ballé, 1997) consists of

- *Fault detection*: detect that an abnormal situation has occurred.
- *Fault isolation*: determine the type and location of the fault.
- *Fault estimation*: estimate the fault magnitude.

Fault diagnosis methods can be divided into model-based methods using mathematical models of the system (Chen and Patton, 1999; Blanke et al., 2006; Ding, 2008), and data-driven methods that only are dependent on measurements, which can be beneficial for large systems (Yoon and MacGregor, 2001; Yin et al., 2012; Ding, 2014). Data-driven methods for multivariate statistical fault diagnosis are presented and discussed in Yoon and MacGregor (2001); Yin et al. (2012); Yu (2012). This paper presents a model-based multivariate statistical fault diagnosis method to detect and isolate the possible incidents. Tests are done on data from the test rig.

Generally, model-based fault diagnosis is based on detecting observable changes that occur due to faults in the system. These changes can appear in residuals, signals that are zero under normal conditions but differ from zero in the presence of faults, or in estimated parameters of the system. One approach to estimate parameters is to use adaptive observers, which estimate states and slowly varying unknown parameters. When the adaptive observer is designed to tolerate unknown input, both abrupt and incipient faults can be captured (Frank and Ding, 1997).

In this paper, fault diagnosis is done by detecting changes, compared to normal operating conditions, of estimated friction parameters and change in flow rates. These estimates will have a random component due to measurements noise propagating though the adaptive observer. Since the magnitude of the different incidents can vary from zero to an unknown magnitude, and the random component is significant, the *generalized likelihood ratio test* (GLRT) can be applied to detect the

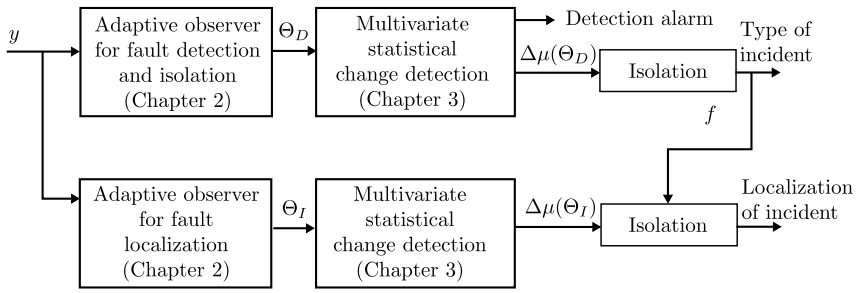

Figure 4.4: Fault detection and isolation based on parameter and state estimation, and statistical change detection.

change (Blanke et al., 2006; Basseville and Nikiforov, 1993; Kay, 1998). The detection problem is to detect a change in a signal x from the *null hypothesis* $\mathcal{H}_0$ to the *alternative hypothesis* $\mathcal{H}_1$, and can be formalized as

$$\mathcal{H}_0: \quad x \sim \mathcal{D}(\Pi_0; \mathcal{H}_0), \tag{4.1a}$$
$$\mathcal{H}_1: \quad x \sim \mathcal{D}(\Pi_1; \mathcal{H}_1), \tag{4.1b}$$

where $\mathcal{D}(\Pi_i; \mathcal{H}_i)$ is the probability distribution of x with statistical parameters Π_i specified at $\mathcal{H}_i$.

The paper focuses on investigation of a methodology to isolate the type of fault that has occurred, to locate where in the well the fault is present and to estimate the magnitude of the incident, i.e., help to assess the severity of the incident. The fault diagnosis methodology is presented graphically in Fig. 4.4. As indicated in the figure, details about design of the adaptive observers are available in Willersrud and Imsland (2013) and derivation of the GLRT detector for a t-distribution is available in Willersrud et al. (2015c).

Detecting that a fault is occurring, and determining the type of fault $f \in \mathcal{F}$, is based on estimated states and parameters in the *adaptive observer for fault detection and isolation*, using available measurements y. The location of the fault is found by the help of the *adaptive observer for fault localization*. Due to noise in the estimated signals, changes are detected using a multivariate statistical change detection algorithm. A univariate test on each estimated parameter would be a possibility, as was done in Willersrud et al. (2013b), but this paper shows that it is possible to achieve much better detection properties using a multivariate method where all parameters are considered jointly (Willersrud et al., 2015c). An alarm is set if the test statistics exceeds a certain threshold. Isolation is done by determining the change direction of the estimated parameters and states, where different faults will give different directions. This approach is similar to Yoon and MacGregor (2001), where isolation was based on vectors in a data-driven principal component analysis (PCA) framework.

4.4 Simplified single-phase hydraulics model

The flow loop was rigged for managed pressure drilling (MPD), and therefore is a model designed for MPD used. Referring to Fig. 4.1, the model can easily be changed to conventional drilling by removing the choke and back-pressure pump.

The process model (Kaasa et al., 2012) is a simplified hydraulics single-phase model with two control volumes connected with a momentum balance at the drilling bit. This model has been verified by offshore MPD commissioning tests, and is suitable for control and detection purposes where unknown parameters can be estimated. Slowly varying effects due to temperature are not included in the model, but can be added to calibrate the physical parameters. The height difference between a real drilling rig and the test rig will only affect the hydrostatic pressure during normal operation with single-phase flow, which will not affect the dynamics noticeably. The model is represented by the ordinary differential equations

$$\frac{dp_p}{dt} = \frac{\beta_d}{V_d}(q_p - q_{\text{bit}}), \tag{4.2a}$$

$$\frac{dp_c}{dt} = \frac{\beta_a}{V_a}\left(q_{\text{bit}} + q_{\text{bpp}} - Q_c(\theta, p_c, u_c)\right), \tag{4.2b}$$

$$\frac{dq_{\text{bit}}}{dt} = \frac{1}{M}\left(p_p - p_c - F(\theta, q_{\text{bit}}) - (\rho_a - \rho_d)gh_{\text{TVD}}\right), \tag{4.2c}$$

where p_p is the pressure downstream the rig pump, p_c pressure upstream the choke, q_p the volumetric pump flow, q_{bit} the flow through the bit, Q_c the flow through the choke, and q_{bpp} the back-pressure flow rate. In each control volume $j \in \{d, a\}$, d for drillstring and a for annulus, β_j is bulk modulus, V_j is volume, ρ_j is fluid density, and L_j is the length. The vertical depth of the well is denoted h_{TVD}, and g is the acceleration of gravity. The integrated density per cross section M is given by $M = M_d + M_a$ where $M_j = \int_0^{L_j} \rho_j(x)/A_j(x)dx$. The total friction $F(\theta, q)$ is dependent on the unknown parameter vector θ of slowly varying parameters which will be estimated. Friction is represented by

$$F(\theta, q) = \theta_d f_d(q) + \theta_b f_b(q) + \theta_a f_a(q), \tag{4.2d}$$

where $f_d(q), f_b(q), f_a(q)$ are the flow characteristics in the drillstring, over the bit, and in the annulus, respectively, and θ_d, θ_b, θ_a are unknown parameters. These parameters are lumped parameters of well geometry, density and viscosity, where the two latter again are functions of pressure and temperature. For normal operation these parameters can be assumed constant. The choke is modeled by

$$Q_c(\theta, p_c, u_c) = \theta_c q_c(p_c, u_c) = \theta_c \operatorname{sgn}(p_c - p_{c,0}) g_c(u_c) \sqrt{|p_c - p_{c,0}|}, \tag{4.2e}$$

where $p_{c,0}$ is the pressure downstream the choke, $g_c(u_c)$ is the choke characteristics as a function of choke opening $u_c \in [0, 100]$, and θ_c is a choke uncertainty parameter. Let p_d and $p_{a,1}$ be the pressure measurements upstream and downstream the bit,

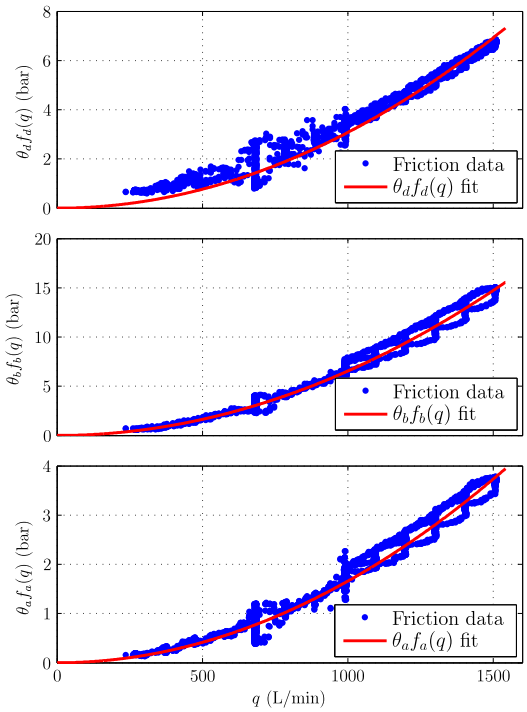

Figure 4.5: Friction characteristics in drillstring, drill bit, and annulus.

respectively. Then the relationship between friction and pressure in the drillstring, over the bit, and in the annulus is, respectively,

$$p_d = p_p - \theta_d f_d(q) + G_d, \tag{4.2f}$$
$$p_{a,1} = p_d - \theta_b f_b(q), \tag{4.2g}$$
$$p_{a,1} = p_c + \theta_a f_a(q) + G_a, \tag{4.2h}$$

where $G_d = \rho_d g h_{\text{TVD}}$ and $G_a = \rho_a g h_{\text{TVD}}$. In addition, if measurements $p_{a,i}$ are available throughout the annulus, the relationship between pressure and friction is

$$p_{a,i} = p_{a,i+1} + \theta_{a,i} f_a(q) + G_{a,i}, \quad i \in \{1, \ldots, N_a\} \tag{4.2i}$$

where $\theta_{a,i}$ is the friction parameter for the annular segment between measurement $p_{a,i}$ at depth $h_{a,i}$ and $p_{a,i+1}$ at $h_{a,i+1}$, with $G_{a,i} = \rho_a g(h_{a,i} - h_{a,i+1})$ and $\theta_a = \sum_{i=1}^{N_a} \theta_{a,i}$. The vector of unknown parameters is thus

$$\theta = \begin{bmatrix} \theta_c, & \theta_d, & \theta_b, & \theta_a, & \theta_{a,1}, & \ldots, & \theta_{a,N_a} \end{bmatrix}^\top. \tag{4.2j}$$

Data from a flow-loop test with different flow rates is used to empirically determine the friction characteristics in the drillstring, over the bit, and in the annulus.

In Fig. 4.5 friction losses for flow rates in the range of 270 L/min to 1500 L/min are plotted, showing a good fit to a quadratic relationship, i.e.,

$$f_d(q) = q^2, \quad f_a(q) = q^2, \quad f_b(q) = q^2, \tag{4.2k}$$

which is typical for turbulent flow, as well as for describing pressure drop over the bit (Bourgoyne Jr. et al., 1986).

4.5 Classification of incidents based on changes to variables

The different downhole drilling contingencies studied in this paper are *lost circulation*, which is loss of fluid to the formation, *influx* of gas from the formation, *drillstring washout* causing leakage from the drillstring to the annulus somewhere in the well, *drill bit nozzle plugging*, and *pack-off* of formation cuttings around the drillstring, restricting flow.

These different incidents will affect friction and flow rates throughout the well differently, and is used in the fault diagnosis method. Changes in mean of the estimated parameters $\hat{\theta}_d$, $\hat{\theta}_b$, and $\hat{\theta}_a$, as well as change in estimated flow rate in and out of the well,

$$\Delta\hat{q} := \hat{q}_c - \hat{q}_p, \tag{4.3}$$

are used to differentiate between the different incidents.

4.5.1 Lost circulation

Loss of fluid to the formation somewhere in the annulus will result in less flow downstream the point of loss. This will again reduce the friction in the segments with less flow, as well as the total annulus friction. Since the friction in the annulus is estimated by $\hat{\theta}_a f_a(\hat{q}_{\text{bit}})$, a reduction in annular flow rate will result in a reduction in the estimated friction parameter. This is due to the fact that the annular flow rate is not estimated, but assumed equal tothe bit flow rate. These effects are illustrated in Fig. 4.6a, showing less flow in the annulus, causing less friction and a negative change of $\Delta\hat{q}$.

4.5.2 Drillstring washout

Drillstring washout is leakage from the drillstring to the annulus due to small holes and cracks in the drillstring. If a washout happens, the lower parts of the drillstring and annulus will have reduced flow, which may result in decreased well pressure and hole cleaning capabilities. The effect on the friction parameters are shown in Fig. 4.6b, where friction in the lower parts of the well is reduced. At the section of the washout, the pressure in the end of the section will be constant due to unchanged flow, but the pressure in the beginning of the section will decrease due to reduced friction in the section. The net effect is an increase in pressure drop at

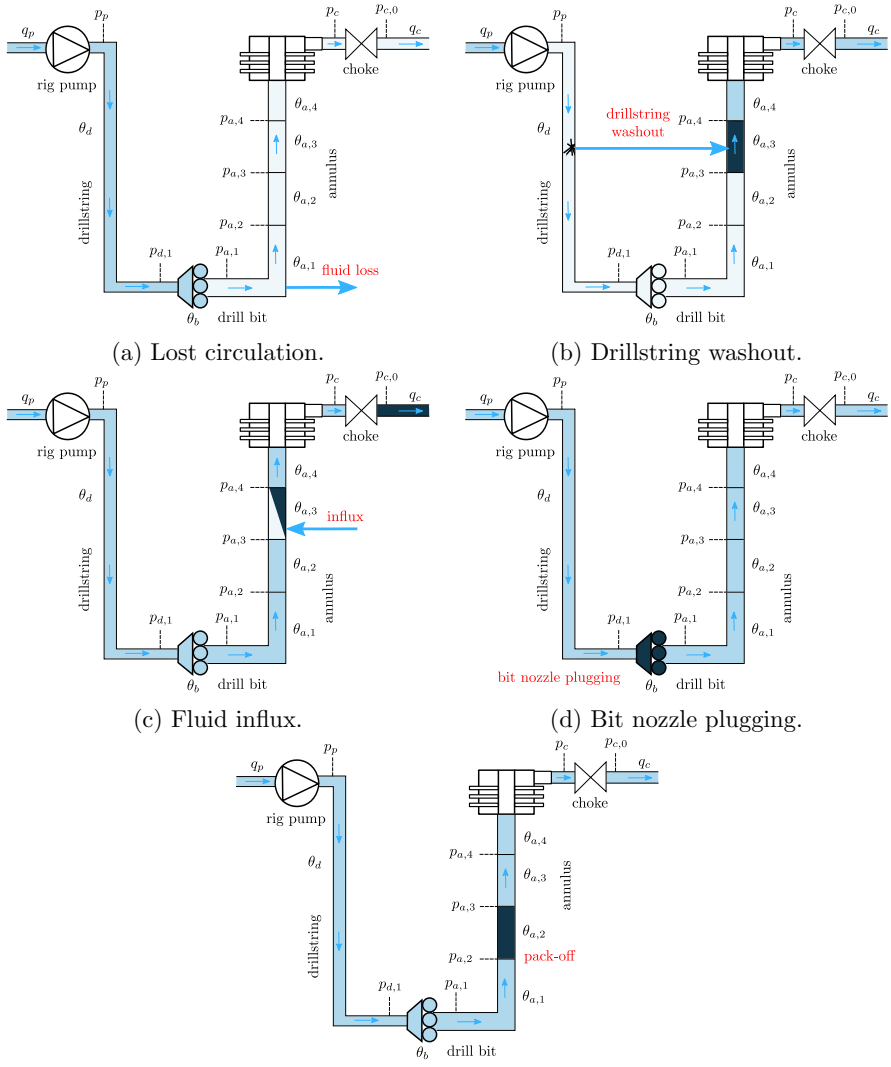

(a) Lost circulation.

(b) Drillstring washout.

(c) Fluid influx.

(d) Bit nozzle plugging.

(e) Pack-off.

Figure 4.6: Changes to flow and parameters due to different incidents. Blue denotes normal flow, light blue is less flow and/or friction, dark blue is increased flow and/or friction.

the washout. The case of drillstring washout was thoroughly studied in Willersrud et al. (2015c).

4.5.3 Gas influx

An influx of formation gas into the well is an incident caused by pressure in the well being lower than the formation pressure. Pressure dynamics will change with gas in the well, requiring a more advanced hydraulic model than (4.2). As the gas percolates up the well its volume will increase due to a smaller hydrostatic head. This will give a smaller pressure drop and thus a smaller estimated friction if the change in density of mixed gas and liquid is not accounted for. However, due to reduced holdup for the liquid in the annulus, its velocity will increase, increasing wall friction. These two effects will either increase or decrease the pressure drop over the annulus, depending on the magnitude of circulating flow rate and well inclination. The multi-phase flow is often classified as either *gravity dominated* or *friction dominated*. For vertical multi-phase flow of gas and liquid, typically 90-99 % of the pressure loss is caused by reduced hydrostatic head (Hasan and Kabir, 1988), i.e., gravity dominated flow.

An influx is thus associated with a decrease in $\Delta\hat{q}$, and change in $\hat{\theta}_a$, with positive change for friction dominated flow and negative for gravity dominated flow. In the particular case of the flow loop the inclination is quite small, hence is it assumed friction dominated flow in the annulus.

4.5.4 Pack-off

In addition to controlling pressure in the well, the drilling fluid is used to transport crushed formation particles (cuttings) or parts of the wellbore out of the well. If the drilling fluid fails to transport this mass, the wellbore can be (partially) plugged around the drillstring, called a *pack-off*. This will be observed in the friction parameters as an increase in $\hat{\theta}_a$, while the rest of the friction parameters and flow rates are unchanged. Pack-off is not emulated in the flow loop, but included here to demonstrate that other incidents are not incorrectly isolated as a pack-off.

4.5.5 Bit nozzle plugging

The drill bit has several nozzles which may be plugged during drilling. Small particles from the cuttings may restrict the flow through one or several of the nozzles, which will be seen as an increased pressure drop over the bit, and thus an increase in the pump pressure. Since the formation is not exposed to this pressure increase, the incident is not as severe as a pack-off (Cayeux et al., 2012a). If pressure sensors are available on both sides of the bit, changes to the pressure drop can be used to indicate a nozzle plugging. However, changes to the corresponding friction parameter may be a result of other incidents happening. A salient feature of the

method proposed here is that changes to the whole drilling process are considered simultaneously.

4.5.6 Overview of changes due to incidents

The effects on friction parameters and flow rates described in the previous subsections are summarized in Tab. 4.1, showing no overlap in the signatures that different incidents have in the estimated parameter and state vector. A vector-based method can thus be applied to isolate the type of incident, using change directions based on this table. Depending on whether the pressure drop during a gas influx is gravity dominated or friction dominated, $\hat{\theta}_a$ will either decrease or increase during the influx. It is assumed that the pressure drop is friction dominated since the flow loop is close to horizontal, giving a positive change in $\hat{\theta}_a$ in Tab. 4.1 for gas influx.

Table 4.1: Change of estimates in different cases of faults. Legend: increasing (+); decreasing (−); unchanged (0).

	$\hat{\theta}_d$	$\hat{\theta}_b$	$\hat{\theta}_a$	$\Delta\hat{q}$
Lost circulation	0	0	−	−
Drillstring washout	−	−	−	0
Gas influx	0	0	+	+
Bit nozzle plugging	0	+	0	0
Pack-off	0	0	+	0

To isolate the position of the different incidents, changes to friction parameters $\hat{\theta}_{a,1}, \ldots, \hat{\theta}_{a,N_a}$ are used. The position of the incident will affect the parameters differently, hence making isolation possible.

The estimated parameter vector Θ_D is used for detection and isolation of incident type, and Θ_I for isolation of position. With $N_a = 4$, the vectors are

$$\Theta_D := \begin{bmatrix} \hat{\theta}_d \\ \hat{\theta}_b \\ \hat{\theta}_a \\ \Delta\hat{q} \end{bmatrix}, \quad \Theta_I := \begin{bmatrix} \hat{\theta}_{a,1} \\ \hat{\theta}_{a,2} \\ \hat{\theta}_{a,3} \\ \hat{\theta}_{a,4} \end{bmatrix}. \tag{4.4}$$

Two separate vectors are used since in general, it may not be possible or desirable to estimate Θ_D and Θ_I in the same observer. Furthermore, the magnitude of change due to an incident may differ between the two vectors. In this specific case, Θ_I represents only a part of the process and will give smaller changes during incidents compared to Θ_D. Scaling would then be a challenge, as well as deteriorating detection and isolation properties, since a trade-off between false alarm and detection rate between Θ_D and Θ_I would have to be considered.

4.6 Parameter estimation using adaptive observers

Two different observers are designed to estimate parameters in the drillstring process. These were illustrated in Fig. 4.4. One observer is used to obtain estimates of incident type (Θ_D), which is used to detect and isolate the type of incident that has occurred; another is used to obtain estimated parameters, Θ_I, which are used for incident localization. For the drilling case with distributed pressure sensors in the annulus, the difference between the observers will be that the detection and isolation observer estimates $\hat{\theta}_a$ for the whole annulus, whereas $\hat{\theta}_{a,i}, i \in \{1, \ldots, N_a\}$ is estimated in the localization observer. When using (4.2) as system model it is possible to estimate all these parameters simultaneously, and hence for simplicity of presentation they are presented in one observer in the current section.

The model (4.2) has nonlinearities in friction (4.2d) and the choke equation (4.2e). In order to estimate states and parameters, a nonlinear adaptive observer is applied. The observer was derived in Willersrud and Imsland (2013), and successfully applied on the washout case in Willersrud et al. (2015c). The model (4.2) can be written on the *nonlinear adaptive observer form*,

$$\dot{x} = \alpha(x, u) + \beta(x, u)\theta, \tag{4.5a}$$
$$z = \eta(x, z) + \lambda(x, u)\theta, \tag{4.5b}$$

where $x(t) \in \mathbb{R}^{N_x}$ are the states, $z(t) \in \mathbb{R}^{N_z}$ are the additional measurements, $u(t) \in \mathbb{R}^{N_u}$ are the inputs, $\theta \in \mathbb{R}^{N_\theta}$ are unknown parameters, and $\alpha(x, u) \in \mathbb{R}^{N_x}$, $\beta(x, u) \in \mathbb{R}^{N_x \times N_\theta}$, $\eta(x, z) \in \mathbb{R}^{N_z}$ and $\lambda(x, u) \in \mathbb{R}^{N_u \times N_\theta}$ are locally Lipschitz functions. It is assumed that (4.5b) is an explicit equation of z, and that x is measured.

The system (4.2) can be written on the form (4.5) using

$$x = \begin{bmatrix} p_p, & p_c, & q_{\text{bit}} \end{bmatrix}^\top, \; u = \begin{bmatrix} q_p, & q_{\text{bpp}}, & u_c \end{bmatrix}^\top, \tag{4.6a}$$
$$z = \begin{bmatrix} q_c, & p_d, & p_{a,1}, & p_{a,1}, & p_{a,1}, & p_{a,2}, & \ldots, & p_{a,N_a} \end{bmatrix}^\top, \tag{4.6b}$$
$$\theta = \begin{bmatrix} \theta_c, & \theta_d, & \theta_b, & \theta_a, & \theta_{a,1}, & \ldots, & \theta_{a,N_a} \end{bmatrix}^\top, \tag{4.6c}$$

$$\alpha(x, u) = \begin{bmatrix} \frac{\beta_d}{V_d}(u_1 - x_3) \\ \frac{\beta_a}{V_a}(x_3 + u_2) \\ \frac{1}{M}(x_1 - x_2 - (\rho_a - \rho_d) g h_{\text{TVD}}) \end{bmatrix}, \tag{4.6d}$$

$$\beta(x, u) = \begin{bmatrix} 0 & 0 & 0 & 0 & \cdots & 0 \\ -\frac{\beta_a}{V_a} q_c(x_2, u_3) & 0 & 0 & 0 & \cdots & 0 \\ -\frac{f_d(x_3)}{M} & -\frac{f_b(x_3)}{M} & -\frac{f_a(x_3)}{M} & 0 & & 0 \end{bmatrix}, \tag{4.6e}$$

$$\eta(x, z) = \begin{bmatrix} 0, & x_1 + G_d, & z_2, & x_2 + G_a, & z_6 + G_{a,1}, & \ldots, & x_2 + G_{a,N_a} \end{bmatrix}^\top, \tag{4.6f}$$
$$\lambda(x, u) = \operatorname{diag}\left\{ q_c(x_1, u_3), \; -f_d(x_3), \; -f_b(x_3), \; f_a(x_3), \; \ldots, \; f_a(x_3) \right\}. \tag{4.6g}$$

Theorem 4.1 (Willersrud and Imsland (2013))**.** *Given an observer on the form*

$$\dot{\hat{x}} = \alpha(x,u) + \beta(x,u)\hat{\theta} - K_x(\hat{x} - x), \tag{4.7a}$$

$$\dot{\hat{\theta}} = -\Gamma\beta^\top(x,u)(\hat{x} - x) - \Lambda\lambda^\top(x,u)(\hat{z} - z), \tag{4.7b}$$

$$\hat{z} = \eta(x,z) + \lambda(x,u)\hat{\theta}, \tag{4.7c}$$

where $K_x, \Lambda, \Gamma > 0$ *are tuning matrices, and with* $\dot{\theta} = 0$*. Let* $e_x = \hat{x} - x$ *and* $e_\theta = \hat{\theta} - \theta$ *be variables for the error dynamics, where* $e = \begin{bmatrix} e_x^\top, & e_\theta^\top \end{bmatrix}^\top = 0$ *is an equilibrium point. Then* $e = 0$ *is globally exponentially stable if*

$$\Gamma^{-1}\Lambda\lambda^\top(\cdot)\lambda(\cdot) - \beta^\top(\cdot)K^\top K\beta(\cdot) > kI_{N_\theta}, \tag{4.8}$$

for some constant $k > 0$*, where* $I_{N_\theta} \in \mathbb{R}^{N_\theta \times N_\theta}$ *is the identity matrix.*

See Willersrud and Imsland (2013) for proof of Thm. 4.1. Requirement (4.8) with $\lambda(\cdot), \beta(\cdot)$ given in (4.6) will be met if there is flow through the system, i.e., for a non-zero and bounded $x_3 = q_{\text{bit}}$, and bounded $x_1 = p_p$.

4.7 Multivariate statistical change detection and fault isolation

Detecting changes to the different estimated parameters and flow rates in Θ_D and Θ_I are done using a generalized likelihood ratio test, described in this section. The diagnosis problem is a set of stepwise problems: First detect that there is a change from normal and isolate which incident is causing this change, then isolate the incident to a particular section of the drillstring and estimate its magnitude. See also Fig. 4.4.

Problem 4.1 (Incident detection)**.** *Given a sampled time sequence of vectors of estimated parameters* $\Theta_D(k)$*, with change from known condition* $\Theta_{D,0}(k)$ *to unknown* $\Theta_{D,1}(k)$ *defined as* $\Delta\Theta_D(k) := \Theta_{D,1}(k) - \Theta_{D,0}(k)$*. Define the index set* $\mathbb{N}_N := \{i \in \mathbb{N} : 1 \leq i \leq N\}$ *and let* $i_D \in \mathbb{N}_{N_f}$ *be the possible fault indices. Let a fault signature matrix be* D*, a unit magnitude fault vector be* $f_{i_D} = [0, \ldots, 0, 1, 0, \ldots, 0]^\top$*, element* i_D *of which is non-zero when fault* i_D *is present, and* $v(k)$ *be an unknown magnitude of change. Further, let the random vector* $w(k)$ *have independent and identically distributed samples with probability density* $f(w)$*, then distinguish between two hypotheses*

$$\mathcal{H}_0 : \ \Delta\Theta_D(k) = 0 + w(k), \ \textit{no fault present}, \tag{4.9a}$$

$$\mathcal{H}_1^D : \ \Delta\Theta_D(k) = Df_{i_D}v(k) + w(k), \ \textit{fault present}. \tag{4.9b}$$

Problem 4.2 (Isolate type of incident)**.** *Given* $\mathcal{H}_1^D$ *has been accepted, determine that a particular fault* i_D^* *is present of the possible faults* $i_D \in \mathbb{N}_{N_f}$*, by determining the best fit of* (4.9b) *for the different fault types.*

Problem 4.3 (Isolate position of incident)**.** *Given that i_D^* has been isolated. Let $G(i_D^*)$ be a known matrix associated with the isolated fault type i_D^*, $\Delta\Theta_I(k)$ be a vector of change in estimated parameters, $j_I \in \mathbb{N}_{N_g}$ be the possible fault positions, f_{j_I} be a fault position vector with element j_I equal to 1 for a fault in position j and 0 otherwise, and $\upsilon(k)$ be the unknown magnitude of the change.*

(A): Determine if localization of a fault is possible by distinguishing between two hypotheses

$$\mathcal{H}_0 : \Delta\Theta_I(k) = 0 + w(k), \textit{localization not possible}, \tag{4.10a}$$
$$\mathcal{H}_1^I : \Delta\Theta_I(k) = G(i_D^*) f_{j_I} \upsilon(k) + w(k), \textit{localization possible}. \tag{4.10b}$$

(B): If hypothesis $\mathcal{H}_1^I$ is accepted, determine the most likely position j_I^* of the positions $j_I \in \mathbb{N}_{N_g}$ along the pipe that explains the estimates (4.10b).

4.7.1 Generalized likelihood ratio test

The GLRT decision function uses the likelihood ratio of the probability density function at the two hypotheses of $\mathcal{H}_0$ and $\mathcal{H}_1$, and can be written as

$$g(k) = \max_{k-N+1 \leq j \leq k-\tilde{N}} \ln \frac{\prod_{i=j}^{k} f(\Theta(i); \mathcal{H}_1)}{\prod_{i=j}^{k} f(\Theta(i); \mathcal{H}_0)}. \tag{4.11}$$

using a data window N to reduce computational cost, and $0 \leq \tilde{N} < N$ (Willsky and Jones, 1976; Lai, 1995). Distinguishing between the two hypotheses is done by using a threshold h of the decision function $g(k)$,

$$\begin{aligned} &\text{accept } \mathcal{H}_0 : \ g(k) \leq h, \\ &\text{accept } \mathcal{H}_1 : \ g(k) > h. \end{aligned} \tag{4.12}$$

4.7.2 Probability distribution of estimated flow and friction parameters

The estimated parameters $\hat{\theta}$ from the adaptive observer (4.7) were found to be multivariate t-distributed in Willersrud et al. (2015c), after the estimated parameters were white-filtered. The t-distribution is a generalization of the Gaussian distribution, with larger probability tails. This means that there is a higher probability of outliers compared to a Gaussian distribution. The p-variate t-distribution with center μ, correlation matrix S and $\nu > 0$ degrees of freedom has the joint probability density function

$$f(x; \mu, S, \nu) = \frac{\Gamma((p+\nu)/2)}{\Gamma(\nu/2)(\pi\nu)^{p/2}|S|^{1/2}} \left[1 + \frac{1}{\nu}(x-\mu)^\top S^{-1}(x-\mu)\right]^{-\frac{p+\nu}{2}}, \tag{4.13}$$

where $\Gamma(z)$ is the Gamma function. The parameter μ is the mean of x when $\nu > 1$ (Kotz and Nadarajah, 2004).

4.7.3 GLRT with multivariate t-distribution

If the mean μ is changing from μ_0 to μ_1, whereas the statistical parameters S and ν are constant, the GLRT decision function $g(k) \in \mathbb{R}$ for the t-distribution (4.13) of vector variable $\Theta(k)$ was found in (Willersrud et al., 2015c) to be given by

$$g(k) = \max_{k-N+1 \leq j \leq k-\tilde{N}} \frac{p+\nu}{2} \sum_{i=j}^{k} \left[-\ln\left(1 + \frac{1}{\nu}(\Theta(i)-\hat{\mu}_1)^\top S^{-1}(\Theta(i)-\hat{\mu}_1)\right) + \ln\left(1 + \frac{1}{\nu}(\Theta(i)-\mu_0)^\top S^{-1}(\Theta(i)-\mu_0)\right)\right], \quad (4.14)$$

with maximum likelihood estimate of the mean after change given by

$$\hat{\mu}_1 = \frac{1}{k-j+1} \sum_{i=j}^{k} \Theta(i). \quad (4.15)$$

4.7.4 Isolate type of incident

The problem of isolating type of incident defined in Problem 4.2 is to find i_D^* of the possible fault types. Let D be the fault signature matrix with unit column vectors D_i defined by

$$D_i := \frac{K_D \Upsilon_{D,i}}{\|K_D \Upsilon_{D,i}\|}, \quad (4.16)$$

where the column vector $\Upsilon_{D,i}$ of Υ_D is the change direction of incident i_D, and K_D are the relative change magnitudes used to scale changes to have approximately similar effects on magnitude υ. Based on Tab. 4.1, the possible change directions Υ_D for Θ_D are

$$\Upsilon_D = \begin{bmatrix} 0 & -1 & 0 & 0 & 0 \\ 0 & -1 & 0 & 1 & 0 \\ -1 & -1 & 1 & 0 & 1 \\ -1 & 0 & 1 & 0 & 0 \end{bmatrix}, \quad (4.17)$$

corresponding to the fault types lost circulation ($i_D = 1$), drillstring washout ($i_D = 2$), gas influx ($i_D = 3$), bit nozzle plugging ($i_D = 4$), and pack-off ($i_D = 5$), respectively.

Determining correct magnitudes K_D can be difficult without prior data of the incidents. Nevertheless, knowledge of certain range of values is maybe possible based on physical considerations. It is assumed that the relative change between friction parameters θ_d, θ_b and θ_d is approximately equal. Furthermore, using (4.2k) with known friction and flow rate, relative change between the friction parameters θ_d, θ_b, θ_d, and change of flow rate Δq is approximately 1/1000, giving the diagonal matrix of relative change

$$K_D = \text{diag}\{1, 1, 1, 1/1000\}. \quad (4.18)$$

The type of fault i_D^* is isolated using a maximum least square solution of magnitude υ given by (4.9b) for each column vector D_i in D, where the mean is $\mathrm{E}(\Delta\Theta_D) = (\hat{\mu}_1^D - \mu_0^D)$, giving

$$i_D^* = \arg\max_i \frac{D_i^\top (\hat{\mu}_1^D - \mu_0^D)}{D_i^\top D_i}. \tag{4.19}$$

4.7.5 Isolating position of incident

The position of the incident refers to the position between two pressure measurements in the annulus, where j_I indicates an incident between pressure sensor $p_{a,j}$ and $p_{a,j+1}$. The different type of incidents $i_D \in \mathbb{N}_{N_f}$ will affect the estimated parameters Θ_I used for isolation differently. As stated in Problem 4.3, it is thus necessary to first determine the type of incident i_D^* and then isolate the position j_I^*. Let $G(i_D)$ be the localization matrix associated with fault type i_D, with unit column vectors $G_j(i_D)$ defined as

$$G_j(i_D) := \frac{K_I \Upsilon_{I,j}(i_D)}{\|K_I \Upsilon_{I,j}(i_D)\|}, \tag{4.20}$$

where $\Upsilon_{I,j}(i_D)$ is the j-th column vector of the localization change direction matrix $\Upsilon_I(i_D)$ associated with fault type i_D, and K_I is a diagonal matrix of relative change magnitudes.

Similarly to (4.19), the position j_I^* of the fault is isolated finding the maximum least square solution to (4.10b), giving

$$j_I^* = \arg\max_j \frac{G_j^\top(i_D^*)(\hat{\mu}_1^I - \mu_0^I)}{G_j(i_D^*)^\top G_j(i_D^*)}. \tag{4.21}$$

It is assumed that the magnitude of change of each estimated parameter is equal for a given incident, giving $K_I = I$, where I is the identity matrix. For the case of lost circulation ($i_D = 1$), drillstring washout ($i_D = 2$), and pack-off ($i_D = 5$), the change direction matrices are, respectively, given by

$$\Upsilon_I(1) = \begin{bmatrix} -1 & 0 & 0 & 0 \\ -1 & -1 & 0 & 0 \\ -1 & -1 & -1 & 0 \\ -1 & -1 & -1 & -1 \end{bmatrix}, \quad \Upsilon_I(2) = \begin{bmatrix} 1 & -1 & -1 & -1 \\ 0 & 1 & -1 & -1 \\ 0 & 0 & 1 & -1 \\ 0 & 0 & 0 & 1 \end{bmatrix}, \tag{4.22a}$$

$$\Upsilon_I(5) = \begin{bmatrix} 1 & 0 & 0 & 0 \\ 0 & 1 & 0 & 0 \\ 0 & 0 & 1 & 0 \\ 0 & 0 & 0 & 1 \end{bmatrix}, \tag{4.22b}$$

where vectors are determined based on discussions in Sec. 4.5. Isolation of gas influx ($i_D = 3$) is not well suited for the current model, and is hence not included. Bit nozzle plugging ($i_D = 4$) does not need additional isolation.

4.7.6 Determining thresholds

Thresholds can be found based on specified probability of false alarms P_{FA} (Kay, 1998), by determining the distribution of the GLRT test statistic $g(k)$ for data under $\mathcal{H}_0$, see, e.g., Galeazzi et al. (2013); Hansen and Blanke (2014). In Willersrud et al. (2015c) the GLRT test statistic (4.14) was found to have a good fit to the Weibull distribution. The Weibull distribution has the cumulative distribution function $F(x;\alpha,\beta)$ and probability density function $f(x;\alpha,\beta)$ given by

$$F(x;\alpha,\beta) = 1 - e^{-(x/\alpha)^\beta}, \quad x \geq 0, \tag{4.23a}$$

$$f(x;\alpha,\beta) = \frac{\beta}{\alpha}\left(\frac{x}{\alpha}\right)^{\beta-1} e^{-(x/\alpha)^\beta}, \quad x \geq 0, \tag{4.23b}$$

where $\alpha > 0$ is the scale and $\beta > 0$ the shape parameter.

Let P_{FA} be the probability of false alarm under $\mathcal{H}_0$. Then the inverse cumulative distribution function gives a threshold h with given probability P_{FA},

$$h = Q(1 - P_{FA}; \mathcal{H}_0, \alpha_0, \beta_0) = \beta_0 \left(-\ln(P_{FA})\right)^{1/\alpha_0}. \tag{4.24}$$

The probability of detecting a fault under the alternative hypothesis $\mathcal{H}_1$ with probability P_D for a given threshold h is

$$P_D = 1 - F(h; \mathcal{H}_1, \alpha_1, \beta_1) = e^{-(x/\alpha_1)^{\beta_1}}. \tag{4.25}$$

Knowledge of data under $\mathcal{H}_1$ is needed to find α_1, β_1, and thus P_D.

4.8 Diagnosis of downhole incidents in flow-loop data

The suggested incident diagnosis method, illustrated in Fig. 4.4, is tested on data from five different cases from the test rig: drillstring washout; lost circulation; two cases of gas influx; and bit nozzle plugging. Data is sampled at 10 Hz and white-filtered using a third order filter. The computational burden of updating the observer (4.7) is well within real-time capability.

Estimation of pump and choke pressure, as well as pump and choke flow rate, is shown for all test cases in Fig. 4.7. Since pressures and choke flow rate are measured, these estimates closely follow the process as expected. Since measured bit flow is assumed equal to pump flow, estimated bit flow closely follows the pump flow. The estimated parameters in (4.2) are plotted in Fig. 4.8, which will determine Θ_D and Θ_I given by (4.4). Measurements indicating the time of the emulated incidents are plotted in Fig. 4.9. Valve position for bit nozzle plugging emulation was not measured and is not shown. This information is shown for reference only, the emulated incidents are not known to the diagnosis algorithm.

The plots in Figs. 4.7, 4.8 and 4.9 show a concatenation of the five different data sets logged at the test rig. Logging was not continuously available and incidents were not always injected in chronological order. Although the different cases were

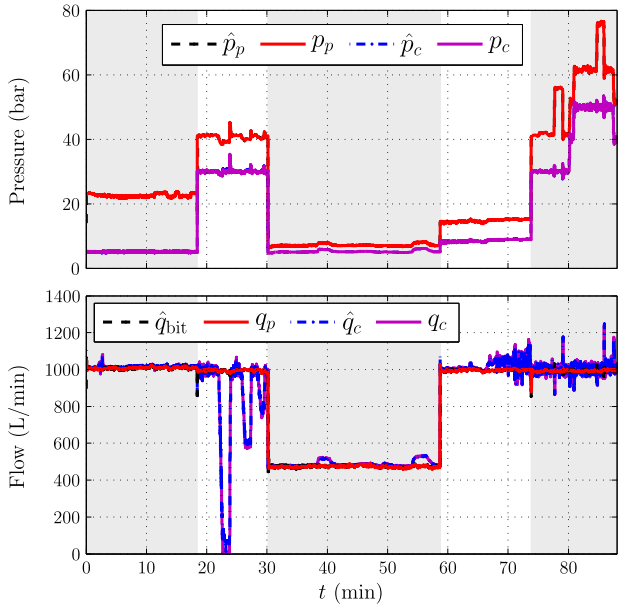

Figure 4.7: State estimation of pressure and flow during washout, loss, gas influx, and bit nozzle plugging. The different cases are separated with alternating grey and white backgrounds.

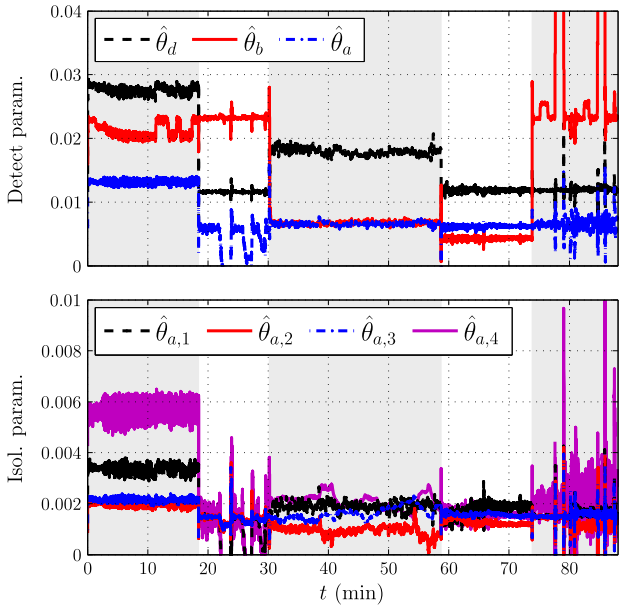

Figure 4.8: Parameter estimation during washout, loss, gas influx, and bit nozzle plugging. The different cases are separated with alternating grey and white backgrounds.

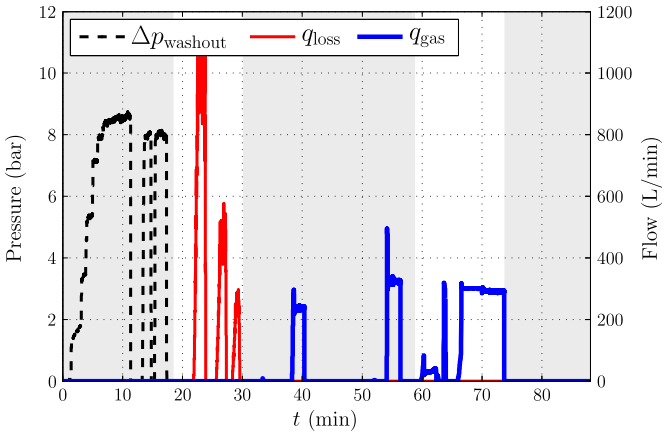

Figure 4.9: Actual incidents: drillstring washout, lost circulation, and gas influx. Bit nozzle plugging not measured. Information not available for diagnosis method. The different cases are separated with alternating grey and white backgrounds.

run on the same experimental rig, physical conditions differ between the experiments and there are therefore differences in the state and parameter estimates between the individual cases. From Fig. 4.8 that shows parameter estimation, it is apparent that the distribution of test statistics under $\mathcal{H}_0$ differ from one experiment to another. In a real drilling process, the estimates would only have small variations during normal operation, and a $\mathcal{H}_0$ calibration could be made from data.

With differences between data sets, different values for the parameters in the t-distribution, i.e., μ_0, S and ν, need to be estimated. The t-distribution parameters under $\mathcal{H}_0$ are estimated using the Expected-Conditional Maximization Either (ECME) algorithm (Liu and Rubin, 1995), using data from test conditions without any incidents. For all data sets $\nu > 1$, meaning that μ is the vector of mean values of parameters. Simultaneous adaptation and change detection could be used to track slowly varying process properties.

A related approach was presented in Blanke and Hansen (2013) where adaptation of model parameters was halted when a $\mathcal{H}_1$ condition was detected, and detection was based on a combination of change in parameters and change in the output estimation error between observer estimated output and measured output.

Threshold values listed in Tab. 4.2 are calculated using (4.24) with the following probabilities of false alarm

$$P_{FA,D} = 10^{-6}, \quad P_{FA,I} = 10^{-4}, \tag{4.26}$$

during detection and type isolation, and localization, respectively.

The chosen GLRT window lengths given in number of samples are

$$N_D = 150, \quad N_I = 400, \tag{4.27}$$

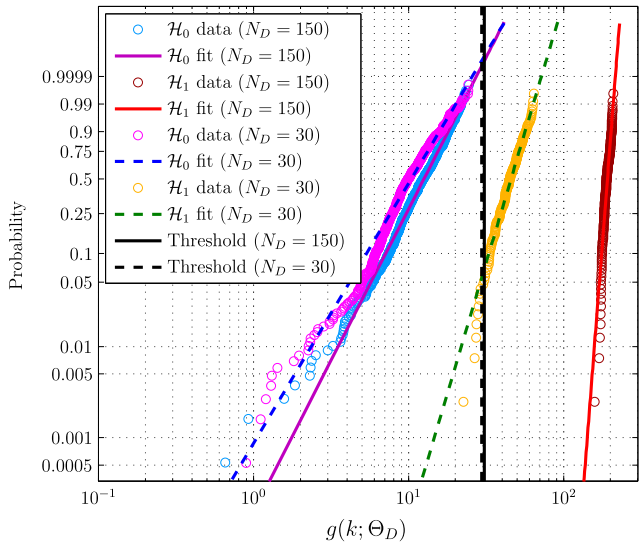

Figure 4.10: Weibull probability plot of decision function $g(k;\Theta_D)$ under $\mathcal{H}_0$, and $\mathcal{H}_1$ with loss of 300 L/min (at 29 min in Fig. 4.9), for window lengths $N_D = 150$ (solid) and $N_D = 30$ (dashed). Thresholds h shown as vertical lines. P_{FA} and P_D are 1−Probability shown on the ordinate axis of the plot.

where a shorter window for detection and type isolation is used to give a fast detection, while localization is based on Θ_I with less changes in the estimated parameters, necessitating a longer window. The necessity for a sufficiently long window size is shown in Fig. 4.10, showing $g(k;\Theta_D)$ fitted to Weibull-distributions for the lost circulation case under $\mathcal{H}_0$ with no loss, and $\mathcal{H}_1$ with lost circulation of 300 L/min shown at 29 min in Fig. 4.9. Two cases are plotted, namely the chosen window size of $N_D = 150$ plotted with solid lines, and a shorter window $N_D = 30$ plotted with dashed lines. Also plotted are the thresholds that give the same false alarm probability for the two window sizes. As Fig. 4.10 shows, in order to obtain high detection probability (P_D) and a satisfactorily low false alarm rate (P_{FA}), $\mathcal{H}_0$-data needs essentially to be below (to the left) of the threshold, and $\mathcal{H}_1$-data essentially to be above. This is the case for $N_D = 150$, which is used in our analysis, but not for a five times shorter window, $N_D = 30$. The window intervals we use in the analysis, see (4.27), are quite short ($N_D = 150$ is equivalent to a 15 s window and $N_I = 400$ is equivalent to 40 s), so the window size could easily be chosen much longer in a real drilling situation, albeit at the expense of slower detection.

This discussion illustrates the necessity of investigating the distribution of test statistics under both $\mathcal{H}_0$ and $\mathcal{H}_1$ in order to choose threshold and window size for a test, and the probability plot approach shown here provides a straightforward and easily applicable methodology. It is a prerequisite that $\mathcal{H}_0$ and at least a few $\mathcal{H}_1$ data are available. If only $\mathcal{H}_0$ data are available, the minimum value of a fault

Table 4.2: Threshold values for different cases.

Incident case	h_{det}	h_{isol}
Lost circulation ($f_{D,1}$)	30.8	27.9
Drillstring washout ($f_{D,2}$)	64.0	82.4
Gas influx A ($f_{D,3}$)	56.3	N/A
Gas influx B ($f_{D,3}$)	48.4	N/A
Bit nozzle plugging ($f_{D,4}$)	57.6	N/A

that can be detected, with a given probability of detection, will be a function of threshold and window length.

With P_{FA} and N specified in (4.26) and (4.27), expected false alarm rates are 0.00024 per hour (2 per year) for detection and type isolation, and 0.009 per hour for localization. Since localization is made subject to prior detection, the localization false alarm does not have as high priority as that of detection. In addition, with a longer window size or a requirement that consecutive hypothesis evaluations confirm a detection, false alarm rates could be further reduced.

4.8.1 Drillstring washout

The first incident studied is a drillstring washout. This case was studied in Willersrud et al. (2015c), but extended in this paper to also include isolation of incident type. Detection and isolation is shown in Fig. 4.11 where the washout is correctly detected and isolated. The true position of the washout is at position 3, which is in the middle of the drillstring. See Fig. 4.3. The position is correctly located after 2 minutes, seen in Fig. 4.12, with the alarm disappearing shortly in the beginning where leakage is fairly small. A multivariate Gaussian test on non-whitened estimates, see, e.g., Basseville and Nikiforov (1993); Blanke et al. (2006) is also shown in the figure.

Using the multivariate t-distribution, the probability of missed detection $P_M := 1 - P_D$ for $g(k; \Theta_D)$ between 2 and 3 minutes is 2.6×10^{-4}, using P_D in (4.25) and P_{FA} specified in (4.26). For localization with $g(k; \Theta_I)$, $P_M = 0.106$. If the multivariate Gaussian distribution is used these values are 1.6×10^{-3} and 0.80, respectively, which is considerably higher. The t-distribution is hence providing better detection properties, where isolation in particular would be challenging using a multivariate Gaussian distribution in the GLRT decision function (4.11). This can also can be seen in Fig. 4.12, where $g(k; \Theta_I)$ is lower using the Gaussian probability density function. The $g(k)$ value of the Gaussian distribution is scaled to have equal threshold h as the t-distribution.

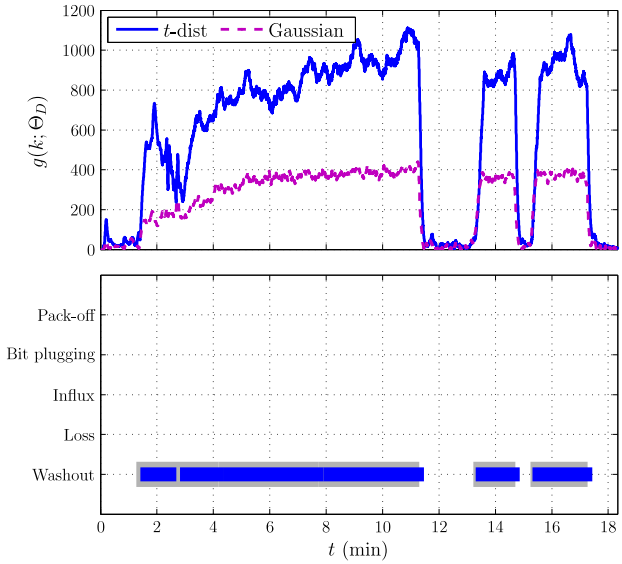

Figure 4.11: Detection and isolation of drillstring washout. GLRT plotted for t-distribution and Gaussian distribution. Gaussian GLRT scaled to have same threshold h as the t-distribution. Actual incident shown in grey.

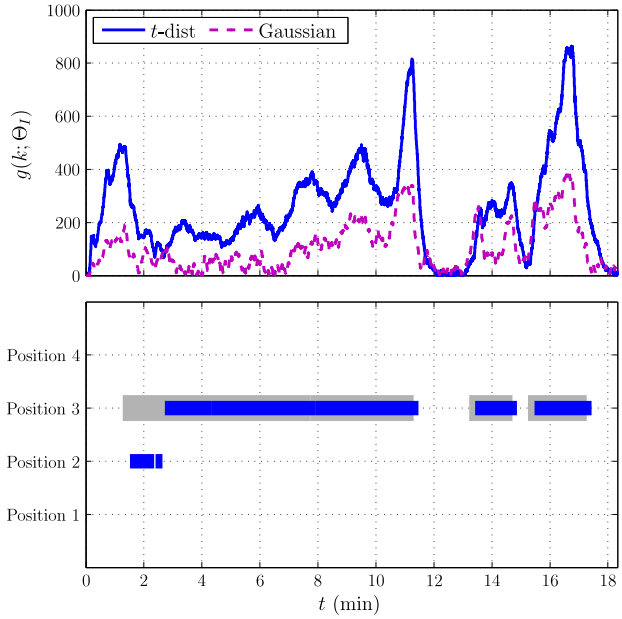

Figure 4.12: Localization of drillstring washout position. GLRT plotted for t and Gaussian distribution (scaled). Actual position shown in grey.

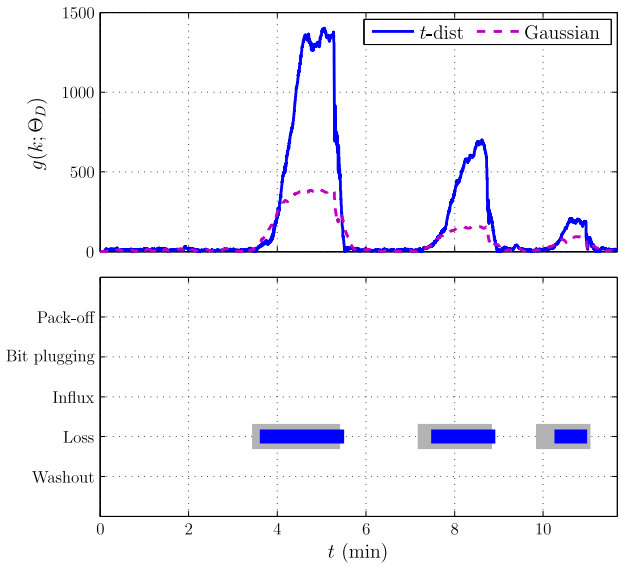

Figure 4.13: Detection and isolation of lost circulation. GLRT plotted for t and Gaussian distribution (scaled). Actual incident shown in grey.

4.8.2 Lost circulation

The next incident is loss of drilling fluid, happening just downstream the bit, which is position 1 in the annulus. The data contains three losses at different magnitudes of approximately 1000 L/m, 500 L/m and 300 L/min. See the actual loss q_{loss} plotted in Fig. 4.9. All of these losses are correctly detected and isolated, as seen in Fig. 4.13. Isolation of the position is also correctly found, as seen in Fig. 4.14. Also here the t-distribution gives better detection and isolation properties.

4.8.3 Gas influx

With gas in the system, some aspects of the model are no longer valid. In the model it is assumed incompressible single-phase flow with constant density in the annulus, whereas during a gas influx the flow will be two-phase and compressible with varying density. For such a case it is expected that a fit-for-purpose multiphase model will describe the fluid dynamics better. Nevertheless, detection in the current framework is still tested, since it is important to have a diagnosis framework that correctly isolates the type of incident.

Detection and isolation of a gas influx is successfully detected in influx case A, shown in Fig. 4.15. Afterwards, there is gas present in the system which is not modeled, and thus causing a slightly increasing value of $g(k;\Theta_D)$ after the first influx. However, this change is less that the threshold h given in Tab. 4.2. Diagnosis in influx case B is shown in Fig. 4.16, which has three instances of gas

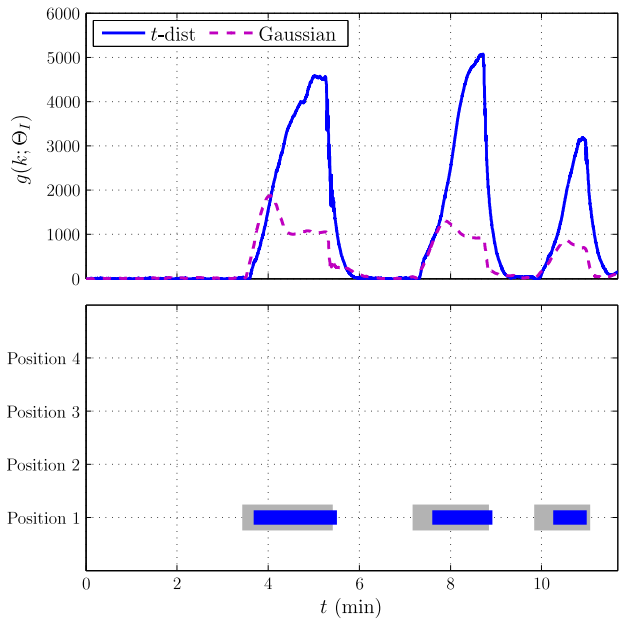

Figure 4.14: Localization of lost circulation position. GLRT plotted for t and Gaussian distribution (scaled). Actual position shown in grey.

influxes, one small, one large over a small time period, and one large continuous influx, see Fig. 4.9 between 60 and 75 minutes. The small influx is successfully detected and isolated, although not at all time instances. The larger ones are also correctly diagnosed. After the first large influx, around the 5 minutes time stamp in Fig. 4.16, there are some false alarms of pack-off and lost circulation. Since the actual incidents plotted is *injection* of gas, there is still gas in the system after injection. Transportation of gas is not modeled, and will affect friction and hydrostatic pressure as discussed in Sec. 4.5.3. Note that when a gas influx is detected in a real drilling operation, the well is typically shut in and normal drilling is stopped in order to remove the influx.

4.8.4 Bit nozzle plugging

The last case studied is a plugging of the drill bit nozzles. In this case only changes in the estimated bit parameter $\hat{\theta}_b$ is expected. By using a multivariate method, changes to all signals in Θ_D can be tested, determining that in fact the bit parameter is the only one changing. Detection and isolation is shown in Fig. 4.17, where all pluggings are detected, with two large pluggings and two small. Studying $\hat{\theta}_b$ from 75 to 88 minutes in Fig. 4.8, the major pluggings will be possible to detect without a statistical method, whereas the smaller ones may be difficult to separate from noise and process disturbances. However, as argued, changes to all parameters should

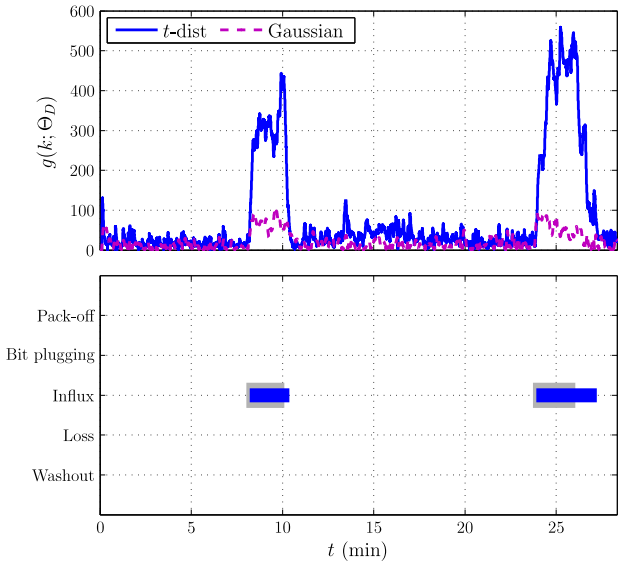

Figure 4.15: Detection and isolation of gas influx case A. GLRT plotted for t and Gaussian distribution (scaled). Actual incident shown in grey.

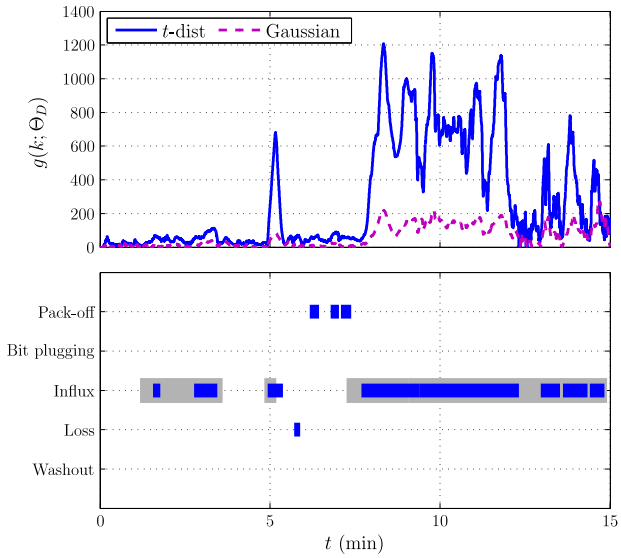

Figure 4.16: Detection and isolation of gas influx case B. GLRT plotted for t and Gaussian distribution (scaled). Actual incident shown in grey.

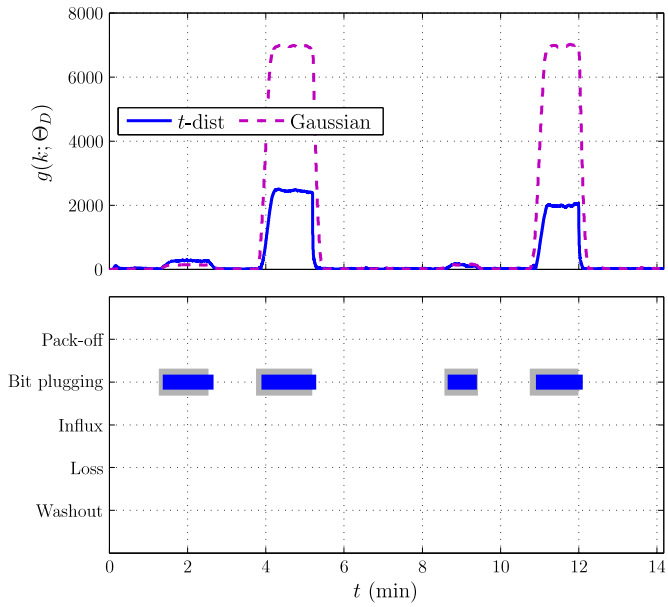

Figure 4.17: Detection and isolation of bit nozzle plugging. GLRT plotted for t and Gaussian distribution (scaled). Actual incident shown in grey.

be considered in order to correctly isolate the type of incident, which is best solved with a multivariate statistical method.

4.8.5 Estimation of incident magnitude

In addition to indicating that an incident is present and finding out where it is, it can be valuable for the operator to get information about the magnitude of the incident. Especially important to know is the magnitude of loss or influx. Estimation of fluid loss to the formation is shown in Fig. 4.18, which for an incompressible fluid is the difference in flow rate in and out of the well. This plot shows that the loss magnitude is correctly estimated, and together with detection and isolation, information about the loss is well diagnosed. Gas influx is more challenging for the current model, since gas is not modeled. Drillstring washout and bit nozzle plugging magnitude is not directly measured, and cannot be verified. Nevertheless, bit nozzle plugging magnitude is possible to estimate based on changes to $\hat{\theta}_b$. Magnitude of drillstring washout flow was calculated in Willersrud et al. (2015c), although the value of washout flow could not be verified from data due to lack of washout flow measurement.

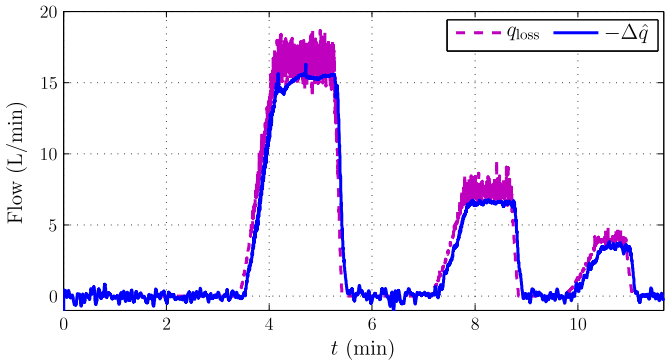

Figure 4.18: Estimation ($-\Delta\hat{q}$) and measurement (q_{loss}) of lost circulation. Measurement not known to estimation algorithm.

4.9 Discussion

The need for statistical change detection was evident from the parameter estimates shown in Fig. 4.8, where most of the incidents would be rather difficult to detect directly from the estimates. An exception was two of the four nozzle pluggings, where the estimated bit parameter $\hat{\theta}_b$ had a large change. However, to ensure that the incident was indeed a bit nozzle plugging, the whole process had to be considered, i.e., a multivariate detection algorithm was needed.

Comparing drillstring washout and lost circulation in the schematic overview in Fig. 4.6, and in Tab. 4.1, shows that the two incidents have equal effect on the annulus parameter $\hat{\theta}_a$. The same applies for gas influx if the pressure drop is gravity dominated. Separation of the incidents requires one to consider changes to all signals in Θ_D.

The proposed methodology successfully detected and isolated the different cases of drillstring washout, lost circulation, gas influx, and bit nozzle plugging. This represents a significant improvement over the results reported in (Willersrud et al., 2013b), where isolation was uncertain. Reasons were that in (Willersrud et al., 2013b), changes to each parameter was considered separately, and that a Gaussian-based detector was used on the non-whitened estimates.

The method was validated using data from the flow loop, representing key parts of the drilling process. During specific drilling operations where tools such as a hole-opener or under-reamer are used, side ports in the bottom hole assembly would slightly modify the flow path. This would have to be accounted for in the process model.

Isolation of the position was based on changes to estimated friction in the annulus, using distributed pressure measurements. With an increased number of measurements, the distance between them decreases, and frictional pressure drop decreases. It is therefore even more difficult to detect changes, making a statistical change detection algorithm necessary if changes to estimated parameters should be detected.

For the drillstring washout case, the position was correctly isolated, except for a few minutes in the beginning with low washout rates. In the lost circulation case, the position was correctly isolated for all three losses, also for the smaller loss. Isolation for the gas influx case was not considered. As discussed in Sec. 4.5.3, changes to pressure drop with a multi-phase flow is dependent on well geometry, where the friction drop could either be gravity dominated or friction dominated. Changes in Θ_I is thus dependent on the geometry, and where in the well the gas is located. This motivates the need for a fit-for-purpose model in order to isolate the position of the gas influx. Nevertheless, the main concern in drilling with respect to gas influx is to detect that it is happening, which the method successfully does.

It was shown in Willersrud et al. (2015c) that the white-filtered estimates are t-distributed. Using the dedicated t-distribution change detector gave superior results over the Gaussian detector for all cases except the bit nozzle plugging. This superiority is especially important for the isolation, where small changes in parameters were experienced.

4.10 Conclusion

Fault diagnosis of downhole incidents during oil and gas drilling was successfully done in this paper by estimating friction parameters and flow rates. Changes to estimates were detected by a multivariate generalized likelihood ratio test, considering a set of estimated well parameters and flow rates simultaneously. Isolation of incident type and position was achieved by determining the direction of change of the estimated parameters. Data from a medium-scale horizontal flow loop of 1400 m was used to test the fault diagnosis method. Parameter and state estimates from data were found to have a non-Gaussian, t-distributed noise component, and this was utilized in the dedicated multivariate statistical change detection algorithm, developed specifically for this distribution. Thresholds were determined based on specified probabilities of false alarms. Diagnosis of drillstring washout, lost circulation, gas influx, and bit nozzle plugging were tested. All of these cases were successfully detected and isolated during the occurrence of the incident. A multi-phase flow model should be considered if isolation of gas influx position is required, whereas the position was correctly isolated for drillstring washout, fluid loss, and bit nozzle plugging.

Chapter 5

Early pack-off diagnosis in drilling using an adaptive observer and statistical change detection

The work in this chapter was published in Willersrud et al. (2015a), and is based on Willersrud et al. (2015c,d).

Summary

Pack-off is a partially or complete blocking of the circulation flow in oil and gas drilling, which can lead to costly delays. Early detection and localization of a pack-off is crucial in order to take necessary actions avoiding downtime. This incident will affect physical friction parameters in the well. A model-based adaptive observer is used to estimate these friction parameters as well as flow rates. Detecting changes to these estimates can then be used for pack-off diagnosis, which due to measurement noise is done using statistical change detection. Isolation of incident type and location is done using a multivariate generalized likelihood ratio test, determining the change direction of the estimated mean values. The method is tested on simulated data from the commercial high-fidelity multi-phase simulator OLGA, where three different pack-offs at different locations and with different magnitudes are successfully detected at an early stage and with low false alarms.

5.1 Introduction

The basic concept of oil and gas drilling is to use a rotating drillstring with a drill bit, crushing the formation and circulating out this mass through the annulus surrounding the drillstring, as shown in Fig. 5.1. If the formed cuttings are not properly transported out of the well, or if parts of the wellbore collapses due to an unstable formation, the well can start to *pack off*, reducing circulation capabilities. If no action is taken the drillstring can become stuck, which will result in expensive delays. Early diagnosis of a pack-off is thus instrumental in maintaining proper hole cleaning, avoiding expensive non-productive time.

Advances in drilling methods and technology, such as *managed pressure drilling* (MPD), bring along improved instrumentation. One such improvement is wired

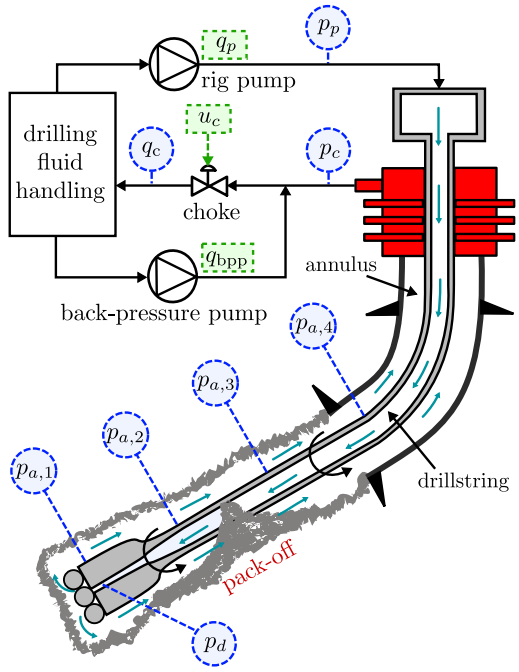

Figure 5.1: Drilling process with a forming pack-off. Measurements in blue, actuators in green.

pipe with pressure (and temperature) measurements along the drillstring, giving real-time data of the wellbore (Godhavn, 2010). This technology has been suggested as a tool for pack-off detection and localization in Long and Veeningen (2011). However, how these measurements should be used in an automatic diagnosis system is left open. In Aldred et al. (1998) and Cayeux et al. (2012b), a pack-off is detected by monitoring the estimated total friction in the well. In Skalle et al. (2013), pack-offs and other incidents are diagnosed using a knowledge-modeling method.

A challenge with all measurement technology is noise. In this paper the goal is to detect small forming pack-offs at an early stage using simple models and fast detection methods, as well as isolating the position, and estimating the magnitude of the incident. This is achieved by applying a multivariate statistical change detection framework on estimated friction parameters and flow rates, giving early diagnosis even with small changes in the estimates.

This paper continues on earlier work on fault diagnosis of downhole incidents in drilling such as *gas influx* from the reservoir, *lost circulation* of drilling fluid to the reservoir, *drillstring washout* (leakage from drillstring to annulus), and *plugging of the drill bit nozzles*, published in Willersrud et al. (2015c,d). There, methods are derived and tested on data from a medium-scale test rig. This paper extends these results by studying how pack-offs, not included in the test rig data, can be diagnosed in simulated data from a full-scale vertical wellbore, using the commercial

high-fidelity multi-phase simulator OLGA (Bendiksen et al., 1991).

The paper is organized as follows: In Sec. 5.2 the model and observer is presented, used to estimate friction parameters and flow rates. Multivariate statistical change detection, and change direction for fault diagnosis are presented in Sec. 5.3. Simulations of three different pack-offs are presented in Sec. 5.4, and fault diagnosis of the simulated data is done in Sec. 5.5. The paper is ended with a conclusion.

5.2 Modeling and estimation

The model-based adaptive observer (Willersrud and Imsland, 2013) is presented in this section, which is used to estimate friction parameters and flow rates. First the model itself is presented, then a brief overview of the observer is shown.

5.2.1 Simplified hydraulics model

The model is a simplified hydraulics model (Kaasa et al., 2012) for managed pressure drilling, given by

$$\frac{dp_p}{dt} = \frac{\beta_d}{V_d}(q_p - q_b), \tag{5.1a}$$

$$\frac{dp_c}{dt} = \frac{\beta_a}{V_a}\left(q_b + q_{\text{bpp}} - g_c(u_c)\sqrt{|p_c - p_{c,0}|}\right), \tag{5.1b}$$

$$\frac{dq_b}{dt} = \frac{1}{M}\left(p_p - p_c - F(\theta, q) - (\rho_a - \rho_d)gh_{\text{TVD}}\right), \tag{5.1c}$$

where p_p is the pump pressure, p_c choke pressure, q_b is the drill bit flow, q_p the pump flow, and q_{bpp} the back-pressure pump flow, see Fig. 5.1. Subscript 'd' denotes drillstring and 'a' annulus for known volume V, bulk modulus β, and density ρ. Parameter M is the integrated density per cross section from pump to choke. Gravitational acceleration is g and h_{TVD} is the depth of the well. The choke flow is modeled as $q_c = g_c(u_c)\sqrt{|p_c - p_{c,0}|}$, where $g_c(u_c)$ is the choke characteristics as a function of choke opening $u_c \in [0, 100]$, and $p_{c,0}$ is the pressure downstream the choke. The total friction is given by

$$F(\theta, q) = \theta_d f_d(q_b) + \theta_b f_b(q_b) + \theta_a f_a(q_b), \tag{5.1d}$$

where f_d, f_b and f_a are friction terms and θ_d, θ_b, and θ_a are unknown parameters nominally equal to one, expressing the change in friction in the drillstring, bit, and annulus due to a pack-off. Changes to the parameters due to changed friction is assumed much slower than changes in pressure and flow rates due to operational changes.

The relationship between the pressure measurements, friction, and hydrostatic

pressure is given by

$$p_d = p_p - \theta_d f_d(q_b) + \rho_d g h_{\text{TVD}}, \tag{5.1e}$$

$$p_{a,1} = p_d - \theta_b f_b(q_b), \tag{5.1f}$$

$$p_{a,1} = p_c + \theta_a f_a(q_b) + \rho_a g h_{\text{TVD}}, \tag{5.1g}$$

where p_d is the pressure at the bottom of the drillstring, and $p_{a,1}$ the pressure at the bottom of the annulus. If distributed pressure measurements $p_{a,i}$ along the annulus are available, the additional equations give pressure relationships

$$p_{a,i} = p_{a,i+1} + \theta_{a,i} f_{a,i}(q_b) + \rho_a g(h_{a,i} - h_{a,i+1}),\ i \in \{1, \ldots, N_a\}, \tag{5.1h}$$

where $\theta_{a,i} f_{a,i}(q_b)$ is the friction of the annular segment between $p_{a,i}$ at depth $h_{a,i}$ and $p_{a,i+1}$ at $h_{a,i+1}$. Note that $f_a = \Sigma_{i=1}^{N_a} f_{a,i}$. The vector of unknown parameters is thus

$$\theta = \begin{bmatrix} \theta_d, & \theta_b, & \theta_a, & \theta_{a,1}, & \ldots, & \theta_{a,N_a} \end{bmatrix}^\top. \tag{5.1i}$$

For typical drilling flow rates, the flow is most commonly turbulent and the friction can be modeled as

$$f_j(q) = k_{j,2} q^2 + k_{j,1}. \tag{5.2}$$

where $j \in \{d, b, a, a1, a2, a3, a4\}$, and where $k_{j,1}$ and $k_{j,2}$ are constant parameters which can be found using regression of historical pressure and flow rate data.

5.2.2 Adaptive observer

The states and parameters in (5.1) are estimated using the adaptive observer in Willersrud and Imsland (2013) with vector of measured states $x = \begin{bmatrix} p_p, & p_c, & q_b \end{bmatrix}^\top$, additional measurements $z = \begin{bmatrix} q_c, & p_d, & p_{a,1}, & p_{a,2}, & p_{a,3}, & p_{a,4} \end{bmatrix}^\top$, inputs $u = \begin{bmatrix} q_p, & q_{\text{bpp}}, & u_c \end{bmatrix}^\top$, and unknown parameters given by (5.1i). It is assumed that bit flow equals pump flow, i.e., $q_b = q_p$, thus ignoring fast drillstring dynamics. The observer is given by

$$\dot{\hat{x}} = \alpha(x, u) + \beta(x)\hat{\theta} - K_x(\hat{x} - x), \tag{5.3a}$$

$$\dot{\hat{\theta}} = -\Gamma \beta^\top(x)(\hat{x} - x) - \Lambda \lambda^\top(x)(\hat{z} - z), \tag{5.3b}$$

$$\hat{z} = \eta(x, z, u) + \lambda(x)\hat{\theta}, \tag{5.3c}$$

where $K_x, \Lambda, \Gamma > 0$ are tuning matrices, and with $\dot{\theta} = 0$. The observer matrices for system (5.1) are given by

$$\alpha(x, u) = \begin{bmatrix} \frac{\beta_d}{V_d}(u_1 - x_3) \\ \frac{\beta_a}{V_a}(x_3 + u_2) \\ \frac{1}{M}(x_1 - x_2 - (\rho_a - \rho_d) g h_{\text{TVD}}) \end{bmatrix}, \tag{5.4a}$$

$$\beta(x) = \frac{1}{M} \begin{bmatrix} 0 & 0 & 0 & 0 & \ldots & 0 \\ 0 & 0 & 0 & 0 & \ldots & 0 \\ -f_d(x_3) & -f_b(x_3) & -f_a(x_3) & 0 & & 0 \end{bmatrix}, \tag{5.4b}$$

$$\lambda(x) = \{-f_d(x_3),\ -f_b(x_3),\ f_a(x_3),\ f_{a,1}(x_3), \ldots,\ f_{a,4}(x_3)\}, \tag{5.4c}$$

$$\eta(x,z,u) = \Big[-\frac{\beta_a}{V_a} g_c(u_c)\sqrt{|x_2 - p_{c,0}|},\ x_1 + \rho_d g h_{\text{TVD}},\ z_2,\ x_2 + \rho_a g h_{\text{TVD}},\ z_4 + \rho_a g(h_{a,1} - h_{a,2}),\ \ldots,\ x_2 + \rho_a g h_{a,N_a} \Big]^\top. \tag{5.4d}$$

5.3 Fault diagnosis

The fault diagnosis method from Willersrud et al. (2015c,d) is presented in this section. Changes to the estimated parameters are detected using multiviariate statistical change detection, and fault isolation is achieved by determining the change direction of the mean of the estimates. The section ends with an overview of the method.

5.3.1 Statistical change detection

Fault diagnosis is done by detecting changes to estimated states and parameters. This can either be done by detecting changes to each signal independently, or by using a multivariate detection method considering a set of signals jointly. Change detection of data from a medium-scaled drilling test setup, using the same model as in this paper, showed superior results using a multivariate method in Willersrud et al. (2015c). Since the parameter values after change is unknown, a multivariate *generalized likelihood ratio test* (GLRT) is applied to detect and localize a pack-off.

The detection problem is to detect a change in a signal $x(k) \in \mathbb{R}^{N_x}$ of sample size N with probability density function $f(x;\Pi)$ and statistical parameters Π, by the two hypotheses $\mathcal{H}_0$ (fault-free) and $\mathcal{H}_1$ (fault). This can be done by using a log-likelihood decision function (Kay, 1998),

$$g(k) = \ln \frac{f(X;\Pi_1)}{f(X;\Pi_0)}, \tag{5.5}$$

where $X = [x(0),\ \ldots,\ x(N)]$, an where Π_0 are the statistical parameters at $\mathcal{H}_0$, and Π_1 at $\mathcal{H}_1$.

The two hypotheses are distinguished by using a threshold h of $g(k)$,

$$\begin{aligned} &\text{accept } \mathcal{H}_0: \ g(k) \leq h, \\ &\text{accept } \mathcal{H}_1: \ g(k) > h. \end{aligned} \tag{5.6}$$

Consider a vector signal with Gaussian noise $x(k) \sim \mathcal{N}(\mu, S)$, with constant covariance matrix S and change in mean μ from μ_0 at $\mathcal{H}_0$ to unknown μ_1 at $\mathcal{H}_1$. Furthermore, let the noise of signals $x(k)$ be independent and identically distributed (IID). Then the decision function (5.5) can be written as

$$g(k) = \sum_{i=k-N+1}^{k} (\hat{\mu}_1 - \mu_0)^\top S^{-1} \left(x(i) - \frac{1}{2}(\hat{\mu}_1 + \mu_0) \right), \tag{5.7}$$

(see, e.g., Basseville and Nikiforov (1993); Blanke et al. (2006)), where

$$\hat{\mu}_1 = \frac{1}{N} \sum_{i=k-N+1}^{k} x(i) \tag{5.8}$$

is the maximum likelihood estimate of the mean after change. A moving window $M < N$ of the data is used to detect changes within the window.

5.3.2 Fault isolation and estimation

Changes to different parameters due to different incident types is discussed in Willersrud et al. (2015d) including lost circulation, drillstring washout, gas influx, bit nozzle plugging, and pack-off. To test isolation of a pack-off, tests for all these different scenarios are included. Let $\Delta\hat{q} := \hat{q}_c - \hat{q}_p$ be the change in estimated flow out and in of the well. Changes to estimated parameters and flow rates due to different incidents are listed in Tab. 5.1. Note that even though only $\hat{\theta}_a$ is changing during a pack-off, all the listed estimated signals need to be checked in order to isolate the pack-off.

Table 5.1: Change of estimates for different incidents with increasing (+), decreasing (−), and unchanged (0) estimates.

	$\hat{\theta}_d$	$\hat{\theta}_b$	$\hat{\theta}_a$	$\Delta\hat{q}$
Lost circulation	0	0	−	−
Drillstring washout	−	−	−	0
Gas influx	0	0	+	+
Bit nozzle plugging	0	+	0	0
Pack-off	0	0	+	0

The change directions for the different incident types can be written as column vectors of

$$\Upsilon_D = \begin{bmatrix} 0 & -1 & 0 & 0 & 0 \\ 0 & -1 & 0 & 1 & 0 \\ -1 & -1 & 1 & 0 & 1 \\ -1 & 0 & 1 & 0 & 0 \end{bmatrix}, \tag{5.9}$$

where each column represents the scaled change direction of

$$\Theta_D := \begin{bmatrix} \hat{\theta}_d, & \hat{\theta}_b, & \hat{\theta}_a, & \Delta\hat{q} \end{bmatrix}^\top, \tag{5.10}$$

for each of the incidents lost circulation, drillstring washout, gas influx, bit nozzle plugging, and pack-off, respectively. Let μ_0^D be the mean of the nominal Θ_D, and $\hat{\mu}_1^D$ the estimate (5.8) of Θ_D after a change. Defining $D_i := \Upsilon_{D,i}/||\Upsilon_{D,i}||$, the fault can be isolated (Willersrud et al., 2015d), finding

$$i_D^* = \arg\max_i \frac{D_i^\top(\hat{\mu}_1^D - \mu_0^D)}{D_i^\top D_i} \tag{5.11}$$

of the possible fault indices $i_D \in \mathbb{N}_{N_f} := \{i \in \mathbb{N} : 1 \leq i \leq N_f\}$, where in this paper, $N_f = 5$. Similarly, (5.11) can be used to find the position of the fault, once the type is isolated. For a pack-off, possible change directions are the column vectors of

$$\Upsilon_I = \begin{bmatrix} 1 & 0 & 0 & 0 \\ 0 & 1 & 0 & 0 \\ 0 & 0 & 1 & 0 \\ 0 & 0 & 0 & 1 \end{bmatrix} \tag{5.12}$$

for the estimated annulus parameters

$$\Theta_I := \begin{bmatrix} \hat{\theta}_{a,1}, & \hat{\theta}_{a,2}, & \hat{\theta}_{a,3}, & \hat{\theta}_{a,4} \end{bmatrix}^\top, \tag{5.13}$$

since a pack-off will be seen as an increase in friction between two pressure sensors $p_{a,i}$ and $p_{a,i+1}$, thus increasing $\hat{\theta}_{a,i}$.

5.3.3 Overview of fault diagnosis method

The fault diagnosis method used in this paper and presented in this section consists of estimating states and parameters, detecting changes to them, and determining in which direction they are changing. The steps in the method are shown in Fig. 5.2 and can be summarized as follows:

1. Friction parameters and flow rates are estimated using the adaptive observer (5.3).

2. Changes to the subset of estimated states and parameters Θ_D given by (5.10) is detected using the GLRT decision function (5.7).

3. The type of fault is isolated using (5.11), with possible change directions of Θ_D as columns in (5.9).

4. The position is located with (5.11), with possible change directions of Θ_I as column vectors in (5.12).

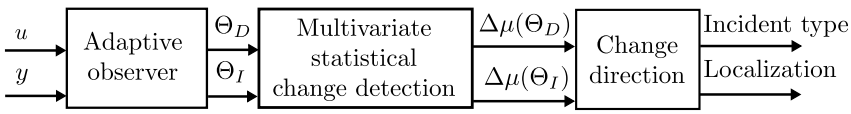

Figure 5.2: Fault diagnosis overview.

5.4 Pack-off simulation in OLGA

OLGA is a high-fidelity dynamic multiphase flow simulator, which is used to simulate a series of pack-offs in a vertical wellbore of 2530 meters. The well is modeled as an annulus with typical radii, including the so-called bottom hole assembly with narrower flow paths, as well as several restrictions representing joints of the drillstring. Water is used as drilling fluid, with a circulation rate of 1000 L/min, a typical flow rate for drilling operation. The model includes an MPD choke, while the back-pressure pump is omitted. A vertical well is chosen for simplicity, but a deviated well would give the same results. The friction coefficients $k_{j,1}$, $k_{j,2}$ for $f_j(q_b)$, $j \in \{d, b, a, a1, a2, a3, a4\}$ are found using regression of the pressure drop adjusted for hydrostatic pressure during a test where the flow rate is varied in the range 300-1100 L/min.

Pack-offs are local build ups of solids in the annulus, partly or fully blocking the flow. This behavior is similar to a choke restriction, and pack-offs are therefore simulated in OLGA using chokes at three different positions in the well. The chokes are gradually opened and then closed with varying magnitude between each one. There are four pressure sensors in the annulus representing a wired drill pipe, in addition to a sensor measuring the choke pressure at the top, see Fig. 5.1. The sensors are located at depth $h_a = \begin{bmatrix} 2530, & 1980, & 1230, & 330 \end{bmatrix}^\top$. The first pack-off choke ($u_{po,1}$) is located between sensor $p_{a,1}$ and $p_{a,2}$, the second ($u_{po,2}$) between $p_{a,2}$ and $p_{a,3}$, and the third ($u_{po,3}$) between $p_{a,3}$ and $p_{a,4}$. A cause of forming pack-offs is insufficient circulation. Therefore is the flow-rate increased to 1100 L/min after the second pack-off, which would be a probable action taken by the drilling operator if a pack-off was detected. Here, this is done to test the diagnosis method for varying pressure and flow rates.

Gaussian distributed white noise is added to all measurements, with standard deviation $\sigma = 0.001\mu_0$ of each measurement, where μ_0 is the mean at the fault-free case $\mathcal{H}_0$, although a larger variance of the signals could easily been used. This fault free case is a time interval known to be without any incidents. In a real case, this would typically be during drilling with constant pressures and flow rates, where the operator has full overview of the situation. In the simulation this interval is between 5 and 40 minutes drilling time.

States and parameters are estimated using the adaptive observer (5.3) with tuning matrices $K_x = \text{diag}(1, 1, 1)$ and $\Gamma = \Lambda = 5 \times 10^{-5} \times \text{diag}(1, 1, 1, 1, 1, 1, 1)$. Simulations and state estimation are shown in Fig. 5.3, illustrating measured and estimated pump pressure, choke pressure, pump flow and bit flow. The bottom panel shows openings of the three different valves. This affects the pump pressure, since the total friction in the well increases. All three pack-offs are visible in p_p, but may be difficult to distinguish from changes due to varying operating conditions.

The resulting parameter estimation is plotted in Fig. 5.4, showing parameters used in Θ_D for incident type isolation in the upper panel, and Θ_I used for localization in the lower. In the upper panel, only $\hat{\theta}_a$ is changing due to a pack-off, in accordance with Tab. 5.1 and (5.9). Furthermore, the need for statistical change

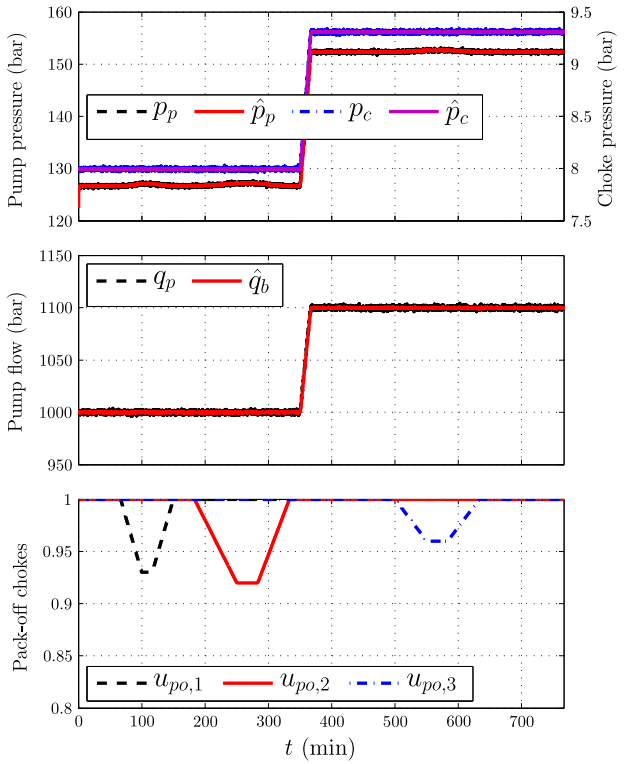

Figure 5.3: Pressure and flow estimation, and valve openings simulating pack-offs.

detection is apparent, since changes are small. In the lower panel, pack-offs at different positions are affecting the estimated annular parameters differently, which is used in incident localization. Note that also here, statistical change detection is needed, in particular to detect changes in $\hat{\theta}_{a,3}$.

5.5 Pack-off diagnosis

Fault diagnosis of pack-offs in simulated OLGA data, shown in Figs. 5.3 and 5.4, is done according to the steps presented in Sec. 5.3.3. Diagnosis results are shown and discussed in this section.

5.5.1 Threshold

Theoretical thresholds for the GLRT (5.5) is given in Kay (1998), where as $N \to \infty$, the test statistic has the asymptotic probability density function (PDF) χ^2_r under $\mathcal{H}_0$ and $\chi^2_r(\lambda)$ under $\mathcal{H}_1$, where r is the number of statistical parameters that are changing and λ is a non-central parameter. This asymptotic distribution can be

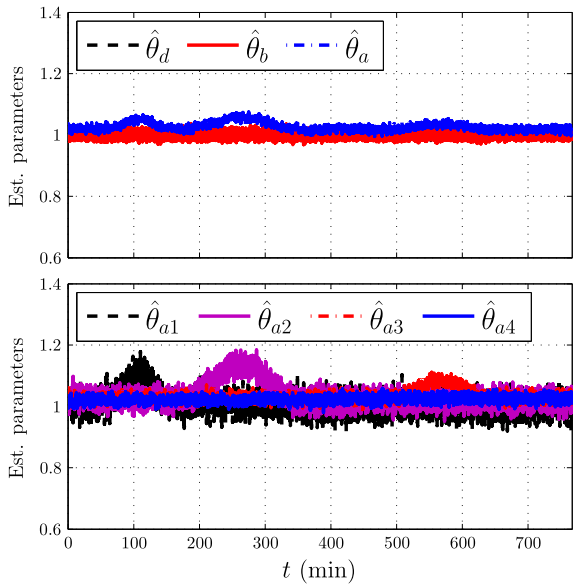

Figure 5.4: Estimation of friction parameters.

used to derive a threshold h as a function of the probability of false alarms P_{FA}. However, this property holds asymptotically, whereas in this case a limited window M is used. Furthermore, the asymptotic PDF of the GLRT assumes IID data. The estimated parameters and flow rates from observer (5.3) are clearly not IID, since the observer acts as a filter of current and previous measurements. Such discrepancy between the asymptotic IID result and a real distribution was also shown to exist in position mooring diagnosis in Blanke et al. (2012).

A Weibull probability plot of $g(k)$ for Θ_D at $\mathcal{H}_0$ is shown in Fig. 5.5 together with a χ^2_r-distribution with $r = 4$ (change in mean of $\Theta_D \in \mathbb{R}^4$), and a fitted Weibull distribution. This plot shows that the test statistic better fits a Weibull distribution, which therefore will be used to determine thresholds. Fitting GLRT statistics to distrubutions other than the χ^2-distribution, such as the Weibull and lognormal distributions, was done in Galeazzi et al. (2013) and Hansen and Blanke (2014).

Table 5.2: Threshold values.

Threshold	Weibull	χ^2_4
h_D	46.6	33.4
h_I	83.7	33.4

Let $Q(x;\alpha,\beta)$ be the inverse cumulative distribution of the Weibull distribution

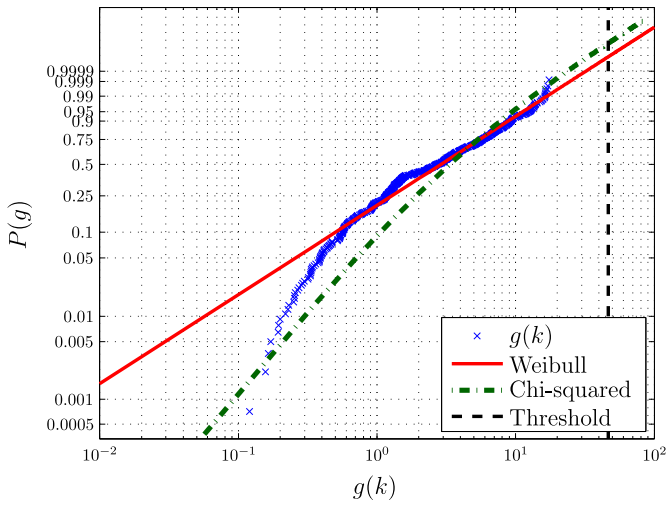

Figure 5.5: Weibull probability plot of $g(k;\Theta_D)$ at $\mathcal{H}_0$ for Weibull and χ^2_4-distribution.

with statistical parameters α, β. Then the threshold for a desired P_{FA} is given by

$$h = Q(1 - P_{FA}; \mathcal{H}_0, \alpha_0, \beta_0) = \beta_0 \left(-\ln(P_{FA})\right)^{1/\alpha_0}, \tag{5.14}$$

where α_0 and β_0 are the statistical parameters fitted to $g(k)$ of data Θ_D and Θ_I under $\mathcal{H}_0$. The thresholds for $g(k;\Theta_D)$ and $g(k;\Theta_I)$ with $P_{\text{FA}} = 10^{-6}$ are given in Tab. 5.2 for the real (Weibull) and theoretical (χ^2) case.

5.5.2 Pack-off detection and isolation

The fault diagnosis method is applied on the estimated parameters and states. Fault type isolation is shown in Fig. 5.6, where the upper panel shows the value of $g(k)$ of Θ_D using a window length $M = 100$, the lower panel shows incident type isolation. In addition, there is a requirement of 100 consecutive samples (10 s) of $g(k)$ above threshold before an alarm is set. This figure clearly shows that all three pack-offs are correctly detected and isolated, with some brief false alarms during change of flow rate, which can be ignored since this change is known. It is assumed that the estimated parameters and states are IID, while they actually are slightly correlated with previous samples. However, assuming IID signals and using (5.7) is shown here to give sufficient detection. If no statistical change detection method was used, and a threshold of the unfiltered $\hat{\theta}_a$ was to be applied directly, detection would be uncertain, and selecting a proper threshold for $\hat{\theta}_{a,3}$ seen in Fig. 5.4 would be difficult if not impossible.

Position localization is shown in Fig. 5.7, showing $g(k)$ for change detection of Θ_I in the upper panel and localization in the lower. Also here, the fault diagnosis method successfully manages to detect the change in parameters and localize the position of the pack-off. It would be possible to estimate the location of the pack-off

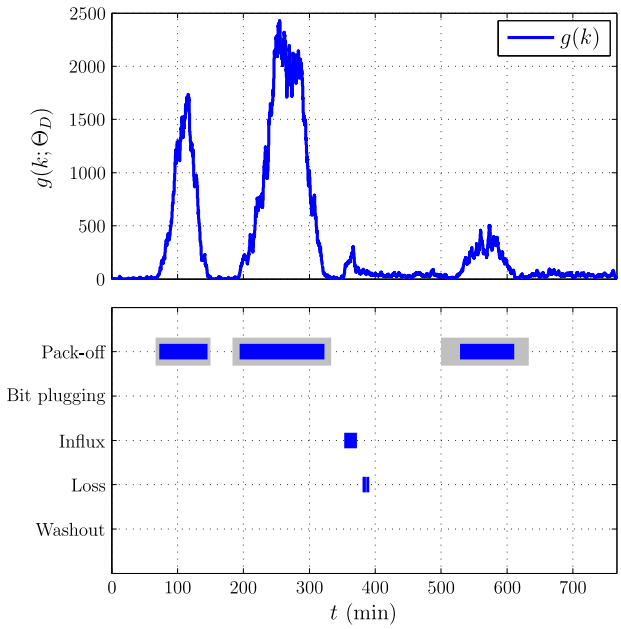

Figure 5.6: Pack-off detection and isolation. Actual pack-offs are shown in grey.

with some uncertainty, but that would require high accuracy modeling of the well geometry. The method in this paper focuses on simple modeling, with position localization limited a segment between two pressure sensors.

Pack-offs are typically building up quite slowly in a real scenario. However, due to limiting simulation times, the simulated pack-offs are occurring quite fast. The strength of the diagnosis method is that both abrupt (fast) and incipient (slowly varying) incidents can be diagnosed.

5.5.3 Pack-off magnitude estimation

The frictional pressure drop due to a pack-off is possible to estimate once the fault is detected and isolated. A pack-off will increase the friction in the annulus with the amount F_{po}. The total estimated annulus friction is given by $\hat{F}_a = \hat{F}_{po} + \hat{F}_{a,0} = (\hat{\theta}_a - \mu_{a,0})\hat{q}_b^2 + \mu_{a,0}\hat{q}_b^2$, where $\hat{F}_{a,0}$ is the annulus friction without pack-offs and $\mu_{a,0} = E(\hat{\theta}_a; \mathcal{H}_0)$ is the mean of the annulus parameter at $\mathcal{H}_0$. The pack-off friction magnitude can thus be estimated as

$$\hat{F}_{po} = (\hat{\theta}_a - \mu_{a,0})\hat{q}_b^2. \tag{5.15}$$

The low-pass filtered estimated pack-off magnitudes are shown in blue in Fig. 5.8, with actual pressure drop from OLGA simulations without noise shown in red. The plots show accurate magnitude estimation of all three pack-offs. By combining

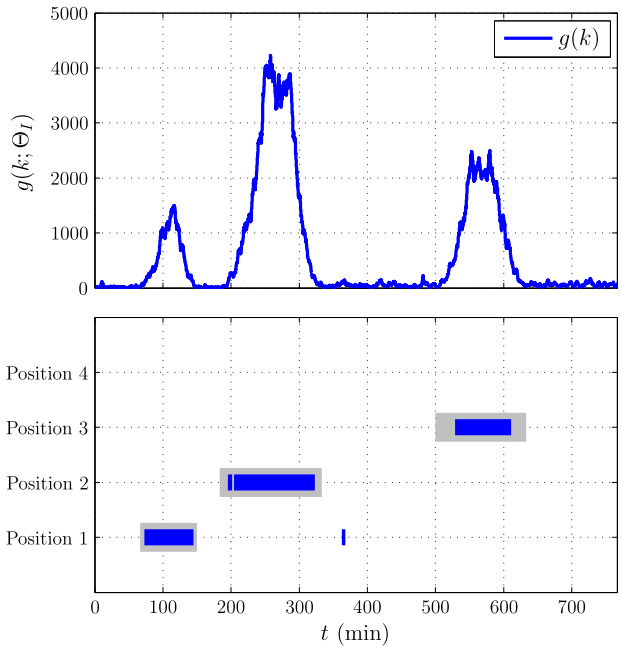

Figure 5.7: Pack-off localization. Actual location shown in grey.

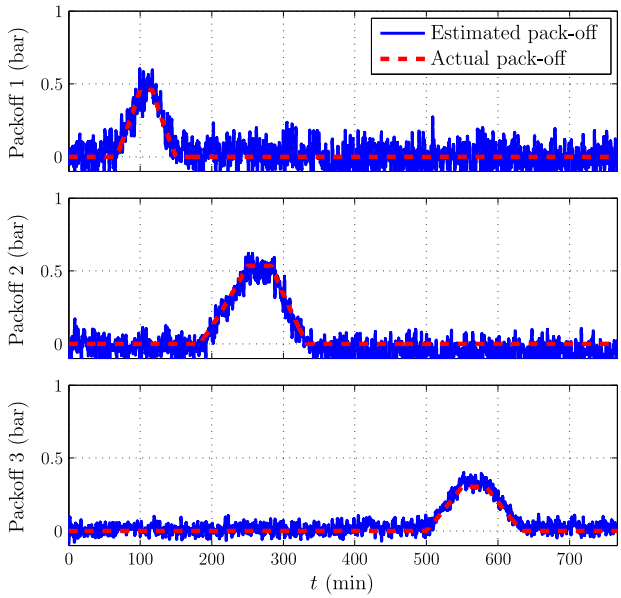

Figure 5.8: Pack-off magnitude estimation.

parameter estimation with a change detection method, fault diagnosis is hence possible, as well as fault magnitude estimation. This is one of the strengths of using estimation of physical parameters, or lumped physical parameters, as a basis for fault diagnosis.

5.6 Conclusion

Pack-off in drilling is a severe event which can lead to costly downtime. Simulations in OLGA are used to test a fault diagnosis method for pack-off detection, isolation, localization, and magnitude estimation. Three pack-offs at different positions and sizes are successfully diagnosed with early detection and low false alarm rates, even with noticeable noise in the measurements. A multivariate generalized likelihood ratio test is applied to detect changes in a set of estimated friction parameters and flow rates affected by noise. By determining the direction of change of a subset of the signals, the type of fault and location is correctly isolated as pack-offs at different positions, and at an early stage with specified probability of false alarms. Once the pack-off is diagnosed, its magnitude is correctly estimated from the estimated friction parameters.

Chapter 6

Fault detection and isolation in drilling using analytical redundancy relations

The work in this chapter was published in Willersrud et al. (2015b).

Summary

Early diagnosis of incidents that could delay or endanger a drilling operation for oil or gas is essential to limit field development costs. Warnings about downhole incidents should come early enough to allow intervention before it develops to a threat, but this is difficult, since false alarms must be avoided. This paper employs model-based diagnosis using analytical redundancy relations to obtain residuals which are affected differently by the different incidents. Residuals are found to be non-Gaussian - they follow a multivariate t-distribution - hence, a dedicated generalized likelihood ratio test is applied for change detection. Data from a 1400 meter horizontal flow loop test facility is used to assess the diagnosis method. Diagnosis properties of the method are investigated assuming either with available downhole pressure sensors through wired drill pipe or with only topside measurements available. In the latter case, isolation capability is shown to be reduced to group-wise isolation, but the method would still detect all serious events with the prescribed false alarm probability.

6.1 Introduction

Drilling for oil and gas is a high-cost operation with risk of delays, and possibly safety and environmental impacts, if an abnormal incident is occurring. A drillstring is rotated with a drill bit at the bottom, crushing the formation. A circulated drilling fluid then transports the formation cuttings back to the surface through the annulus surrounding the drillstring, see Fig. 6.1. Pressure in the well is controlled by the hydrostatic and friction pressure drop of the drilling fluid, as well as a possible topside back-pressure. For some wells, the pressure window of operation between the pressure of the formation fluid and the formation fracture pressure is quite narrow. Incidents happening can make it difficult to maintain this operational window, and may lead to costly delays in progress.

Monitoring of the drilling process has traditionally been done manually by drilling operators. With new sensor technology, giving an increased number of measurements available, manual monitoring may be overwhelming and tiresome for operators, whose main task is to drill deeper into the formation, maintaining operating requirements. An automatic diagnosis algorithm can be used to interpret the signals and alarming the operators at an earlier stage if something abnormal is about to develop. Abnormal downhole incidents include *influx* of fluids from the formation, or *lost circulation* of drilling fluid to the formation, *plugging of the drill bit*, *pack-off* of formation solids around the drillstring, and leakage from the drillstring to the annulus caused by wear and tear, called *drillstring washout*. Sensors may stop working, or have a slowly varying bias drift giving incorrect readings, and actuators may stop or be partially defective. If the drilling technology *managed pressure drilling* (MPD) is applied, the installed choke may be *plugged*.

Detection of influxes was studied in Gravdal et al. (2010a); Hauge et al. (2013). Detection of other incidents was studied in (Cayeux et al., 2012b) using a high-fidelity model, and a knowledge-based method was used in (Skalle et al., 2013). Lost circulation, formation fluid influx, and drillstring washout have many similarities to the problem of leak diagnosis in open water channels, see, e.g., Bedjaoui and Weyer (2011).

Model-based fault diagnosis methods can often be divided into methods detecting changes in estimated parameters or states, or using residuals which are zero in the fault-free case and non-zero during a fault Zhang and Jiang (2008). Diagnosis based on parameter estimation in drilling was the topic in Willersrud et al. (2015c,d), while this paper presents a *fault detection and isolation* (FDI) method based on residuals generated using *analytical redundancy relations* (ARR), see, e.g., Chow and Willsky (1984); Staroswiecki and Comtet-Varga (2001); Blanke et al. (2006). Model-based fault diagnosis of sensors in aircrafts using an extended Kalman filter was studied in Van Eykeren and Chu (2014), and in Odendaal and Jones (2014) diagnosis of actuator faults was done using analytical redundancy relations and a cumulative sum (CUSUM) method, while Knüppel et al. (2014) applied ARR for an electrical distribution system.

Analytical redundancy relations offer an alternative to parameter and/or state estimation, where a structured method is used to generate residuals based on the model equations. This avoids the need for a stable adaptive observer. In addition, the ARR residual generation framework offers possibilities to detect and isolate actuator and measurements faults such as bias drift, differentiating them from process faults in a systematic manner.

Measurement noise will affect the residuals, and with small changes in the residuals due to faults, a statistical change detection algorithm is necessary. To increase detection and isolation capabilities it was demonstrated in (Willersrud et al., 2015c) that a multivariate change detection algorithm using a *generalized likelihood ratio test* (GLRT) was superior to univariate change detection of estimated parameters. Statistical evaluation of residual signals for fault detection and isolation was studied in Basseville (1988); Gertler and Yin (1996); Peng et al. (1997); Heyns et al. (2012),

while the use of directional residuals was studied in (Gertler and Monajemy, 1995; Yin, 1998; Venkatasubramanian et al., 2003c).

In this paper actuator faults, sensors faults, and downhole drilling incidents are detected and isolated using a model-based fault diagnosis method. The different incidents are illustrated in Fig. 6.1, highlighted in red. Residuals are generated using analytical redundancy relations, which due to use of sensor measurements are affected by noise. Therefore, statistical change detection is applied using GLRT, detecting changes in the vector residual. This method will increase detectability of small changes to the process due to an incident, decreasing the false alarm rate. The different incidents will affect the residuals differently, making isolation possible by determining the residual change direction.

The method is tested on a series of data sets from a medium-scale flow loop test carried out in Stavanger, Norway. The flow loop is a horizontal loop of 1400 meters, using water as drilling fluid. The paper describes two scenarios of fault detection and isolation possibilities. In the first scenario, downhole pressure measurements are available assuming the use of *wired drill pipe* technology, see, e.g., Jellison et al. (2003); Pixton et al. (2014). The second scenario describes what can and cannot be detected and isolated with only topside sensors available, a case still most common in the industry.

The paper is organized into ten sections. After the introduction, details about the flow-loop test setup is described in Sec. 6.2. Model-based fault diagnosis is briefly introduced in Sec. 6.3, and the system model is presented in Sec. 6.4. Analytical redundancy relations are derived in Sec. 6.5, and methods for change detection and incident isolation are suggested in Sec. 6.6. Results of incident detection and isolation using downhole sensors are shown in Sec. 6.7, and without downhole sensors in Sec. 6.8. A discussion and a conclusion finalize the paper.

6.2 Flow loop for testing of incidents in drilling

Data from a medium-scale horizontal flow loop is used to test fault diagnosis of downhole incidents, actuator fault, and sensor bias drift. The flow loop shown in Fig. 6.2 is a 1400 meter test rig located in Stavanger, Norway, circulating water in circular pipes with typical drilling diameters. During the tests the flow loop was rigged for managed pressure drilling (MPD). This is a drilling method where the annulus is sealed off with a choke as illustrated in Fig. 6.1. Doing so, the downhole pressure is controlled by the choke back-pressure, which is affected by hydrostatic pressure due to density, and friction due to fluid flow. The model used in the diagnosis is thus adapted to MPD, which could be applied to conventional drilling by omitting the choke. The test setup was rigged to test the incidents bit nozzle plugging, drillstring washout, lost circulation, gas influx and choke plugging. Pack-off was not tested. No tests were done for bias drift, and this is therefore tested by artificially adding a noise-free signal to specific measurements, ramping up from zero to a constant bias.

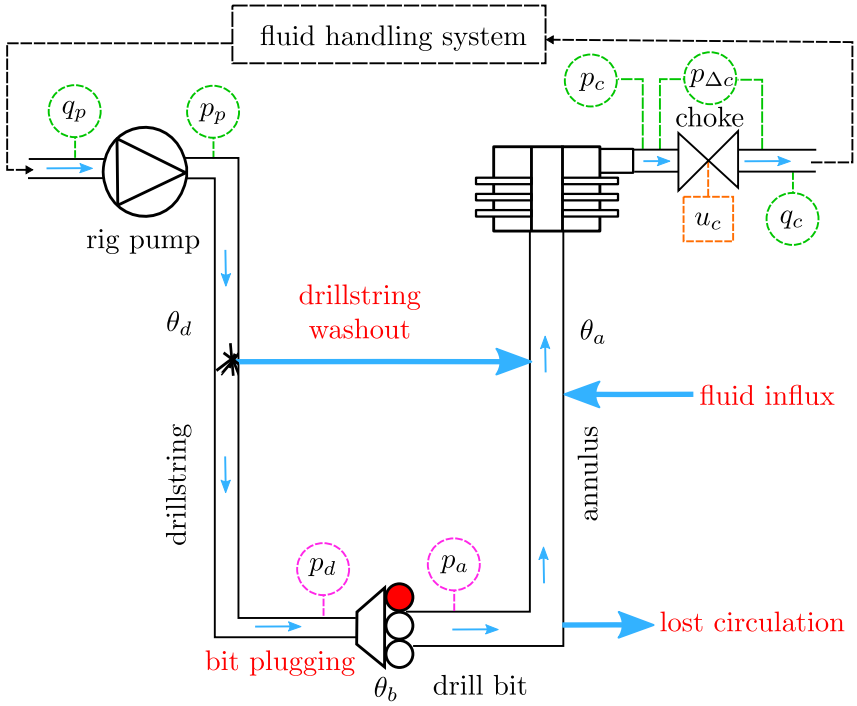

Figure 6.1: Managed pressure drilling process with possible downhole incidents shown in red, including lost circulation, drillstring washout, formation fluid influx, and bit nozzle plugging. Topside sensors shown in green, downhole sensors in magenta, and the actuator in orange.

There are some obvious differences between the test setup and real drilling. One discrepancy is the lack of difference in height between the bit at the bottom of the well and the choke at the top. This will result in different hydrostatic pressure, where during an influx the height difference will affect the now multi-phase flow. However, for normal drilling conditions, this issue only adds a constant hydrostatic pressure. Other characteristics that differ are the lack of transported solids due to drilling ahead, as well as lack of annular effects since circular pipes are used in the test setup. Nevertheless, for testing drilling incidents the flow loop produces realistic scenarios, only preceded by a full-scale test rig or actual drilling with logged incidents.

Figure 6.2: Stand pipe with pressure measurement p_p (left) and chokes with pressure measurement p_c (right).

6.3 Model-based fault detection and isolation

Fault diagnosis methods may be divided into model-based and data-based techniques Zhang and Jiang (2008). Model-based methods are typically used if mathematical models of the process and faults are available, whereas data-driven methods use historical data of complex systems to determine occurring faults, see, e.g., Svärd et al. (2014). Although complex, the drilling process is limited in size and can be divided into two subsystems separated by the drill bit. With a quite simple hydraulics model available, this paper uses a model-based diagnosis method, namely analytical redundancy relations to generate residuals, together with statistical change detection to detect changes to the residuals.

Model-based fault detection and isolation (FDI) is defined in Isermann and Ballé (1997) as

- *Fault detection:* Determination of the presence of a fault in the system.
- *Fault isolation:* Determination of the kind and location of the fault.

The FDI procedure can be divided into function blocks. A *residual generator* which provides signals that ideally deviate from zero only if a fault happens, and a *decision system* giving a hypothesis about which parts of the system are faulty Blanke et al. (2006), see Fig. 6.3.

Residuals in a model-based fault detection and isolation method can be generated using state estimation, parameter estimation, joint state and parameter estimation, or analytical redundancy relations, see, e.g., Patton and Chen (1997); Gertler (1997). Joint state and parameter estimation is achieved using an adaptive observer, or extending the state vector in a Kalman filter by relevant parameters. Adaptive observers for state and parameter estimation was the topic in Willersrud et al. (2015c,d). This paper focuses on using analytical redundancy relations. Benefits and drawbacks of the two methods are compared in Tab. 6.1, which is a shortened version of Tab. 14.1 in Isermann (2006).

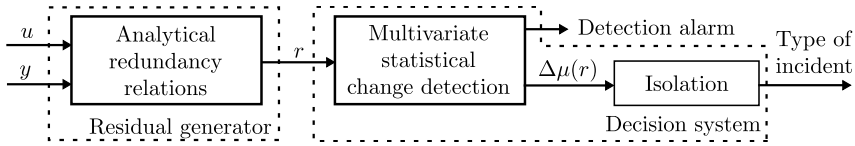

Figure 6.3: Fault detection and isolation using analytical redundancy relations to generate residuals r as a function of measured inputs u and outputs y. Changes in mean $\Delta\mu(r)$ are detected using statistical change detection, and incident type isolation is determined using change direction of the mean.

6.4 System representation

The model of the drilling process including system dynamics, algebraic equations, inputs, and measurements are presented in this section. Consider the system

$$\dot{x} = f(x, u, \theta), \tag{6.1a}$$
$$y = h(x, u, \theta), \tag{6.1b}$$

where $x \in \mathbb{R}^{n_x}$ is the state vector, $u \in \mathbb{R}^{n_u}$ is the input vector, and $\theta \in \mathbb{R}^{n_\theta}$ is a constant parameter vector. Each equation $\dot{x}_i = f_i(x, u, \theta)$, $y_i = h_i(x, u, \theta)$, and u_i in (6.1) will represent a constraint

$$c_i \in \mathcal{C} \tag{6.2}$$

in the constraint set $\mathcal{C}$, used in generating the analytic redundancy relations, as well as analyzing the relationship between the ARR and the faults.

The analytic redundancy relations are easily generated from simple model equations. In general, simple models give faster and easier real-time diagnostic classifiers Venkatasubramanian et al. (2003c), while unmodeled dynamics can be treated as model uncertainty. Motivated by this, the dynamics in the well is modeled with

Table 6.1: Comparison of combined state and parameter estimation with analytical redundancy relations for fault diagnosis, with the preferred method highlighted. Adapted from Isermann (2006).

Characteristics	**Combined state and parameter estimation**	**Analytical redundancy relations**
Fast detection	Relatively fast, dependent on tuning	*Fast*
Detecting and isolating sensor and actuator bias	Dependent on model and setup	*Inherent*
Estimation of fault magnitude	*Possible, but dependent on model and setup*	Requires additional estimation
Propagation of measurement noise	*Dependent on tuning*	Needs to be handled if measurement differentiation is required
Design of method	Dependent on model, may require expert knowledge to derive observer	*Straightforward if tools are available*
Model parameters	*Unknown, time-varying*	Known, constant
Excitation requirements	Possibly	*No*

a modification of the simplified model from Kaasa et al. (2012) for the drilling hydraulics,

$$(c_1): \quad \frac{dp_c}{dt} = \frac{\beta_a}{V_a}(q_p - q_c) \tag{6.3a}$$

$$(c_2): \quad \frac{dq_p}{dt} = \frac{1}{M}((\rho_a - \rho_d)gh + p_c - p_p + \theta_d q_p^2 + \theta_b q_p^2 + \theta_a q_p^2) \tag{6.3b}$$

where p_p is the pressure at the pump, p_c the pressure upstream the choke, q_p the pump flow and q_c flow through the choke, see Fig. 6.1. The pressure drop $p_{\Delta c}$ over the choke is measured by a dedicated pressure difference sensor. The parameters β_a and V_a represent the bulk modulus and volume of the annulus, respectively, and M is the integrated density of the total liquid in the drillstring and the annulus per cross section area. The density of the fluid in the annulus is ρ_a, and ρ_d in the drillstring, g is the gravitational acceleration, and h is the depth of the well. The pressure dynamics in the drillstring is ignored, assuming in (6.3) that the flow q_p from the rig pump equals the flow through the bit. This pressure dynamics is typically orders of magnitude faster than the occurring incidents, making the assumption valid.

The friction through the system is modeled using a turbulent friction relationship $\theta_i q_b^2$ for the drillstring, bit, and annulus, respectively with $i \in \{d, b, a\}$. As shown in Willersrud et al. (2015d), this relationship matches the flow loop data well. For laminar flow, a linear relationship can be applied. The friction coefficients θ_i can be

found offline using some form of parameter identification, while all other parameters are assumed constant and known.

The algebraic equations of friction and choke flow are given by

$$(c_3): \ p_d = p_p - \theta_d q_p^2 + \rho_d g h, \tag{6.3c}$$
$$(c_4): \ p_a = p_d - \theta_b q_p^2, \tag{6.3d}$$
$$(c_5): \ p_a = p_c + \theta_a q_p^2 + \rho_a g h, \tag{6.3e}$$
$$(c_6): \ q_c = g_c(u_c)\sqrt{p_{\Delta c}}, \tag{6.3f}$$

where p_a is the pressure in the annulus, downstream the bit. This pressure is commonly named the *bottomhole pressure*. The pressure upstream the bit is denoted p_d. The choke opening input constraint is

$$(c_7): \ u = u_c, \tag{6.3g}$$

and the measurements are

$$(c_8 - c_{14}): \ y = \begin{bmatrix} p_p, & p_d, & p_a, & p_c, & p_{\Delta c}, & q_p, & q_c \end{bmatrix}^\top. \tag{6.3h}$$

Note that both states p_c and q_p in (6.3) are measured, as well as the downhole pressures p_a and p_d. In the following sections these downhole sensors are first assumed available. Analysis and discussion of the case without the downhole sensors follows subsequently.

6.5 Analytical redundancy relations

Analytical redundancy relations (ARR) are functions of the system inputs and outputs and their derivatives, and can be used to derive nonlinear residuals (Staroswiecki and Comtet-Varga, 2001). Analytical redundancy in fault diagnosis can be used to check for inconsistencies between the actual system and the system model, and residuals can be used for fault detection and isolation Venkatasubramanian et al. (2003c). The residuals should be (close to) zero during the fault free case, and significantly non-zero during a fault. Detection of change from zero to non-zero of the residuals can then be used for fault detection and isolation.

The residuals designed based on system (6.1) can be written as

$$r(\bar{y}^{(q)}, \bar{u}^{(q)}, \theta) = 0, \tag{6.4}$$

where $\bar{y}^{(q)}$ and $\bar{u}^{(q)}$ are vectors of y and u and their time derivatives up to order q, respectively, see, e.g., (Staroswiecki and Comtet-Varga, 2001; Blanke et al., 2006; Trave-Massuyes et al., 2006; Sundström et al., 2014). In case of measurement noise, the residuals (6.4) are not identically zero in the fault-free case. Thus, a fault is detected using hypothesis testing by differentiating between the *null hypothesis* $\mathcal{H}_0$, and the *alternative hypothesis* $\mathcal{H}_1$,

$$\mathcal{H}_0: \quad r(\bar{y}^{(q)}, \bar{u}^{(q)}, \theta) = w, \tag{6.5}$$
$$\mathcal{H}_1: \quad r(\bar{y}^{(q)}, \bar{u}^{(q)}, \theta) = A + w, \tag{6.6}$$

where w is white noise with probability distribution $f(x;\Pi)$ with statistical parameters Π, and where $A \neq 0$ is representing the effect of the fault. Computing ARR is done by eliminating the state in the system equations. Different tools and methods available for generating ARR and *minimal structurally overdetermined sets* (Trave-Massuyes et al., 2006; Blanke et al., 2006; Krysander et al., 2008) for residuals are compared in Armengol et al. (2009). The MATLAB toolbox SaTool Blanke and Lorentzen (2006) comprises algorithms to find complete matchings between the constraints and the unknown system variables, and is used to generate the residuals in this paper.

6.5.1 ARR for the drilling model

From the system constraints defined in (6.3), the Matlab tool SaTool is used to find the following residuals,

$$r_1 = \frac{d}{dt}y_4 - \frac{\beta_a}{V_a}(y_6 - y_7), \tag{6.7a}$$

$$r_2 = \frac{d}{dt}y_6 + \frac{1}{M}\left((\rho_a - \rho_d)gh - y_1 + y_4 + \theta_a y_6^2 + \theta_b y_6^2 + \theta_d y_6^2\right), \tag{6.7b}$$

$$r_3 = \theta_d y_6^2 - \rho_d gh - y_1 + y_2, \tag{6.7c}$$

$$r_4 = \theta_b y_6^2 - y_2 + y_3, \tag{6.7d}$$

$$r_5 = \theta_a y_6^2 + \rho_a gh - y_3 + y_4, \tag{6.7e}$$

$$r_6 = y_7 - g_c(u_c)\sqrt{y_5}, \tag{6.7f}$$

which will be used for fault detection and isolation.

Differentiating a signal with noise leads to obvious challenges. A common procedure to reduce noise is to low-pass filter the signal, in this case the residuals. However, if the residuals are low-pass filtered the result will be slower detection. Furthermore, since both of $y_6(t)$ and dy_6/dt appear in r_2, the derivative of the signal is not needed for detectability nor isolability and the presence of $y_6(t)$ ensures that a change in y_6 is strongly detectable. With respect to dy_4/dt, $y_4(t)$ itself appear in r_2 and r_5, which assures strong detectability and isolability. Therefore, the derivatives of $y_4(t)$ and $y_6(t)$ in (6.7) are not needed and they are omitted in the further analysis and application. This is equivalent to considering the algebraic version of constraints c_1 and c_2 in (6.3), that follow with $dy_4/dt \equiv 0$ and $dy_6/dt \equiv 0$. Rapid changes do not take place in the normal drilling operation, and the derivatives would be within the noise floor. If, nevertheless, dy_6/dt should change rapidly, r_2 might give a short deviation from zero but $[r_1, r_3, r_4, r_5]^T \simeq 0$, so a $\mathcal{H}_1$ hypothesis would be rejected. If dy_4/dt should change rapidly, r_2 would deviate for a short while, but since none of the other residuals would deviate from zero, a false $\mathcal{H}_1$ alarm would be rejected, also in this case.

6.5.2 Relations between faults in analytic and structural domains

In the structural domain, we consider violations of normal behaviors and analyze the ability to detect whether a violation has happened. Isolation in this domain means to determine which constraint has been violated. When translating to the analytic domain, residuals (6.7) are expressed as functions of measured signals y, of input u, and of process parameters in θ, ρ, V_a, etc.

6.5.3 ARR and constraint dependency

The matching between residuals (6.7) and constraints (6.3) was found using the ranking algorithm implemented in SaTool (Blanke and Lorentzen, 2006). Subsequent calculation of the analytical redundancy relations is achieved by expressing that $c_k = 0$ is an ARR when c_k is an unmatched constraint, i.e., redundant in the calculation of the unknown variables but valid and useful as a test quantity. With c_k being a function of the variables in the system and with all unknown variables being calculable as prescribed by the complete matching, a backtracking along the path found by the matching will lead to c_k being a function expressed solely by known variables. The calculation of c_k will be a function also of the constraints c_i along the paths of the backtracking.

As a next step, the ARR $c_i = 0$ is replaced by the test quantity $r_j = c_i$ where r_j is a residual. The resulting dependencies between the constraints and the residuals are listed in Tab. 6.2. An 'X' in the table at position (j, i) means that a constraint c_i is used in the calculation of residual r_j. A violation of c_i will therefore influence r_j such that the function $r_j(t)$ will be nonzero for some or all t after $c_i(t) \neq 0$ has happened. This is referred to as *detectability*. *Isolability* means that it is possible to determine which particular constraint was violated. Precise definitions can be found in Blanke et al. (2006).

Table 6.2: Dependency matrix between residuals and constraints.

Residual	c_1	c_2	c_3	c_4	c_5	c_6	c_7	c_8	c_9	c_{10}	c_{11}	c_{12}	c_{13}	c_{14}
r_1	X										X		X	X
r_2		X						X			X		X	
r_3			X					X	X				X	
r_4				X					X	X			X	
r_5					X					X	X		X	
r_6						X	X					X		X

Tab. 6.3 shows structural detectability and isolability of each constraint using the residuals r. *Structural detectability*, denoted d, follows if the corresponding column i in Tab. 6.2 is non-zero, i.e., comprises an 'X'. *Structural isolability*, denoted i, requires that the signature in column i in Tab. 6.2 differs from the signature of all other columns. Constraints c_6, c_7 and c_{14} are only detectable, denoted 'd' in

Tab. 6.3. This means that it is not possible to distinguish between a violation of these three constraints or, in other words, that it is not possible to distinguish between faults in sensors q_c, $p_{\Delta c}$ and choke opening u_c. This can be also seen in the constraint dependency table shown in Tab. 6.2, giving the same matching for r_6 with c_6, c_7 and c_{12}. Fortunately, all these sensors are topside and easily available. If a low reliability is experienced in these sensors, redundant sensors could be installed to enhance isolability. Pressure sensors in particular are quite small and easy to install.

Table 6.3: Detectability and isolability of constraints.

c_1	c_2	c_3	c_4	c_5	c_6	c_7	c_8	c_9	c_{10}	c_{11}	c_{12}	c_{13}	c_{14}
i	i	i	i	i	d	d	i	i	i	i	d	i	i

Localization of the position of an incident, which was done in Willersrud et al. (2015d) based on parameter and state estimation, would also be possible using ARR by including additional measurements in the annulus and extending the model (6.3) to include friction parameters representing friction between the measurements. However, this will lead to quite many constraints and residuals. To narrow down the scope of this paper, localization is omitted in the fault diagnosis, focusing on incident detection and type isolation.

6.5.4 Fault isolation with analytical redundancy relations

The faults are not modeled explicitly in (6.3). This has been done for mechanical systems in, e.g., Svärd et al. (2013), where faults in an automotive engine were modeled explicitly. This would result in a mapping between the faults and the residuals. In this paper, this relationship is implicit, and a physical change to the process will affect the residuals as indicated in Tab. 6.2 as a match between residual r_j and constraint c_i.

The challenge with explicit modeling of the faults lies both in the nature of some of the faults and the difficulty of modeling any possible incident or fault. The methodology of Svärd et al. (2013) is aimed at isolating only the specific fault included in the model. The generic approach used here will be sensitive to any deviation from the normal behavior that was described by (6.3).

A drillstring washout, a loss of circulating drilling fluid, or an influx will change the flow in parts of the process. However, the position of the fault is unknown, and therefore difficult to implement in the model. The different faults and sensor bias drifts are listed in Tab. 6.4. An 's' in Tab. 6.4 denotes *strong detectability* of the corresponding fault (as opposite to weak detectability), meaning that the affected residual reaches a non-zero steady state, see, e.g., Blanke et al. (2006).

The incidents are defined as:

- A *drillstring washout* (f_{wo}) is a leakage from the drillstring to the annulus, and will reduce flow in the lower parts of the system. This will be seen as a reduced friction loss in the drillstring, over the bit, and in the annulus.
- *Lost circulation* (f_{ls}) of drilling fluid to the reservoir will reduce friction in the annulus.
- An *influx* (f_{in}) of reservoir fluids will have an opposite effect as lost circulation giving larger flow out of the well than in, and an increased friction in the annulus.
- A *plugging of the drill bit nozzles* (f_{bp}) will cause an increased pressure drop over the drill bit. This will then give a higher back-pressure at the bit, giving increasing values of pump pressure and upstream bit pressure.
- A *pack-off* (f_{po}) is a partial or fully plugging of of solids around the drillstring in the annulus, giving increased pressure drop in this section. It will therefore behave similar as a bit nozzle plugging, but with an increased friction drop in the annulus rather than over the bit.
- A *choke plugging* (f_{cp}) is a partially or fully blocking of the MPD choke, caused by formation solids. This will change the characteristics of the choke.
- Bias drifts in pressure sensors p_p, p_c, p_d and p_a are denoted as Δp_i for sensor p_i for a positive drift.

All the sensor faults and process incidents are possible to isolate, as seen in Tab. 6.4, except from a negative bias drift in choke pressure ($-\Delta p_c$) and a pack-off (f_{po}) which have the same signature. Note that the method does not necessarily handle isolation of simultaneous incidents. However, for drilling this is not considered a limitation, since each of the incidents are quite severe. If an incident is detected and isolated, drilling should be suspended and appropriate actions should be taken immediately to reduce possible consequences.

Table 6.4: Fault dependency table with downhole measurements. Strong detectability is denoted 's'.

Residual	Δp_p	Δp_c	Δp_d	Δp_a	f_{wo}	f_{ls}	f_{in}	f_{bp}	f_{po}	f_{cp}
r_1						$-$	$+$			
r_2	$-$	$+$			$+$	$+$	$+$	$-$	$-$	
r_3	$-$		$+$		$+$					
r_4			$-$	$+$	$+$			$-$		
r_5		$+$		$-$	$+$	$+$	$-$		$-$	
r_6										$-$
	s	s	s	s	s	s	s	s	s	s

6.5.5 Analytical redundancy relations with only topside measurements

Analysis up until now assumed available downhole pressure sensors through a wired drill pipe. However, this is a novel technology without a large user base in operating drilling rigs. More commonly, only a single downhole pressure sensor is available, with high latency, low bandwidth transmission and with a relatively high rate of downtime. In many cases no downhole measurement is available at all. It is hence interesting to investigate what can be done using only topside measurements, in other words, not using p_d and p_a in the measurement vector (6.3h).

Conducting the same analysis as before, but removing p_d and p_a from (6.3), the alternative residuals $\tilde{r}$ are

$$\tilde{r}_1 = \frac{d}{dt}\tilde{y}_2 - \frac{\beta_a}{V_a}(\tilde{y}_4 - \tilde{y}_5), \tag{6.8a}$$

$$\tilde{r}_2 = \frac{d}{dt}\tilde{y}_4 + \frac{1}{M}\left((\rho_a - \rho_d)gh - \tilde{y}_1 + \tilde{y}_2 + \theta_f \tilde{y}_4^2\right), \tag{6.8b}$$

$$\tilde{r}_3 = \tilde{y}_2 - \tilde{y}_1 + \theta_f \tilde{y}_4^2, \tag{6.8c}$$

$$\tilde{r}_4 = \tilde{y}_5 - g_c(u_c)\sqrt{\tilde{y}_3}, \tag{6.8d}$$

the topside measurements are

$$\tilde{y} = \begin{bmatrix} p_p, & p_c, & p_{\Delta c}, & q_p, & q_c \end{bmatrix}^\top, \tag{6.9}$$

and

$$\theta_f = \theta_d + \theta_b + \theta_a \tag{6.10}$$

is the friction coefficient of the total friction from pump to choke, represented by the parameter θ_f. Since no downhole measurements are available, θ_d, θ_b and θ_a are not possible to identify individually.

Table 6.5: Fault dependency table with no downhole measurements. Strong detectability is denoted 's'.

	Δp_p	Δp_c	f_{wo}	f_{ls}	f_{in}	f_{bp}	f_{po}	f_{cp}
$\tilde{r}_1$				$-$	$+$			
$\tilde{r}_2$	$-$	$+$	$+$	$+$	$+$	$-$	$-$	
$\tilde{r}_3$	$-$	$+$	$+$	$+$	$+$	$-$	$-$	
$\tilde{r}_4$								$-$
	s	s	s	s	s	s	s	s

With a possibility of both positive and negative drift of the pressure sensors, it is not possible to separate washout (f_{wo}), bit nozzle plugging (f_{bp}) and pack-off (f_{po}) from bias drift, as seen in Tab. 6.5, although subgroups of sensor faults and physical incidents can be isolated. This is as expected, since drillstring washout, bit nozzle plugging and pack-off only change the pressure drop seen from pump to

choke, without changing flow rate. Without downhole measurements, it is difficult to separate these from bias drift. However, since the measurements are located topside, they are more easily accessible than downhole measurements. One could install redundant pressure sensors making it easy to isolate a sensor with bias drift and exclude it from the diagnostic algorithm. Drillstring washout could then be isolated from either a bit nozzle plugging or a pack-off.

6.6 Multivariate change detection and change direction for FDI

Detecting changes to the residuals are done by using a multivariate generalized likelihood ratio test (GLRT). By using a multivariate scheme, changes to all residuals are considered jointly. For diagnosis based on change detection in Willersrud et al. (2015c), this approach was found to be superior compared with using independent univariate tests on each signal.

It is common to assume that the noise is Gaussian distributed. However, noting that the residuals are sums of pressure measurements, and squares of flow measurements, residuals are not likely to be Gaussian. The distribution is checked using a Kolmogorov-Smirnov test for the Gaussian, Student t, Laplace, and Cauchy distributions in Tab. 6.6, showing a high p-value for all residuals with the t-distribution, which furthermore is the only distribution with all p-values above 0.05, a typical statistical threshold. To save space, only the p-values for the lost circulation case is shown, but the t-distribution is well suited for all cases. Non-Gaussian distributions on estimated parameters and residuals are studied in Willersrud et al. (2015c,d); Hansen and Blanke (2012, 2014).

Table 6.6: Kolmogorov-Smirnov test of the residuals r for the lost circulation case at $\mathcal{H}_0$, with p-values above 0.05 highlighted.

Residual	Gaussian	Student t	Laplace	Cauchy
r_1	**0.064**	**0.79**	**0.059**	1.0×10^{-6}
r_2	0.034	**0.70**	0.010	1.5×10^{-7}
r_3	2.8×10^{-9}	**0.76**	**0.75**	5.6×10^{-3}
r_4	$< 10^{-12}$	**0.87**	**0.053**	0.048
r_5	0.0031	**0.99**	0.0011	4.6×10^{-7}
r_6	0.0082	**0.19**	3.2×10^{-7}	4.2×10^{-10}

The detection problem of change in a signal x is to distinguish between the *null hypothesis* $\mathcal{H}_0$ and the *alternative hypothesis* $\mathcal{H}_1$, which can be presented as

$$\mathcal{H}_0 : \quad x \sim \mathcal{D}(\Pi_0; \mathcal{H}_0), \tag{6.11a}$$

$$\mathcal{H}_1 : \quad x \sim \mathcal{D}(\Pi_1; \mathcal{H}_1), \tag{6.11b}$$

where x has the probability distribution $D(\Pi_i; \mathcal{H}_i)$ with statistical parameters Π_i under hypothesis $\mathcal{H}_i$.

6.6.1 Generalized likelihood ratio

The window limited generalized likelihood ratio of signal $x(k)$ with noise distributed by probability density function $f(x;\Pi)$, and with statistical parameters Π, is given by

$$g(k) = \max_{k-N+1\leq j\leq k-\tilde{N}} \ln \frac{\prod_{i=j}^{k} f(x(i);\Pi_1)}{\prod_{i=j}^{k} f(x(i);\Pi_0)}, \tag{6.12}$$

where Π_0 denotes statistical parameters during the $\mathcal{H}_0$ hypothesis, and Π_1 during the $\mathcal{H}_1$ hypothesis. The window is given by $0 \leq \tilde{N} \leq N$, and is used to reduce computational cost (Willsky and Jones, 1976).

The p-variate t-distribution of a vector signal x with mean μ, correlation S, and degrees of freedom ν is

$$f(x;\mu,S,\nu) = \frac{\Gamma((p+\nu)/2)}{\Gamma(\nu/2)(\pi\nu)^{p/2}|S|^{1/2}} \left[1+\frac{1}{\nu}(x-\mu)^\top S^{-1}(x-\mu)\right]^{-\frac{p+\nu}{2}}, \tag{6.13}$$

where $\Gamma(z)$ is the Gamma function. Note that μ is the mean of x when $\nu > 1$ (Kotz and Nadarajah, 2004). The corresponding GLRT statistic was derived in Willersrud et al. (2015c) for a change in mean μ from μ_0 to μ_1 with S and ν constant, and was shown to be

$$\begin{aligned} g(k) = \max_{k-N+1\leq j\leq k-\tilde{N}} \frac{p+\nu}{2} \sum_{i=j}^{k} \Bigg[&- \ln\left(1+\frac{1}{\nu}(x(i)-\hat{\mu}_1)^\top S^{-1}(x(i)-\hat{\mu}_1)\right) \\ &+ \ln\left(1+\frac{1}{\nu}(x(i)-\mu_0)^\top S^{-1}(x(i)-\mu_0)\right)\Bigg], \end{aligned} \tag{6.14}$$

where $\hat{\mu}_1$ is the maximum likelihood ratio of the mean after change,

$$\hat{\mu}_1 = \frac{1}{k-j+1}\sum_{i=j}^{k} x(i). \tag{6.15}$$

6.6.2 Fault isolation by determining change direction of the residuals

The GLRT statistic (6.14) is scalar, and an estimate of the magnitude of change is provided by (6.15). To determine the type of fault, the direction of change can be considered, which was done for parameter estimation in Willersrud et al. (2015c) and Willersrud et al. (2015d), and is similar to Yin (1998) where the direction of change of residuals was considered.

Problem 6.1 (Fault detection)**.** *Given a sampled time sequence of vectors of residuals $r(k)$, with change from known condition $r_0(k)$ to unknown $r_1(k)$. Define the index set $\mathbb{N}_N := \{i \in \mathbb{N} : 1 \leq i \leq N\}$ and let $i_f \in \mathbb{N}_{N_f}$ be the possible fault indices. Let a fault signature matrix be D, with column vector D_i corresponding to fault index i_f. Then distinguish between two hypotheses*

$$\mathcal{H}_0 : \quad r(k) = 0 + w(k), \qquad \textit{no fault present}, \tag{6.16a}$$

$$\mathcal{H}_1 : \quad r(k) = D_i v(k) + w(k), \qquad \textit{a fault is present}. \tag{6.16b}$$

Problem 6.2 (Fault isolation)**.** *Given that $\mathcal{H}_1$ has been accepted, determine that a particular fault i_f^* is present of the possible faults $i_f \in \mathbb{N}_{N_f}$, by determining the best fit of* (6.16b) *for the different fault types.*

The matrix D is constructed based on Tab. 6.4, where each fault type in the table corresponds to one column vector D_i. An element with '$-$' in the table gives a value of -1 in D, '$+$' gives a value of 1, and 0 is used otherwise. Negative bias drift is isolated using changed signs for the corresponding positive drift.

The fault type i_f^* is isolated using a projection of the change in mean $\hat{\mu}_1 - \mu_0$ of the residual r onto the different column vectors D_i corresponding to different faults, finding the largest projection,

$$i_f^* = \arg\max_i \frac{D_i^\top (\hat{\mu}_1 - \mu_0)}{D_i^\top D_i}. \tag{6.17}$$

6.6.3 Deciding on threshold value for the GLRT statistic

By finding the distribution of the test statistic $g(k)$ at $\mathcal{H}_0$, a threshold value h can be chosen with a desired probability of false alarm P_{FA}. If test statistic data is available at $\mathcal{H}_1$, the probability P_D of detecting a fault may also be found. An asymptotic distribution may be estimated from data. A Weibull distribution was fitted to the the test statistic of the residuals in Hansen and Blanke (2012) and estimated parameters in Willersrud et al. (2015c,d). A lognormal distribution is used in Galeazzi et al. (2013).

The test statistic data of r for the influx case at $\mathcal{H}_0$ is plotted in Fig. 6.4, showing a good fit of the tail to the Weibull distribution. The lognormal distribution gives a good fit overall, but not of the last 10 % of the tail, which is the part of the distribution that is most important for threshold selection. The Weibull distribution is applied for all cases to determine the threshold h of $g(k)$.

The Weibull distribution has the probability density function $f(x; \alpha, \beta)$ and cumulative distribution $F(x; \alpha, \beta)$ given by

$$f(x; \alpha, \beta) = \frac{\beta}{\alpha} \left(\frac{x}{\alpha}\right)^{\beta - 1} e^{-(x/\alpha)^\beta}, \quad x \geq 0, \tag{6.18}$$

$$F(x; \alpha, \beta) = 1 - e^{-(x/\alpha)^\beta}, \quad x \geq 0, \tag{6.19}$$

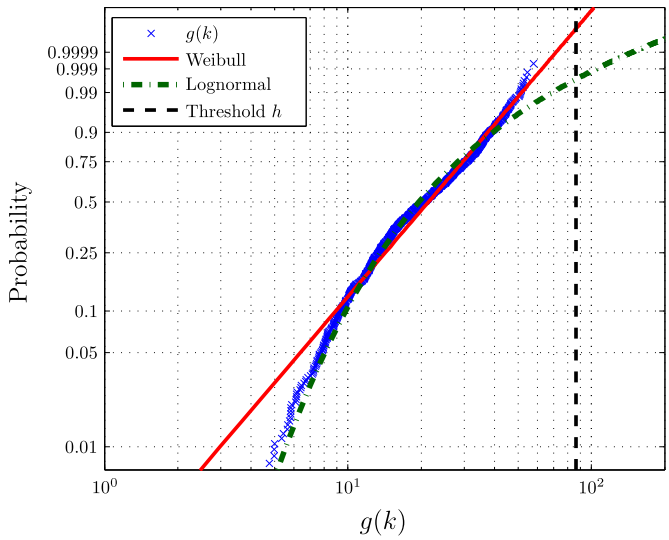

Figure 6.4: Weibull probability plot of $g(k)$ at $\mathcal{H}_0$ for the influx case. Test statistic data fitted to Weibull distribution (red solid line) and lognormal distribution (green dashed dotted line). The threshold h is calculated from a fitted Weibull distribution with $P_{FA} = 10^{-6}$, plotted as a vertical black dashed line.

where $\alpha > 0$ is the scale parameter and $\beta > 0$ is the shape parameter. The inverse cumulative distribution can be used to determine the threshold h as a function of the probability of false alarms P_{FA}, even if the residuals are not independent and identically distributed Galeazzi et al. (2013); Blanke et al. (2012); Fang et al. (2015). The threshold is then given by

$$h = Q(1 - P_{FA}; \mathcal{H}_0, \alpha_0, \beta_0) = \beta_0 \left(-\ln(P_{FA})\right)^{1/\alpha_0}, \tag{6.20}$$

where α_0 and β_0 are the parameters of the Weibull distribution fitted to $g(k)$ under $\mathcal{H}_0$. If $\mathcal{H}_1$ data is available, the probability of detecting a fault P_D is given as a function of the threshold h,

$$P_D = 1 - F(h; \mathcal{H}_1, \alpha_1, \beta_1) = e^{-(x/\alpha_1)^{\beta_1}}, \tag{6.21}$$

where α_1 and β_1 are the statistical parameters of the test statistic at $\mathcal{H}_1$.

6.7 FDI of flow loop data using downhole measurements

Fault detection and isolation of different incidents in data from the flow loop tests is done using the methods described in Secs. 6.5 and 6.6. This section presents fault detection and isolation where downhole measurements are available. The cases studied are lost circulation, gas influx, bit nozzle plugging, choke plugging,

and a positive bias drift in the downhole sensor p_a. The measured pressure and flow rates are plotted in Fig. 6.5, which are sampled at 10 Hz. The plot shows a concatenation of different test cases recorded over a time period of several weeks, and are not necessarily plotted in chronological order. In the test setup some of the incidents are also measured, used only as ground truth about the time interval and magnitude of the incident, and shown in Fig. 6.6. Note that bit nozzle plugging and choke plugging occurring during the interval 40 to 60 minutes are not measured.

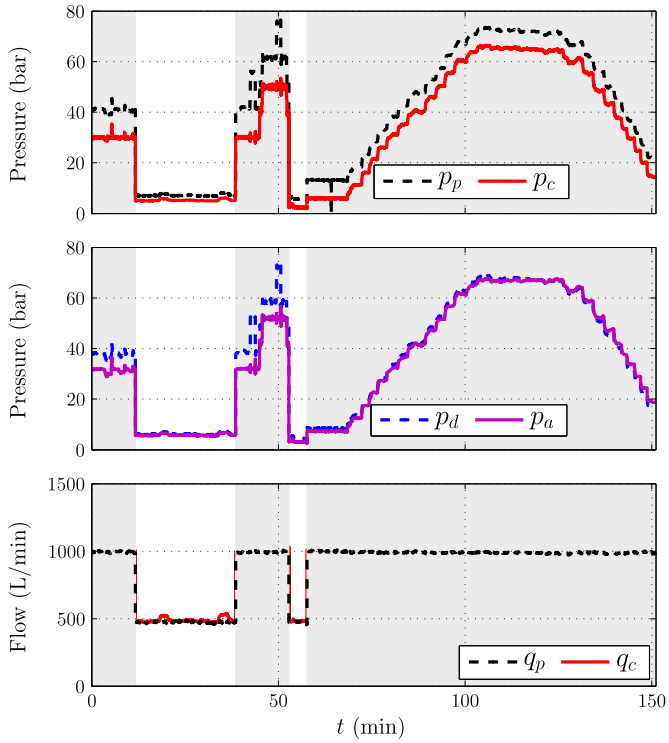

Figure 6.5: Topside pressure measurements (top), downhole pressure measurements (middle), and flow measurements (bottom) of the five cases of lost circulation, gas influx, bit nozzle plugging, choke plugging, and positive bias drift in sensor p_a. The different cases are separated with alternating grey and white backgrounds. There is significant noise in the data.

The residuals r given by (6.7) are plotted in Fig. 6.7 for all five cases of incidents. The physical parameters of the flow loop are found using available information about the drilling process and are listed Tab. 6.7. The friction parameters θ_a, θ_b and θ_d in (6.7) are found using an off-line parameter estimation method. The parameters are assumed constant or varying much slower than the dynamics in the process, and thus kept constant in r. In this case the parameters are found using the adaptive observer in Willersrud and Imsland (2013) of data $\mathcal{H}_0$ known to be

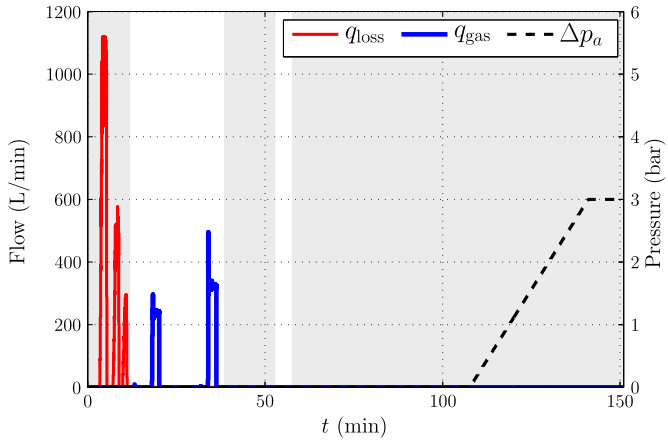

Figure 6.6: Downhole incidents of lost circulation and gas influx in the first 40 minutes of data. Bit nozzle plugging and choke plugging from 40 to 60 minutes are not measured. Artificially added bias drift in p_a starts at 110 minutes. None of this information is available to the diagnosis method.

fault free. Since the flow-loop setup was used extensively for a various number of tests, many not included in this paper, there are some differences between the cases, giving slightly different friction parameters, representing natural variation during operation.

Table 6.7: Physical flow loop parameters.

β_a	2.2×10^9 Pa	Effective bulk modulus
ρ_d, ρ_a	$1000\,\text{kg/m}^3$	Drilling fluid density
M_a	$3.74 \times 10^7\,\text{Pa s}^2/\text{m}^3$	Integrated density per cross section
V_a	$13.2\,\text{m}^3$	Volume of fluid in annulus
h	2.14 m	Depth of well at bit
L_d, L_a	700 m	Length of drillstring/annulus

From Fig. 6.7 it is apparent that different faults affect the residuals in some manner, giving non-zero values. However, due to measurement noise, these changes are very difficult to detect reliably without some change detection method. The methods in Sec. 6.6 are used for fault detection and isolation in the different cases described in the following subsections. For all cases a window length of

$$N = 200 \tag{6.22}$$

samples is used, corresponding to 20 seconds and is considered sufficiently long. A too short window length decreases the detection rate, whereas an increasing window length increases the computational cost. Choosing a sufficiently long window length was discussed in Willersrud et al. (2015d). A probability of false alarm

$$P_{FA} = 10^{-6} \tag{6.23}$$

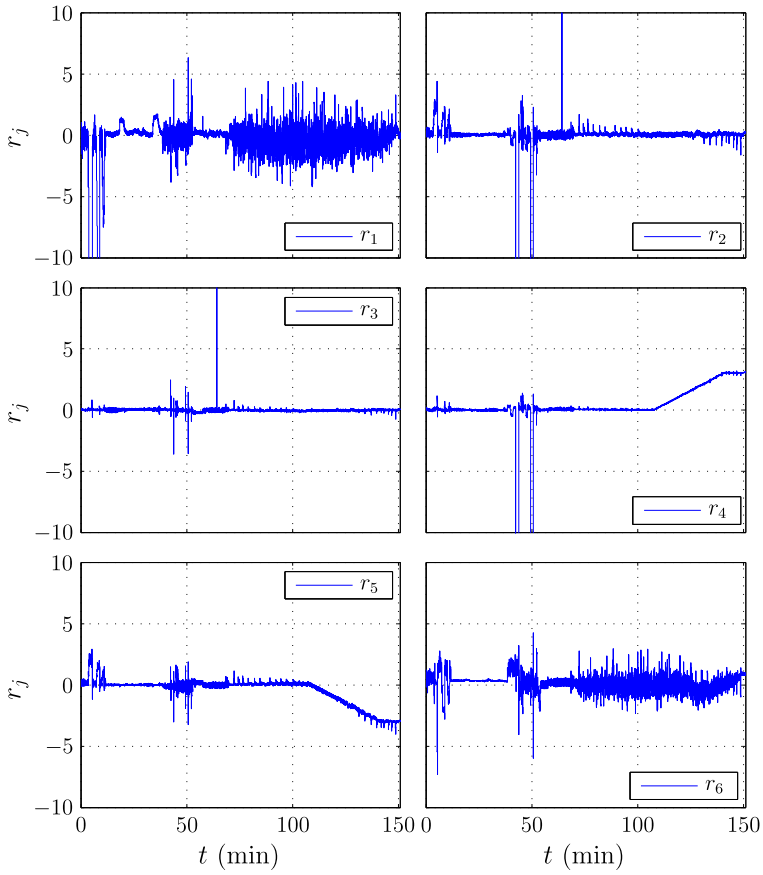

Figure 6.7: Residuals r_1 - r_6 for lost circulation, gas influx, bit nozzle plugging, choke plugging, and positive bias drift in sensor p_a, using downhole measurements.

is used to determine thresholds, which corresponds to an expected false alarm rate of 0.00018 per hour (under 2 per year). Due to process disturbances, there has been used an additional requirement that an alarm is set off only if 200 samples (20 s) of $g(k)$ is above the threshold. The spikes in residuals r_2 and r_3 happening at 64 minutes are caused by a 2 second temporal artifact in p_p.

6.7.1 Lost circulation

The first case studied is lost circulation of drilling fluid to the reservoir, which is labeled as fault f_{ls} in Tab. 6.4. From this table, loss of drilling fluid is detected and isolated if $g(k)$ is above the threshold, and that the mean of r is changing in a negative direction for r_1, and positive direction for r_2 and r_5. Three different loss rates are tested with different magnitude, plotted in red in Fig. 6.6. The first loss is at over 1000 L/min, which is a complete loss of drilling fluid. The last one is around 250 L/min, or 25 % of circulation rate. All three loss rates are quite large, and as expected, detection and isolation are quite manageable. Fault detection is shown in the upper panel of Fig. 6.8, showing a value of $g(k)$ above threshold for all three losses. The actual loss intervals are shown in grey in the lower panel, where fault isolation is correctly achieved using change direction of r, shown in blue.

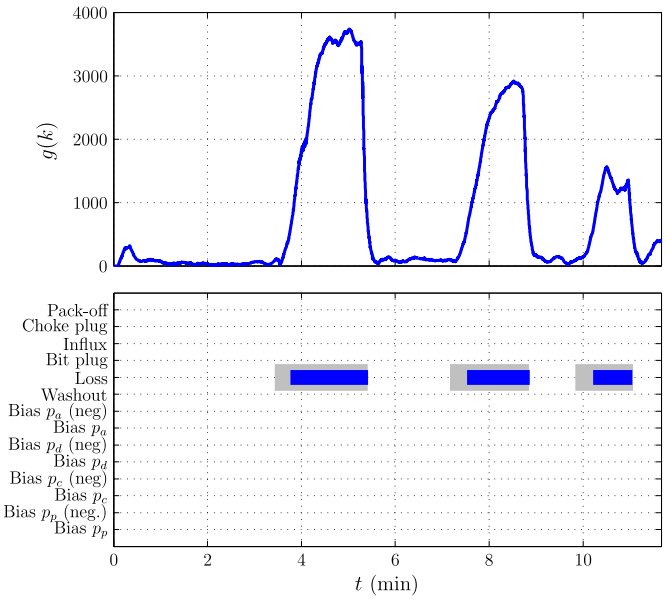

Figure 6.8: Detection and isolation of lost circulation. Actual loss shown in grey.

6.7.2 Gas influx

Gas influx is a complex case to correctly diagnose. When gas enters the annulus, the dynamics changes drastically from single-phase to multi-phase flow. Limitations of the model (6.3) during an influx is discussed in Willersrud et al. (2015d), where the model is not well suited to determine information about the gas influx once it has entered the annulus. However, detecting and isolating the initial occurrence of an influx is still possible, by determining change in the total annular friction and change in the flow rate difference in and out of the well. The procedure once an influx is detected is to shut in the well, which is done by closing the blow-out preventer (BOP) around the drillstring, blocking annular flow. It is therefore still possible to use the method described in this paper. Two influxes of gas in the annulus are plotted in blue in Fig. 6.6. Corresponding detection is shown in Fig. 6.9. Both influxes are correctly detected and isolated. However, after the first influx, the gas is transported through the annulus, giving different dynamics and friction. This gives some incorrectly isolated incidents, while most are correctly isolated as gas in the system. Nevertheless, as discussed above, once the first influx is detected and isolated the drilling crew will most probably decide to shut in the well and remove the gas in the system by circulating a heavier drilling fluid.

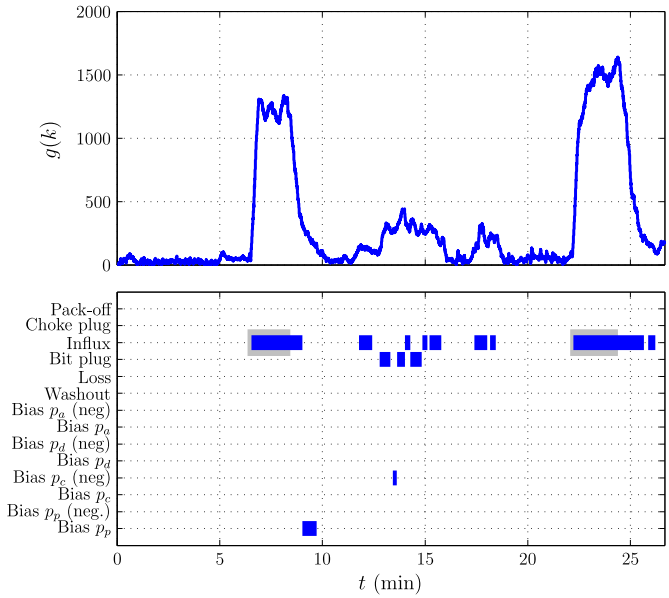

Figure 6.9: Detection and isolation of two influxes of gas into the well. Note that there is gas in the well also after injection. Some of it is correctly isolated as gas, some incorrectly as a bit nozzle plugging.

6.7.3 Plugging of drill bit nozzles

Plugging of the drill bit nozzles is not as severe as formation fluid influx and lost circulation, since the pressure in the well is not affected. Nevertheless, monitoring of the bit status is important in order to maintain drilling. A partial blocking of the nozzles will be seen as a higher pressure in the drillstring, which the operator has great benefits of determining the cause of. A full blocking of the nozzles will stop circulation of drilling fluid, halting progress.

Four pluggings of the bit nozzles are successfully detected and isolated in Fig. 6.10, two small and two large. Detecting a bit nozzle plugging may be possible by directly measuring the pressure drop over the bit, $p_d - p_a$. However, this pressure drop is a function of flow. In addition, changes to pressure measurements may be caused by other incidents. Thus is a complete diagnosis method favorable for distinguishing nozzle plugging from other incidents.

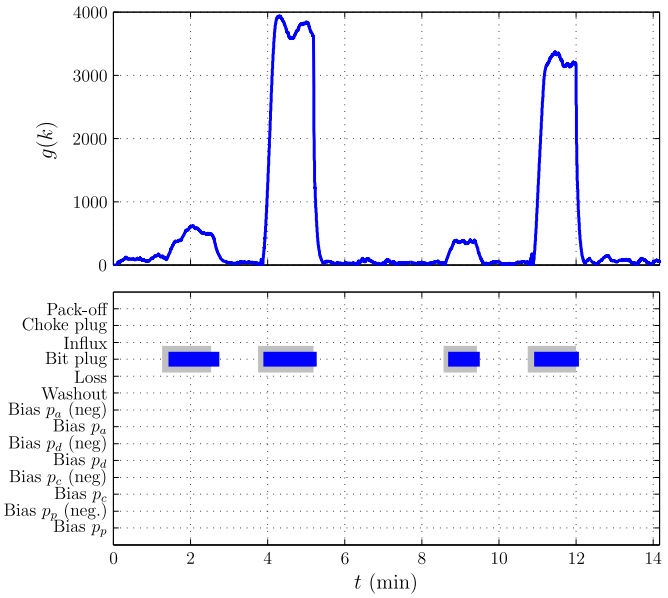

Figure 6.10: Detection and isolation of a plugging of the drill bit nozzles.

6.7.4 Plugging of MPD choke

If the choke in a managed pressure drilling operation becomes partially plugged, control of the back-pressure may be difficult. This pressure will directly affect the downhole pressure, which should be controlled within a pressure window. If the pressure is too low the well can start to produce, causing influxes, while a too high pressure may cause damage to the formation, which may result in lost circulation due to cracks in the formation.

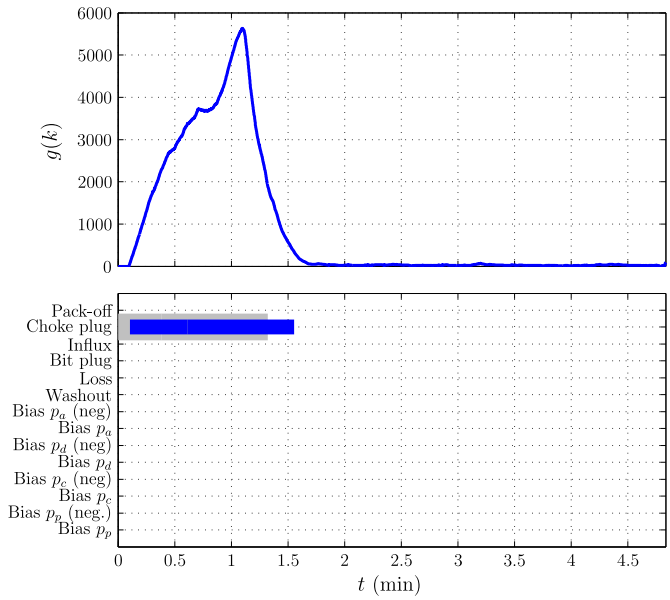

Figure 6.11: Detection and isolation of a plugging of the MPD choke.

Detection and isolation of a partial plugging of the MPD choke is shown in Fig. 6.11. The partial plugging is simulated in the flow loop as partially closing a dedicated valve upstream the choke. The plugging occurs in the very beginning of the recorded data set, and is correctly detected and isolated.

6.7.5 Bias drift in bottomhole pressure sensor p_a

The four previous cases describe incidents which are physical changes in the process due to some induced physical incidents. Detection and isolation is based on residuals which again are functions of measurements of process variables and actuators. For such a method to be successful, the measurements must be reliable. In real life, uncertainty in measurements, such as bias drift, affects the diagnosis method. It is therefore important to also detect and isolate such effects.

In this case a positive drift in the downhole pressure sensor p_a is tested. The bias drift is artificially added to the pressure signal as a ramp function from 0 to 3 bar, starting at around 110 minutes in Fig. 6.6. This is occurring simultaneously as the choke opening is ramped up, giving a significant increase in choke pressure p_c, and thus also in p_d, p_a and p_p, shown in Fig. 6.5. Diagnosis of the bias drift is shown in Fig. 6.12, with an early detection of the drift where the bias is quite small. Determining that a bias drift is occurring from the measurements directly would be difficult for an operator, while it is successfully detected and isolated with the methodology in this paper.

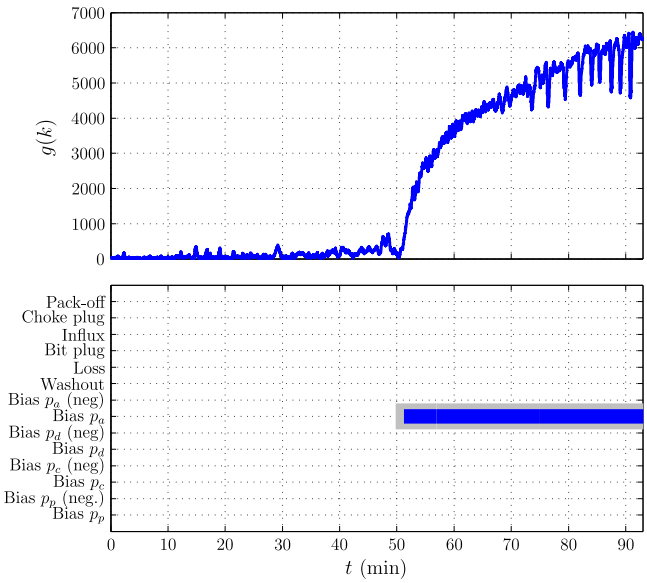

Figure 6.12: Detection and isolation of a positive bias drift in pressure sensor p_a.

6.8 FDI of flow loop data with only topside measurements

All cases in the previous section utilized downhole pressure sensors available when wired drill pipe technology is at hand. However, in most drilling rigs only a few downhole sensors are available, if any. This section investigates to what extent analytical redundancy relations are capable of fault detection and especially fault isolation with only topside sensors available. Two cases are studied: drillstring washout, and a negative bias drift in the choke pressure sensor p_c.

6.8.1 Drillstring washout without downhole measurements

Without downhole sensors, it is difficult to distinguish between a negative drift in p_p, a positive drift in p_c, and drillstring washout (f_{wo}), as shown in Tab. 6.5. However, detecting that something has happened, and narrowing down the possibility to these three different scenarios, is still of great value for the drilling crew.

Topside pressure and flow measurements are plotted in Fig. 6.13, where the washout case consists of the first 19 minutes. In Fig. 6.14, the actual washout is measured as pressure drop over a valve, where there is no washout if the pressure drop is zero. The corresponding effects on the residuals are shown in Fig. 6.15, showing an increase in $\tilde{r}_2$ and $\tilde{r}_3$ during the washout. Also here, a statistical change detection algorithm is necessary to get sufficient detection with a low false alarm rate. The GLRT statistic is plotted in Fig. 6.16, showing detection of the incident, with isolation narrowed down to either positive bias in p_c, negative bias in p_p or a drillstring washout, which is the actual case.

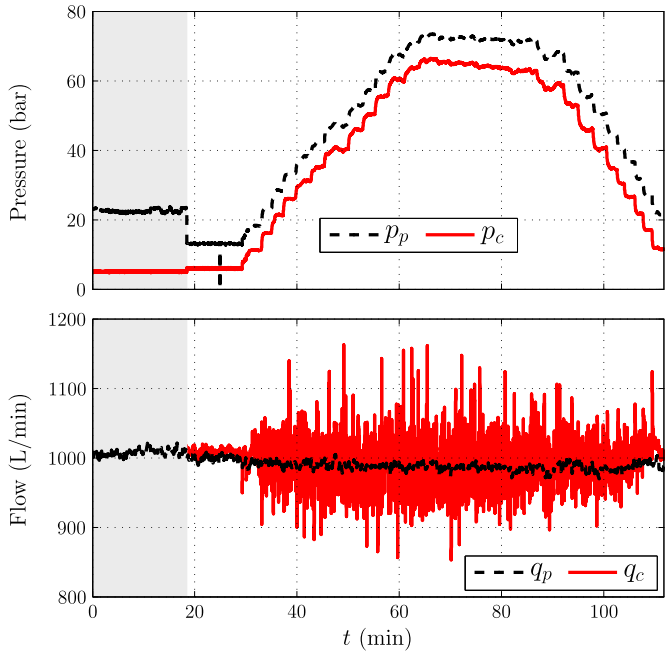

Figure 6.13: Pressure measurements (top) and flow measurements (bottom) of drillstring washout (grey background) and a negative bias drift in sensor p_c without downhole measurements.

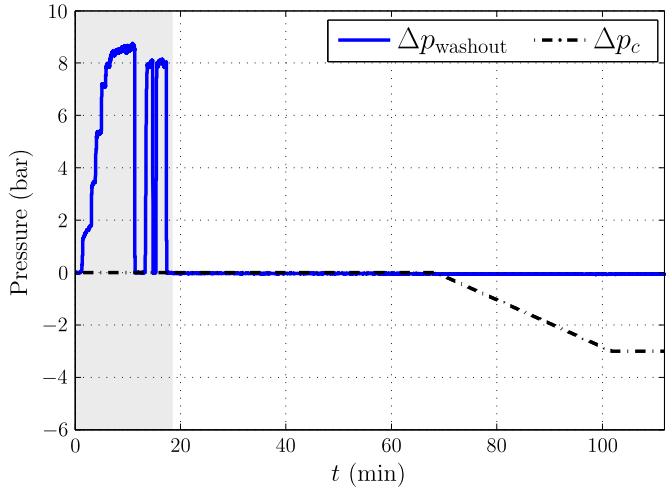

Figure 6.14: Drillstring washout (grey background), and artificially added negative bias drift in p_c starting at 69 minutes. None of this information is available to the diagnosis method.

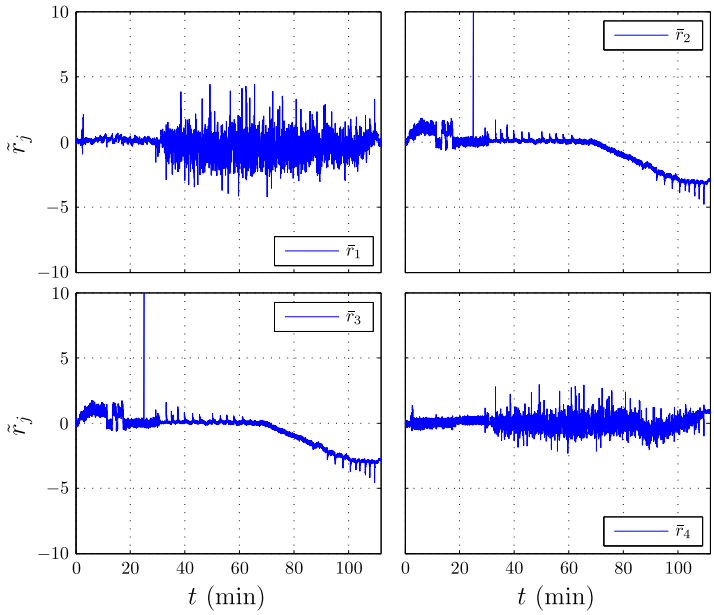

Figure 6.15: Residuals $\tilde{r}_1$ - $\tilde{r}_4$ for drillstring washout and negative bias drift in p_c, without downhole measurements.

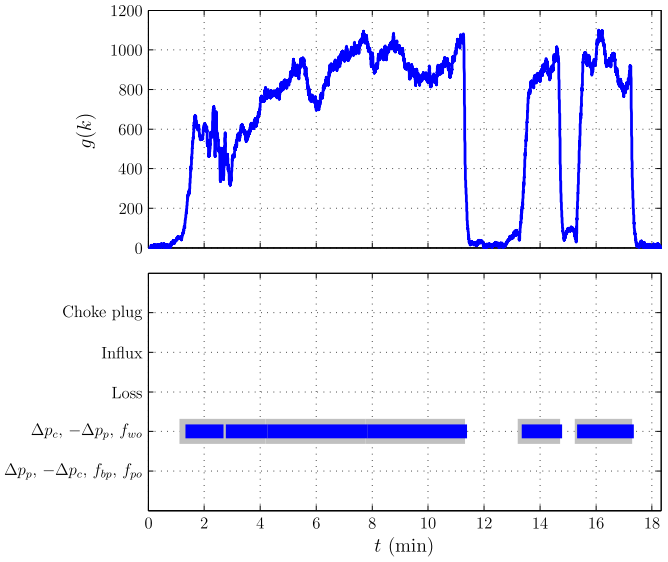

Figure 6.16: Detection and isolation of a washout without downhole measurements. The incident is isolated to be either a positive bias drift in p_c, a negative drift in p_p, or a drillstring washout.

6.8.2 Negative bias drift in choke pressure sensor without downhole measurements

Detection and isolation of a negative bias drift in the choke pressure sensor p_c is shown in Fig. 6.17, where no downhole measurements are available. The drift is ramped up from 0 to 3 bar quite slowly. For bias drift under around 1 bar (before 60 minutes), the value of $g(k)$ is below the threshold value, while for increasing drifting values the bias is isolated to the correct subgroup of incidents.

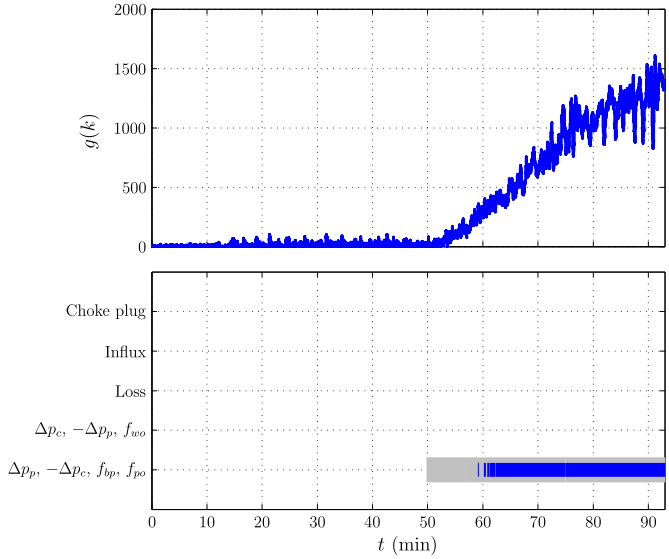

Figure 6.17: Detection and isolation of a negative bias drift in pressure sensor p_c without downhole measurements. The sensor fault is isolated as either a positive bias drift in p_p, a bit nozzle plugging, a pack-off, or the actual negative bias drift in p_c.

6.9 Discussion

Two different diagnosis scenarios using flow-loop data were tested, assuming in the first scenario that downhole pressure sensors were available, while in the second only topside sensors were used. Using downhole pressure sensors, all incidents are detectable and isolable using analytical redundancy relations, except separating a pack-off from a negative drift in the measured choke pressure. Detection and isolation was successfully achieved at an early stage, with temporal false alarms only for the gas influx incident.

When using only topside measurements, the number of residuals were reduced from six to four, with the effect of greatly reducing isolation capabilities. As can be seen in Tab. 6.5, there are several overlaps between the different cases, especially if

both negative and positive bias drift of the pressure sensors are considered. However, there is still important information in the existing isolation. A possibility to separate a drillstring washout from either a bit nozzle plugging or a pack-off is of great value for the drilling personnel.

The model used to generate the residuals is limited to hydraulic relationships between pressures and flow rates. In a real drilling rig system, there is also information about drillstring torque and the weight of the drillstring and bottomhole assembly, called weight on bit, as well as the rate of penetration. This information can be included as constraints in (6.3), giving increased detection and isolation capabilities. An influx can be a result of drilling into a gas pocket, called a *drilling break*, increasing the rate of penetration drastically. A pack-off will not only increase fluid friction, but also increase the rotational friction of the drillstring. This would be seen as an increase in the torque measured topside. The diagnosis framework described in this paper could easily be extended with these features, illustrating its flexibility for extending the detection and isolation capabilities.

Diagnosis of downhole incidents is also possible using adaptive observers, which was done in Willersrud et al. (2015c,d). Tab. 6.1 made a comparison between the methods, where one method was favorable for some properties, while the other method was best suited for others. Adaptive observers make it possible to estimate the fault magnitude, at least in some cases. This is not directly possible using analytical redundancy relations. ARR, however, make it possible to distinguish between sensor faults and actuator faults from physical incidents, a property not directly possible using adaptive observers. A complete diagnosis system may thus implement both methods, possibly combining them for improved diagnosis.

6.10 Conclusion

Analytical redundancy relations were used to generate residuals based on a simple hydraulics drilling model. Despite significant measurement noise, statistical change detection of the residuals was achieved with early detection and low false alarm rates using a multivariate generalized likelihood ratio test. Data from a medium-scale horizontal flow-loop rig of 1400 meters was used to test incident diagnosis capabilities. Successful detection and isolation was achieved with the specified low false alarm rates for all of the incidents: drillstring washout; fluid loss; gas influx; bit nozzle plugging; choke plugging; as well as bias drift of the pressure sensors. The method was first tested using downhole pressure sensors, showing successful isolation of all of the different incidents. Then, using only cheaper and readily available topside measurements, the different incidents were shown to be successfully detected and isolated into subgroups of possible incidents.

Chapter 7

Concluding remarks

Diagnosis of downhole incidents in oil and gas drilling was studied in this thesis, including diagnosis of reservoir fluids influx, lost circulation of drilling fluid to the formation, pack-off of formation solids around the drillstring, plugging of the drill bit nozzles, washout of the drillstring, as well as plugging of chokes if *managed pressure drilling* is applied. A model-based fault diagnosis approach has been applied, where a simple hydraulics model was used to describe the relationship between pressure, friction and flow rates in the system. Due to noticeable measurement noise in the test data, a statistical change detection approach for fault diagnosis was shown to be necessary for sufficiently low false alarms and high detection rate. Discrepancies between the process and the model in the form of *residuals* were determined based on changes in estimated parameters using *adaptive observers*, or by using *analytical redundancy relations* (ARR). Benefits and limitations of using the two methods for fault diagnosis were compared, where ARR inherently include diagnosis possibilities for sensor and actuator faults, whereas adaptive observers facilitates fault magnitude estimation.

The distribution of the noise of the residuals were determined, and changes were detected using the statistical change detection method of the *generalized likelihood ratio test* (GLRT). Both *univariate* and *multivariate* change detection methods were tested, where a multivariate method was found to give much better diagnosis results in Chapter 3, and was therefore chosen as the preferred method in Chapters 4-6. A multivariate method may, however, be limited by computational complexity for high dimensions of the considered signal vector. The different drilling incidents were isolated from each other in the multivariate methods using the direction of change of the mean of the residuals. The position of the incident was found in a similar manner, isolating the position to be in between two downhole pressure sensors. By determining the statistical distribution of the GLRT statistic under the null hypothesis, the threshold value for change detection was given as a function of probability of false alarm. Where data of the fault was available, the detection probability could also be determined.

The methods were thoroughly tested on data from a medium-scale horizontal flow loop of 1400 m, with realistic pressure and flow rate operating conditions, with very convincing diagnosis results. The high-fidelity simulator OLGA was also applied, where pack-off diagnosis was successfully achieved in Chapter 5. The developed methods could easily be adapted to a real drilling case, integrating the diagnosis

algorithms in the drilling control and monitoring system, although additional tests and adaptions to a real rig would be required. There is limited existing diagnosis tools for drilling on the marked today, and the solutions which do exist are typically based on very simple methods. There is great potential of increasing the efficiency and reliability of these methods, which should be easy to use, implement and maintain, while the theory behind may be more complex. This thesis presents several solutions to the research objective of developing efficient diagnosis methods for oil and gas drilling, which are easy to use and require little tuning, and can be implemented in a real diagnosis system.

Comparison between using adaptive observers and analytical redundancy relations for fault diagnosis

The objective of the thesis has been to investigate diagnosis possibilities of incidents occurring in drilling with the available sensors at hand. Two main methods for generating the residuals were presented. In the first approach adaptive observers were used, estimating friction parameters and flow rates, which was the topic of Chapters 2-5. Then analytical redundancy relations were studied as an alternative in Chapter 6. Comparison between the methods were given in Sec. 1.4.1 in Chapter 1 as well as in Sec. 6.4 in Chapter 6. The main differences in terms of results were that the adaptive observers could handle unknown system parameters and provided inherent estimation of physical magnitudes, whereas ARR provided a systematic method for generating residuals, while requiring known or estimated system parameters. The resulting diagnostic property for the adaptive observers gave a possibility to estimate the fault magnitudes, at least some of them, which was the topic in Chapters 4 and 5. This was not directly applicable using ARR. However, these residuals are shown in Chapter 6 to have isolation properties for sensor bias and actuator faults, in addition to downhole incidents. Chapter 6 also showed possibilities and limitations for fault detection and isolation without available downhole sensors, where all incidents were detected, albeit with decreased isolation capabilities. This is an important result for the industry since most wells are drilled with limited downhole measurements.

Another difference between the methods is that parameter estimation in general reacts slower to abrupt changes, where the detection rate is dependent on observer tuning that should be chosen carefully. Residuals generated from analytical redundancy relations can, however, react quite fast, but may be more affected by measurement noise. Nevertheless, these differences in detection rate were not noticeable in the results presented in this thesis. By combining the residual generation methods with statistical change detection, the problem with noise was successfully handled.

The conclusion from this comparison is that both adaptive observers and ARR work satisfactory in diagnosing downhole incidents, where both methods have some properties not applicable to the other. A complete diagnosis system may thus imple-

ment both methods, and possibly combine them for increased diagnosis properties.

Noise distribution of the residuals and threshold selection

The ARR residuals, and estimated friction parameters and flow rates in the flow-loop data were found to best fit the t-distribution in Chapters 3, 4 and 6, after the residuals were white filtered. This is a continuous probability distribution with heavier tails compared with the Gaussian distribution. Detection capabilities assuming the t-distribution was compared with assuming the Gaussian distribution in Chapter 4, achieving a higher detection rate of the generalized likelihood ratio test using the t-distribution. Combining this distribution with univariate and multivariate GLRT change detection methods required derivation of the decision function in Chapter 3, which is novel work based on similar known results for the Gaussian case.

The Gaussian distribution is often chosen due to simplicity and availability of developed methods. However, in this thesis it was shown that a more thorough analysis of the noise distribution gave better and more reliable results. Estimated states and parameters, as well as generated ARR residuals, may be nonlinear functions of the measurements, which will easily become non-Gaussian, possibly non-IID, even if the measurements are normally distributed IID signals.

Due to measurement noise and modeling error, a threshold on the decision function was required. Often, the thresholds are obtained by using trial and error, which was done in Chapter 2. However, by using test statistic data under the null hypothesis $\mathcal{H}_0$, the thresholds were defined as functions of the probability of false alarm. In Chapters 3-6, the Weibull distribution was found be be a good fit for the right-tail of the test statistic. Where data under the alternative hypothesis $\mathcal{H}_1$ also was available (data with faults), it was possible to determine the probability of detecting an incident. This approach of obtaining thresholds greatly simplifies the diagnosis method, increasing robustness and requiring much less tuning.

Possible future research directions for drilling diagnosis

The methods proposed in this thesis were tested on data from a medium-scale drilling test facility and in a high-fidelity simulator. The next research step could be to test the methods on real drilling data where downhole incidents are occurring. However, this requires close collaboration with the industry, since confidential drilling data must be made available. In addition, data where actual drilling incidents are occurring may prove difficult and time consuming to acquire.

The main idea in change-detection algorithms is to detect a change from a known fault-free case to an, in some cases, unknown fault scenario. The challenge for such methods to be implemented in a industry drilling system is the requirement of determining that the system is in the fault-free case, as well as producing good estimates for the null hypothesis. In a first implementation version this will have to be determined by the expert user, e.g., the drilling operators and engineers.

For future implementations, this could be done in a more automated matter where the system updates the null hypothesis estimates regularly after predetermined scheduled changes to the process.

The use of adaptive observers and analytical redundancy relations are thoroughly tested in this thesis for drilling incident diagnosis. The methods are compared, each with a set of benefits and limitations. For even increased diagnosis properties, the methods may be combined in one model-based diagnosis method. Promising preliminary results of this combination are published in Blanke and Hansen (2013), which could be applied to the diagnosis framework presented in this thesis.

Bibliography

Aadnoy, B., Cooper, I., Miska, S., Mitchell, R. F., and Payne, M. L. (2009). *Advanced Drilling and Well Technology*. Society of Petroleum Engineers, Richardson, TX.

Abdollahi, J., Carlsen, I. M., Randhol, P., Tenold, E., Haga, H. B., and Jakobsen, T. (2008). A Case-Based Approach To Understand the Complexity of Causal Connections Related to Well Integrity Problems. In *IADC/SPE Drilling Conference, SPE 111129*, pages 1–14, Orlando, Florida.

Agamennoni, G., Nieto, J. I., and Nebot, E. M. (2012). Approximate Inference in State-Space Models With Heavy-Tailed Noise. *IEEE Transactions on Signal Processing*, 60(10):5024–5037.

Alcorta García, E. and Frank, P. (1997). Deterministic nonlinear observer-based approaches to fault diagnosis: A survey. *Control Engineering Practice*, 5(5):663–670.

Aldred, W., Cook, J., Carpenter, B., Hutchinson, M., Rezmer-cooper, I., and Leder, P. C. (1998). Using Downhole Annular Pressure Measurements to Improve Drilling Performance. *Oilfield Review*, (Winter):40–55.

Ambrus, A., Ashok, P., and van Oort, E. (2013). Drilling Rig Sensor Data Validation in the Presence of Real-Time Process Variations. In *SPE Annual Technical Conference and Exhibition, SPE 166387*, New Orleans, LA.

API (2006). API Recommended Practice 13D, Recommended Practice on the Rheology and Hydraulics of Oil-Well Drilling Fluids. Technical Report 5th ed., American Petroleum Institute.

Arehart, R. A. (1990). Drill-Bit Diagnosis With Neural Networks. In *SPE Annual Technical Conference and Exhibition*, pages 24–28, San Antonio, TX.

Armengol, J., Bregon, A., Escobet, T., Gelso, E., Krysander, M., Nyberg, M., Olive, X., Pulido, B., and Trave-Massyues, L. (2009). Minimal Structurally Overdetermined sets for residual generation: A comparison of alternative approaches. In *Proc. IFAC Safeprocess*, pages 1480–1485, Barcelona, Spain.

Ashok, P., Ambrus, A., and van Oort, E. (2013). Automatic Sensor Data Validation: Improving the Quality and Reliability of Rig Data. In *SPE Digital Energy Conference, SPE 163726*, pages 1–14, The Woodlands, TX.

Basseville, M. (1988). Detecting Changes in Signals and Systems - A Survey. *Automatica*, 24(3):309–326.

Basseville, M. and Nikiforov, I. (2002). Fault isolation for diagnosis: Nuisance rejection and multiple hypotheses testing. *Annual Reviews in Control Reviews Control*, 26(2):189–202.

Basseville, M. and Nikiforov, I. V. (1993). *Detection of Abrupt Changes: Theory and Applications*. Prentice Hall, Englewood Cliffs, NJ.

Bedjaoui, N. and Weyer, E. (2011). Algorithms for leak detection, estimation, isolation and localization in open water channels. *Control Engineering Practice*, 19(6):564–573.

Bellarby, J. (2009). *Well completion design*, volume 56 of *Developments in Petroleum Science*. Elsevier, Amsterdam, The Netherlands.

Bendiksen, K. H., Maines, D., Moe, R., and Nuland, S. (1991). The Dynamic Two-Fluid Model OLGA: Theory and Application. *SPE Production Engineering*, 6(2):171–180.

Bert, D., Storaune, A., and Zheng, N. (2009). Case Study: Drillstring Failure Analysis and New Deep-Well Guidelines Lead to Success. *SPE Drilling & Completion*, 24(4):508–517.

Besançon, G. (2000). Remarks on nonlinear adaptive observer design. *Systems & Control Letters*, 41(4):271–280.

Besancon, G. and Zhang, Q. (2002). Further developments on adaptive observers for nonlinear systems with application in fault detection. In *Proc. IFAC World Congress*, pages 732–732, Barcelona, Spain.

Blanke, M., Fang, S., Galeazzi, R., and Leira, B. J. (2012). Statistical Change Detection for Diagnosis of Buoyancy Element Defects on Moored Floating Vessels. In *Proc. IFAC Safeprocess*, pages 462–467.

Blanke, M. and Hansen, S. (2013). Towards self-tuning residual generators for UAV control surface fault diagnosis. In *Proc. Conf. Control Fault-Tolerant Systems*, pages 37–42, Nice, France.

Blanke, M., Kinnaert, M., Lunze, J., and Staroswiecki, M. (2006). *Diagnosis and fault-tolerant control*. Springer, Berlin, 2nd edition.

Blanke, M. and Lorentzen, T. (2006). SaTool - A software tool for structural analysis of complex automation systems. In *Proc. IFAC Safeprocess*, pages 629–634.

Bourgoyne Jr., A. T., Millheim, K. K., Chenevert, M. E., and Young, F. (1986). *Applied Drilling Engineering*. Society of Petroleum Engineers, Brookfield, CT, USA, 2nd edition.

Caccavale, F., Pierri, F., and Villani, L. (2008). Adaptive Observer for Fault Diagnosis in Nonlinear Discrete-Time Systems. *Journal of Dynamic Systems, Measurement, and Control*, 130(2):021005.

Cayeux, E., Daireaux, B., Dvergsnes, E., Leulseged, A., Bruun, B., and Herbert, M. (2012a). Advanced Drilling Simulation Environment for Testing New Drilling Automation Techniques and Practices. *SPE Drilling & Completion*, 27(4):559–573.

Cayeux, E., Dvergsnes, E. W., and Sælevik, G. (2012b). Early Symptom Detection on the Basis of Real-Time Evaluation of Downhole Conditions: Principles and Results From Several North Sea Drilling Operations. *SPE Drilling & Completion*, 27(4):546–558.

Chen, J. and Patton, R. J. (1999). *Robust Model-Based Fault Diagnosis for Dynamic Systems*. Springer, Boston, MA.

Choe, J., Schubert, J. J., and Texas, A. (2007). Analyses and Procedures for Kick Detection in Subsea Mudlift Drilling. *SPE Drilling & Completion*, 22(4):296–303.

Chow, E. and Willsky, A. (1984). Analytical redundancy and the design of robust failure detection systems. *IEEE Transactions on Automatic Control*, 29(7):603–614.

Clark, R. N. (1978). Instrument Fault Detection. *IEEE Transactions on Aerospace and Electronic Systems*, 14(3):456–465.

Coley, C. J. and Edwards, S. T. (2013). The Use of Along String Annular Pressure Measurements to Monitor Solids Transport and Hole Cleaning. In *SPE/IADC Drilling Conference and Exhibition, SPE 163567*, pages 1–35.

Daison, P. A. and Belavadi, M. N. (2008). Early Detection of Drillstring Washouts Based on Downhole Turbine RPM Monitoring Prevents Twist-offs in Challenging Drilling Environment in India. In *IADC/SPE Asia Pacific Drilling Technology Conference and Exhibition, SPE 115290*, pages 1–8, Jakarta, Indonesia.

Dalton, C., Paulk, M., and Stevenson, G. (2003). The Benefits of Real-Time Downhole Pressure and Tension Data With Wired Composite Tubing. *Journal of Canadian Petroleum Technology*, 42(5):67–77.

Ding, S. X. (2008). *Model-based Fault Diagnosis Techniques*. Springer, Berlin.

Ding, S. X. (2014). Data-driven design of monitoring and diagnosis systems for dynamic processes: A review of subspace technique based schemes and some recent results. *Journal of Process Control*, 24(2):431–449.

Elliott, D., Montilva, J., Francis, P., Reitsma, D., Shelton, J., and Roes, V. (2011). Managed Pressure Drilling Erases the Lines. *Oilfield Review*, 23(1):14–23.

Fan, J., Zhang, Y., and Zheng, Z. (2013). Adaptive Observer-Based Integrated Fault Diagnosis and Fault-Tolerant Control Systems Against Actuator Faults and Saturation. *Journal of Dynamic Systems, Measurement, and Control*, 135(4):041008.

Fang, S., Blanke, M., and Leira, B. J. (2015). Mooring system diagnosis and structural reliability control for position moored vessels. *Control Engineering Practice*, 36:12–26.

Frank, P. and Ding, X. (1997). Survey of robust residual generation and evaluation methods in observer-based fault detection systems. *Journal of Process Control*, 7(6):403–424.

Frank, P. M. (1990). Fault diagnosis in dynamic systems using analytical and knowledge-based redundancy. *Automatica*, 26(3):459–474.

Frank, P. M., Schreier, G., and Alcorta García, E. (1999). Nonlinear observers for fault detection and isolation. In *New Directions in nonlinear observer design*, pages 399–422. Springer-Verlag.

Galeazzi, R., Blanke, M., and Poulsen, N. K. (2013). Early Detection of Parametric Roll Resonance on Container Ships. *IEEE Transactions on Control Systems Technology*, 21(2):489–503.

Gallier, J. (2011). *Geometric Methods and Applications*. Springer, New York, 2nd edition.

Gertler, J. (1991). Analytical Redundancy Methods in Fault Detection and Isolation. In *Proc. IFAC Safeprocess*, pages 9–21, Baden-Baden, Germany.

Gertler, J. (1997). Fault detection and isolation using parity relations. *Control Engineering Practice*, 5(5):653–661.

Gertler, J. (1998). *Fault Detection and diagnosis in engineering systems*. Marcel Dekker, New York.

Gertler, J. and Monajemy, R. (1995). Generating directional residuals with dynamic parity relations. *Automatica*, 31(4):627–635.

Gertler, J. and Singer, D. (1990). A new structural framework for parity equation-based failure detection and isolation. *Automatica*, 26(2):381–388.

Gertler, J. and Yin, K. (1996). Statistical decision making for dynamic parity relations. In *Proc. IFAC World Congress*, pages 13–18, San Fransisco, CA.

Ghilardi, P., de Mari, A., Lins, D. G., Martins, A. L., Gandelman, R. A., Aragao, A. F. L., Teixeira, G. T., Castaneda, R. M., and Lenz, C. (2013). Real Time Drilling Data Diagnosis Implemented In Deepwater Wells - A Reality. In *Offshore Technology Conference, OTC 24275*, pages 1–9, Rio de Janeiro, Brazil.

Godhavn, J.-M. (2010). Control Requirements for Automatic Managed Pressure Drilling System. *SPE Drilling & Completion*, 25(3):336–345.

Godhavn, J.-M., Pavlov, A., Kaasa, G.-O., and Rolland, N. L. (2011). Drilling Seeking Automatic Control Solutions. In *Proc. IFAC World Congress*, pages 10842–10850, Milan, Italy.

Gravdal, J., Nikolaou, M., Breyholtz, Ø., and Carlsen, L. (2010a). Improved Kick Management During MPD by Real-Time Pore-Pressure Estimation. *SPE Drilling & Completion*, 25(4):577–584.

Gravdal, J. E., Lorentzen, R., and Time, R. (2010b). Wired Drill Pipe Telemetry Enables Real-Time Evaluation of Kick During Managed Pressure Drilling. In *SPE Asia Pacific Oil and Gas Conference and Exhibition*, Brisbane, Australia. Society of Petroleum Engineers.

Grip, H. F., Johansen, T. A., Imsland, L., and Kaasa, G.-O. (2010). Parameter estimation and compensation in systems with nonlinearly parameterized perturbations. *Automatica*, 46(1):19–28.

Gulsrud, T. O., Nybø, R., and Bjørkevoll, K. S. (2009). Statistical Method for Detection of Poor Hole Cleaning and Stuck Pipe. In *Proc. Offshore Europe, SPE 123374*, Aberdeen, UK.

Gundersen, O. E., Sørmo, F., Aamodt, A., and Skalle, P. (2013). A Real-Time Decision Support System for High Cost Oil Well Drilling Operations. *AI Magazine*, Spring:21–32.

Gundersen, O. E., Sørmo, F., Aamot, A., and Skalle, P. (2012). A Real-Time Decision Support System for High Cost Oil-Well Drilling Operations. In *Proc. Innovative Applications of Artificial Intelligence Conference*, pages 2209–2216, Toronto, Canada.

Hansen, S. and Blanke, M. (2012). In-Flight Fault Diagnosis for Autonomous Aircraft Via Low-Rate Telemetry Channel. In *Proc. IFAC Safeprocess*, pages 576–581, Mexico City, Mexico.

Hansen, S. and Blanke, M. (2014). Diagnosis of Airspeed Measurement Faults for Unmanned Aerial Vehicles. *IEEE Transactions on Aerospace and Electronic Systems*, 50(1):224–239.

Hargreaves, D., Jardine, S., and Jeffryes, B. (2001). Early Kick Detection for Deepwater Drilling: New Probabilistic Methods Applied in the Field. In *SPE Annuual Technical Conference and Exhibtion, SPE 71369*, New Orleans, LA.

Hasan, A. R. and Kabir, C. S. (1988). A Study of Multiphase Flow Behavior in Vertical Wells. *SPE Production Engineering*, 3(2):263–272.

Hauge, E., Aamo, O. M., Godhavn, J.-M., and Nygaard, G. (2013). A novel model-based scheme for kick and loss mitigation during drilling. *Journal of Process Control*, 23(4):463–472.

Heyns, T., Godsill, S., de Villiers, J., and Heyns, P. (2012). Statistical gear health analysis which is robust to fluctuating loads and operating speeds. *Mechanical Systems and Signal Processing*, 27(2012):651–666.

Hwang, I., Kim, S., Kim, Y., and Seah, C. E. (2010). A Survey of Fault Detection, Isolation, and Reconfiguration Methods. *IEEE Transactions on Control Systems Technology*, 18(3):636–653.

Isermann, R. (1984). Process fault detection based on modeling and estimation methods – a survey. *Automatica*, 20(4):387–404.

Isermann, R. (1997). Supervision, fault-detection and fault-diagnosis methods – an introduction. *Control Engineering Practice*, 5(5):639–652.

Isermann, R. (2005). Model-based fault-detection and diagnosis – status and applications. *Annual Reviews in Control*, 29(1):71–85.

Isermann, R. (2006). *Fault-Diagnosis Systems*. Springer, Berlin.

Isermann, R. (2011). *Fault-Diagnosis Applications*. Springer-Verlag, Berlin.

Isermann, R. and Ballé, P. (1997). Trends in the application of model-based fault detection and diagnosis of technical processes. *Control Engineering Practice*, 5(5):709–719.

Jablonowski, C. and Podio, A. (2011). The Impact of Rotating Control Devices on the Incidence of Blowouts: A Case Study for Onshore Texas, USA. *SPE Drilling & Completion*, 26(3):364–370.

Jardine, S. I., White, D. B., and Billingham, J. (1994). Computer-Aided Real-Time Kick Analysis and Control. *SPE Drilling & Completion*, 9(3):199–204.

Jellison, M. J., Prideco, G., Hall, D. R., Howard, D. C., Tracy, H., Long, R. C., National, D. O. E., Technology, E., Chandler, R. B., and Pixton, D. S. (2003). Telemetry Drill Pipe: Enabling Technology for the Downhole Internet. In *SPE/IADC Drilling Conference*, pages 1–10, Amsterdam, The Netherlands.

Jiang, B., Staroswiecki, M., and Cocquempot, V. (2004). Fault diagnosis based on adaptive observer for a class of non-linear systems with unknown parameters. *International Journal of Control*, 77(4):367–383.

Johnson, A., Leuchtenberg, C., Petrie, S., and Cunningham, D. (2014). Advancing Deepwater Kick Detection. In *IADC/SPE Drilling Conference and Exhibition, SPE 167990*, pages 1–10, Fort Worth, Texas.

Johnson, E., Land, J., Lee, M., and Robertson, R. (2013). Landing the Big One – The Art of Fishing. *Oilfield Review*, 24(4):26–35.

Kaasa, G.-O., Stamnes, Ø. N., Aamo, O. M., and Imsland, L. (2012). Simplified Hydraulics Model Used for Intelligent Estimation of Downhole Pressure for a Managed-Pressure-Drilling Control System. *SPE Drilling & Completion*, 27(1):127–138.

Kay, S. M. (1998). *Fundamentals of Statistical Signal Processing: Detection Theory*. Prentice Hall, Upper Saddle River, NJ.

Khalil, H. K. (2002). *Nonlinear Systems*. Prentice Hall, Upper Saddle River, NJ, 3rd edition.

Knüppel, T., Blanke, M., and Østergaard, J. (2014). Fault diagnosis for electrical distribution systems using structural analysis. *International Journal of Robust and Nonlinear Control*, 24(8-9):1446–1465.

Kotz, S. and Nadarajah, S. (2004). *Multivariate t-distribution and their applications*. Cambridge University Press, Cambridge, United Kingdom.

Krysander, M., Aslund, J., and Nyberg, M. (2008). An Efficient Algorithm for Finding Minimal Overconstrained Subsystems for Model-Based Diagnosis. *IEEE Transactions on Systems, Man, and Cybernetics - Part A: Systems and Humans*, 38(1):197–206.

Kucs, R., Thonhauser, G., Regan, M., Hanson, J., and Haugen, J. (2015). An Holistic Approach to Improving Drilling Performance in Realtime: Integrating Measured, Analysed, Modelled and Reported Drilling Data. In *SPE/IADC Drilling Conference and Exhibition, SPE 173115*, pages 1–18, London, UK.

Lai, T. L. (1995). Sequential Changepoint Detection in Quality Control and Dynamical Systems. *Journal of the Royal Statistical Society*, 57(4):613–658.

Landet, I. S., Pavlov, A., and Aamo, O. M. (2013). Modeling and Control of Heave-Induced Pressure Fluctuations in Managed Pressure Drilling. *IEEE Transactions on Control Systems Technology*, 21(4):1340–1351.

Liu, C. and Rubin, D. B. (1995). ML estimation of the t distribution using EM and its extensions, ECM and ECME. *Statistica Sinica*, 5:19–39.

Ljung, L. (1979). Asymptotic behavior of the extended Kalman filter as a parameter estimator for linear systems. *IEEE Transactions on Automatic Control*, 24(1):36–50.

Long, R. and Veeningen, D. (2011). Networked drill pipe offers along-string pressure evaluation in real time. Technical report, National Energy Technology Laboratory.

Macdonald, K. A. and Bjune, J. (2007). Failure analysis of drillstrings. *Engineering Failure Analysis*, 14(8):1641–1666.

Macpherson, J. D., de Wardt, J. P., Florence, F., Chapman, C., Zamora, M., Laing, M., and Iversen, F. (2013). Drilling-Systems Automation: Current State, Initiatives, and Potential Impact. *SPE Drilling & Completion*, 28(04):296–308.

Mahdianfar, H., Pavlov, A., and Aamo, O. M. (2013). Joint Unscented Kalman Filter for State and Parameter Estimation in Managed Pressure Drilling. In *Proc. European Control Conference*, pages 1645–1650, Zürich, Switzerland.

Manring, N. D. (2005). *Hydraulic Control Systems*. Wiley, New York.

Martins, A. L., Gandelman, R. A., Folsta, M. G., Resende, E. L., Vega, M., Aguiar, R., Pirovolou, D., and Gullo, R. M. D. (2013). On the Path for Offshore Drilling Automation. In *SPE/IADC Drilling Conference and Exhibition, SPE163453*, pages 1–13, Amsterdam, The Netherlands.

Mitchell, R. F. and Miska, S. Z. (2011). *Fundamentals of Drilling Engineering*, volume 12 of *SPE Textbook Series*. Society of Petroleum Engineers, Richardson, TX.

Nagy-Kiss, A. M. and Schutz, G. (2013). Estimation and diagnosis using multi-models with application to a wastewater treatment plant. *Journal of Process Control*, 23(10):1528–1544.

Niedermayr, Michael Pearse, J., Banks, M., Zoellner, P., and Thonhauser, G. (2010). case study – field implementation of automated torque-and-drag monitoring for maari field development. In *IADC/SPE Drilling Conference and Exhibition, SPE 128243*, pages 1–14.

Norwegian Petroleum Directorate (2014). Petroleum resources on the norwegian continental shelf - fields and discoveries. Technical report, NPD, Stavanger, Norway.

Nybø, R. (2010). Fault detection and other time series opportunities in the petroleum industry. *Neurocomputing*, 73(10-12):1987–1992.

Nygaard, V., Jahangir, M., Gravem, T., Nathan, E., Evans, J., Reeves, M., Wolter, H., and Hovda, S. (2008). A Step Change in Total System Approach Through Wired Drillpipe Technology. In *IADC/SPE Drilling Conference, SPE 112742*, Orlando, Florida.

Odendaal, H. M. and Jones, T. (2014). Actuator fault detection and isolation: An optimised parity space approach. *Control Engineering Practice*, 26:222–232.

Page, E. S. (1954). Continuous Inspection Schemes. *Biometrika*, 41(1):100–115.

Patton, R. and Chen, J. (1997). Observer-based fault detection and isolation: Robustness and applications. *Control Engineering Practice*, 5(5):671–682.

Patton, R. J., Clark, R. N., and Frank, P. M. (2000). *Issues of Fault Diagnosis for Dynamic Systems*. Springer-Verlag, London.

Pearson, R. (2002). Outliers in process modeling and identification. *IEEE Transactions on Control Systems Technology*, 10(1):55–63.

Peng, Y., Youssouf, A., Arte, P., and Kinnaert, M. (1997). A complete procedure for residual generation and evaluation with application to a heat exchanger. *IEEE Transactions on Control Systems Technology*, 5(6):542–555.

Pixton, D. S., Intelliserv, N. O. V., Shishavan, R. A., Perez, H. D., Hedengren, J. D., and Craig, A. (2014). Addressing UBO and MPD Challenges with Wired Drill Pipe Telemetry. In *SPE/IADC Drilling Conference and Exhibition, SPE 168953*, pages 1–16, Madrid, Spain.

Raja, H., Sørmo, F., and Vinther, M. L. (2011). Case-Based Reasoning: Predicting Real-Time Drilling Problems and Improving Drilling Performance. In *SPE Middle East Oil and Gas Show and Conference, SPE 141598*, pages 1–12.

Rajamani, R. and Hedrick, J. (1995). Adaptive observers for active automotive suspensions: theory and experiment. *IEEE Transactions on Control Systems Technology*, 3(1):86–93.

Redman Jr., K. P. (1991). Understanding Kick Tolerance and Its Significance in Drilling Planning and Execution. *SPE Drilling Engineering*, 6(4):245–249.

Reitsma, D. (2010). A simplified and highly effective method to identify influx and losses during Managed Pressure Drilling without the use of a Coriolis flow meter. In *SPE/IADC MPD and UBO Conference, SPE 130312*, Kuala Lumpur, Malaysia.

Rommetveit, R., Bjørkevoll, K., Ødegård, S. I., Herbert, M., Halsey, G., Kluge, R., and Korsvold, T. (2008). eDrilling used on Ekofisk for Real-Time Drilling Supervision, Simulation, 3D Visualization and Diagnosis. In *SPE Intelligent Energy, SPE 112109*, pages 1–14, Amsterdam, The Netherlands.

Rommetveit, R., Bjørkevoll, K. S., Ødegård, S. I., Sandve, O., Larsen, B., and Herbert, M. (2007). eDrilling: Linking advanced models and 3D visualization to drilling control systems in real time. In *Offshore Mediterranean Conference and Exhibition*, Ravenna, Italy.

Röver, C., Meyer, R., and Christensen, N. (2011). Modelling coloured residual noise in gravitational-wave signal processing. *Classical and Quantum Gravity*, 28(015010):20.

Santos, H., Catak, E., Kinder, J., and Sonnemann, P. (2007). Kick Detection and Control in Oil-Based Mud: Real Well-Test Results Using Microflux Control Equipment. In *SPE/IADC Drilling Conference, SPE 105454*, Amsterdam, The Netherlands.

Schlumberger (2014). FLAG Fluid Loss & Gain Detection Service, www.slb.com/flag, Retrived May 2015.

Skalle, P., Aamodt, A., and Gundersen, O. E. (2013). Detection of Symptoms for Revealing Causes Leading to Drilling Failures. *SPE Drilling & Completion*, 28(2):182–193.

Stamnes, Ø. N., Aamo, O. M., and Kaasa, G.-O. (2011a). Adaptive Redesign of Nonlinear Observers. *IEEE Transactions on Automatic Control*, 56(5):1152–1157.

Stamnes, O. N., Aamo, O. M., and Kaasa, G.-O. (2011b). Redesign of adaptive observers for improved parameter identification in nonlinear systems. *Automatica*, 47(2):403–410.

Staroswiecki, M. and Comtet-Varga, G. (2001). Analytical redundancy relations for fault detection and isolation in algebraic dynamic systems. *Automatica*, 37(5):687–699.

Sundström, C., Frisk, E., and Nielsen, L. (2014). Selecting and Utilizing Sequential Residual Generators in FDI Applied to Hybrid Vehicles. *IEEE Transactions on Systems, Man, and Cybernetics: Systems*, 44(2):172–185.

Svärd, C., Nyberg, M., and Frisk, E. (2013). Realizability Constrained Selection of Residual Generators for Fault Diagnosis With an Automotive Engine Application. *IEEE Transactions on Systems, Man, and Cybernetics: Systems*, 43(6):1354–1369.

Svärd, C., Nyberg, M., Frisk, E., and Krysander, M. (2014). Data-driven and adaptive statistical residual evaluation for fault detection with an automotive application. *Mechanical Systems and Signal Processing*, 45(1):170–192.

Swanson, B., Gardner, A., Brown, N., and Murray, P. (1997). Slimhole Early Kick Detection by Real-Time Drilling Analysis. *SPE Drilling & Completion*, 12(1):27–32.

Trave-Massuyes, L., Escobet, T., and Olive, X. (2006). Diagnosability Analysis Based on Component-Supported Analytical Redundancy Relations. *IEEE Transactions on Systems, Man, and Cybernetics - Part A: Systems and Humans*, 36(6):1146–1160.

Van Eykeren, L. and Chu, Q. (2014). Sensor fault detection and isolation for aircraft control systems by kinematic relations. *Control Engineering Practice*, 31(2014):200–210.

Veeningen, D., Palmer, J., Steinicke, G., Saenz, J., and Hansen, T. (2012). From Field Test to Successful Integration of Broadband Drillstring System for Offshore Extended Reach Wells. In *SPE/IADC Drilling Conference and Exhibition, SPE 151386*, San Diego, CA.

Venkatasubramanian, V., Rengaswamy, R., and Kavuri, S. N. (2003a). A review of process fault detection and diagnosis Part II: Qualitative models and search strategies. *Computers & Chemical Engineering*, 27(3):313–326.

Venkatasubramanian, V., Rengaswamy, R., Kavuri, S. N., and Yin, K. (2003b). A review of process fault detection and diagnosis Part III: Process history based methods. *Computers & Chemical Engineering*, 27(3):327–346.

Venkatasubramanian, V., Rengaswamy, R., Yin, K., and Kavuri, S. N. (2003c). A review of process fault detection and diagnosis Part I: Quantitative model-based methods. *Computers & Chemical Engineering*, 27(3):293–311.

Vestavik, O. M., Aas, B., and Podio, A. L. (1990). Downhole Gas Detection Method in Drilling Fluids. In *IADC/SPE Drilling Conference, SPE 19971*, Houston, TX.

Willersrud, A., Blanke, M., and Imsland, L. (2015a). Early pack-off diagnosis in drilling using an adaptive observer and statistical change detection. In *Proc. IFAC Workshop on Automatic Control in Offshore Oil and Gas Production*, Florianopolis, Brazil.

Willersrud, A., Blanke, M., and Imsland, L. (2015b). Incident detection and isolation in drilling using analytical redundancy relations. *Control Engineering Practice*, 41:1–12.

Willersrud, A., Blanke, M., Imsland, L., and Pavlov, A. (2015c). Drillstring Washout Diagnosis using Friction Estimation and Statistical Change Detection. *IEEE Transactions on Control Systems Technology*, PP(99).

Willersrud, A., Blanke, M., Imsland, L., and Pavlov, A. (2015d). Fault diagnosis of downhole drilling incidents using adaptive observers and statistical change detection. *Journal of Process Control*, 30:90–103.

Willersrud, A. and Imsland, L. (2013). Fault Diagnosis in Managed Pressure Drilling Using Nonlinear Adaptive Observers. In *Proc. European Control Conference*, pages 1946–1951, Zürich, Switzerland.

Willersrud, A., Imsland, L., Blanke, M., and Pavlov, A. (2015e). Early Detection and Localization of Downhole Incidents in Managed Pressure Drilling. In *Managed Pressure Drilling and Underbalanced Drilling Operations Conf. and Expo., SPE/IADC 173816*, pages 1–9, Dubai, UAE.

Willersrud, A., Imsland, L., Hauger, S. O., and Kittilsen, P. (2013a). Short-term production optimization of offshore oil and gas production using nonlinear model predictive control. *Journal of Process Control*, 23(2):215–223.

Willersrud, A., Imsland, L., Pavlov, A., and Kaasa, G.-O. (2013b). A Framework for Fault Diagnosis in Managed Pressure Drilling Applied to Flow-Loop Data. In *Proc. Dynamics and Control of Process Systems*, pages 625–630, Mumbai, India.

Willsky, A. and Jones, H. (1976). A generalized likelihood ratio approach to the detection and estimation of jumps in linear systems. *IEEE Transactions on Automatic Control*, 21(1):108–112.

Willsky, A. S. (1976). A survey of design methods for failure detection in dynamic systems. *Automatica*, 12(6):601–611.

Wu, W.-R. (1993). Target racking with glint noise. *IEEE Transactions on Aerospace and Electronic Systems*, 29(1):174–185.

Xu, A. and Zhang, Q. (2004). Nonlinear system fault diagnosis based on adaptive estimation. *Automatica*, 40(7):1181–1193.

Yin, K. (1998). Minimax methods for fault isolation in the directional residual approach. *Chemical Engineering Science*, 53(16):2921–2931.

Yin, S., Ding, S. X., Haghani, A., Hao, H., and Zhang, P. (2012). A comparison study of basic data-driven fault diagnosis and process monitoring methods on the benchmark Tennessee Eastman process. *Journal of Process Control*, 22(9):1567–1581.

Yoon, S. and MacGregor, J. F. (2001). Fault diagnosis with multivariate statistical models part I: using steady state fault signatures. *Journal of Process Control*, 11(4):387–400.

Yu, J. (2012). A particle filter driven dynamic Gaussian mixture model approach for complex process monitoring and fault diagnosis. *Journal of Process Control*, 22(4):778–788.

Zhang, Q. (2000). A new residual generation and evaluation method for detection and isolation of faults in non-linear systems. *International Journal of Adaptive Control and Signal Processing*, 14(7):759–773.

Zhang, Q. (2002). Adaptive observer for multiple-input-multiple-output (MIMO) linear time-varying systems. *IEEE Transactions on Automatic Control*, 47(3):525–529.

Zhang, Q. (2005). Revisiting different adaptive observers through a unified formulation. In *Proceedings of the 44th IEEE Conference on Decision and Control*, pages 3067–3072. IEEE.

Zhang, X., Polycarpou, M. M., and Parisini, T. (2002). A robust detection and isolation scheme for abrupt and incipient faults in nonlinear systems. *IEEE Transactions on Automatic Control*, 47(4):576–593.

Zhang, X., Polycarpou, M. M., and Parisini, T. (2010). Fault diagnosis of a class of nonlinear uncertain systems with Lipschitz nonlinearities using adaptive estimation. *Automatica*, 46(2):290–299.

Zhang, Y. and Jiang, J. (2006). Issues on integration of fault diagnosis and reconfigurable control in active fault-tolerant control. In *Proc. IFAC Safeprocess*, pages 1437–1448, Beijing, China.

Zhang, Y. and Jiang, J. (2008). Bibliographical review on reconfigurable fault-tolerant control systems. *Annual Reviews in Control*, 32(2):229–252.

Zhou, J., Stamnes, Ø. N., Aamo, O. M., and Kaasa, G.-O. (2011). Switched Control for Pressure Regulation and Kick Attenuation in a Managed Pressure Drilling System. *IEEE Transactions on Control Systems Technology*, 19(2):337–350.

Zhou, W.-W. and Blanke, M. (1989). Identification of a class of nonlinear state-space models using RPE techniques. *IEEE Transactions on Automatic Control*, 34(3):312–316.